Titre: Title:	Magnetic Powdered Activated Carbon for Drinking Water Treatment
Auteur: Author:	Kim Maren Lompe
Date:	2018
Type:	Mémoire ou thèse / Dissertation or Thesis
Référence: Citation:	Lompe, K. M. (2018). Magnetic Powdered Activated Carbon for Drinking Water Treatment [Ph.D. thesis, École Polytechnique de Montréal]. PolyPublie. https://publications.polymtl.ca/3038/

UNIVERSITÉ DE MONTRÉAL

MAGNETIC POWDERED ACTIVATED CARBON FOR DRINKING WATER TREATMENT

KIM MAREN LOMPE

DÉPARTEMENT DES GÉNIES CIVIL, GÉOLOGIQUE ET DES MINES

ÉCOLE POLYTECHNIQUE DE MONTRÉAL

THÈSE PRÉSENTÉE EN VUE DE L'OBTENTION

DU DIPLÔME DE PHILOSOPHIAE DOCTOR

(GÉNIE CIVIL)

AVRIL 2018

UNIVERSITÉ DE MONTRÉAL

ÉCOLE POLYTECHNIQUE DE MONTRÉAL

Cette thèse intitulée :

MAGNETIC POWDERED ACTIVATED CARBON FOR DRINKING WATER TREATMENT

présentée par : LOMPE Kim Maren

en vue de l'obtention du diplôme de : Philosophiae Doctor

a été dûment acceptée par le jury d'examen constitué de :

Mme PRÉVOST Michèle, Ph. D., présidente

M. BARBEAU Benoit, Ph. D., membre et directeur de recherche

M. MÉNARD David, Ph. D., membre et codirecteur de recherche

M. COMEAU Yves, Ph. D., membre

M. SOLTAN Jafar, Ph. D., membre

DEDICATION

Es gibt nichts Gutes, außer:Man tut es!

(Erich Kästner)

Roughly translates to: No change without action!

Wissen ist Nacht!

(Prof. Abdul Nachtigaller – Walter Moers)

Roughly translates to: Knowledge is night!

ACKNOWLEDGEMENTS

First and foremost, I would like to thank my advisor Benoit Barbeau for the opportunity to work on this subject at the Chair of drinking water at Polytechnique. Your enthusiasm and optimistic attitude have inspired me. During our many discussions on the various topics of this thesis or some side projects, you were always available and you guided me to solve occurring problem. I appreciate especially that you have always motivated and encouraged me.

Thanks also to my co-advisor, David Menard, not only for your guidance into the exotic world of magnetism but also for your thorough reading of our papers and your positive feedback during our discussions.

Also, I would like to thank the whole lab/chair team (Jacinthe, Julie, Mireille, Yves, Gabriel, Laura) for your support with knowledge, protocols, material and analysis as well as your moral support. Thanks also to Mélanie and Dénis for lending me material and providing all kinds of tools that you can only find in the precious collection of the waste water lab. Thanks also to my interns and Master students: Sarah, Hélène and Maria for your support and help in the lab.

All the hours spent in the lab would not have been fun or even doable, without all my colleagues and friends. Thank you Elise, for welcoming me into the group - with a big friendly smile on day one - and for being my friend ever since. Thank you my dear friend Sanaz, for your strength, for being my emotional support, my confidant and my mischievous partner in crime. Thank you, Evelyne, for your friendship and for being my eternal source of information, cupcakes and my link to the Quebecois culture. Thank you, Fatemeh, for your humor, all the nuts and the introduction to lavashak. Thank you, Laleh, for the fun and your immense kindness. Thank you, all my present and past colleagues and office friends (Emile, Flavia, Mathieu, Félix, Hadis, Veronika, Nargess…). Thank you, dear Christoph, for all the shared years and adventures.

Thanks, also to all my friends outside Polytechnique: Humberto, Céline, Ricardo, Mona.

One of the best things of this whole experience was the opportunity to make international friends. Thank you Lety, Sampada, Isabel, Sanaz, Mauricio, Sandra, Thomas, Rajesh, Xin and Celso for forming this extraordinary second family. Thank you, Andrés, for your love, care and support.

Thank you, my dear parents, for sending parcels to Canada and for being interested in my work, your support and for always being there for me and thanks Adrian and loved ones at home!

RÉSUMÉ

En combinant la capacité d'adsorption du charbon actif en poudre (CAP) avec des nanoparticules d'oxyde de fer magnétiques (NP) on obtient un matériau composite prometteur, le CAP magnétique (CAPM). Le CAPM présente l'avantage de pouvoir être séparé de l'eau dans lequel il est en suspension au moyen de séparateurs magnétiques. Cette étape de séparation est essentielle pour re-circuler le CAPM dans le réacteur et permettre son utilisation à long terme, dans l'objectif d'épuiser complètement sa capacité d'adsorption ou d'augmenter l'âge du matériau jusqu'à sa colonisation. Un CAPM biologique (colonisé) permettrait d'éliminer certains polluants biodégradables. Jusqu'à présent, le CAPM a été étudié comme adsorbant pour différents contaminants tels que les métaux lourds, des colorants et quelques polluants organiques à l'état de traces. Cependant, l'influence de la fraction massique des NP sur la capacité d'adsorption des polluants typiques de l'eau potable ainsi que l'application du CAPM dans un procédé biologique n'ont pas encore été étudiées. Dans cette thèse, un CAPM a été développé et évalué comme adsorbant alternatif pour la matière organique naturelle (MON) et certains micropolluants (MP). Finalement, la colonisation du CAPM en biomasse hétérotrophe et nitrifiante a été mesurée.

D'abord, trois CAPM ont été produits en utilisant un procédé de co-précipitation et des fractions massiques de NP de 10 %, 38 % et 54 % respectivement. Les CAPM ont été comparés avec du CAP régulier en termes de distribution de taille de pores et d'aire de surface, de charge de surface, de taille de particules et de propriétés magnétiques. Ensuite, les isothermes et la cinétique d'adsorption de la MON et de 9 MP ont été étudiés pour les matériaux composites, frais ou colonisés. Dans une prochaine étape, les CAPM et du CAP régulier ont été colonisés dans des petits réacteurs biologiques pour une période d'au moins 90 jours. Leurs performances d'enlèvement biologique du carbone organique dissous et de l'ammonium, ainsi que la quantité de biomasse hétérotrophe et la communauté bactérienne développée sur les différents CAP ont été comparées. Finalement, la séparabilité du CAPM a été évaluée dans un séparateur magnétique de haut gradient, construit avec des aimants permanents.

Les résultats ont montré que les NP couvrent principalement la surface du CAP microporeux utilisé durant ce projet. La diminution du volume des micropores était proportionnelle à la quantité de CAP dans le composite. Le volume des mésopores augmentait par rapport au CAP, de par la présence de vides entre les NP à la surface. Les NP n'ont pas contribué à l'adsorption de la

MON et des MP. En effet, la capacité d'adsorption pour ces composés était principalement proportionnelle à la quantité de CAP dans le composite. Cependant, lorsque la fraction massique des NP dépassait 38 %, les mésopores propres au CAP étaient bloqués et en conséquence, la capacité d'adsorption pour la MON était réduite. Par ailleurs, la présence des NP n'a pas influencé la cinétique d'adsorption lente de la MON, cependant elle a diminué celle, plus rapide, des MP. La MON était en compétition avec les MP pour les sites d'adsorption sur le CAPM. Ainsi, le CAPM devrait être appliqué préférablement comme étape de polissage après enlèvement de la MON dans la filière de traitement. Après vieillissement des CAPM pour 90 jours et confirmation de la présence d'un biofilm, une capacité d'adsorption résiduelle des MP persistait. Elle était cependant dix fois moins élevée que le CAPM frais. L'étude sur le long terme a montré que la même quantité de biomasse hétérotrophe active se développe sur le CAP et sur le CAPM, et ce même pour les fractions massiques les plus élevées de NP testées. Par ailleurs, une fois l'état stationnaire atteint, les NP n'ont pas réduit l'enlèvement du carbone organique dissous et de l'ammonium. Cependant, la nitrification était retardée de 6 jours sur les CAPM, ce qui a été attribué à l'inhibition initiale des bactéries nitrifiantes. En terme de stabilité du CAPM, une baisse de magnétisation entre 10 % et 34 % a été mesurée entre le début et la fin des essais (90 jours). Cet effet s'explique par la perte de NP par des effets d'abrasion dans la solution de CAPM. En effet, comparativement à du CAP, une vitesse d'agitation plus élevée était nécessaire pour maintenir les matériaux composites lourds en suspension. Finalement, les essais de séparation de CAPM ont montré que 10 % de NP dans le matériau composite n'était pas suffisant pour isoler le CAPM de la suspension avec un séparateur magnétique à haut gradient, et ce même à des vitesses de filtration faibles (0.04 m/s).

Ce projet de recherche a démontré l'aptitude du CAPM pour l'adsorption de la MON et des MP. En choisissant le CAP microporeux comme matrice de CAPM, l'adsorption de la MON et des MP était proportionnelle à la quantité de CAP dans le matériau composite. De plus, le CAPM peut agir à titre de support de biomasse dans le réacteur biologique puisque les NP n'ont pas inhibé l'enlèvement du carbone organique dissous et l'ammonium. En général, des fractions massiques de NP variant entre 10% et 38 % devraient être choisies pour la préparation de CAPM afin de maximiser la quantité d'adsorbant actif (CAP) tout en évitant des vitesses élevées d'agitation pouvant accélérer l'abrasion du matériau.

ABSTRACT

Combining the high adsorption capacity of powdered activated carbon (PAC) with magnetic iron oxide nanoparticles (IONP), leads to a promising composite material, magnetic PAC or MPAC, which can be separated from water using magnetic separators. The possibility to separate the adsorbent from the suspension and to recirculate it into the reactor opens the door for the long-term use of PAC - either to fully exhaust its adsorption capacity or to increase the adsorbent age until the adsorbent particles are fully colonized. The adsorbent particles will then act as a growth support and contribute to the elimination of certain biodegradable pollutants. So far, MPAC has been studied as an adsorbent for various contaminants such as heavy metals, dyes and some organic trace pollutants. Yet, the influence of IONP mass fraction on the adsorption capacity for typical drinking water pollutants or MPAC's usability in a biological process, have not yet been clarified. In this thesis, MPAC was evaluated as an alternative adsorbent for natural organic matter (NOM) and micropollutants and as a growth support for heterotrophic and nitrifying bacteria.

First, we produced three MPAC composites with mass fractions of 10 %, 38 % and 54 % maghemite nanoparticles using a co-precipitation process. The adsorbents were then compared to bare PAC and pure nanoparticles with respect to pore size and surface area distribution, surface charge, particle size and magnetic properties. Second, the composites were studied regarding their NOM adsorption kinetics and isotherms. Third, we tested the adsorption properties of fresh and colonized MPAC for 9 organic micropollutants representing pharmaceuticals, hormones and pesticides. Subsequently, the three MPAC composites and regular PAC were colonized in small bioreactors for over 90 days to compare their removal performance regarding dissolved organic carbon (DOC) and ammonia. Finally, we explored the separability of MPAC in a high gradient magnetic separator built with permanent magnets.

The results have shown that IONP cover mostly the surface of the microporous PAC used during this project. Reductions in the micropore volumes were mostly proportional to the PAC content in MPAC. Mesopore volume of MPAC on the other hand was increased compared to PAC due to the presence of voids in the IONP crust.

The IONP did not contribute to the adsorption of NOM or MP and thus the adsorption capacity for these compounds was mainly proportional to the PAC mass fraction in MPAC. Only at IONP mass fractions exceeding 38 %, intrinsic PAC mesopores were blocked by IONP, which limited the adsorption capacity of the larger NOM molecules. The presence of IONP did not influence the already slow adsorption kinetics of NOM while the usually fast kinetics of MP were slower on MPAC compared to PAC. NOM competed with MP for adsorption sites on MPAC and the application of MPAC should consequently be considered as a polishing step after NOM has been removed in a previous treatment step such as coagulation-flocculation. A residual but tenfold lower adsorption capacity for micropollutants exists even for aged MPAC (90 days) that are colonized and covered with biofilm. The long-term study of MPAC has shown that the same amount of active heterotrophic biomass (48 µg C/cm³) developed on MPAC with a mass fraction of 54 % IONP as on the non-magnetic PAC control. Moreover, IONP did not influence the DOC and ammonia biological removals once steady state was reached. However, we observed a slightly slower onset of nitrification (6 days) in reactors containing MPAC which might be an indicator for the initial inhibition of nitrifying bacteria. In terms of long-term stability of MPAC, a loss in magnetization between 10 % and 34 % was recorded at the end of the 90 day aging period, which was attributed to a loss of IONP due to attrition. Higher agitation speeds were necessary to keep the heavier composites in suspension. Regarding the separation of MPAC in a HGMS using permanent magnets, 10 % IONP were not sufficient to separate MPAC even at low flow velocities of 0.04 m/s.

Overall, this research project has shown the suitability of MPAC for the adsorption of NOM and micropollutants. With the microporous PAC that was chosen as MPAC template, the adsorption capacity of NOM and micropollutants was mostly proportional to the PAC content in the composite material. Moreover, MPAC can serve as a growth support in a bioreactor as IONP did not inhibit dissolved organic and ammonia biological removal by MPAC. In general, IONP mass fractions between 10 % and 38 % should be chosen for the preparation of MPAC in order to maximize the content of the active adsorbent (PAC) per unit weight and to avoid high agitation speeds and attrition due to high MPAC densities.

TABLE OF CONTENTS

LIST OF TABLES

LIST OF FIGURES

LIST OF SYMBOLS AND ABBREVIATIONS

AC	Activated carbon
ARE	Average relative error (%)
BDOC	Biodegradable dissolved organic carbon
BET	Brunauer-Emmett and Teller theory
CUR	Carbon usage rate
DBP	Disinfection by-products
DOC	Dissolved organic carbon
EDS	Energy dispersive X-ray spectroscopy
EPS	Extracellular polymeric substances
GAC	Granular activated carbon
HA	Humic acid
HGMS	High gradient magnetic separator
HIMS	High intensity magnetic separator
HMP	Hybrid membrane process
HRT	Hydraulic retention time
HSDM	Homogeneous surface diffusion model
IONP	Iron oxide nanoparticle(s)
MAC	Magnetic activated carbon(s)
MF	Microfiltration
MPAC	Magnetic powdered activated carbon(s)
NLDFT	Non-local density function theory
NOM	Natural organic matter

NP	Nanoparticles
OTU	Operational taxonomic unit(s)
PAC	Powdered activated carbon
PES	Polyethersulfone
PGR	Potential glucose respiration rate
RMSE	Root mean squared error
ROS	Reactive oxygen species
SEM	Scanning electron microscopy
SR-NOM	Suwannee River NOM
$SUVA_{254}$	Specific ultraviolet absorbance at 254 nm
TEM	Transmission electron microscopy
TOC	Total organic carbon
UF	Ultrafiltration
UVA	UV absorbance
VSM	Vibrating sample magnetometer
XRD	X-ray diffraction

LIST OF APPENDICES

CHAPTER 1 INTRODUCTION - WHY DO WE NEED A MAGNETICALLY SEPARABLE ADSORBENT FOR WATER TREATMENT?

Magnetic powdered activated carbons (MPAC) are magnetically enhanced adsorbents that combine two desired qualities: high adsorbent capacities for many organic pollutants and their magnetic properties that allow for simple and highly efficient recovery via magnetic separation (Anzai et al. 2016, Borghi and Fabbri 2014, Kim et al. 2013). The magnetic properties of MPAC are achieved by combining PAC with iron oxide nanoparticles (IONP) such as the ferrimagnetic maghemite or magnetite. It is the magnetic separability that makes these novel adsorbents attractive for a variety of powdered activated carbon (PAC) applications in drinking water as it allows returning PAC into the process and thus to increase the solid retention time.

Conventional PAC has successfully been employed in water treatment for decades to deal with organic molecules at trace level, as it efficiently removes a wide range of organic pollutants via adsorption. However, the short contact times of a few minutes typically prevailing within water treatment processes do not allow to fully exhaust the PAC adsorption capacity (Kim et al. 2014). As PAC is a costly expense for a water treatment plant (currently around 1.0 - 2.5 $ CAD/kg), techniques are sought for to use PAC longer until its adsorption capacity is fully exhausted or even longer (> 30 days) until PAC particles are colonized with bacteria to work in a combined adsorption/biodegradation process (Stoquart et al. 2012). Processes using colonized PAC are especially promising as they can be used to remove not only trace contaminants via adsorption but also biodegradable precursors of disinfection by-products (DBP) such as biodegradable dissolved organic carbon (BDOC) and ammonia (Markarian et al. 2010). In both cases (pure adsorption or combined biodegradation PAC processes) efficient PAC separation is necessary to return the adsorbent particles back into the carbon contactor until the desired PAC age is achieved. Separating PAC, however, remains a challenge as it entails the problem of separating fine and stable suspensions (Tarleton and Wakeman 2007).

Conventional separation technologies for fine PAC suspensions are filtration, flotation, gravity sedimentation, and centrifugal sedimentation. Sedimentation following a pre-treatment of coagulation/ flocculation is the most common PAC separation step in water treatment and is often followed by sedimentation basins, lamella separators or deep bed filters where a flocculation aid

is added to enhance the filter's removal efficiency. The pre-treatment is required as the PAC particles have nearly the same density as water and are too small for efficient sedimentation (Svarovsky 2000). Coagulation/flocculation aims at increasing the diameter of PAC to allow for faster sedimentation. However, separation via sedimentation is time and space-consuming and chemical products such as coagulants and flocculation aids are expensive or in the case of polyacrylamide might be forbidden in the nearer future on the European market.

Current designs of processes using highly concentrated PAC suspensions, so-called hybrid membrane processes (HMP), are low pressure membranes such as microfiltration (MF) and ultrafiltration (UF) membranes which are either immersed in the PAC reactor or in direct contact with the PAC suspension. In this configuration the membrane is acting as a barrier for PAC particles but also particulate contaminants such as *Cryptosporidium* or other protozoan pathogens (Lebeau et al. 1998). The compact layout and the complete separation of PAC particles are a considerable advantage of this design which was tested in several pilot studies (Lebeau et al. 1998, Leveillé et al. 2013). The HMP design with immersed membranes and PAC retention times < 7 days exist as full-scale processes (e.g. as the commercialized Opaline C process (Veolia Water 2013) and the Cristal process (Suez Environment)). However, contacting the membrane directly with highly concentrated PAC suspensions can lead to abrasion and clogging of the membranes which is a constraint of this technology (Oligny et al. 2016, Seo et al. 2005).

The issue of PAC separation becomes more important when the process is designed to work at high PAC age, where PAC particles do not only serve as adsorbents but also as a support for heterotrophic and nitrifying biomass. When operated in biological mode, a direct contact of colonized PAC with the membrane can lead to increased fouling as biomass develops a gel layer on the membrane surface that functions as adhesive between membrane and PAC (Seo et al. 2005). Severe membrane fouling resulting from the direct contact of the membranes with highly concentrated and colonized PAC suspensions have limited so far the industrial application of biologically working HMP. A separation step for PAC or colonized PAC that efficiently removes PAC from the membrane feed flow is the missing element for the application of the HMP as a combined adsorption/biodegradation process.

The advantage of magnetic separation is obvious: there is no need to add any chemical products to the process which could affect the carbon's capacity. Also, separation with magnetic separators and re-dispersion of PAC into the water can be fast. Recently, Zahoor (2014) proposed MPAC as

an alternative to the use of PAC in a lab-scale HMP with low PAC age where problems related to cake formation and membrane fouling were successfully avoided using magnetic separation to provide a low-particle membrane feed.

Previous adsorption studies have shown the suitability of MPAC for different organic dyes such as methylene blue, acid orange, methyl orange and humic acid (Ai and Jiang 2010, Kondo et al. 2010, Yang et al. 2008), a range of micropollutants (MP) such as bisphenol-A (endocrine disruptor) (Koduru et al. 2016, Nakahira et al. 2006, Nakahira et al. 2007, Park et al. 2015), atrazine (herbicide) (Castro et al. 2009), imidacloprid (insecticide) (Zahoor and Mahramonlioglu 2011), ciprofloxacin (antibiotic) (Shi et al. 2013), carbamazepine (anti-epileptic drug) (Baghdadi et al. 2016), and naproxen (anti-inflammatory) (Ilbay et al. 2015). Using MPAC for the removal of NOM has been proposed by Kondo et al. (2010),Anzai et al. (2016), Kim et al. (2013), Park et al. (2015) and Zahoor (2014).

The studies show promising results as adsorption capacities of MPAC seem only partly affected by the presence of magnetite nanoparticles. Several considerations, however, are still missing towards the application of MPAC for the HMP:

- While removal of inorganic and organic molecules by MPAC has been demonstrated, the interplay between IONP content in MPAC, pore size distribution of PAC and contaminant properties had not yet been investigated.
- While studies on the impact of pure IONP on environmental systems exist (Ju-Nam and Lead 2008, Klaine et al. 2008, Moore 2006), the impact of magnetically enhanced carbon materials in biological processes have not been undertaken.

Applying easily separable MPAC opens up new possibilities for both: MPAC use at high PAC ages to exploit the benefits of colonized adsorbents that allow for biodegradation of dissolved contaminants and for typical applications of PAC where contact times are short and PAC is returned into the process to exhaust its adsorption capacity. Investigating the influence of IONP content in MPAC on adsorption properties and biological growth are necessary to design processes that help to solve the current and future challenges of removing dissolved organic contaminants from drinking water.

The main research questions that were addressed in this thesis are :

i) How do IONP change the physical properties of PAC (pore size distribution, surface area, surface charge, size, magnetic properties)?

ii) How does IONP content of MPAC influence the adsorption capacity for NOM?

iii) How does IONP content of MPAC influence the adsorption capacity for MP?

iv) What is the role of NOM in MP adsorption on MPAC?

v) Is there a significant residual MP adsorption capacity on 90 days aged MPAC?

vi) Do IONP inhibit the development of heterotrophic and nitrifying biomass on MPAC?

vii) How does IONP content influence the biodegradation of NOM and ammonia?

viii) Are MPAC particles stable composites even at high adsorbent age?

This thesis is structured in 8 chapters.

A critical review of the state of the art of magnetic PAC synthesis and application is presented in Chapter 2 and leads to the objectives, hypotheses and methodology that are formulated in Chapter 3. Chapters 4 through 6 represent the research results in the form of published or submitted articles. The first article presents the synthesis and characterization of the magnetic adsorbent and systematic and quantitative evaluation of IONP mass fractions on NOM adsorption (research questions i and ii). NOM removal was evaluated with respect to the distribution of pore volume and surface area as well as the NOM characteristics such as molecular size and aromaticity. The second article demonstrates the suitability of fresh and colonized MPAC for the removal of trace pollutants in natural waters (research questions iii through v). The third article evaluates MPAC performance both as an adsorbent and as a support for biological growth within a bioreactor operated for 90 days (research questions vi to viii). Chapter 7 reports findings on the separability of MPAC in a magnetic separator. Finally, a general discussion is provided in Chapter 8 followed by conclusions and recommendations.

CHAPTER 2 CRITICAL LITERATURE REVIEW

2.1 A promising magnetic adsorbent

In the last decade the preparation of magnetic adsorbents gained attention due to their qualities as adsorbents and their simple and highly efficient recovery via magnetic separation (Figure 2.1). Magnetic separation has many advantages over conventional separation techniques such as gravitational or centrifugal separation as also very fine particles can be separated, no chemicals have to be added, separation is fast and the equipment is space-saving (Svarovsky 2000). Of course, magnetic separation requires magnetically susceptible particles that can be separated applying a magnetic field. This constraint would normally exclude conventional PAC from the field of application. Magnetically modified PAC (MPAC) which is presented with its specific properties in this Chapter, however, is in the scope of applications for magnetic separators. MPAC are composite materials with a non-magnetic structure of activated carbon that serves as an adsorbent and magnetic labels such as iron oxides (mainly maghemite and magnetite) at nano- or micro scale that are responsible for the strong magnetic behaviour of the composite (Safarik et al. 2013).

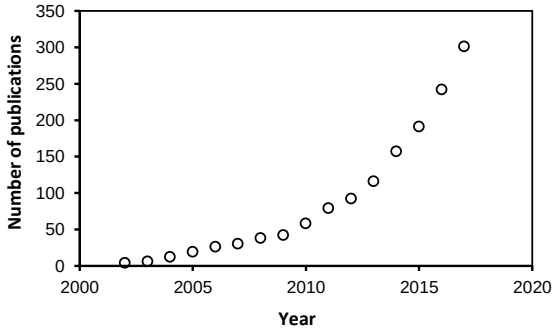

Figure 2.1: Publications on magnetic activated carbons since 2002[1].

Aside from the additional advantage of magnetic separability, the role of MPAC remains that of an adsorbent in the first place. If PAC is to be replaced by MPAC as an alternative adsorbent, the

[1] Search strategy with Web of Science: TS=(carbon OR biochar) AND TS=(activated OR porous OR powdered) AND TS=(adsorbent) AND TS=(magnetic OR magnetite OR Fe3O4 or Fe2O3 OR iron oxide) NOT TS=(tube OR nanotube* OR multiwall* OR sheet OR silica OR template OR dioxide OR multi* OR electro* OR calcium OR nanosphere* OR catalyst OR copper OR nuclear OR resonance OR Frequency OR magnetic suspension balance OR MIEX OR Resin OR chitosan OR microsphere* OR polymer OR graph* OR zeolite*)

properties of MPAC that allow for high adsorption capacity and fast kinetics for the target contaminant should remain similar to PAC. The challenge regarding the design of this composite material is thus to

(i) Choose either the best PAC or the best PAC template to allow for maximum adsorption of the specific target pollutant;

(ii) Optimize the MPAC synthesis method to preserve/enhance the adsorption properties of PAC while producing magnetic nanoparticles of highest quality regarding their magnetic properties;

(iii) Optimize the ratio of PAC and magnetic nanoparticles to ensure good adsorption properties while at the same time obtaining sufficient magnetic properties for separation.

The first part of this literature review focuses on adsorption theory to provide the necessary background to take on the challenge (i). The next part is dedicated to the theory of magnetism and magnetic materials addressing challenge (ii). This is followed by a critical review of the existing literature on MPAC with respect to the synthesis methods, MPAC properties and adsorption studies (iii). Finally, the compatibility of magnetic nanoparticles with heterotrophic and nitrifying bacteria is reviewed to set the basis for the application of MPAC in a biological drinking water process as suggested for the first time in this project.

2.2 Adsorption theory and models

Adsorption is a process where dissolved contaminants (adsorbates) are removed from the aqueous solution via adsorption onto a solid surface (adsorbent) (Worch 2012). This mass transfer process for porous materials such as PAC involves (i) the transport of the adsorbate from the bulk liquid to the external surface of PAC, (ii) the diffusion into the inner pore system and (iii) its attachment to the inner surface. The kinetics of this process are determined by the rate controlling external and internal mass transfer whereas the attachment itself is fast (Worch 2012). The adsorption of organic pollutants on PAC is governed by the nature of the adsorbent, the nature of the adsorbate and the properties of the water matrix. The interactions between adsorbate and adsorbent influence the adsorption kinetics and capacity. For practical applications, adsorption experiments have to be conducted. Models that have been developed to represent in a

simplified way the equilibrium behaviour via isotherms and time dependence of adsorption processes via kinetic models can be applied to the data obtained.

2.2.1 Factors that influence adsorption kinetics and capacity

2.2.1.1 **Nature of the adsorbent**

The basic raw materials (e.g. wood, coconut shells, lignite coal or bituminous coal), the carbonization method (temperature and holding time) as well as the method of activation (acid, base or steam) determine the chemical composition, the surface chemistry, the surface structure and porosity of PAC (Çeçen and Aktas 2012, Chattopadhyaya et al. 2006). These properties can vary widely between products and define their adsorption characteristics (Çeçen and Aktas 2012). The surface of PAC is mainly hydrophobic but can contain charged functional groups such as oxygen groups that lead to a (slightly) negatively charged surface when suspended in water at a neutral pH (Tarleton and Wakeman 2007). The particle size influences mainly adsorption kinetics as diffusion pathways are shorter in smaller particles. This effect has recently been exploited in applications using superfine powdered activated carbon (0.1 – 1 µm particle diameter) (Partlan et al. 2016). The accessibility of adsorption sites inside the porous structure is determined by the pore size distribution. Steric effects hinder molecules to enter pores that are smaller than the molecule diameter (Çeçen and Aktas 2012).

2.2.1.2 **Nature of the adsorbate**

The properties of the adsorbate such as molecular weight, hydrophobicity, polarity and aromaticity determine its interaction with PAC and have been discussed in various studies (Crittenden et al. 2012, Worch 2012). The affinity of adsorbates for PAC can differ very largely and competition for adsorption sites can occur by molecules of similar properties. Generally it has been found that PAC is most effective to remove non-polar, more hydrophobic, uncharged compounds that have a lower solubility and thus a higher affinity for the carbon surface than for water (Crittenden et al. 2012). Among molecules with similar affinity for PAC, the molecular weight (that determines the size) of the adsorbate determines the accessibility to the inner pore spaces of PAC (Crittenden et al. 2012).

2.2.1.3 **Water matrix**

The properties of the water matrix such as temperature, pH and ionic force influence the PAC surface chemistry as well as the properties of the adsorbate. In natural waters NOM reduces the removal efficiency of PAC for the organic target molecules such as organic MP due to competition effects. NOM is a complex multi-component mixture originating from natural as well as non-natural sources and its actual composition varies in waters of different geographical origin (Crittenden et al. 2012). It consists mainly of humic substances with a molecular weight between 500 and 3000 Da which corresponds to a size of < 10 nm. The size of NOM molecules is thus in the same range as PAC mesopores (2 nm < Ø < 50 nm) and one order of magnitude larger than organic MP (< 1 nm) (Crittenden et al. 2012). The different fractions of NOM, have different adsorbability and the competitive effect of NOM depends on their character and concentration (Çeçen and Aktas 2012). Mainly two competition mechanisms have been identified: direct competition with the target molecule for adsorption sites and/or pore blocking (Çeçen and Aktas 2012). Direct competition between NOM molecules and MP can be attributed to small NOM molecules with a molecular size that is similar to the target pollutant (Kovalova et al. 2013) as well as to the higher concentration of NOM (mg/L) compared to the organic MP (ng/L) (Çeçen and Aktas 2012, Worch 2012). The pore blocking phenomenon occurs when relatively large NOM molecules block the access to the pore system of PAC.

2.2.2 Isotherm and kinetic models

2.2.2.1 **Adsorption equilibrium**

The following section gives an overview of the most common adsorption models. The intention is to set the foundation for the methods used in this thesis rather than to provide a complete review of existing models and theories.

The evaluation of pollutant adsorbability or the comparison of PAC performances is usually done in batch experiments at equilibrium state. Adsorption equilibrium is reached when the concentration of the adsorbate in the liquid phase is not changing anymore with time. The pollutant loading on a specific PAC in equilibrium is dependent on the adsorbate concentration and the temperature. This relation is described by an appropriate adsorption isotherm that is recorded at constant temperature (Worch 2012).

$$q_{eq} = f(C_{eq}), \qquad T = constant \qquad \text{Eq. 2.1}$$

The loading of adsorbate on PAC in equilibrium q_{eq} (e.g. in µg/mg) is obtained from the concentration difference between initial and final concentrations C_0 and C_{eq} of the solute *(µg/L)*, the known solute volume V_L (L) and the known mass of adsorbent m_{PAC} (mg/L) :

$$q_{eq} = \frac{V_L}{m_{PAC}} (C_0 - C_{eq}) \,. \qquad \text{Eq. 2.2}$$

The best known isotherm models describe single solute adsorption. Although in most applications in water treatment many solutes are present simultaneously, these models are sufficient to compare adsorbabilities of solutes or capacities of adsorbents (Worch 2012).

The Langmuir and the Freundlich models are the most frequently used. While the former is based on theoretical considerations, the latter is empirical (Crittenden et al. 2012).

The Langmuir model considers saturation of the adsorbent at high equilibrium concentrations (formation of a mono-layer on the adsorbent) and has the form:

$$q_{eq} = \frac{q_m b C_{eq}}{1 + b C_{eq}}, \qquad \text{Eq. 2.3}$$

where q_m (same unit as the adsorbent loading q_{eq}) and b (reciprocal unit of the concentration) are the isotherm parameters. The Freundlich isotherm – although empirical – shows often much better fit to experimental data with PAC (Worch 2012) and has the form:

$$q_{eq} = K_F {C_{eq}}^{1/n}, \qquad \text{Eq. 2.4}$$

where K_F (unit depends on units of q_{eq} and C_{eq}, e.g. µg/mg (µg/L)$^{1/n}$) and n (unitless) are the isotherm parameters. The adsorption coefficient K characterizes the strength of adsorption and can be used to compare adsorption capacities if n-values of the respective models are similar. The exponent n determines the curvature of the isotherm. The lower the value n the more concave the isotherm and the more favourable the adsorption on PAC (Worch 2012).

2.2.2.2 **Rate of adsorption**

PAC applications such as taste and odour control often work at contact times much smaller than the time necessary to reach equilibrium. Adsorption kinetics describe the time dependence of the adsorption process until equilibrium is reached:

$$q_t = f(t). \qquad \text{Eq. 2.5}$$

The kinetics of adsorption in porous materials such as PAC are determined by diffusion processes (external film diffusion and internal pore or surface diffusion). In experiments with high shaking velocities, external diffusion of the solute towards the PAC surface is not limiting and the mass transfer can be described by pore or surface diffusion models. The most frequently used model is the ***homogeneous surface diffusion model*** (HSDM) which describes the rate of surface loading change q with time t at any distance r from the PAC particle centre. The loading of the PAC particles, considered spherical and homogeneous, is described by the diffusion equation:

$$\frac{\partial q}{\partial t} = D_s \left(\frac{\partial^2 q}{\partial r^2} + \frac{2}{r} \frac{\partial q}{\partial r} \right), \qquad \text{Eq. 2.6}$$

with the initial condition:

$$\text{at } t = 0,\ 0 \le r \le R: \qquad q = 0, \qquad \text{Eq. 2.7}$$

and two boundary conditions :

$$\text{at } r = 0,\ t \ge 0: \qquad \frac{\partial q}{\partial r} = 0 \qquad \text{Eq. 2.8}$$

$$\text{at } r = R,\ q_s = K C_{eq}^{1/n} \ . \qquad \text{Eq. 2.9}$$

The surface diffusion coefficient D_s (m²/s) represents the rate of diffusion of the target compound along the surface of PAC (Najm 1996). As can be seen from Eq. 2.8 and Eq. 2.9 the loading rate in the center of the particle is zero and the solid concentration of the adsorbate at the outer surface of the particle (r = R) is in Freundlich equilibrium with the liquid adsorbate concentration C_{eq}. To determine D_s from experimental data, batch tests can be carried out. For a batch reactor the HSDM can be expressed by combining Eq. 2.10 that describes the total mass M_t of adsorbent on the surface of all particles in the reactor (where C_{PAC} is the PAC concentration and R is the particle radius) with a mass balance for a plug flow reactor (Najm 1996):

$$M_t = \frac{3 C_{PAC}}{R^3} \int_0^R q\, r^2\, dr \ , \text{ with initial condition at } t = 0\text{: } C = C_0 \qquad \text{Eq. 2.10}$$

$$\frac{dC}{dt} = \frac{dM_t}{dt} = -\frac{3 C_{PAC}}{R^3} \frac{\partial}{\partial t} \int_0^R q\, r^2\, dr \qquad \text{Eq. 2.11}$$

The resulting system of equation has been approximated by a nonlinear algebraic equation (Eq. 2.12) and can be solved iteratively for D_s by minimizing the sum of squared residuals between the model result and the measured kinetic data as described by Edzwald (2011):

$$0 = C_0 - C - 3C_{PAC}KC_{eq}{}^{1/n} \cdot \left\{ \begin{matrix} 0.33334 - 0.04903\, e^{\left(-142.634\frac{tD_S}{R^2}\right)} \\ -0.05399\, e^{\left(-39.996\frac{tD_S}{R^2}\right)} \\ -0.20240\, e^{\left(-9.8686\frac{tD_S}{R^2}\right)} \end{matrix} \right\}. \qquad \text{Eq. 2.12}$$

Also ***reaction kinetic models*** are often used to describe adsorption kinetics for PAC despite the fact that they are not based on the well-known diffusion process that determines adsorption kinetics (Worch 2012). Rate kinetic equations were developed for chemical reaction kinetics and have no physical meaning for adsorption processes. However, they are simple to use and this makes them attractive as a tool to compare adsorbents.[2] Most authors fit a pseudo-second order reaction kinetic model developed by Ho and McKay (1998) to their adsorption data as this model is applicable for low adsorbate concentrations (a common condition in drinking water treatment). This model is given by the following equation:

$$q_t = \frac{tk_2 q_{eq}^2}{1+k_2 q_{eq} t} \ , \qquad \text{Eq. 2.13}$$

where k_2 (e.g. in mg/µg/min) is the kinetic constant. For higher concentrated contaminants such as NOM, the pseudo-first order model developed by Lagergren (1898) often fits experimental data:

$$q_t = q_e(1 - e^{-k_1 t}) \ , \qquad \text{Eq. 2.14}$$

where k_1 (1/min) is the kinetic constant. After linearizing the equations of these two models, the constant can be determined using a linear regression with the experimental data (Ho and McKay 1998).

[2] The reviewers of the article "Influence of iron oxide nanoparticles upon the adsorption of organic matter on MPAC" presented in Chapter 4 specifically asked to add reaction kinetic model results to the initially presented diffusion coefficients (HSDM result) in order to compare to other published studies. For MPAC, no other published study using the HSDM exists so far.

2.3 Theoretical background of magnetic separation

2.3.1 Magnetism and magnetic materials

In this chapter some fundamental principles of the phenomenon of magnetism are introduced since they are essential for the proper design of magnetic separation. The theory section is mainly based on Spaldin (2003) and Teja and Koh (2009) and the SI unit system is used.

Suspensions of magnetically susceptible particles can be separated applying a magnetic field. The necessary magnetic field, its gradient and process designs of the magnetic separator depend on the particle's magnetic properties such as its magnetization in a magnetic field.

Magnetization within a magnetic field is a property of the material and depends on the individual magnetic dipole moments of the constituent elementary particles and how these moments interact and vary with the applied magnetic field and temperature (Spaldin 2003). The observed magnetic moments of a material arise from the spin and orbital angular moments of the electrons that circulate around the nucleus of an atom. The net or total angular moment of the electrons determine the magnetic moment of an atom (Spaldin 2003). Without going into the details of quantum mechanics, a short overview on different magnetic states is given in order to understand the interactions between magnetic particles and the magnetic field in particle separation.

In the case of ***ferro- or ferrimagnetic*** particles, separation is quite simple. These materials such as iron (and its oxides maghemite and magnetite), but also cobalt and nickel are strongly attracted by a magnetic field. On an atomic scale, this means that the intrinsic magnetic moments of the atoms are aligned parallel even without an external magnetic field below a critical temperature (Curie temperature). Characteristic for ferromagnetic materials is the formation of small regions of uniform alignment of the intrinsic magnetic moments (Weiss domains) that tend to minimize the total magnetic energy. When an external magnetic field is applied, the orientation of these domains is changed in such a way that they are aligned parallel to the applied magnetic field (Figure 2.2). Due to the parallel orientation, ferro- and ferromagnetic materials are likewise attracted by the South- and North Pole of the external magnet. The difference between ferro- and ferrimagnets is only "visible" on a microscopic scale. In ferrimagnets the net magnetic moment results from two types of atoms with moments of different strengths that are arranged in an antiparallel fashion (Teja and Koh 2009). Most ferrimagnets are oxides such as magnetite (the

two atoms Fe^{2+} and Fe^{3+} lead to the opposing moments) whereas most ferromagnets are metals (Spaldin 2003).

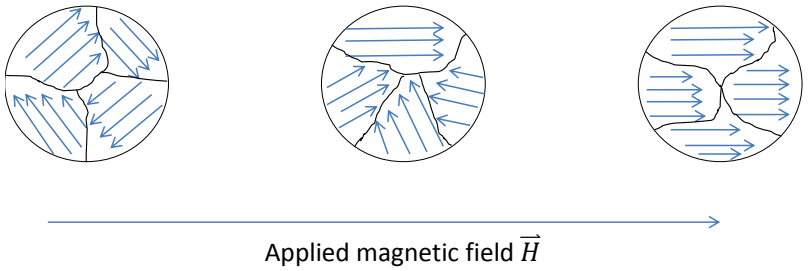

Figure 2.2 : Orientation of the Weiss domains within a ferromagnetic material. The arrow indicates the direction of increasing strength of the applied magnetic field $\vec{H}$.

Another characteristic of ferro- and ferrimagnetic materials is the phenomenon of remanence. Magnetization of ferro- and ferrimagnetic materials increases with growing magnetic field strength until saturation but does not disappear completely when the magnetic field is removed. A certain magnetization $\vec{M}_R$ remains (Weiss domains remain aligned) leading to the so-called typical hysteresis loop (Figure 2.3a). The remaining magnetization can be removed by applying the opposite magnetic field. The magnitude of this opposing field $\vec{H}_C$ is called coercivity. The susceptibility χ, which is defined as the ratio of $\vec{M}$ to $\vec{H}$ indicates how responsive a material is to an applied magnetic field. The susceptibility is large and positive for ferro- and ferrimagnetic materials and a function of the applied field (Spaldin 2003).

If the size of ferro- or ferrimagnetic materials becomes very small, ***superparamagnetic*** effects dominate below the Curie temperature. In this regime, thermal fluctuations of the magnetization of each particles lead to a vanishing average magnetization, when no field is applied. Whenever magnetic fields are applied, the magnetization curve of superparamagnetic materials does thus not exhibit hysteresis (Teja and Koh 2009) which means that no remanent magnetization is present after the magnetic field is removed (Figure 2.3 b). This phenomenon makes these materials very attractive for several technical applications as superparamagnetic particles do not form agglomerates and can easily be redispersed in water when the magnetic field is removed. At a microscopic scale this can be explained with an energy approach. The number of Weiss domains decreases with decreasing length scale until a critical diameter below which only a single domain remains as it becomes energetically unfavourable to form domain walls (Spaldin 2003, Teja and Koh 2009, Westwood 1993). The energy required to align the direction of

magnetic moments is very low and in the order of thermal energy. In the absence of a magnetic field the magnetization can randomly change direction under the influence of thermal energy and thus the net magnetization averages zero (Spaldin 2003). IONP such as maghemite and magnetite with diameters smaller than about 20 nm display superparamagnetic behavior at room temperature (Teja and Koh 2009).

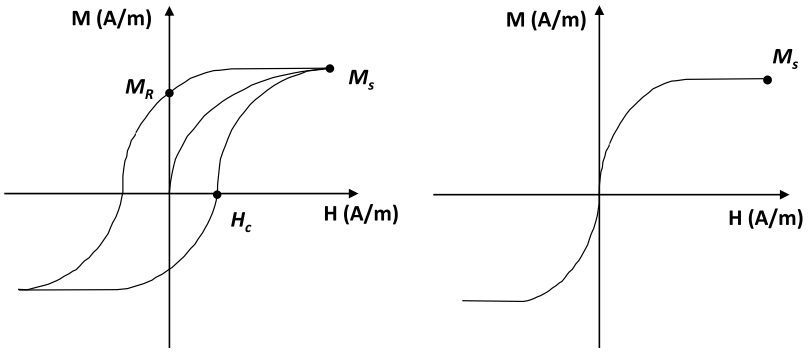

Figure 2.3 : a) Hysteresis curve for ferro- and ferromagnetic materials, b) Magnetization curve for superparamagnetic materials (taken from Spaldin, 2003).

Powdered activated carbon particles are not attracted by a magnet, they are ***diamagnetic*** – a magnetic state that exists in all components independently of other magnetic states. A diamagnetic material will exhibit an extremely weak magnetization that is antiparallel to the applied field. The susceptibility of diamagnetic materials is small and negative (Spaldin 2003). On a microscopic scale, this effect is due to a change in orbital motion of the electrons that is imposed by an applied magnetic field. This change in orbital motion takes place in all materials; however, this effect is very weak and is overshadowed in materials with stronger magnetic states such as ferri- and ferromagnetism (Spaldin 2003). Magnetic separation of PAC particles is therefore only possible, if the particles are seeded with magnetic particles. Then diamagnetic PAC becomes attractive to be separated from the likewise diamagnetic water.

2.3.2 Theory of magnetic separation

For efficient separation of magnetic particles from the surrounding water, ***magnetic forces*** $\vec{F}_m$ that act on the particles and the ***field gradient*** $\mathrm{grad}(\vec{H})$ are of paramount importance. Other forces such as the hydrodynamic drag force $\vec{F}_m$, gravity $\vec{F}_g$ or inter-particle forces interact or

counteract magnetic separation. Effective separation requires a magnetic force that is higher than the sum of the counteracting forces (Jin et al. 2000).

The magnetic force $\vec{F}_m$ (kg m/s^2) that acts on a particle in a magnetic field can be written as:

$$\vec{F}_m = \mu_0 V_p \vec{M}_p \cdot \mathrm{grad}(\vec{H}) \ , \qquad \text{Eq. 2.15}$$

where μ_0 (kg m/s²/A²) is the magnetic permeability in air, V_p is the particle volume and $\vec{M}_p$ (A/m) is the magnetization of the particle in the applied field $\vec{H}$. The equation can also be expressed in terms of susceptibility of the particle χ_p (unitless) :

$$\vec{F}_m = \mu_0 V_p \chi_p \vec{H} \cdot \mathrm{grad}(\vec{H}) \ . \qquad \text{Eq. 2.16}$$

Given that the susceptibility is a given material property, then the force $\vec{F}_m$ can only be enhanced using stronger magnetic fields $\vec{H}$ or/and by increasing the gradient $\mathrm{grad}(\vec{H})$ or by increasing the particle volume e.g. by aggregation (Andreu et al. 2012).

Superparamagnetic particles are very small and thus have a small volume V_p which leads to a low magnetic force acting on the particles (Ohara et al. 2001). When employed in medical applications, the magnetic response of superparamagnetic particles is often enhanced by embedding the nanocrystals in a matrix of non-magnetic material to create larger particles (Andreu et al. 2012). With regard to MPAC the same principle applies as IONP are concentrated on the surface and in the pores of a non-magnetic PAC matrix.

The enhancement of the magnetic force through the use of stronger magnetic fields is limited for ferro- and ferrimagnetic or superparamagnetic particles such as magnetite or maghemite nanoparticles as they become saturated at relatively low magnetic fields. This means that the magnetization remains small even if the magnetic field is increased beyond the point of saturation and the magnetic force acting on ferromagnetic particles cannot increase (Ohara et al. 2001). In contrast to ferri- or ferromagnetic particles that exhibit a magnetic moment without external field, the magnetic moment in superparamagnetic particles has to be induced by an external magnetic field. The conditions for a magnetic field for the separation of superparamagnetic particles are twofold: (i) it has to be strong enough to generate the magnetic moment within the particle and thus a large magnetization and (ii) needs a magnetic gradient in order to produce a magnetic force on the particle (Andreu et al. 2012).

As mentioned before, the magnetic force has to be stronger than the counteracting force of gravity or the hydrodynamic drag force. The drag force $\vec{F}_D$ is a function of the flow velocity in the separator and the particle diameter:

$$\vec{F}_D = 3\,\pi\,\eta\,d_p\,\vec{v}_r \quad , \qquad \text{Eq. 2.17}$$

where η (kg/m/s) is the dynamic viscosity of the fluid and $\vec{v}_r$ (m/s) is the relative flow velocity of the particle. The velocity of the fluid is thus a parameter that needs to be optimized within a magnetic separator (Georgeaud 1999). Especially for small particles, the hydrodynamic drag force is an important constraint which can be seen with regards to the particle diameter as $\overrightarrow{F_D} \propto {d_p}^1$. With decreasing particle size the relative importance of the hydrodynamic drag increases in comparison to the magnetic force where $\vec{F}_M \propto {d_p}^3$.

2.3.3 Magnetic separation in water treatment

Using magnetic separation in water treatment is not a new idea and several commercialized processes are available on the market such as the Sirofloc process (Masuda et al. 2006, Svarovsky 2000) and the BioMag^{TM} or CoMag^{TM} process (Evoqua LLC formerly Siemens Water Technologies). These processes are based on micron-sized magnetite particles that are added to the water either to adsorb anionic water pollutants (Sirofloc, Gregory et al. (1988) or as ballasting agent during coagulation-flocculation (CoMag^{TM}) and in biological flocs (BioMag^{TM}). The particles added to the treatment process are separated from the sludge with the help of magnetic separators. In the case of micron-sized magnetite particles, the ballasting agents have to be demagnetized before their recirculation to the process by applying the opposite magnetic field.

In general, magnetic separators can be classified in terms of their separation mechanism, the applied magnet type and their separation intensity (Gerber and Birss 1983, Masuda et al. 2006).

In the case of micron sized (10 - 15 µm) ferromagnetic particles in the BioMag^{TM} and CoMag^{TM} process, wet drum filters have successfully been applied to achieve 96 – 99.8 % removal (Evoqua 2017). These separators are ***low- and medium-intensity*** magnetic separators where the magnetic field is generated by ***permanent magnets*** based on iron, nickel, cobalt or rare earth compounds. Besides magnetic drum filters, belt separators also fall in this category. Wet drum separators have low capital and operation costs, they work continuously and can be operated with concurrent or counter rotation at a permeate flow of 20 m³/hour and meter of drum length (Svarovsky 2000).

When it comes to MPAC however, ***high intensity/high gradient*** separators are necessary that can effectively separate ***weakly magnetic and small volumetric particles***. Weakly magnetic and small particles lead to the necessity to increase the magnetic field and to apply a high gradient to induce a sufficiently high magnetization and magnetic force to allow their attraction and separation from the liquid flow. High gradient magnetic separators (HGMS) exhibit magnetic fields of 1600 kA/m (more than 10 times higher than low intensity separators) and gradients between 16000 and 160000 MA/m² (about 10^4 times higher) that are mostly generated by ***electromagnets*** (Masuda et al. 2006). Different types of HGMS exist for wet separation such as the Jones separator or matrix-loaded separators that produce highly inhomogeneous fields with high gradients (Gerber and Birss 1983). The matrix-loaded HGMS consists of a filtration unit which is filled with fine steel wool or other filling elements to which a magnetic field is applied. The fluid to be separated is passed through the matrix when the magnetic field is switched on. The weakly magnetic and small particles are captured and held on the matrix. When the matrix is loaded with particles the magnetic field is removed and backwash takes place to flush out the magnetic particles and to recycle them (Cummings et al. 1976). An advantage of HGMS is the high separation efficiency at relatively high flow rates and minimum pressure drops across the filter (Svarovsky 2000).

Two applications in the water treatment industry are currently available: (i) The Hitachi Ballast Purification System, resembles the CoMag™ process and is an application to treat polluted ballast water of vessels. Non-magnetic solids are separated by seeding and flocculation with finely ground magnetite (Ambashta and Sillanpaa 2010, Svarovsky 2000). (ii) The HGMS commercialized by MS-Engineering Co., LTD in Japan is designed to separate fine MPAC from water (volume fraction of 25 – 35 % magnetite, MPAC diameter 40 – 50 nm, aggregate size 1 - 3µm). Their system is relying on a superconducting magnet and is able to treat 500 – 2000 m³/day, separation efficiency is not reported (MS-Engineering 2006).

Using superconducting magnets for HGMS is the newest development. Their magnetic field is much higher than the previously mentioned magnetic separators. Field strength of 4000 kA/m and gradients between 16000 and 200000 MA/m² are reached with the help of superconducting systems that work at cryogenic temperatures (Masuda et al. 2006, Ohara et al. 2001).

For separating MPAC in a drinking water treatment plant, a matrix loaded HGMS is a promising separator. It provides a high magnetic field and gradient to allow for fast separation and recycling of this composite material, where small volumetric superparamagnetic IONP are concentrated on diamagnetic PAC. A downside of the reported HGMS systems using electromagnets are the higher capital costs compared to conventional magnetic separators (Svarovsky 2000) and energy consumption adds to the operational costs. In the case of superconducting HGMS, the large footprint due to the superconducting magnets, along with the cost of maintaining the cryogenic fluid at low temperature, add other constraints. HGMS systems using permanent magnets would reduce capital and operation costs. Applications and designs, however, are limited. An overview of separators for MPAC separation at lab-scale is provided in Chapter 7.

2.4 Synthesis of magnetic powdered activated carbons

A wide variety of MPAC synthesis methods have been developed over the past years aiming at producing specific iron oxide types and shapes and/or specific properties of the composite material and/or facile, low-cost methods that are easy to scale up to industrial size.

Physical methods such as blending of carbon and particulate magnetic oxides via ball-milling or compression as proposed by Rudge et al. (2000) and Yang et al. (2010) seem to lead to MPAC with low porosity and surface. Better MPAC in terms of adsorption properties are achieved with ***chemical processes*** such as precipitation and impregnation methods followed by heat treatment or, more recently, by microwave or γ-irradiation (Safarik et al. 2013, Wang et al. 2012). Some authors use commercially available activated carbon (AC) as base material, others use AC precursors such as organic material such as nut shells, vegetable peel and residues (Bastami and Entezari 2012, Chun et al. 2012, Mohan et al. 2011), silica templates (Lee et al. 2005, Liu et al. 2011) or phenolic resins (Wang et al. 2008) which are impregnated with magnetic IONP followed by ***carbonization*** to create highly porous carbon structures such as PAC. In the following the most common methods to produce MPAC will be explained in more details.

Simple precipitation methods involve the ***co-precipitation*** of magnetic IONP from a supersaturated solution of iron salts at high pH directly onto the surface of AC. Often, a stoichiometric mixture of ferric iron as iron(III)chloride ($FeCl_3$) and ferrous iron as iron(II)sulphate ($FeSO_4$) is prepared and heated to 60-90°C to target the precipitation of a specific iron oxide such as magnetite or maghemite (Castro et al. 2009, Mohan et al. 2011, Oliveira et al.

2002, Zhang et al. 2007). Activated carbon is added to the solution and impregnated with the salt solution while stirring. The drop-wise addition of highly concentrated NaOH leads to the precipitation of solid iron oxides at nano-scale on the carbon surface. At a microscopic scale, precipitation is the particle birth by nucleation from a supersaturated solution. The formed particles start growing and form crystallites if the conditions are favourable (Li 2011). Also other iron oxide precursors can be used. Several authors propose $FeCl_3$ as ferric and $FeCl_2$ as ferrous iron salt instead of $FeSO_4$; precipitation of NP is then realized with NH_4OH at 60 – 90°C (Bastami and Entezari 2012, Kahani et al. 2007, Luo and Zhang 2009). Nakahira et al. (2007) used $Fe_2(SO_4)_3$ and $FeSO_4$ as iron salt in solution followed by precipitation with NaOH at room temperature. Most of the co-precipitation processes aim at producing magnetic magnetite and maghemite and high pH and low redox potential are necessary to obtain these iron oxides. Some authors suggest working under inert nitrogen or argon atmosphere (Gong et al. 2009, Kahani et al. 2007, Wang et al. 2012) to avoid the production of other non-magnetic particles such as hematite or goethite. Both non-magnetic oxides precipitate at much higher redox potentials, e.g. when oxygen is present in the solution. The chemical reaction for magnetite can be written as follows:

$$Fe^{2+} + 2Fe^{3+} + 8OH^- \rightarrow Fe_3O_4\ (black\ solid) + 4\ H_2O \qquad \text{Eq. 2.18}$$

If this reaction takes place in oxygen containing media, the oxidation of Fe^{2+} to Fe^{3+} ($Fe^{2+} + O_2 \rightarrow Fe^{3+}$) leads to a Fe^{2+}/Fe^{3+} ratio lower than 0.5. If the pH is high, goethite can be produced (Tajabadi and Khosroshahi 2012):

$$Fe_3O_4 + 0.25\ O_2 + 4.5\ H_2O \rightarrow 3Fe(OH)_3 \qquad \text{Eq. 2.19}$$

The purity of the final product is thus dependent on the ratio of ferrous and ferric iron, the pH and redox potential of the solution. Also particle size and shape of iron oxides is governed by pH and the initial concentration and type of cations, temperature, ionic force and aging time (Li 2011, Lu et al. 2007). NaOH with Na^+ as cation was identified as the precipitation agent leading to the smallest NP. NaOH is also easily available, easy to handle and inexpensive (Li 2011).

Besides the above-mentioned co-precipitation method, it is also possible to form IONP applying ***high energy methods***. For this purpose, AC is impregnated with an iron salt solution and then transformed to magnetite or maghemite IONP via supply of energy such as heating at 750°C

(Yang et al. 2008) or γ-irradiation under nitrogen atmosphere (Wang et al. 2012). Chun et al. (2012) uses Ar/H_2-atmosphere and 400°C to produce magnetite IONP and Kondo et al. (2010) reports on heat treatment at 800°C under air atmosphere followed by heat treatment at 850°C under CO_2-atmosphere to obtain a ferromagnetic composite. Yang et al. (2008) suggest enhanced impregnation of AC in an ultrasonic bath to accelerate the reaction via acoustic cavitation.

Instead of mixing AC directly into the iron salt solution before precipitation of IONP, it is also possible to prepare first a slurry of magnetic IONP and then to ***impregnate*** AC with the slurry at room temperature while stirring (Kahani et al. 2007, Wang et al. 1994, Zhang et al. 2007). Most authors prepared the IONP slurry with one of the above-mentioned precipitation methods.

After the synthesis of MPAC, ***post-treatment*** of the final composite product often involves washing with ultra-pure water and ethanol followed by drying at room temperature or at temperatures between 50 and 100°C (Bastami and Entezari 2012, Castro et al. 2009, Faulconer et al. 2012, Kahani et al. 2007, Mohan et al. 2011, Zhang et al. 2007). Often the precipitation conditions favoured the development of several iron oxides although a pure phase of magnetite or maghemite was desired. Heating at high temperatures between 200 and 450°C for several hours was found to transform non-magnetic iron oxides to magnetic maghemite or magnetite via oxidation under normal air atmosphere or H_2-atmosphere (Faulconer et al. 2012, Nakahira et al. 2007). At temperatures above 400°C the transformation to non-magnetic hematite can occur (Faulconer et al. (2012). Also, the researcher observed that heat treatment at high temperatures works at the expense of carbon quality as micropores collapse and the specific surface area of the carbon composite is reduced (Faulconer et al. (2012).

Among the presented methods, co-precipitation of IONP onto the carbon surface seems to be the most promising method as it is simple, reproducible and easily scalable which favours its application at large scale. Commercial activated carbons can be used as a starting material combined with ferrous and ferric iron salts that are inexpensive and easily available chemicals. Some problems regarding co-precipitation methods are the difficulty to control particle size and size distribution and sometimes the simultaneous presence of different iron oxides other than magnetite and maghemite.

2.5 Material properties of MPAC and characterization

2.5.1 Type of iron oxides and magnetic properties

Most of the published literature on magnetic AC reports on the synthesis of magnetite or maghemite IONP. These iron oxides are magnetic and lead to the desired magnetic properties of MPAC. As described in the previous chapter, some authors also precipitated hematite and goethite as impurities alongside the target iron oxide, which is mainly related to high oxygen contents in the suspension during co-precipitation (Castro et al. 2009, Gong et al. 2009, Mohan et al. 2011). Particle size of maghemite and magnetite IONP, as calculated from XRD data or measured via scanning or transmission electron microscopy (SEM/TEM) images, varied between 5 – 200 nm and was lowest for co-precipitating or impregnation methods with average IONP diameters as low as 5 nm (Zhang et al. 2007). The targeted IONP diameter is 20 nm or smaller to obtain a superparamagnetic adsorbent[3].

Superparamagnetism makes these IONP attractive for applications in water treatment as MPAC particles do not form agglomerates and can easily be redispersed in water when the magnetic field is removed. As the size of IONP obtained via co-precipitation or impregnation is not completely homogenous, the magnetization curves often reveal weak coercivity and remanent magnetization although the material is classified as superparamagnetic. Saturation magnetization for magnetite IONP < 20 nm varies between 50.3 Am²/kg (Kahani et al. 2007) and 70 Am²/kg (Bastami and Entezari 2012). These values are smaller than that of the bulk material of magnetite and maghemite (80 – 100 Am²/kg) (Cornell and Schwertmann 2003). Wang et al. (2008) explain the reduction as a consequence of the non-magnetic or weak magnetic interfaces with carbon. But also for IONP that are not attached to carbon surfaces, saturation magnetization values seem to be smaller than the bulk value. Lu et al. (2007) report values in the range of 30 – 50 Am²/kg for magnetite IONP.

[3] See Chapter 2.3.1 for more information on superparamagnetism

2.5.2 Long-term stability

Long-term stability of the adsorbent is critical for industrial applications where changes in magnetization or dissolution of IONP are not desired. Magnetite IONP are not very stable under ambient conditions and can easily be oxidized to maghemite (Mohan et al. 2011). Also, structural modifications of the surface of magnetite IONP via oxidation to maghemite in the presence of bacteria in water were observed by Auffan et al. (2008). According to their study, this phenomenon is related to the high mobility of electrons within the Fe(II)/Fe(III) structure of magnetite and the undesirable release of Fe(II) ions into solution. As maghemite is a ferrimagnet with similar magnetic properties as magnetite (Cornell and Schwertmann 2003), oxidation to maghemite is not a constraint for MPAC applications. Lee et al. (2005) checked the stability of MPAC that had been exposed to air for 5 months. The saturation magnetization at 2 K was 40.9 Am^2/kg shortly after preparation and decreased by nearly 50% after 5 months. MPAC prepared by Safarik et al. (2013) was stable for at least several months. An experiment with a magnetic composite that was stirred in water for two months showed no performance decrease (Yang et al. 2008).

Besides oxidation, dissolution of IONP might impact their stability. The pH-dependent dissolution of magnetic IONP was studied by Zahoor and Mahramonlioglu (2011) in a range of pH 1 to 8. Below pH 4.8, dissolution occurred and led to a loss of iron content in MPAC. With typical pH values between 6 and 8 in drinking water treatment processes, dissolution of magnetic IONP is therefore not expected. To the author's knowledge, no long-term studies have been carried out at pilot or industrial scale where additional stability issues such as abrasion due to shear forces during mixing and pumping might occur. The effect of colonization and the consequent contact of IONP with bacteria and biofilms in long-term applications is another aspect that has not been studied so far.

2.5.3 Surface area and porosity

Surface area and porosity are of paramount importance for all adsorption processes as these parameters define the availability of adsorption sites. The combination of PAC and IONP in the composite material can lead to a modification of these parameters, depending on the carbon/IONP ratio, the PAC template and the MPAC preparation method.

Most studies report a loss of surface area and/or pore volume of MPAC compared to PAC (Baghdadi et al. 2016, Bastami and Entezari 2012, Castro et al. 2009, Chun et al. 2012, Kim et al. 2013, Kondo et al. 2010, Mohan et al. 2011, Oliveira et al. 2002, Park et al. 2015, Yang et al. 2008, Zahoor and Mahramonlioglu 2011, Zahoor 2014, Zhang et al. 2007). Specific surface area and pore volumes in all studies are expressed as surface area or volume per mass of the composite material (m^2/g and mL/g). Yet, it is misleading to compare composite materials if no information about the final IONP mass fraction is reported. For most of the cited studies it remains unclear if the reduction in specific surface area is a consequence of lower PAC content or blocked pore volume. One has to bear in mind that the composite material has less PAC present per unit weight than the non-magnetic counterpart. Adding IONP that have a higher density (e.g. 5 g/cm^3 Fe_3O_4) than PAC (e.g. 0.4 g/cm^3) increases the density of the composite and the observed differences in specific surface area or specific pore volumes are thus partially due to the smaller fraction of carbon present. When plotting e.g. the reduction of specific surface area as a function of IONP content (Figure 2.4) it becomes visible that the loss of specific surface area is at least partly a consequence of lower PAC content.

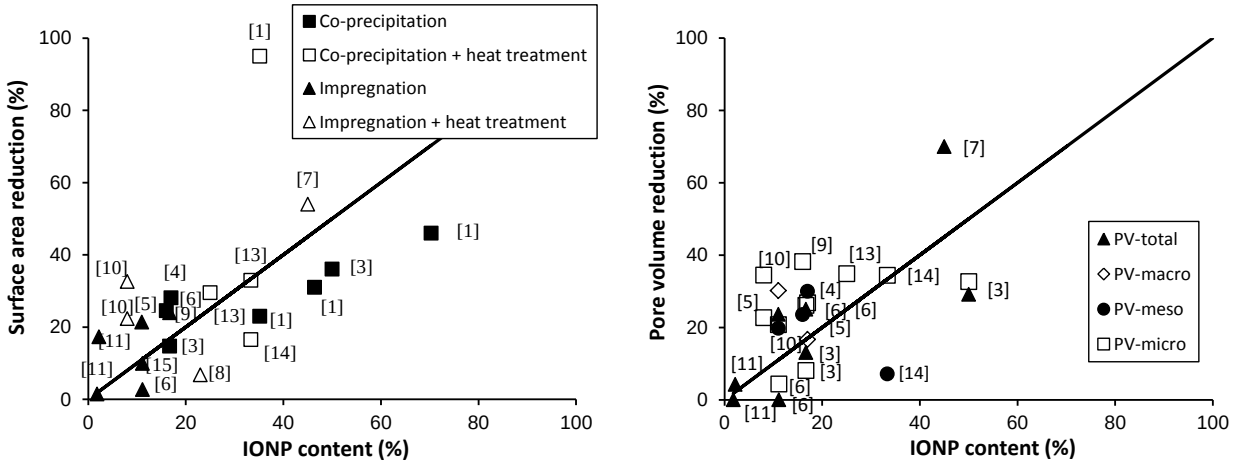

Figure 2.4 : Reduction of specific surface area and pore volumes as a function of IONP content in MPAC. The IONP contents were calculated from provided material characteristics (desired/measured Fe-content in the composite material combined with XRD/VSM data), surface area and pore volume reduction from reported BET surface and pore volume data. [1] (Faulconer et al. 2012), [2] (Castro et al. 2009), [3] (Mohan et al. 2011), [4] (Zhang et al. 2007), [5] (Bastami and Entezari 2012), [6] (Saroyan et al. 2017), [7] (Chun et al. 2012), [8] (Yang et al. 2008), [9] (Zahoor 2014), [10] (Kim et al. 2013), [11] (Park et al. 2015), [12] (Kondo et al. 2010), [13] (Oliveira et al. 2002), [14] (Zahoor and Mahramonlioglu 2011), [15] (Baghdadi et al. 2016).

Most of the authors mention only the initial synthesis ratio (e.g. mass ratios of iron salts and PAC) but did not analyze the ratio in the final composite. Especially for the co-precipitation methods, the initial PAC/Fe ratio is not necessarily identical to the final composite ratio as it is not guaranteed that all iron from the solution precipitates onto the PAC surface. A certain amount might remain freely as IONP in solution and are subsequently removed by washing procedures.

Due to their size of 5 – 20 nm IONP can deposit on the inner walls of meso- and macropores with diameters of around 20 – 50 nm and > 50 nm respectively or they can block the smaller micro-pores that have diameters around 2 nm. Published data discriminating between micro-, meso- and macropore volumes are limited. Zhang et al. (2007) impregnated granular activated carbon (GAC) with an IONP slurry (8 wt-% Fe or approx. 11 % IONP) and measured a higher decrease of the macropore volume (30 %) than of the mesopore and the micropore volume (20 %). Mohan et al. (2011) covered PAC via co-precipitation with a mass fraction of 17 % IONP and reported the highest pore volume reduction in mesopores (30 %) compared to micro- (27 %) and macropores (17 %).

2.5.4 Surface chemistry

The surface of regular PAC is mainly hydrophobic but can contain functional groups formed during the activation process (Delgado et al. 2012). The charged functional groups at the surface of PAC, mainly oxygen groups (such as e.g. carboxyl, lactone, phenol, carbonyl or phenol groups (Marsh and Rodriguez-Reinoso 2006)), lead to a (slightly) negatively charged surface when suspended in a polar medium such as water at neutral pH (Tarleton and Wakeman 2007). The surface oxygen groups of PAC also determine the surface hydrophobicity which in turns governs the strong hydrophobic interactions with hydrophobic adsorbates (Marsh & Rodriguez-Reinoso, 2006). IONP can change the zeta-potential and add iron oxide specific surface groups. IONP are positively charged and several authors observed a change from negatively charged PAC with pH_{pzc} of 2 to positively charged composites with pH_{pzc} around 6 (Bastami and Entezari 2012, Mohan et al. 2011). The surface functional groups of iron oxides are hydroxyl groups (Cornell and Schwertmann 2003) and the surface density of hydroxyl groups determines the adsorption capacity of different iron oxides. As the surface density depends on the crystal structure, on the extent of development of the crystal faces and the crystal morphology, the adsorption capacity can slightly vary between iron oxides (Cornell and Schwertmann 2003).

2.6 Adsorption of water pollutants on MPAC

MPAC has been proposed as an adsorbent for various water pollutants such as heavy metals, NOM, dyes and trace contaminants. Adding IONP to PAC is generally proposed to either increase the adsorption affinity/capacity of PAC and/or to make PAC magnetic and thus separable in a magnetic separator. As seen in Chapter 2.5.3, IONP can reduce the adsorption sites in PAC via pore blocking and can change the surface chemistry of PAC (Chapter 2.5.4). For organic trace contaminants that mainly adsorb on PAC, adding IONP decreases the adsorption capacity (at least proportional to the mass fraction of IONP), with regards to heavy metals that usually do not adsorb well on PAC, adding IONP increases the removal of these compounds. The following review gives an overview of MPAC products developed and their performance with respect to removal capacity and kinetics for a variety of water pollutants.

2.6.1 MPAC as enhanced adsorbents for heavy metals and NOM

Adsorption of different heavy metals was tested by various authors with a focus on ***arsenic*** in the form of the anions arsenate As(V) and arsenite As(III) as a major pollutant of ***ground water*** (Faulconer et al. 2012, Liu et al. 2010, Mayo et al. 2007, Vaughan Jr. and Reed 2005, Zhang et al. 2007). In the case of metal anions, IONP often enhance the adsorption compared to conventional PAC due to surface complexation of the anion with the surface functional hydroxyl groups of IONP (Cornell and Schwertmann 2003). Briefly, the Fe-atoms of iron oxides coordinate with water and hydroxyl ions leading to the complete coverage of the IONP surface with these functional groups. The main mechanism of anion adsorption is ligand exchange (OH ion exchanges against the adsorbate anion). In the case of cation adsorption, the cation can interact with the deprotonated surface hydroxyl group. Adsorption is thus in both cases (anion and cation adsorption) pH dependent (Cornell and Schwertmann 2003) and the carbon particles in MPAC serve merely as a support for IONP, which fulfill the actual adsorbent function. Studies on pH dependent arsenic As(V) adsorption on pure maghemite IONP (3.8 – 18.4 nm) showed adsorption capacities of 20 mg/g at pH 7 (Tuutijarvi et al. 2009). The benefit of working with nano-sized Fe_3O_4 (12 nm) compared to micron-sized Fe_3O_4 (0.3 µm) was demonstrated by Mayo et al. (2007) who observed 200 times higher adsorption capacities for As(III) and As(V) on the smaller Fe_3O_4 particles because of the higher surface to volume ratio (more surface groups). Combining IONP with PAC then resulted in an adsorbent with improved arsenic removal as

demonstrated by Zhang et al. (2007). The authors studied the adsorption of As(V) onto maghemite/magnetite loaded GAC (mass fraction IONP 11 %) prepared via impregnation method and observed a higher adsorption capacity of MGAC compared to GAC at 25°C and pH 5 (0.99 mmol/g versus 0.81 mmol/g). Vaughan Jr. and Reed (2005) modelled pH-dependent As(V) removal by GAC impregnated with maghemite and magnetite IONP using the HSDM coupled to a surface complexation model. They could show that adsorption was predominantly governed by IONP (not PAC) and they confirmed ligand exchange with the –OH groups on IONP as the dominant adsorption mechanism.

MPAC were also shown to adsorb cationic lead (80.6 mg Pb(II)/g) and copper (48.3 mg Cu(II)/g) at pH 5.5 on MPAC (pH_{pzc} = 6.8) produced via co-precipitation (Parlayici and Pehlivan 2017). Lead and copper adsorption were also studied by Han et al. (2015) who prepared magnetic coal and coconut-based MPAC via co-precipitation with a mass fraction of 63 % magnetite/maghemite IONP (calculated from provided data). They achieved similar or better removal with MPAC compared to PAC when correcting for IONP mass fraction indicating that IONP contributed to the adsorption of both heavy metals. Mercury (HgII) removal of 90 % from a 100 µg/L solution was achieved at pH 4.5 within 1 min by Faulconer et al. (2012) using MPAC prepared via co-precipitation.

In ***surface water***, one of the main compounds of concern for drinking water production is ***NOM***. Removing NOM from water using regular PAC is usually not very efficient as NOM adsorption capacities of PAC are low and adsorption is slow compared to trace organic pollutants (Dastgheib et al. 2004). MPAC has also been proposed as an alternative to regular PAC for the removal of NOM (Anzai et al. 2016, Kim et al. 2013, Park et al. 2015). As the carboxyl groups of NOM show an affinity for iron oxides' hydroxyl groups via ligand exchange (Gu et al. 1994), IONP were suggested to enhance the adsorption capacity of PAC. Micron-sized iron oxides have been proposed as antifouling agents in water treatment and were successfully tested by Choo and Kang (2003), Cui and Choo (2013) in adsorption/membrane processes. Combining nano-sized iron oxides with PAC for the removal of NOM has been proposed by Kondo et al. (2010), Anzai et al. (2016), Kim et al. (2013), Park et al. (2015) and Zahoor (2014). In a study by Park et al. (2015), NOM removal in the presence of IONP was found to be up to 10 times higher with MPAC containing mass fractions of 1.8 % – 2.6 % ferrihydrite, hematite and magnetite IONP compared to regular PAC, even though the Brunauer-Emmett and Teller (BET) surface area was reduced by

up to 50 %. In contrast, Zahoor (2014) measured 20 % lower humic acid adsorption capacity of MPAC compared to PAC and attributed this to a lower available surface area (1150 m^2/g vs. 868 m^2/g). However, as discussed previously (Chapter 2.5.3), no IONP mass fraction has been analyzed in this study and the observed reduction of NOM adsorption capacity might also originate from the 20 % lower PAC mass fraction present in their MPAC (estimated from the 20 % difference in bulk density). Similarly, Kim et al. (2013) found reduced NOM adsorption on MPAC compared to PAC which they attributed to reduced micropore volume and surface area (23 % – 33 % lower than for PAC). Yet, as no mass fraction of magnetite was analyzed, the link between reduced pore volume, surface area, and adsorption capacity was not evident. Anzai et al. (2016) prepared MPAC from rice husk that showed 30 % reduced humic acid adsorption capacity when prepared at higher IONP content (no mass fraction analyzed). Once again, it remained unclear if the observed reduction was related to the lower PAC mass fraction in MPAC or pore volume and surface area reduction due to pore blocking. The question thus remains: Do iron oxide nanoparticles on PAC improve or reduce its NOM adsorption capacity? With NOM being one of the main compounds of interest in drinking water treatment, more studies are necessary to understand the interactions of IONP and NOM in the composite material.

2.6.2 MPAC as magnetically recoverable adsorbent for organic dyes and micropollutants

For small organic pollutants such as dyes and trace organics MPAC has been tested as an easily separable magnetic adsorbent where IONP fulfill their function as the magnetic vector whereas PAC serves as the adsorbent.

Several studies focussed on organic dye removal with MPAC to treat industrial wastewater discharges such as cationic dyes:, Safranin O, crystal violet, Bismarck brown, acridine orange (Safarik et al. 1997, Safarik et al. 2013), drimaren red (Oliveira et al. 2002), methylene blue (Ai et al. 2011a, Luo and Zhang 2009) and anionic dyes: reactive black (Saroyan et al. 2017), congo red and aniline blue (Safarik et al. 1997). Experiments with methylene blue showed that this medium sized cationic molecules are preferentially adsorbed in mesopores (here: 2 – 5 nm) of negatively charged PAC (Bansal and Meenakshi 2005). Ai et al. (2011b) tested adsorption of methylene blue on pure magnetite IONP and confirmed that IONP did not contribute to methylene blue removal.

With regard to MPAC applications in drinking water treatment, trace organic pollutants of natural and anthropogenic origin in surface waters are the main concern. Among these contaminants, taste and odour causing bacterial metabolites such as geosmin and 2-methylisoborneol are nontoxic but can be smelled already at concentrations as low as 10 ng/L. Organic pollutants that are released by humans such as pesticides and herbicides can be found in drinking water sources due to agricultural activities and pharmaceuticals and personal care products due to wastewater discharges. These anthropogenic compounds are generally found only at trace levels in the range of µg/L. Many of these so-called micropollutants (MP) are considered a potential risk for human health and the ecosystems and regulation for these molecules become more and more stringent. The USEPA added hormones, pesticides, insecticides, fungicides and pharmaceuticals to their contaminant candidate list (CCL) which in its most recent version (CCL-4) includes 55 MP that are candidates for future regulation in drinking water (EPA 2016). The US EPA proposes PAC or GAC as best available technology for the removal of organic MP in drinking water (Barceló 2012). Previous adsorption studies have shown the suitability of novel magnetic adsorbents for a range of MP such as the endocrine disruptor bisphenol-A (Koduru et al. 2016, Nakahira et al. 2006, Nakahira et al. 2007, Park et al. 2015), the herbicide atrazine (Castro et al. 2009) and metribuzin (Essandoh et al. 2017), the insecticide imidacloprid (Zahoor and Mahramonlioglu 2011), the antibiotics ciprofloxacin (Shi et al. 2013), amoxicillin (Saucier et al. 2017), tetracycline and quinolone antibiotics (Ma et al. 2017a), the anti-epileptic drug carbamazepine (Baghdadi et al. 2016, Shan et al. 2016), the anti-inflammatory drug naproxen (Ilbay et al. 2015), and the pain killer paracetamol (Saucier et al. 2017). In most studies adsorption isotherms and kinetics were recorded (see Table B-2).

Concerning adsorption of MP on pure magnetic IONP, the hydroxyl moieties found on iron oxides are the functional groups that can interact with the functional groups of organic MP according to Gu et al. (1994). The dominant adsorption mechanism between the iron oxide surface functional groups and the ones of ciprofloxacin was found to be surface complexation in two studies by Rakshit et al. (2013) and Gu et al. (1994). In a study with the antibiotic chlorotetracycline the formation of Fe-O bonds between magnetite IONP and MP was found to be the effective adsorption mechanism (Zhang et al. 2011). The antibiotic oxytetracycline interacted through the surface groups $CONH_2$, OH and $N(CH_3)_2$ groups with magnetite IONP surface groups (Rakshit et al. 2013).

While interactions between magnetic IONP and MP are possible, the adsorption capacities of IONP are low. A study by Shi et al. (2013) with the antibiotic ciprofloxacin suggests that the MP adsorption capacity of pure IONP is low compared to PAC (20 times lower adsorption capacities of magnetite IONP (2.62 µg/mg) compared to PAC (48 µg/mg)). Also Shan et al. (2016) found lower adsorption capacity on pure Fe_3O_4 IONP compared to PAC and MPAC (no values given).

With pure IONP contributing little to the adsorption of MP on MPAC, the adsorption capacities of MPAC are expected to be lower than those of regular PAC when compared based on total adsorbent mass. And indeed, among the authors who compared the adsorption capacity of magnetic adsorbents with a non-magnetic control, most found lower adsorption capacities on the magnetic adsorbent (Bastami and Entezari 2012, Castro et al. 2009, Ma et al. 2017b, Shan et al. 2016, Zahoor and Mahramonlioglu 2011). The reason for the loss of adsorption capacity is two-fold: First the adsorption capacities of AC and IONP are different and second (as discussed previously in Chapter 2.5.3) the mass ratio of both sorbents should be considered when comparing PAC with MPAC. However, only few authors study the adsorption capacity of both materials separately or report the mass fraction of IONP in their composite material. Therefore many studies claiming a loss of adsorption sites due to pore blockage by IONP might be misleading as the reason for the loss of adsorption capacity is more probably linked to the reduced mass fraction of the efficient adsorbent PAC in MPAC. In a study by Castro et al. (2009) this becomes clear: The authors measured maximum adsorption capacities for atrazine on PAC and MPAC with IONP mass fractions of 17 % and 50 %. They observed maximum atrazine adsorption capacities of 30 mg/g (PAC), 22 mg/g (MPAC 17 %) and 15 mg/g (MPAC 50 %) and attributed the loss of adsorption capacity to the IONP that occupy active adsorption sites. However, when normalizing their results to the mass fraction of PAC it becomes obvious that the loss of adsorption capacity in these adsorbents is approximately equivalent to the mass fraction of IONP. A systematic study evaluating the contributions of IONP and PAC separately and comparing the adsorption capacities and kinetics normalized to PAC mass content is still missing.

In natural waters NOM reduces the removal efficiency of AC for MP. The effects of NOM on MP adsorption using MPAC are not yet well understood. Most of the cited studies above were carried out in pure water. In a study with the endocrine disruptor Bisphenol-A (BPA) MPAC with 2.2 % Fe_3O_4 had higher BPA adsorption capacity (K_F = 6.23 (no unit given) in the presence of NOM than PAC (K_F = 0.08) (Park et al. 2015). The increased BPA removal was attributed to the

good adsorption of NOM to IONP and the molecular coordination between NOM and BPA. An adsorption study carried out for different antibiotics and a chitosan-magnetite-PAC composite in the absence and presence of humic acid showed only negligible decrease of adsorption performance (Ma et al. 2017b). More systematic studies are needed to understand the interactions of competition between NOM and MP on MPAC. Also, the effect of MPAC aging on MP removal capacities has not yet been evaluated. As MPAC offers the opportunity to work at higher adsorbent age (returning MPAC into the process), the residual MP adsorption capacity after NOM preloading or biofilm formation is a crucial information for the application of MPAC.

2.7 Compatibility of magnetic nanoparticles with heterotrophic and nitrifying bacteria

IONP have been intensively studied for their biomedical application (targeted drug delivery, contrast enhancement agents for magnetic resonance imaging applications and for hyperthermia treatment of tumours) and are generally considered biocompatible (Pankhurst 2003, Reddy et al. 2012, Valdiglesias et al. 2016). Most in vivo, in vitro and epidemiological studies on magnetic IONP for biomedical applications suggest low toxicity towards human cells (Valdiglesias et al. 2016). Since 1996 the use of certain IONP as contrast agents for imaging in the human body is already approved by the US Food and Drug Administration (Wang 2011). Due to the increase of nanoparticle usage and their subsequent release into the environment, also the IONP bacteria interactions move into the focus of many researchers. The following literature review evaluates (i) the interaction pathways of IONP with microorganisms and (ii) examines the observed cytotoxicity towards planktonic and sessile bacteria and the relevance for the biological MPAC process.

2.7.1 Potential interaction pathways of IONP with microorganisms

Considering MPAC as an alternative adsorbent and growth support for heterotrophic and nitrifying bacteria in a biological drinking water process raises the question: are nanosize iron oxides on the surface of PAC deleterious to biological activity?

Even though bulk iron, magnetite or maghemite are not cytotoxic, the small size of nanoparticles (NP) in general (< 100 nm by definition) makes them behave very differently from the bulk material and potentially toxic for bacteria (Ju-Nam and Lead 2008, Luyts et al. 2013). They are

less thermodynamically stable but highly reactive at their surface because of the high surface area per unit mass (Luyts et al. 2013). The toxicity of NP in general (not only IONP) also depends on their composition, solubility and concentration, shape, charge and stability (Klaine et al. 2008, Simonet and Valcarcel 2009). Toxicity can arise from either the ***direct interaction*** of NP with the bacteria cell or ***indirectly*** via the adsorption of toxic elements such as heavy metals or organic pollutants on their surface. Simonet and Valcarcel (2009) suggest that toxicity effects occur due to changes in the bioavailability of toxins or nutrients and indirect effects result from the interaction of NP with natural organic compounds. Concerning the direct interactions between NP and bacterial cells, several mechanisms have been proposed by Klaine et al. (2008): (a) disruption of membranes or membrane potential, (b) formation of reactive oxygen species (ROS), (c) oxidation of proteins, (d) genotoxicity, (e) interruption of energy transduction, and (f) release of toxic constituents. The most relevant mechanisms described specifically for IONP will briefly be presented in this section.

2.7.1.1 **IONP attachment and uptake by the cell membrane**

The semipermeable membrane of cells serves to regulate transport of substances, to transduce energy and for intercellular communication. An intact cell membrane is thus essential for the microorganism's survival (Prescott et al. 2005). Neal (2008) discovered that close contact is necessary for interaction between NP and the cell membrane. Attachment to the cell membrane surface of *E.coli* has been observed for IONP but no evidence of cellular incorporation of IONP or membrane damage was observed (Auffan et al. 2008). In the case of silicon NP and fullerenes, NP attached and were embedded into the membrane which compromised its integrity and functions (Klaine et al. 2008). Also carboxyl fullerenes and gold NP have shown to puncture or weaken the cell membrane of gram-positive bacteria and *E. coli* which lead to cell death or heat shock responses (Auffan et al. 2008). Relevant pathways for NP uptake are diffusion through cell membranes, endocytosis (engulfing of large polar molecules) and adhesion (Klaine et al. 2008, Luyts et al. 2013). While quantum dots < 5 nm or silver NP < 80 nm have been shown to enter the cells (Klaine et al. 2008), no study has yet shown the uptake of IONP via the cell membrane. IONP on the carbon surface of MPAC are in the critical size range for uptake (of 5 – 30 nm) (Bastami and Entezari 2012, Li 2011) but as they are attached to the carbon surface microbial

uptake might not be an issue. Direct contact with the cells of microorganisms, however, is possible, as the MPAC surface is proposed as a growth support in this project.

2.7.1.2 **Cell damage via reactive oxygen species**

At the surface of many NP reactive oxygen species (ROS) can be generated such as the hydroxyl radical OH•, superoxide anion $O_2^{\bullet -}$ and non-radical hydrogen peroxide H_2O_2 (Arora et al. 2012). When in contact with the bacterial cell wall, these ROS cause oxidative stress for the cell and they are responsible for several cell damaging reactions such as the oxidation of membrane phospholipids (lipid peroxidation) or the oxidation of other cell components such as proteins, and DNA (Klaine et al. 2008). The damaged membrane becomes more permeable and susceptible to osmotic stress which hinders nutrient uptake (Klaine et al. 2008).

ROS can be generated at the surface of magnetite IONP in aerobic solutions when structural Fe(II) is oxidized. Reduced iron oxides are efficient ROS producer via the Fenton reaction (Auffan et al. 2008):

$$Fe^{2+} + H_2O_2 \longrightarrow Fe^{3+} + OH^{\bullet} + OH^{-} \qquad \text{Eq. 2.20}$$

Oxidative stress has also been found to be the reason for dose-dependent cytotoxicity of magnetite and maghemite IONP in tests with pure culture of two strains of *E .coli* with different tolerance towards oxidative stress by Auffan et al. (2008). Bacterial strains with higher tolerance towards oxidative stress were less affected by high IONP dose. The survival rate ranged between 85 % ± 11 % and 100 % ± 20 %. A significant decrease was only observed at very high concentrations of 175 mg/L (magnetite) and 700 mg/L (maghemite) IONP.

2.7.1.3 **Release of toxic ions by IONP**

The release of metal ions from the metal containing NP can cause increased membrane permeability and uptake of these ions through the cell wall. This dissolution is inversely proportional to the NP size (Dinali et al. 2017). However, in the case of IONP, the release of iron ions did not show inhibitory effects. On the contrary: IONP have been found to promote bacterial cell growth by acting as an iron source (Borcherding et al. 2014). Furthermore, studies with fullerenes and zinc oxide NP have shown that bacteria can develop protection mechanisms against toxicity such as altering membrane lipid composition, membrane fluidity or the production of extracellular proteins to neutralize toxic ions (Dinesh et al. 2012).

2.7.1.4 **Adsorption of toxic elements by IONP**

Although IONP do not seem to have a pronounced toxic effect on microorganisms, toxicity might occur indirectly due to the adsorption of toxic elements on the surface of IONP. The adsorption of toxic elements from water could be a significant limitation for a biological MPAC process. *e.g.* high heavy metal concentrations can be damaging to living organisms (Athar and Vohora 2001) among them: silver, copper, nickel, barium, chromium, mercury, arsenic, zinc, cadmium. This good adsorption capacity for metal ions onto IONP could lead to high heavy metal loadings on MCAP in bioreactors. Inhibition effects in biological HMP, where PAC is replaced by MPAC, will depend on heavy metal concentrations in the raw water and the necessary PAC/IONP ratio for optimal separation. With typically low heavy metal concentrations in drinking water sources and the conventional coagulation-flocculation pretreatment, inhibition effects due to adsorbent heavy metals are not likely to occur.

2.7.1.5 **Modification of IONP by bacteria**

While most studies focus on the inhibitory effect of IONP towards bacteria, Auffan et al. (2008) found that magnetite and to a lesser degree maghemite IONP were subjected to structural modifications in the presence of *E. coli.* The surface of the magnetite IONP was entirely oxidized to the more stable maghemite. The high mobility of electrons within the structure of magnetite and the diffusion of Fe(II) from the solid into solution are the reasons for its unstable surface against oxidation. On the contrary, maghemite, composed of fully oxidized crystals and therefore highly stable, did not show significant structural transformations after contact with bacteria (Auffan et al. 2008).

2.7.2 Observed cytotoxicity of IONP towards planktonic bacteria and biofilms

The above discussed mechanisms suggest only low cytotoxic potential for IONP. Indeed, studies with pure culture of ***planktonic bacteria*** such as *E. coli* (Auffan et al. 2008, Hu et al. 2009) and *Pseudomonas aeruginosa* (Kafayati et al. 2013) at very high concentrations of 500 – 700 mg/L magnetite or maghemite IONP revealed low or moderate cytotoxicity. Hu et al. (2009) determined an LD_{50} of 638 mg IONP/L for pure culture of *E. coli* strains for maghemite IONP. In contrast, Arakha et al. (2015) measured inhibition of *E .coli* and *Bacillus subtilis* by magnetite IONP even at 50 mM (11.6 mg/L).

For the application of MPAC in a bioreactor, IONP toxicity towards ***biofilms*** is of great interest as MPAC is proposed in this project as a support for sessile biofilm forming bacteria. Bacteria in biofilms are far less susceptible to antimicrobial agents, due in part to the extracellular polymeric substance (EPS) in which they are embedded (Prescott et al. 2005). The protective nature of EPS was confirmed in a study with EPS capped silver NP that showed reduced toxicity towards *E. coli* and other strains of pure culture (Sudheer Khan et al. 2011). Also microcosm tests on soil bacterial communities indicate no or only low inhibitory effects as for example shown by He et al. (2011) and Vittori Antisari et al. (2013) with Fe_3O_4 IONP loads of 0.14 to 260 mg IONP per kg of soil. In some cases, IONP even stimulated bacterial activity such as seen during a study with soil bacteria (*Actinobacteria*), where increased enzymatic activity was detected during microcosm tests (He et al. 2011). Changes in the bacteria community in the presence of IONP were observed although cell viability (He et al. 2011) or bacterial metabolism remained constant (Vittori Antisari et al. 2013). IONP were also studied with respect to their effects on activated sludge of waste water treatment plants. In response to initial shock loads of IONP, performance of activated sludge often initially decreases, but stabilized in long-term exposure: Ni et al. (2013) for example, observed inhibited nitrification and suppressed EPS when dosing 50 mg/L magnetite IONP into aerobic wastewater sludge. During long-term operation, however, nitrogen removal increased as did the abundance of nitrifying bacteria (Ni et al. 2013). Similar observations were reported in a study by Zhang et al. (2018), where maghemite IONP were added to an anammox sludge reactor. During long-term operation, bacteria community richness and diversity increased with 1 – 5 mg/L IONP and decreased at 200 mg/L IONP dose, while functional specific anammox community was enhanced. The authors attributed the changes to the availability of Fe^{3+} as a micronutrient. EPS content of the sludge nearly doubled in the presence of 200 mg/L IONP. Wang et al. (2016) observed improved methane production and activity of key enzymes and increased abundance of bacteria and *archae* in anaerobic granular sludge with 100 mg/L magnetite IONP. While most studies suggest that microorganisms develop protection strategies against IONP such as increased EPS formation and shifts in the bacterial community, also negative effects of magnetite IONP were observed: in a study by Ma et al. (2017a) changes in performance of activated sludge in a sequencing batch reactor were measured (decreased chemical oxygen demand removal, but stable ammonia removal) in the presence of 60 mg/L magnetite IONP. At 60 mg/L IONP the authors detected increased ROS formation and membrane

damage. Although most studies show low or only moderate cytotoxicity of IONP for biofilms, more research is necessary to tests MPAC as an IONP covered growth support for heterotrophic and nitrifying bacteria.

2.8 A critique of anterior MPAC synthesis and application

MPAC have repeatedly been proposed as easily separable adsorbents for water treatment and an increasing number of laboratory studies are published on synthesis techniques or adsorption of various contaminants (Chapter 2.6). While most research has focussed on the adsorption of dyes and metals, few studies are directed at adsorption of typical drinking water contaminants such as NOM (Chapter 2.6.1) or MP such as pharmaceuticals or herbicides (Chapter 2.6.2). The majority of these studies are of exploratory character and the causal links between IONP mass fraction and adsorption properties for major drinking water contaminants or magnetic separability are not yet established. For an application of MPAC at larger scale for drinking water treatment, the role of IONP content in the composite material is of paramount importance. While for separation in a magnetic field, the rule "the more the better" might apply, this does not seem to be the case for its function as an adsorbent. While several studies stated a loss of adsorption sites in MPAC compared to PAC (Chapter 2.5.3), adsorbents are often at the same time poorly characterized and it remains unclear if the observed loss is simply related to an increase in density (equated with lower PAC content) or to IONP blocking pores and adsorption sites. A thorough understanding of mass fraction dependent pore volume and surface area changes in MPAC compared to PAC is needed. The relative importance of IONP in adsorption (e.g. for NOM) remains unclear as the discrimination between adsorption capacity of IONP vs. PAC has not yet been investigated for MPAC.

In existing studies, the easy magnetic separability of MPAC compared to PAC is highlighted as its major advantage. Yet, in none of the reported tests has this advantage already been exploited. Easy (and fast) magnetic separation opens the door for a long-term use of the adsorbent – either to fully exhaust its adsorption capacity or to make the transition to a combined adsorption/biodegradation process. Increasing the adsorbent age has the benefits of minimizing adsorbent consumption and reducing operation costs. When used in a biological process, MPAC would serve as a growth support for heterotrophic and nitrifying bacteria allowing for the removal of ammonia and biodegradable NOM. Highly concentrated suspensions of aged regular

PAC combined with low pressure membranes have repeatedly been suggested to reduce ammonia-related taste and odour problems and to reduce the formation of NOM related disinfection by-products (Stoquart et al. 2012). Yet, separation of these aged PAC suspensions has proven difficult due to fouling, clogging and abrasion of the membrane and large-scale applications have remained scarce (Leveillé et al. 2013, Stoquart et al. 2012). Replacing regular PAC by magnetically separable MPAC could help to overcome the current limitation by adding a separation step between carbon reactor and membrane. The potential of MPAC as an adsorbent in a biological process is still unknown and issues related to colonization of an IONP covered adsorbent have not yet been addressed. Studies on cytotoxicity of IONP for pure culture of planktonic bacteria suggest that biological activity might be imparted while microcosm tests on sessile soil bacteria showed no or low inhibitory effects (Chapter 2.7.1). Due to the lack of long-term studies on aged MPAC suspensions, nothing is known so far on residual adsorption capacities for drinking water contaminants such as MP on fully colonized MPAC. Additionally, questions on the physical and magnetic stability of MPAC arise. While published data on MPAC stability exists (Chapter 2.5.2), the data is neither consistent nor taken under real operating conditions as for example continuous agitation in a reactor with a flat blade stirrer (vs. laboratory magnetic stir bar or shaking) or stability during long-term colonization of MPAC. Although some studies have reported a lack of magnetic susceptibility after keeping MPAC for a couple of months in a lab flask on a shaker, they seldom identify the origin of this loss (change of iron oxide, loss of IONP).

In summary, the weaknesses of anterior studies on MPAC are the following:

1) The adsorption of drinking water contaminants such as NOM or MP was tested but the relation between IONP mass fraction and adsorption capacity or kinetics was never systematically and thoroughly established;
2) Easy separability of MPAC has been highlighted as its major advantage over regular PAC but has never been exploited for the long-term (re-)use of MPAC; thus nothing is known about MPAC's potential to be colonized;
3) The effect of long-term use of MPAC concerning its physical and magnetic stability is poorly studied and has never been evaluated for aged MPAC suspensions;
4) IONP mass fraction dependent separation of MPAC has never been studied.

CHAPTER 3 RESEARCH OBJECTIVES, HYPOTHESES AND METHODOLOGY

3.1 Research objectives and hypotheses

The general objective of this project is to evaluate magnetically separable PAC as an alternative adsorbent for drinking water treatment. Specifically, the focus is on its application in a mixed adsorption/biodegradation/separation process which has often been referred to in the scientific literature as the hybrid membrane process.

On a more detailed level, the objectives of this project are to:

1. Compare the properties of MPAC with increasing IONP mass fraction and PAC: pore size and surface area distribution, surface charge, IONP size and magnetic properties;
2. Identify the role of IONP in MPAC concerning adsorption kinetics and capacity for typical drinking water contaminants such as NOM, hormones, pharmaceuticals, pesticides and taste and odour metabolites;
3. Assess the possibility to use MPAC as a growth support for heterotrophic and nitrifying bacteria in a high concentration carbon contactor and identify the interference of IONP with biodegradation;
4. Determine the residual adsorption capacity of aged MPAC concerning pharmaceuticals, hormones and pesticides;
5. Evaluate the long-term degradation of MPAC in a biological process concerning its magnetic properties;
6. Identify the major factors (and their relative importance) that govern magnetic separation of MPAC.

Achieving these objectives will allow us to answer fundamental questions concerning the suitability of MPAC as an adsorbent in a mixed adsorption/biodegradation process.

- How do increasing mass fractions of IONP in MPAC change the pore size and surface area distribution of the adsorbent?
- Do magnetic IONP on PAC improve or reduce its NOM adsorption capacity?
- How does the IONP content of MPAC influence their adsorption capacity for MP?

- Is the same quantity and activity of heterotrophic and nitrifying biomass developing on MPAC with increasing IONP content as on regular PAC or are IONP inhibiting growth and reduce activity?
- Is there a significant residual MP adsorption capacity on 90-days aged MPAC?
- Do agitation and colonization of MPAC change its magnetic properties over time?
- Which IONP mass fraction in MPAC is necessary for efficient separation in a magnetic separator?

The project objectives are derived from the following research hypotheses:

1. IONP in MPAC are deposited mainly on the surface of a microporous PAC and therefore do not change the pore size or surface area distribution of PAC even at increased IONP mass fractions.

   Originality: In several studies, the pore volume and surface area of MPAC was analyzed and a loss of specific pore volume or surface area has been attested for MPAC compared to PAC. However, a systematic study that analyzes pore size distribution and surface area of MPAC and links these results to the presence of a specific IONP mass fraction has not yet been carried out. An in-depth understanding of the location of IONP (inside pores or only on the outer surface?) and their effect on pore size and surface area distributions will help to understand their impact on contaminant adsorption.

   The hypothesis will be discarded if the surface area and/or a certain pore size fraction are significantly reduced in MPAC compared to PAC after results are normalized to the PAC mass fraction.

2. The reduction of adsorption capacity and rate constants for DOC and MP that occurs in MPAC compared to PAC is proportional to the PAC/IONP ratio.

   Originality: Although single MPAC adsorption studies exist with humic acids and some MP such as imidacloprid, atrazine and biphenol-A, the influence of the PAC/IONP ratio on sorption has not yet been evaluated.

   The hypothesis will be refused if modelled adsorption capacity parameters are not linearly dependent on the PAC/IONP ratio.

3. IONP on the PAC surface do not prevent biological growth or inhibit activity of heterotrophic and nitrifying bacteria.

   Originality: Although several studies revealed only low or no cytotoxicity of IONP towards pure culture of bacteria and fixed bacteria (microcosm), no study exists for colonized MPAC. If IONP do not prevent biomass development, MPAC could replace PAC in a biological process which would entail the advantage of being easily separable and thus MPAC could be easily recycled into the process to adjust PAC age.

   The hypothesis will be refused if less active heterotrophic biomass is found on aged MPAC compared to PAC and/or if nitrification and DOC removal performances of MPAC bioreactors are significantly ($p < 0.05$) lower than that of regular PAC.

4. MPAC aged for 90 days exhibits a residual adsorption capacity for MP.

   Originality: MPAC has never been used in a biological drinking water process and thus no data on MP adsorption capacities or kinetics of aged MPAC is available. Studies on colonized PAC suggest that a residual adsorption capacity exists.

   The hypothesis will be proven wrong if no significant difference in MP removal is measured on 90-day-old MPAC compared to aged PAC ($p>0.05$).

5. The physical and magnetic properties of MPAC are not altered during aging in a bioreactor.

   Originality: While magnetic stability has been confirmed by several authors for MPAC prepared via co-precipitation in water for a couple of months, nothing is known about the stability of agitated MPAC in highly concentrated aged suspensions.

   The hypothesis is refused if higher iron concentrations (Fe_{tot}) can be found in the treated effluent than in the influent of the carbon contactor (physical stability) or if the magnetic properties of MPAC are significantly ($p < 0.05$) lower than that of freshly prepared MPAC.

6. There exists an optimal PAC/IONP ratio for DOC and MP removal, on the one hand, and satisfying separation efficiency (> 90 %) on the other hand.

   Originality: No systematic approach has been published identifying the optimal PAC/IONP ratio for the elimination of typical drinking water pollutants, on the one hand, and MPAC separability, on the other hand.

The hypothesis is refused if no PAC/IONP ratio is found that allows high DOC removal (final DOC < 2 mg/L) and MP removal (> 90%) with simultaneous high MPAC separation efficiency (> 90%).

3.2 Research Strategy and Methodology

The experimental approach was organized in 8 main parts to validate or invalidate the research hypotheses:

1) Synthesis of three MPAC with increasing IONP mass fraction (Hyp. 1-6);
2) Characterization of the material properties of PAC and MPAC (Hyp. 1-6);
3) Recording adsorption isotherms and kinetics for NOM and MP on fresh PAC and MPAC (Hyp. 2);
4) Design, operation and monitoring (DOC and ammonia) of bioreactors containing PAC and MPAC with increasing IONP mass fraction for 90 days (Hyp. 3 to 5);
5) Measure the quantity of active heterotrophic biomass on aged PAC and MPAC and compare the bacterial community structure (Hyp. 3);
6) Record adsorption isotherms and kinetics for MP on aged PAC and MPAC to evaluate the residual adsorption capacity and the influence of biofilm on adsorption rates (Hyp. 4);
7) Monitor iron export from the bioreactors, measure the magnetic properties and identify the type of iron oxide of aged MPAC (Hyp. 5);
8) Design and operate a small-scale magnetic separator with varying flow rate, filter element density and MPAC dose (Hyp. 6)

The experimental protocol is described for each part, with reference to the specific analysis performed.

3.2.1 Synthesis of magnetic powdered activated carbon with distinct IONP mass fractions (Hyp. 1-6)

In the first step of this research project, MPAC was produced to serve as test material throughout the rest of the project. The requirements were to obtain a composite material that (i) is an effective adsorbent for typical drinking water contaminants such as NOM, taste and odour

metabolites and MP, (ii) contains iron oxides that are superparamagnetic and of homogeneous size and shape (iii) can be produced at a known and adjustable IONP mass fraction, (iv) can repeatedly be produced with the same quality and properties.

3.2.1.1 **Choice of powdered activated carbon**

As a base material, a commercial carbon was chosen that was certified for applications in drinking water treatment (NSF60). The specific adsorption characteristics of PAC such as surface area, pore size distribution and surface chemistry are defined by the interplay of its raw material (wood, peat, lignite and bituminous coal), the carbonization and activation method and the particle size (Snoeyink and Summers 1999). As the main application in drinking water treatment is DOC, colour and taste and odour removal (Crittenden et al. 2012), DOC adsorption pretests with 6 PAC of high iodine numbers and small median diameter (ca 25 µm) were carried out in coagulated/flocculated water from the Ste-Rose drinking water treatment plant. Taste and odour removal of the bacterial metabolites geosmin and 2-methylisoborneol was tested among 11 PAC in three pre-filtered raw waters (St-Lawrence River, Rivière des Milles-Îles and Rivière l'Assomption). In both tests, a mineral-based PAC (AquaSorb® CB1-MW by Jacobi) with a mean diameter of 23 µm (by volume) and an iodine number of 900 mg/g PAC showed the best performances and was therefore chosen as the MPAC base material. Before being used for MPAC synthesis, this PAC was washed with demineralized water to reduce its basicity below pH 8 and dried at 105°C.

3.2.1.2 **Deposition of IONP on PAC**

Among the existing MPAC synthesis routes, an alkaline co-precipitation process was chosen as proposed by Oliveira et al. (2002). Various pretests concerning synthesis temperature, initial pH, NaOH dosage, stirring velocity and NaOH dosage rate and reactor design were carried out to refine the protocol and to develop a synthesis reactor that allows for maintaining constant and repeatable synthesis conditions and product quality. The challenge was to produce IONP with a size < 20 nm of uniform shape that are superparamagnetic and to avoid the presence of non-magnetic IONP such as goethite or hematite. Briefly, the final protocol involved the addition of $FeCl_3 \cdot 6H_2O$ and $FeSO_4 \cdot 7H_2O$ solutions (molar ratio 1:2) to a stirred (700 rpm) and heated (70°C) suspension containing between 2 and 10 g of PAC under inert conditions (constant N_2 stream). Ferric and ferrous iron solutions were added through syringe ports on the reactor lid once the

synthesis temperature was reached. Co-precipitation of both Fe^{2+} and Fe^{3+} ions was initiated by raising the pH to 14 using concentrated NaOH. A closed batch reactor was designed and equipped with a peristaltic pump to add NaOH solution drop-wise (10 mL/min) to the suspension. A condenser was added to the reactor to avoid evaporation during the heating period. The suspension was agitated until cooled, washed with demineralized water to pH 8, dried at 105°C and stored in a desiccator until use. The quantity of PAC during the synthesis was varied to produce MPAC with iron oxide mass fractions of 20%, 40%, and 50% as well as pure IONP (100%). For the total number of experiments during this project, several batches of each MPAC were produced and characterized to obtain a total of approx. 12 – 20 g for each MPAC type. A detailed description and flow scheme of the reactor can be found in Chapter 4.

3.2.2 Characterization of the material properties (Hyp. 1-6)

Several characterization methods for PAC, MPAC and IONP were used throughout this project. The results were used as the basis for all data interpretation regarding adsorption, colonization and separation studies carried out to evaluate hypotheses 1-6.

3.2.2.1 **Iron oxide identification**

Identifying the type of iron oxide in MPAC was necessary throughout the project to

(i) verify if the three produced MPAC are only different concerning their IONP mass fraction and not concerning the iron oxide type present. Knowing the present iron oxide is essential for hypotheses 1, 2, 3 and 6 where properties such as pore size distributions, adsorption capacities, biomass development and separability are evaluated as a function of IONP mass fraction;

(ii) compare the iron oxides before and after the 90 days aging period (Hyp. 5);

Samples (PAC, MPAC and pure IONP) were analyzed using ***powder X-ray diffraction*** (XRD). XRD is the most common technique to identify the type of iron oxide in a mixture (Cornell and Schwertmann 2003). The principle is the interaction of electromagnetic radiation (wavelength ca. 0.1 nm) with the atoms in the crystal structure leading to compound specific diffraction patterns as a function of the angle of incidence θ. This is possible because the wavelength λ is the same order of magnitude as the spacing d between atoms within a crystal. The relation is described by Bragg's law (Cornell and Schwertmann 2003):

$$n\lambda = 2d \sin \theta \qquad \text{Eq. 3.1}$$

Where λ is the wavelength of the incident wave (nm), d is the distance between the lattice planes in the crystal (nm), θ is the scattering angle (degrees) and n is an integer value.

The peaks of the spectra obtained (intensity I versus angle θ) are compared to spectra of known oxides (Cornell and Schwertmann 2003). XRD devices which are employed in routine analysis use a copper anode to create X-rays; however, discriminating between the iron oxides maghemite and magnetite is difficult with these devices as the copper radiation bears the risk of fluorescence with iron (Nicol 1975). We therefore opted for cobalt as a radiation source where this fluorescence does not occur (XRD D5000 Bruker, Sol-X detector with Co $K\alpha$ radiation (1.79 Å) in the 2θ range 5°- 94°).

3.2.2.2 **Magnetic properties of MPAC**

Measurements with a ***vibrating sample magnetometer*** (VSM) were employed to analyze the hysteresis behaviour, magnetization saturation and magnetic susceptibility of pure IONP and all MPAC batches produced in the synthesis reactor as well as the magnetic properties of aged MPAC. The results of the magnetic properties analysis were used to (i) optimize the MPAC synthesis protocol (needed for Hyp. 1) and (ii) to validate (or invalidate) hypothesis 5 where magnetic properties before and after colonization are compared.

Briefly, an aliquot of the powdered sample with known mass is exposed to an external magnetic field $\vec{H}$ (A/m). Due to the vibration of the sample (vibration with 100 Hz) a voltage is produced in the coils of the magnetometer. This voltage is proportional to the sample's magnetic moment, but does not depend on the strength of the applied field $\vec{H}$. Knowing the magnetization saturation of the sample $\vec{M}$ (Am²/kg) can help to (i) quantify the mass fraction of magnetic IONP in the composite and (ii) identify the prevailing iron oxides (Cornell and Schwertmann 2003). However, the characterization of mixtures is not as evident as the magnetization curve is the integral signal of all iron oxides present (Cornell and Schwertmann 2003). Therefore, supplementary analyses such XRD were necessary.

3.2.2.3 **PAC/IONP ratio of MPAC**

Knowing the mass fractions of PAC and IONP in the composite material is crucial for the understanding of adsorption phenomena (Hyp. 2) and separation (Hyp. 6). Indeed, previous studies often fell short analyzing the exact mass fraction of IONP in MPAC and simply related reduced adsorption capacities of MPAC to the presence of IONP that block important adsorption sites. Knowing the mass fraction of the active adsorbent (PAC) and IONP allows identifying the contribution or the reduction of adsorption sites due to IONP. Among the tested methods to determine the quantity of IONP in the composite material, a thermo-gravimetric method combined with the determination of the saturation magnetization, were found to be the most accurate.

The developed protocol for a ***thermo-gravimetric*** method involved the incineration of MPAC samples in triplicate at 900°C. During the combustion the carbon fraction transforms to CO_2 and only the iron oxides and ash content of PAC remains. The advantage of this method is that all the different iron oxide species present on MCAP are transformed to one single species: hematite (Chun et al. 2012). The exclusive presence of hematite in the calcined samples was confirmed in XRD measurements. Knowing the weight ratios of PAC to hematite and its molecular mass, it is thus possible to calculate the ratio of PAC to elementary iron. The result has to be corrected for the ash content of PAC. Finally, the iron content can be used in combination with XRD data to calculate the mass fraction of PAC and the specific iron oxide.

In contrast to the thermo-gravimetric method which reveals the iron content in the sample (and thus only indirectly the specific iron oxide content), recording the saturation magnetization of MPAC compared to pure PAC and pure IONP allows detecting directly the percentage of the magnetic iron oxide. Combining both methods can reveal if a non-magnetic iron phase is present in the composite.

3.2.2.4 **Location of IONP on the surface and inside the carbon matrix**

Locating IONP in the composite material was crucial to validate (or invalidate) hypothesis 1. In order to understand where the iron oxides precipitate (on the surface or in the pores of the carbon matrix), ***scanning electron microscopy*** (SEM, Hitachi S-4700 at 1 -15 kV, max resolution of 1,2 nm) and ***energy-dispersive X-ray spectroscopy*** (EDS, JEOL JSM-7600F at 10 kV with Oxford, XMax 80 detector) were chosen. The topography of the MPAC sample is provided by SEM

where a fine electron beam scans the surface and the various emitted signals are collected to create a 3D image of the surface (Nicol 1975). EDS allowed mapping of elemental iron in the cross-section of MPAC-54% particles. The principle is based on the excitation of electrons on an inner shell of the atom using X-rays. When an inner-shell electron is excited it emits an X-ray that is characteristic for the element (Shindo and Oikawa 2002). To obtain cross-sections of micron-sized particles, MPAC were immersed into an epoxy matrix, hardened and polished to obtain a smooth surface that exposes the inner matrix of MPAC.

3.2.2.5 **Particle size of PAC, MPAC and IONP**

Particle size distribution of the adsorbents and IONP are essential material properties for adsorption phenomena (hypothesis 2) and particle separation (hypothesis 6). Particle ***size distribution of PAC and MPAC*** was analyzed using the ***dynamic particle counter*** Mastersizer 3000^{TM} (Malvern Instruments) that detects particles in the range of 0.01 – 3500 µm. This optical technique is based on the diffraction of light at the particle surface. The angular variation of the signal is dependent on particle size e.g. small particles diffract light at higher angles than big particles. The device generates volume weighted distributions that can be transformed into a number weighted distribution with the help of the Mastersizer software for spherical or non-spherical particles. The ***size of IONP*** is an essential aspect of their quality as super-paramagnetism occurs below a diameter of 20 nm. IONP size was analyzed using ***SEM*** and image processing tools to measure the diameter of 30 randomly selected IONP. A mean diameter of the crystalline iron oxides was also calculated from XRD data using the ***Debeye-Scherrer equation***:

$$\tau = \frac{K\,\lambda}{\beta\,cos\theta}\,, \qquad \text{Eq. 3.2}$$

which relates the crystalline size to the broadening of a peak in a diffraction pattern. K is a dimensionless shape factor with values of about 0.89; β is the peak broadening of half the maximum intensity (rad) and λ is the wavelength (nm).

3.2.2.6 **Bulk and particle density**

Precipitated IONP add primarily weight to the PAC particles, thus changing their density and separation behaviour. For different PAC/IONP ratios the bulk density (mass of the porous

material per volume) was analyzed using gravimetric methods. The particle or true density (mass of the material without pores) was analyzed using an Archimede's balance. The principle is based on the known mass of material in air and water:

$$\varphi_{PAC} = \varphi_{water} \cdot \frac{m_{PAC,air}}{m_{PAC,air} - m_{PAC,water}} \quad . \qquad \text{Eq. 3.3}$$

3.2.2.7 **Surface charge**

The surface charge of adsorbents is a parameter that influences its adsorption behaviour. Results from this analysis were needed to validate (or invalidate) hypothesis 2. As iron oxides are reported to be slightly positively charged at neutral pH (Baalousha et al. 2008) while the surface of PAC is mostly negatively charged (Worch 2012) the net charge of the magnetic adsorbent was expected to change with increasing IONP mass fraction. To determine the net charge of MPAC with different IONP mass fractions, the ***point of zero charge*** was determined which is defined as the pH where the net surface charge is zero. Higher surface acidity leads to lower pH_{pzc}. If the pH of a solution is above the pH_{pzc} the surface of the particle is negatively charged. For the determination of the point of zero charge (pH_{pzc}), pre-weighted masses of PAC and MPAC were immersed in 40 mL NaCl solutions (ionic strength of 0.01 M) adjusted to variable pH of 3-11 with NaOH and HCl. The suspensions were shaken and measured after 48 h and the pH_{pzc} determined as the crossing point between the potentiometric curve of the suspension and the blank solution (Bourikas et al. 2003).

3.2.2.8 **Surface area and pore size distribution**

Measurements of pore size and surface area distribution of MPAC were used to address hypothesis 1, where the effect of IONP deposition on PAC is to be investigated. The standard method for analyzing surface area and pore size distribution in PAC is the measurement of ***nitrogen adsorption isotherms***. The amount of nitrogen adsorbed was recorded at varying relative pressure P/P_0 between 10^{-6} and 10^{0} at 77 K (Quantachrome Autosorb 1MP). Subsequently, the data was used to calculate pore size and surface area distributions with the non-linear density functional theory (NLDFT with slit/cylindrical pore shape for carbon) using the Autosorb-1 (FL, USA) software. The total pore volume was calculated from the adsorbed volume of gas near the saturation point (P/P_0 = 0.99). To compare results to the so-called BET surface area, data was also fitted to the multi-point Brunauer-Emmett and Teller (BET) isotherm.

However, as the BET equation is in a strict sense not applicable to microporous materials (Thommes 2010), the NLDFT results were taken for all subsequent calculations concerning surface area or pore volume.

3.2.3 Adsorption studies (Hyp. 2 & Hyp. 4)

The role of IONP in MPAC concerning adsorption kinetics and capacity for NOM and MP was identified by (i) discriminating between the adsorption capacity of IONP and PAC for NOM and MP and by (ii) measuring the adsorption capacities (fit to isotherm models) and kinetics (fit to pseudo-second order reaction kinetic model and homogeneous surface diffusion model) in the composite material at increasing IONP mass fraction.

All adsorption experiments comparing capacities and kinetics between PAC and MPAC were carried out using the bottle point technique (Worch 2012). Briefly, each bottle contained a known adsorbent/pollutant ratio and represented a point of the isotherm or kinetic curve. Bottles and sampling vials were combusted at 550°C prior to all experiments and septa were cleaned with a 5 % potassium persulfate solution at 60°C and rinsed with ultra-pure water to remove organic carbon. Experiments carried out in ultra-pure water were adjusted for ionic strength with NaCl and buffered at pH 7 using phosphate buffer. For experiments with natural water, all solutions were pre-filtered through 0.45 µm polyethersulfone filters (PES) (Pall Supor®-450) before spiking with the target pollutant to avoid adsorption on particulate matter.

The adsorbents were dried at 105°C and cooled in a desiccator before the experiments to know their dry weight. To avoid diffusion barriers due to air filled pores in the adsorbents, PAC and MPAC were pre-wetted by soaking them in known volumes of buffered ultra-pure water with adjusted ionic strength. Colonized PAC and MPAC were used as humid filter cakes and their humidity was analyzed in triplicate according to *Standard Methods* (2540-B, APHA 2012).

Concentrated primary solutions of the pollutants were prepared prior to the experiments. In case of experiments with NOM, Suwannee River NOM (Internation Humic Substance Society) was dissolved in ultra-pure water and filtered through 0.45 µm PES filters after adjusting pH and ionic strength. Primary solutions of MP were prepared as a mixture of individual stock solutions prepared in HPLC grade methanol. The mixture was left to be evaporated to dryness using a gentle N_2 stream and mild heating (40 °C). HPLC-grade water was then added to obtain stock

solutions in water. These concentrated primary solutions were diluted to the desired initial concentrations for each experiment.

To stop the reaction between adsorbents and target pollutant, samples were filtered through 0.3 µm glass fiber syringe filters (Sterlitech GF-75) for all MP adsorption experiments or through 0.45 µm PES filters (Pall Supor®-450) for all NOM adsorption experiments. All filters were pre-washed with ultra-pure water. The filter materials were previously selected by the involved analytic laboratories to avoid adsorption of the target pollutant by the filter material.

A challenge when manipulating MPAC during long-term adsorption experiments is the shaking technique. Among all tested shakers, an orbital shaker and a rotary shaker were leading to good results without degrading the adsorbent via abrasion.

3.2.4 Colonization study in bioreactors (Hyp. 3, 4 & 5)

In order to validate (or invalidate) hypotheses 3 to 5, which are related to aged PAC and MPAC, the adsorbents were colonized for 95 days in bioreactors. Specifically for hypothesis 3, monitoring DOC and NH_4 removal, nitrate and nitrite production was crucial to detect the transition from a mostly adsorption dominated to a mainly biological process. Imaging techniques were supporting evidence for the presence of living bacteria and biofilm. Finally, the quantity of active heterotrophic and nitrifying biomass was measured on adsorbents at the end of the colonization study and the DNA was extracted from biomass samples to analyze the community structure on PAC and MPAC.

3.2.4.1 **Experimental setup and design**

MPAC with mass fractions of 23; 38 and 54% maghemite was colonized in small bioreactors for over 90 days. Two reactors contained unmodified PAC (control reactors) to evaluate the significance of differences between the adsorbent types. The reactors were operated without adsorbent replacement to obtain uniform adsorbent age within each reactor. During the aging period the adsorbents were colonized passing from mainly adsorption to mainly biological mode after ca. 30 days. Each reactor contained the same approximate number of adsorbent particles to facilitate the evaluation of biomass development as a function of IONP concentration. This was achieved by working at an equivalent PAC concentration of 10 g PAC/L rather than at the same

adsorbent concentration (g MPAC/L) which involves adding higher mass concentrations of the MPAC with higher iron oxide content, to compensate for the density differences.

The five pressurized bioreactors consisted of a clear PVC container of 1 L each. They were alimented with temperature buffered and dechlorinated water from a 1.7 m^3 tank with peristaltic pumps. A blade stirrer at 120 rpm prevented settling of the adsorbents within the reactors and a 10 µm nylon mesh strainer at the effluent side of the reactor held back the PAC particles. A detailed flow scheme of the reactors can be found in Chapter 6. To promote the growth of heterotrophic and nitrifying bacteria, this matrix was amended with a nutrient composed of acetate as carbon source as well as NH_4Cl and K_2HPO_4 as nitrogen and phosphate sources to yield a C:N:P ratio of 100:20:1.

Figure 3.1: Bioreactor setup in the laboratory.

3.2.4.2 **Monitoring of DOC and ammonia removal**

DOC and ammonia were monitored in the influent and effluent of the reactors on a bi-weekly basis to follow colonization of the adsorbents. Nitrate and nitrite nitrogen were measured weekly, to differentiate between adsorption and biodegradation of ammonia. The results of these analyses were used to validate (or invalidate) hypothesis 3).

3.2.4.3 **Presence and quantification of biomass**

Qualitative and quantitative measurements of MPAC colonization with heterotrophic and nitrifying bacteria were used to validate or (invalidate hypothesis 3).

The presence of biological activity on the adsorbents was qualitatively proven using ***imaging techniques*** such as ***fluorescence microscopy*** of stained bacteria with the viable/dead Baclight™ staining kit (Boulos et al. 1999) on a bi-weekly basis on the adsorbents of all five bioreactors and using an ***environmental SEM*** (ESEM Quanta 200 FEG at 20 kV) to visualize humid biofilm on the adsorbents at the end of the colonization study. The images allowed identifying the presence of viable bacteria and biofilm on the surface of the adsorbents.

Quantification of active heterotrophic biomass was achieved using the ***potential glucose activity technique*** (Servais et al. 1991). Briefly, adsorbents were filtered to remove the surrounding liquid and wet mass of the obtained filter cakes were re-suspended in a nutrient solution containing radio-labelled glucose. The maximal heterotrophic activity is then derived from the respiration product, radio-labelled CO_2 detected via scintillation.

The analysis of the ***microbial community*** differences on PAC and MPAC with increasing IONP content was carried out on fully colonized samples at the end of the study. The technique involved detaching biomass from the adsorbent particles with a blender and subsequent filtrations to (i) remove adsorbent particles and (ii) concentrate bacteria on filter papers (Camper et al. 1985). DNA was extracted according to a protocol developed by Bédard et al. (2014) and sent to an external laboratory for next generation sequencing targeting a specific region on the 16s rRNA of bacteria and archae. Results on the class-level were obtained using the SilvaBacteria reference database.

3.2.5 Stability of the aged adsorbents (Hyp. 5)

To validate (or invalidate) hypothesis 5 the physical and magnetic stability of the of MPAC in a long-term biological process was addressed by (i) measuring the total and dissolved iron concentrations in the inlet and outlet of the bioreactors on a weekly basis (ICP-OES, model iCAP 6000, cf. Chapter 4), (ii) analyzing the iron oxide type with XRD (cf. 3.2.2.1) and by (iii) analyzing the magnetic properties of MPAC before and after the 90 days aging period (cf. 3.2.2.2).

3.2.6 Separation study (Hyp. 6)

A study for separation efficiency was carried out to identify the factors that govern the magnetic separation of MPAC. Briefly, the three MPAC with maghemite IONP mass fractions of 10 %,

38 % and 54 % and known magnetic properties were sieved (< 100 µm) prior to the separation tests to eliminate agglomerates. A magnetic separator was built consisting of two squared rare-earth magnets ($Nd_2Fe_{14}B$, grade N42) mounted in parallel in a Plexiglas casing to provide a relatively uniform magnetic field to magnetize ferromagnetic stainless steel fibres forming the high gradient magnetic separator column (HGMS). The magnetic field between the external magnets was modelled with the commercial numerical software Quickfield (student version, © Tera Analysis Ltd). MPAC suspensions with different particle concentrations were fed into the separator at different flow rates. Three HGMS columns were prepared with increasing mass of stainless steel wool to investigate the influence of the filter element density on separation efficiency. Adsorbent concentrations, expressed in mg PAC/L, were calculated with the help of a calibration curve relating MPAC concentration to absorbance at 850 nm. A more detailed description and parameterization of the separator can be found in Chapter 7.

Samples were collected every 1 or 2 minutes in 40 mL vials at the outlet of the separator and analyzed for MPAC concentration Separation efficiency *E* at time *t* was calculated as:

$$E(t) = \frac{m_r\,(t)}{m_f\,(t)} \cdot 100\%, \qquad \text{(Eq. 3.4)}$$

where m_r is the mass retained in the separator and m_f is the mass that is fed into the separator.

Table 3.1 : Experimental approach developed to validate (or invalidate) the research hypotheses and corresponding articles.

	Hypothesis	Scale	Experimental approach	Expected results	Article
1	IONP in MPAC are deposited mainly on the surface of a microporous PAC and therefore do not change the pore size or surface area distribution of PAC even at increased IONP mass fractions.	Laboratory	Synthesis of three MPAC with IONP mass fraction of 0; 20; 40 and 50 %. Analysis of pore size and surface area distribution. Imaging of IONP distribution on PAC surface and inside PAC.	Relation between IONP content, their location in PAC and changes in pore size and surface area distribution.	1
2	The reduction of adsorption capacity and rate constants for DOC and MP that occurs in MPAC compared to PAC is proportional to the PAC/IONP ratio.	Laboratory & modelling	Adsorption isotherms and kinetic experiments for NOM and a mixture of MP on virgin PAC and MPAC. Fitting of isotherm and kinetic models to the data.	Discrimination between adsorption capacity on IONP and PAC for NOM and MP. Impact of IONP/PAC ratio on adsorption capacity and rate constant/diffusion coefficients for DOC and MP.	1 & 2
3	IONP on the PAC surface do not prevent biological growth or inhibit activity of heterotrophic and nitrifying bacteria.	Small scale bioreactors & laboratory	Monitoring of DOC and NH_4 removal, and nitrite and nitrate production. Qualitative proof of colonization via imaging techniques. Comparison of active heterotrophic biomass quantity between colonized PAC and MPAC with increasing IONP content. Comparison of the bacterial community on aged PAC and MPAC	Demonstration of PAC and MPAC colonization (heterotrophic and nitrifying bacteria) after 30 days. Quantification of the active heterotrophic biomass on 90-d old adsorbents. Impact of IONP on adsorbent colonization (quantity, activity and community composition).	3

Table 3.1 : Experimental approach developed to validate (or invalidate) the research hypotheses and corresponding articles (continued).

	Hypothesis	Scale	Experimental approach	Expected results	Article
4	MPAC aged for 90 days exhibit a residual adsorption capacity for MP.	Small scale bioreactors & laboratory	Adsorption isotherms and kinetic experiments for mixture of MP on aged PAC and MPAC. Comparison of isotherm and kinetic constants of aged and virgin PAC and MPAC.	Demonstration of the potential of aged MPAC to face a peak concentration of MP. Quantification of the residual adsorption capacity.	2
5	The physical and magnetic properties of MPAC are not altered during aging in a bioreactor.	Small scale bioreactors & laboratory	Comparison of magnetic properties before and after colonization. Monitoring of total and dissolved iron in the bioreactor influent and effluent.	Demonstration of the magnetic stability of MPAC in long-term applications. Quantification of the magnetization loss.	3
6	There exists an optimal PAC/IONP ratio for DOC and MP removal, on the one hand, and satisfying separation efficiency (> 90 %) on the other hand.	Small scale magnetic separator & laboratory	Comparison of separation efficiency between MPAC with increasing IONP content under different operation parameters.	Demonstration of magnetic separability for MPAC. Relative importance of flow velocity, IONP mass fraction, magnetic gradient and adsorbent concentration for the separation of MPAC in a magnetic field. Identification of the best PAC/IONP mass ratio for adsorption of NOM and MP.	

CHAPTER 4 ARTICLE 1 - THE INFLUENCE OF IRON OXIDE NANOPARTICLES UPON THE ADSORPTION OF ORGANIC MATTER ON MAGNETIC POWDERED ACTIVATED CARBON

Our objective was to clarify where IONP are located in MPAC and if they contribute significantly to NOM adsorption. In this work, we present a systematic investigation of the adsorption properties of magnetic activated carbons for NOM, showing for the first time the individual contributions in terms of isotherms and kinetics of PAC and maghemite nanoparticles in this composite material. We were able to show that NOM removal is achieved primarily by adsorption on PAC - not iron oxide nanoparticles - and that the latter block the mesopores of PAC – an effect that becomes important only at high mass fractions of IONP. This chapter was published as a research paper in the journal *Water Research* in 2017.

THE INFLUENCE OF IRON OXIDE NANOPARTICLES UPON THE ADSORPTION OF ORGANIC MATTER ON MAGNETIC POWDERED ACTIVATED CARBON

Kim Maren Lompe[a*], *David Menard*[b], *Benoit Barbeau*[a]

[a]NSERC Industrial Chair on Drinking Water, Department of Civil, Geological and Mining Engineering, Polytechnique Montreal, P.O. Box 6079, Downtown Station, Montreal, QC, Canada H3C 3A7.

[b] Department of Engineering Physics, Polytechnique Montreal, Montreal, Qc, Canada

***** corresponding author. Tel: +1 514 340-4711 ext. 2983.

E-mail: kim-maren.lompe@polymtl.ca (Kim Maren Lompe)

ABSTRACT

Combining powdered activated carbon (PAC) with magnetic iron oxides has been proposed in the past to produce adsorbents for natural organic matter (NOM) removal that can be easily separated using a magnetic field. However, the trade-off between the iron oxides' benefits and the reduced carbon content, porosity, and surface area has not yet been investigated systematically. We produced 3 magnetic powdered activated carbons (MPAC) with mass fractions of 10 %, 38 % and 54 % maghemite nanoparticles and compared them to bare PAC and

pure nanoparticles with respect to NOM adsorption kinetics and isotherms. While adsorption kinetics were not influenced by the presence of the iron oxide nanoparticles (IONP), as shown by calculated diffusion coefficients from the homogeneous surface diffusion model, nanoparticles reduced the adsorption capacity of NOM due to their lower adsorption capacity. Although the nanoparticles added mesoporosity to the composite materials, they blocked intrinsic PAC mesopores at mass fractions > 38 % as measured by N_2-adsorption isotherms. Below this mass fraction, the adsorption capacity was mainly dependent on the carbon content in MPAC and mesopore blocking was negligible. If NOM adsorption with MPAC is desired, a highly mesoporous PAC and a low IONP mass fraction should be chosen during MPAC synthesis.

KEYWORDS

Magnetic powdered activated carbon, Adsorption, Natural organic matter, Iron oxide nanoparticles

4.1 Introduction

Understanding adsorption of natural organic matter (NOM) on powdered activated carbon (PAC) is of importance in drinking water treatment for the removal of disinfection by-product precursors and the competition effect with trace organic pollutants. As NOM adsorption capacities of PAC are low and adsorption is slow compared to trace organic pollutants (Dastgheib et al. 2004), several authors have suggested enhancing its affinity for NOM by combining activated carbon with iron oxides (Anzai et al. 2016, Kim et al. 2013, Park et al. 2015). Hydroxyl groups are the surface functional groups of iron oxides (Cornell and Schwertmann 2003). Previous studies have shown affinity of NOM carboxyl groups for iron oxides' hydroxyl groups and ligand exchange between these groups has been identified as the principal adsorption mechanism in a study conducted with hematite and Suwannee River fulvic acid (Gu et al. 1994). The surface density of hydroxyl groups determines the adsorption capacity of different iron oxides. As the surface density depends on the crystal structure, on the extent of development of the crystal faces and the crystal morphology it can slightly vary between iron oxides (Cornell and Schwertmann 2003). In a NOM adsorption study from wastewater goethite and hematite had similar adsorption capacities compared to ferrihydrite that adsorbed up to three times more NOM (Choo and Kang 2003). The authors attributed the higher adsorption capacity of ferrihydrite to the lower degree of

crystallinity leading to a higher available surface area for adsorption compared to crystalline goethite and hematite. Iron oxides have been proposed as antifouling agents in water treatment and were successfully tested by Choo and Kang (2003), Cui and Choo (2013) and Kang and Choo (2010) in adsorption/membrane processes. The latter compared ferrihydrite to PAC and found five times higher adsorption capacity on ferrihydrite when normalizing to surface area instead of adsorbent mass. Several researchers combined PAC with maghemite or magnetite nanoparticles, two ferrimagnetic iron oxides that allow for easy magnetic separation of the adsorbent from water using a magnetic field (Anzai et al. 2016, Borghi and Fabbri 2014, Kim et al. 2013). Magnetic PAC (MPAC) properties make it an attractive sorbent for water treatment as its recovery by magnetic separation could be fast without the production of coagulated sludge. MPAC have been widely studied for their ability to remove contaminants of emerging interest such as herbicides (Castro et al. 2009) insecticides (Zahoor and Mahramonlioglu 2011), pharmaceuticals (Shi et al. 2013), various dyes (Oliveira et al. 2002, Safarik et al. 1997, Safarik et al. 2013) and metals (Faulconer et al. 2012, Han et al. 2015, Liu et al. 2010, Nethaji et al. 2013). Using MPAC for the removal of NOM has been proposed by Kondo et al. (2010), Anzai et al. (2016), Kim et al. (2013), Park et al. (2015) and Zahoor (2014). It is unclear, though, if magnetic iron oxide nanoparticles (IONP) enhance or reduce NOM adsorption as the trade-off between the benefits of IONP sorption capacity and the reduction of activated carbon content, porosity and surface area has not been investigated systematically to this day. Recently, our group showed the suitability of MPAC as biomass support media and as an adsorbent in a mixed biological/adsorption drinking water treatment process (Lompe et al. 2016). PAC and MPAC with different mass fractions of maghemite IONP showed the same removal performance for dissolved organic carbon (DOC) when normalized based on the available PAC content in MPAC indicating negligible NOM adsorption capacity of maghemite IONP. In contrast, Zahoor (2014) measured 20 % lower humic acid adsorption capacity of MPAC compared to PAC and attributed this to a lower available surface area (1150 m^2/g vs. 868 m^2/g) although the reduction might also originate from the 20 % lower PAC mass fraction in their MPAC that can be estimated from the 20 % difference in bulk density. Similarly, Kim et al. (2013) found reduced NOM adsorption on MPAC compared to PAC which they attributed to reduced micropore volume and surface area (23 % – 33 % lower than for PAC). Yet, the link between reduced pore volume, surface area, and adsorption capacity was not evident as no mass fraction of magnetite was analyzed. Anzai et al.

(2016) prepared MPAC from rice husk that showed 30 % reduced humic acid adsorption capacity when MPAC was prepared by impregnating PAC with a 1.6 M iron nitrate solution (vs. impregnated with a 0.4 M iron nitrate solution). However, the authors did not investigate further the adsorption mechanisms and it remains unclear if the observed reduction was related to the lower PAC mass fraction in MPAC or pore volume and surface area reduction due to pore blocking. Enhanced NOM removal in the presence of IONP was found in a study by Park et al. (2015) who observed up to 10 times higher adsorption of NOM on MPAC containing mass fractions of 1.8 % – 2.6 % ferrihydrite, hematite and magnetite IONP, even though the Brunauer-Emmett and Teller (BET) surface area was reduced by up to 50 %. An overview of past adsorption studies performed with MPAC is given in Table A-1 of the supplementary information. It remains unclear whether magnetic IONP improved the adsorption capacity of PAC or not considering the diverging conclusions in the scientific literature. Therefore, our aim is to address the following research question: Do magnetic nanoparticles on PAC improve or reduce its NOM adsorption capacity?

Three MPAC containing mass fractions of 10 %, 38 % and 54 % maghemite IONP were prepared using a co-precipitation process. The role of IONP in NOM adsorption was studied with respect to PAC content, along with the distribution of pore volume and surface area as well as the NOM characteristics such as molecular size and aromaticity. The originality of this project lies in the systematic and quantitative evaluation of IONP mass fractions on NOM adsorption and the applications of isotherm and kinetic models to highlight the dominant adsorption mechanisms.

4.2 Materials and Methods

4.2.1 Water matrix

Suwannee River NOM purchased from the International Humic Substance Society (IHSS) was chosen as well characterized NOM source to allow for better comparison with the existing literature. The NOM powder was stirred for 12 hours in Milli-Q water (18 µS/cm, DOC 0.174 mg/L ± 0.018 mg/L standard deviation) with a background ionic strength of 1 mM (NaCl) to produce a stock solution of 500 mg DOC/L. The latter was adjusted to pH 7.0 with phosphate buffer and NaOH and filtered through a 0.45 µm polyethersulfone filter (Pall Supor®-450), previously rinsed with 1 L of Milli-Q water. For adsorption experiments, the stock solution was

diluted to the desired initial DOC concentration with phosphate buffered Milli-Q water (pH 7, ionic strength 1 mM with NaCl).

4.2.2 Preparation of PAC and MPAC adsorbents

Coal-based Aquasorb® CB1-MW (Jacobi, formerly Picahydro MP23 from PICA™) was washed with demineralized water to reduce its basicity below pH 8 and dried at 105°C before serving as the base material for MPAC synthesis. This carbon with an iodine number of 900 mg/g and a median volume diameter of 15-35 µm was chosen among others in adsorption pretests for its good DOC and MIB/geosmin removal from the water matrix used during this study (data not shown). MPAC was prepared by an alkaline co-precipitation process as proposed by Oliveira et al. (2002). $FeCl_3 \cdot 6H_2O$ and $FeSO_4 \cdot 7H_2O$ solutions (molar ratio 1:2) were injected into a stirred (700 rpm) deoxygenized carbon suspension (containing between 2 to 10 g of PAC) while the temperature was maintained at 70°C by a water bath.

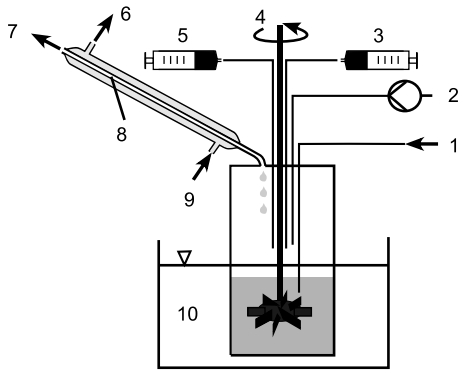

Figure 4.1 : MPAC synthesis reactor: 1 - Nitrogen gas, 2 - NaOH addition 10 mL/min, 3 - Addition of ferric chloride, 4 - Agitation at 700 rpm, 5 - Addition of Ferrous sulphate, 6 - Warm water outlet condenser, 7 - Air outlet condenser, 8 – Condenser to avoid changes of volume due to evaporation, 9 - Cold water inlet condenser, 10 - Hot water bath (70°C).

A peristaltic pump added 5 M NaOH solution dropwise (10 mL/min) into the suspension for 5 min. To allow for controlled precipitation conditions, we operated a closed glass batch reactor with an additional condenser to avoid evaporation during the heating period. Chemicals were added through ports on the reactor lid (Figure 4.1). The suspension was agitated until cooled, washed with demineralized water to pH 8, dried at 105°C and stored in a desiccator until use. The quantity of PAC during the synthesis was varied to produce MPAC with iron oxide mass

fractions of 23 %, 38 %, and 54 % as well as pure IONP (100 %). Bare PAC was also used as a negative control (0 %) throughout this project.

4.2.3 PAC and MPAC characterization

X-ray diffraction (XRD) patterns of pure IONP, PAC and MPAC were recorded with a D5000 Bruker, Sol-X detector with Co Kα radiation (1.79 Å) in the 2θ range 5°- 94° to identify the types of iron oxides and the average crystallite size. The content of iron oxide was analyzed by comparing the magnetic saturation value of pure IONP, PAC and MPAC as recorded by a vibrating sample magnetometer (VSM) as well as with a thermo-gravimetric approach. Briefly, a known mass (triplicates) of MPAC, PAC and IONP were incinerated at 900°C for 24 h. After correcting for ash content in the residues, the iron content was determined from the remaining pure hematite phase (as confirmed by XRD). Surface characteristics of PAC and MPAC were evaluated using scanning electron microscopy (SEM Quanta 200 FEG). Maps of the iron distribution on the surface and inside of MPAC were obtained with X-ray microanalysis from MPAC particles mounted in a polished epoxy disc (SEM JEOL JSM-7600F with energy dispersive X-ray spectroscopy (EDS) at 10 kV and Oxford XMax 80 detector). The size distribution of PAC and MPAC were analyzed by a light scattering method (Mastersizer 3000 Malvern Instruments Ltd.). Nitrogen adsorption isotherms from relative pressure P/P_0 varying between 10^{-6} and 10^{0} at 77 K for PAC and MPAC (Quantachrome Autosorb 1MP) were recorded to analyze multi-point BET surface area as well as pore size and surface area distributions with the non-linear density functional theory (NLDFT with slit/cylindrical pore shape for carbon) using the Autosorb-1 (FL, USA) software. The total pore volume was calculated from the adsorbed volume of gas near the saturation point ($P/P_0 = 0.99$). For the determination of the point of zero charge (pH_{pzc}), pre-weighted masses of PAC and MPAC were immersed in 40 mL NaCl solutions (ionic strength of 0.01 M) adjusted to variable pH of 3 – 11 with NaOH and HCl. The suspensions were shaken and measured after 48 h and the pH_{pzc} determined as the crossing point between the potentiometric curve of the suspension and the blank solution (Bourikas et al. 2003).

4.2.4 Adsorption isotherms and kinetics

The equilibrium adsorption capacity (24 hours) and kinetic experiments were carried out using the bottle point technique. Carbon-free (combusted at 500°C for 5 hours) 125 mL serum bottles

were used as reactors and equipped with aluminum crimp caps and Teflon-lined septa and agitated on a vertical wheel rotary shaker at 22°C. Pre-tests had shown the vulnerability of the composite materials to the high agitation necessary to keep the dense MPAC materials in suspension on a linear shaker (decomposition of MPAC < 24 h due to abrasion). The bottles were therefore mounted horizontally to a motorized wheel that turned at a speed of 50 rpm and initiated a movement of constantly falling particles through the liquid. The adsorbents (0.005 g) were pre-wetted for 24 hours in 4 mL Milli-Q water before adding 100 mL of NOM solution (preparation described in section 4.2.1). Concentrations ranged between 0.89 – 241 mg DOC/L for the constant dose isotherms and samples were taken after 24 hours. Pre-tests demonstrated < 10 % differences between the 24 h values and the adsorption equilibrium (data not shown). Adsorption kinetics were recorded for an initial concentration of 4.36 ± 0.24 mg DOC/L (standard deviation) for 10 contact times up to 24 h. To stop the adsorption reaction, samples were filtered immediately through a 0.45 µm polyethersulfone filters (Pall Supor®-450), previously rinsed with 1 L of Milli-Q water. Controls and blanks from the adsorption assays confirmed that the chosen bottles and septa did neither adsorb nor release any carbon. The pH remained constant at 7.0 ± 0.06 during the tests. Two conditions per isotherm and kinetic test were carried out in duplicate to estimate the experimental error. As the resulting standard deviations on the replicates (0 to 0.2 mg DOC/L) and coefficients of variation (0 % – 2.5 %) were very low, no error bars are shown in the graphics of isotherms and kinetics.

DOC (Standard Methods APHA 2012, TOC meter Sievers 5310-C), UVA_{254} (Standard Methods APHA 2012, 5910B) and pH were measured before and after the assay for each test condition. All DOC samples were analyzed in duplicate revealing a precision of ± 0.01 mg DOC/L. The specific ultraviolet absorbance ($SUVA_{254}$) was calculated to evaluate the selectivity of PAC and IONP for the aromatic SR-NOM fraction. $SUVA_{254}$ is defined as the UV_{254} absorbance divided by the DOC concentration of the sample (reported as L/mg/m) and characterizes the aromatic character of the organic matter (Weishaar et al. 2003). One sample per isotherm with an initial DOC concentration of 4.45 mg DOC/L (representing a point in the middle of the isotherm) was analyzed using size exclusion chromatography (SEC) with UV detection (wavelength 254 nm) with a High-Performance Liquid Chromatograph (HPSEC/UV, Perkin Elmer, Canada with TSK HW-50S column (Tosoh, Japan) as stationary phase and phosphate buffer (2.5 g/L KH_2PO_4 + 1.5

g/L $Na_2HPO_4 \cdot H_2O$) as the mobile phase and polystyrene sulfonate standards) to determine the size fractions of NOM that was adsorbed by MPAC compared to PAC.

To distinguish between the impact of surface area, porosity and surface chemistry, the adsorption isotherms of PAC, MPAC and pure IONP were normalized by equivalent PAC mass, accessible surface area as well as pore volume. The empirical Freundlich model was fitted to the experimental data. The surface diffusion coefficient D_s was calculated from kinetic data applying the homogeneous surface diffusion model (HSDM) for PAC batch tests as described by Najm (1996). The HSDM predicts the diffusion of the adsorbate from the external surface of the PAC particle along the surface of the pores to the final internal adsorption sites. PAC particles are considered to be spherical, homogeneous and equal in size. Therefore, the mass median diameters of PAC and MPAC particles were chosen as input parameters. The nonlinear algebraic equation was solved iteratively for D_s by minimizing the sum of squared residuals between the model result and the measured kinetic data, as described by Edzwald (2011).

4.3 Results

4.3.1 PAC and MPAC characterization

The IONP detected on the PAC surface were mainly formed of maghemite and had an average diameter of 17 nm, as estimated by the line width of XRD spectra (Figure 4.2 and Table 4.1). The incineration test of the three MPAC samples confirmed the presence of the iron mass fractions added during MPAC synthesis. A complete transformation of this iron into maghemite during co-precipitation would have led to maghemite mass fractions of 54 %, 38 %, and 23 %. VSM measurements confirmed mass fractions of 38 % and 54 % magnetic iron oxide in the samples referred to as MPAC-38% and MPAC-54% hereafter (Table 4.1). However, only 10 % (instead of 23 %) maghemite, was present in the sample referred to as MPAC-10% hereafter. The remaining mass fraction of 13 % was present as a non-magnetic iron phase and the XRD diffractogram confirmed low crystallinity for this sample. While one could speculate that this is ferrihydrite, which is generally nano-sized and poorly ordered, it is also difficult to identify it unambiguously. During this study, the structure and properties of the non-magnetic iron phase in sample MPAC-10% were not further investigated.

Table 4.1 : Characteristics of the adsorbents.

Adsorbents	Fe_2O_3 mass fraction (%)	Magnetic saturation (Am^2/kg)	pH_{pzc} (-)	d_{10} (µm)	d_{25} (µm)	d_{50} (µm)	d_{75} (µm)	d_{90} (µm)
PAC	0	0	7.5	6	11	23	47	82
MPAC-10%	10	5.20	8.6	-	-	-	-	-
MPAC-38%	38	20.1	7.3	-	-	-	-	-
MPAC-54%	54	30.3	7.0	6	11	23	49	100
Fe_2O_3 IONP	100	57.8	-	-	-	17 (nm)[a]	-	-

[a] Calculated from XRD data using the Scherrer equation for the average crystallite diameter

The particle size distribution remained the same for MPAC-54% compared to PAC for diameters < d_{75} (~ 48 µm) as the volume of MPAC particles was not significantly increased, even at high IONP mass fractions. Due to the high density of maghemite (5.0 g/cm³) compared to PAC (apparent density of 0.4 g/cm³), the deposition of IONP on MPAC can increase its mass without much increasing its volume (Table 4.1). Deviations between both distributions observed for particle diameters above d_{75} was a consequence of MPAC particles not being well dispersed during the measurement. Applying ultrasound and stronger stirring during the measurements decreased the differences but also led to the decomposition of the composite over time (the MPAC suspension turned brown and an increase of the small particle fraction was detected).

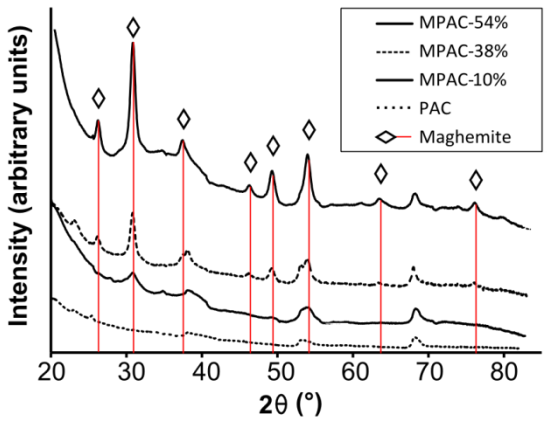

Figure 4.2 : X-ray diffractogram with highlighted positions of identified maghemite phase. Low crystallinity is visible in the MPAC-10% sample.

The point of zero charge of PAC and MPAC varied between pH_{pzc} 7.0 and 8.6 with no clear correlation to the IONP mass fraction. All adsorbents were thus neutral or slightly positively charged during the adsorption experiments carried out at pH 7.

The specific micropore volume (primary and secondary) of MPAC decreased disproportionally with increasing mass fraction of maghemite (up to 66 % for MPAC-54%) compared to bare PAC (76 % of the pore volume < 2 nm) (Figure 4.3c). Normalizing micropore volumes to PAC mass (data not shown) confirmed that the lower mass fraction of PAC in the magnetic adsorbents could not solely explain this difference. EDS spectra of elemental iron (Figure A-2 and Figure A-3 in the SI) in the cross section of MPAC-54% shows the presence of the metal inside the carbon matrix of the composite material. Pore blocking of the micropores by IONP might therefore have contributed to the disproportional reduction of micropore volume in MPAC. How IONP affect the mesopore volume is more difficult to evaluate: according to the size of IONP (average diameter of 17 nm) one would expect blocking and filling of the mesopores (2 – 50 nm); yet, the N_2-adsorption isotherm revealed a consistent trend of mesopore increase for the increasing IONP mass fraction (Figure 4.3 and Table A-2). SEM images and EDS mapping of elemental iron show dispersed IONP on the MPAC surfaces as well as larger IONP clusters forming an irregular spongy crust on the MPAC surface thus adding porosity to the material (Figure 4.4 b and Figure A-2). As a plausibility check, we estimated the pore volume that is formed by the respective IONP mass fraction in MPAC. To do so, we calculated the expected number of IONP per g of MPAC, assuming homogeneously shaped, spherical IONP with a diameter of 17 nm and a density of maghemite (5 g/cm³). The voids that form between these IONP then depend on the arrangement of spheres which can be simplified as e.g. tetrahedral lattice, close cubic lattice or hexagonal lattice. The calculated, specific pore volumes in the IONP crust per g of MPAC matched the measured increase of mesopore volume - with range values (depending on the arrangement of spheres) of 0.21– 0.56 mL/g (MPAC-54%), 0.15 – 0.39 mL/g (MPAC-38%) and 0.08 – 0.22 mL/g (MPAC-10%). The total pore volume as calculated applying the NLDFT method increased for MPAC-38% and MPAC-54% compared to bare PAC. The IONP crust thus compensates the loss of pore volume in the micropores and mesopores of the PAC matrix in MPAC-38% and MPAC-54%. The total pore volume of the MPAC-10% sample, however, decreased despite a 30 % increase in mesoporosity, which can be attributed to the additional

amorphous iron phase that reduced the micropore volume disproportionally to the IONP mass fraction of 10 % (Figure 4.3).

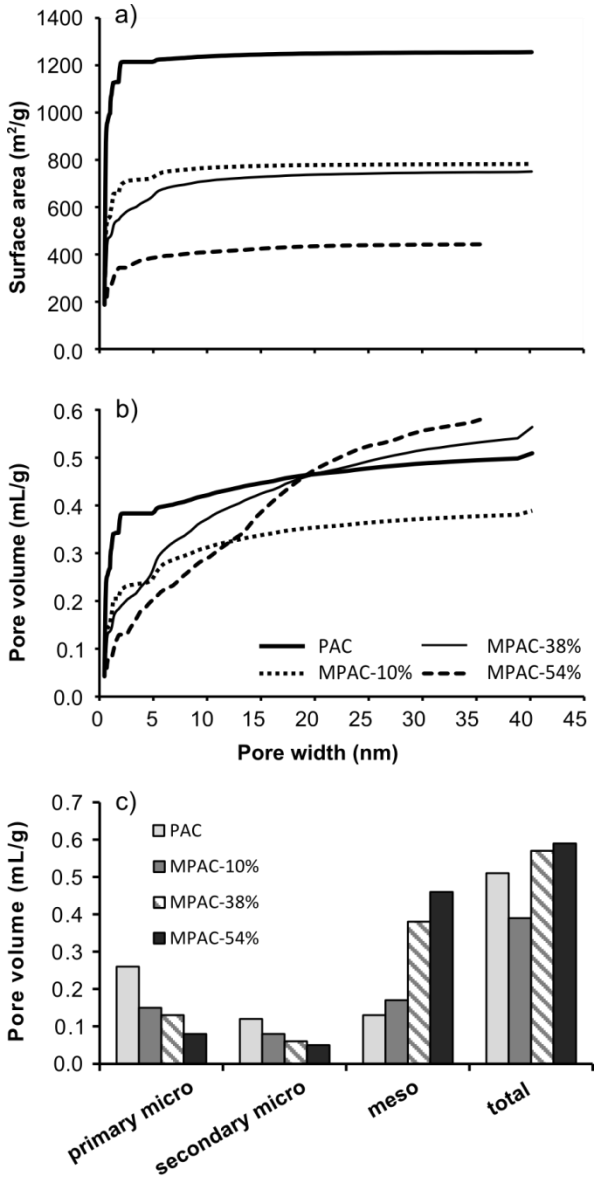

Figure 4.3 : a) Surface area and b) pore volume distribution, both recorded from nitrogen adsorption isotherms and calculated as NLDFT distributions. c) Pore volume constitution with primary micropores < 0.8 nm, secondary micropores 0.8 nm < Ø < 2 nm, mesopores 2 nm < Ø < 50 nm.

The cumulative surface area as calculated using the NLDFT method was larger than the BET surface area for all adsorbents (up to 40 % in the case of bare PAC). The NLDFT results were taken for all subsequent calculations considering that the BET equation is in a strict sense not applicable to microporous materials (Thommes 2010). The micropores contribute the most to the total specific surface area and thus, this characteristic is greatly reduced for all MPAC compared to PAC (Figure 4.3a). Although the IONP crust contributes to the surface area in the mesopore range, it cannot balance the surface loss in the micropores and the reduction of the total specific surface area is thus not proportional to the IONP mass fraction of the composite material. The inconsistent trend of MPAC-10% with respect to the total surface area (values similar to the MPAC-38% sample despite higher PAC content) can be attributed again to the presence of the low crystalline iron oxide.

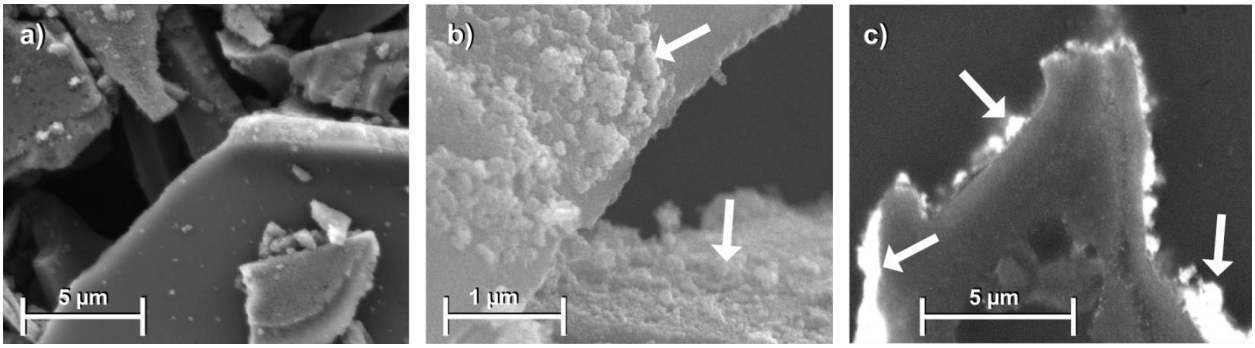

Figure 4.4 : a) PAC surface without IONP, b) arrows point to crust of IONP on the surface of MPAC-54% and c) cross section of a MPAC-54% particle embedded in a polished epoxy matrix, arrows pointing to the IONP cover on the surface of PAC. Element mapping confirmed the presence of iron and oxygen on the outer surface of PAC and inside the particle (s. SI for recorded EDS spectra in Figure A-2 and Figure A-3).

For NOM adsorption, only the fraction of the pores that is accessible for the NOM molecules is relevant. To evaluate this accessible pore fraction, the total surface area and the pore volume from the NLDFT measurements were limited to the contribution of pores with diameters larger than the size of SR-NOM molecules. Pores smaller than this critical diameter were considered inaccessible for SR-NOM. In the literature, SR-NOM diameters between 0.77 nm (fulvic acid) (Averett and Geological 1994) and 2.1 nm (fulvic acid) (Lead et al. 2000) are reported. Tests with small (<500 Da) and large NOM fractions (500 – 3000 Da) by Newcombe et al. (1997) have

shown that NOM adsorbs primarily in mesopores or secondary micropores (> 0.8 nm). Our own size distribution measurements of SR-NOM show that all NOM molecules were > 500 Da (Figure 4.8). For this study, pores smaller than 1 nm were therefore considered inaccessible for NOM molecules. The accessible surface area and pore volume is thus a mixture of micropores (fraction 1 – 2 nm), mesopores in the PAC matrix and mesopores formed by the IONP crust and no clear trend is visible with IONP mass fraction (Table A-2 in the SI).

4.3.2 Adsorption isotherms

Compared to PAC, all MPAC adsorbents had lower adsorption capacities for SR-NOM with increasing IONP content (Figure 4.5 a). The linearized empirical Freundlich isotherm fitted the data with coefficients of determination of $0.95 < R^2 < 0.99$ (Table 4.2). Yet, the adsorption capacity expressed on the basis of adsorbent mass (q_m) does not account for the different material bulk densities (PAC: 0.4 g/cm³, maghemite: 5.0 g/cm³). To provide a better comparison, the solid concentrations were normalized by accessible surface area q_A and pore volume q_{PV} (Figure 4.5 b) and Figure 4.5 c). The q_A values show that pure IONP adsorb 10 times less than PAC even when only the accessible surface is taken into account. The q_A values for MPAC also indicate significantly (p-value all < 0.05) lower amounts of NOM adsorption than pure PAC. Similar conclusions were derived from the q_{PV} isotherms (Figure 4.5 c). Changing the accessible pore volume definition, e.g. as (i) the pore volume in pores > 2 nm, (ii) as the pore volume in secondary micropores and mesopores (0.8 – 50 nm), or as (iii) the pore volume in pores larger than the micropores calculated with the Dubinin-Radushkevich equation (Quantachrome software) (Table A-2 in the SI) led to similar conclusions (data not shown). All these approaches have in common that they do not differentiate between adsorption sites in the carbon matrix or in the IONP crust. The measurements of the pore size distribution revealed that IONP reduced the microporosity (pores < 2 nm) and increased the overall mesopore volume of the composite material but could not show how IONP affect specifically the mesopores associated with the carbon matrix of MPAC. As IONP have a low adsorption capacity for NOM the presence of accessible adsorption sites in the carbon matrix is crucial for NOM adsorption.

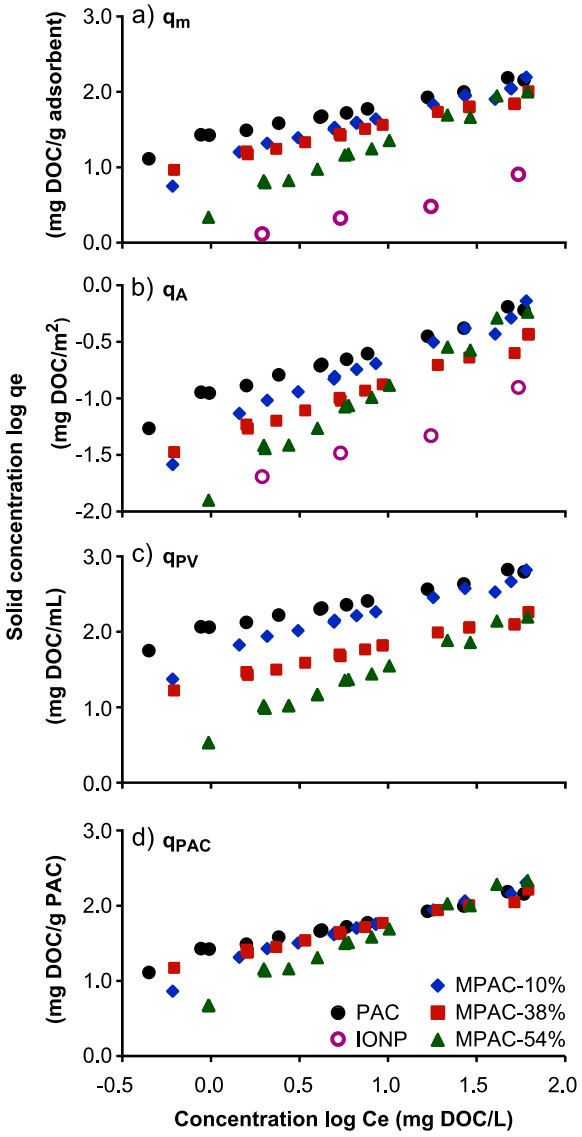

Figure 4.5 : Linearized DOC solid concentration q_e normalized by a) adsorbent mass, b) accessible surface area (pores > 1 nm), c) accessible pore volume (pores > 1 nm) and d) PAC mass fraction.

To find out if IONP reduce the adsorption sites located in the mesopores of the carbon matrix of MPAC the solid concentration of NOM was normalized to the PAC mass fraction q_{PAC} (mg NOM/g PAC). The resulting isotherms reveal that IONP do reduce the adsorption capacity of these mesopores (Figure 4.5 d): If IONP had no influence on the adsorption capacity of the carbon matrix, MPAC should show higher solid concentrations q_{PAC} in equilibrium than pure PAC because of the additional, albeit low, NOM quantity adsorbed on IONP. Yet, for all MPAC,

q_{PAC} values are lower or equal to bare PAC. This shows that the adsorption sites in the mesopores of the PAC matrix were reduced by the presence of IONP. The reduction is small and not statistically significant (t-tests with calculated p-values of 0.4 – 0.7) at low IONP mass fractions in MPAC (10 % and 38 %). The presence of the poorly crystalline iron phase in sample MPAC-10% did not influence this result. However, the reduction is clearly visible and statistically significant (p-value of 0.006 – 0.03) at an IONP content of 54 % (Figure 4.5 d).

To confirm the reduction of adsorption capacity for the MPAC with high IONP mass fraction, measured isotherms of the composite materials MPAC-10%, MPAC-38% and MPAC-54% were compared to theoretical mixed isotherms calculated from isotherms of pure PAC and pure IONP (Figure 4.6). Assuming independent effects of both adsorbents, the visible deviations of these theoretical isotherms from the measured mixed isotherms indicate the loss of adsorption capacity due to a loss of blocked mesopores in the carbon matrix. The loss is most important in the sample MPAC-54% while for the other two MPAC (10 % and 38 %) the loss of adsorption due to pore blocking is compensated by the sorption capacity of IONP.

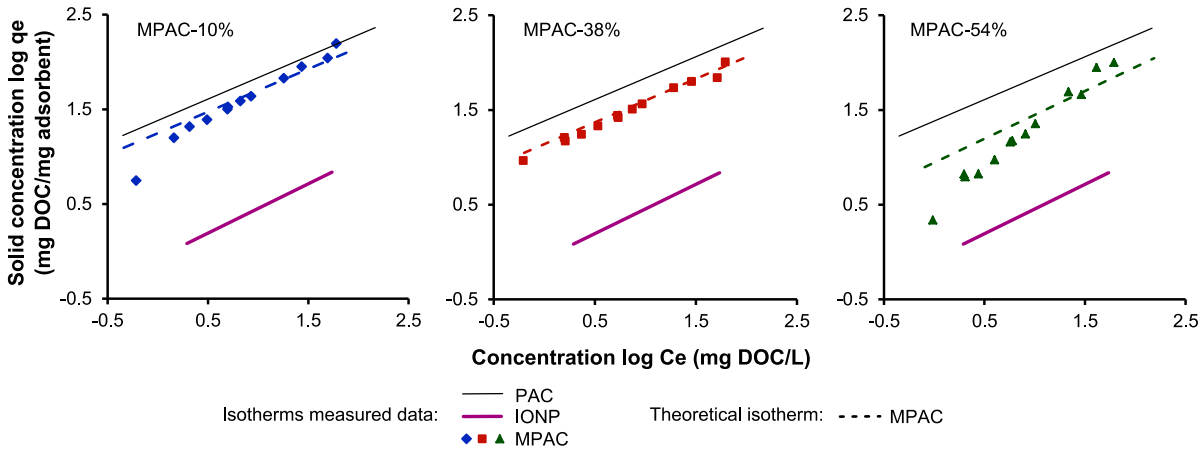

Figure 4.6 : Measured isotherms compared to theoretical isotherms composed from pure PAC and pure IONP isotherms. Theoretical isotherms assume independent effects of both sorbents and deviations between measured and theoretical isotherms thus indicate the loss of adsorption capacity due to blocked mesopores in the carbon matrix.

Table 4.2 : Freundlich[a] coefficients for the adsorption of NOM onto PAC, MPAC and IONP.

Adsorbent	Normalized to adsorbent mass				Normalized to PAC mass			
	K_F (mg/g)(L/mg)$^{1/n}$	1/*n*	R^2	ARE (%)[b]	K_F (mg/g) (L/mg)$^{1/n}$	1/*n*	R^2	ARE (%)[b]
PAC	24.15	0.45	0.98	7.6	24.15	0.45	0.98	7.6
MPAC-10%	11.20	0.62	0.96	12.8	14.23	0.64	0.98	10.5
MPAC-38%	12.10	0.47	0.98	7.2	19.21	0.49	0.99	4.9
MPAC-54%	2.91	0.88	0.99	11.4	6.33	0.88	0.98	11.4
Fe_2O_3 IONP	0.86	0.52	0.95	12.3	-	-	-	-

[a] $q_e = K_F C_e^{1/n}$, [b] As a measure for the quality of the non-linear fit the average relative error ARE (also known as the mean absolute percentage error) was calculated as ARE (%) = 100/n * $\sum$ ($|\Delta x|/x$)

4.3.3 Adsorption kinetics

For both PAC and MPAC, > 85 % removal of the adsorbable NOM was reached after 400 min and > 75 % was adsorbed after 150 min (Figure 4.7). The surface diffusion coefficients D_s as calculated from the HSDM model were $1.21 \cdot 10^{-14}$ m²/s (MPAC-38%) and $1.18 \cdot 10^{-14}$ m²/s (MPAC-54%), which is marginally higher for MPAC than for bare PAC ($0.91 \cdot 10^{-14}$ m²/s). However, the differences between the diffusion coefficients are low considering the fact that these coefficients typically vary on a log-scale. Varying D_s (in the range of $0.91 \cdot 10^{-14}$ m²/s to $1.21 \cdot 10^{-14}$ m²/s) for each adsorbent did not change the quality of fit (coefficient of determination R^2) between model and data as confirmed in paired t-test (all p-values > 0.55). Even for a high IONP mass fraction - as for the MPAC-54% - the IONP did thus not inhibit the adsorption rate. The differences between the curves are therefore only related to the different equilibrium adsorption capacities and not by the internal transport process. Identical conclusions were derived analyzing the kinetic constants k_2 (PAC: $1.21 \cdot 10^{-3}$ g/mg/min, MPAC-38%: $2.53 \cdot 10^{-3}$ g/mg/min and MPAC-54%: $1.89 \cdot 10^{-3}$ g/mg/min) derived by fitting the data to a pseudo-second order model (Ho and McKay 1998) (Table A-3 in the SI).

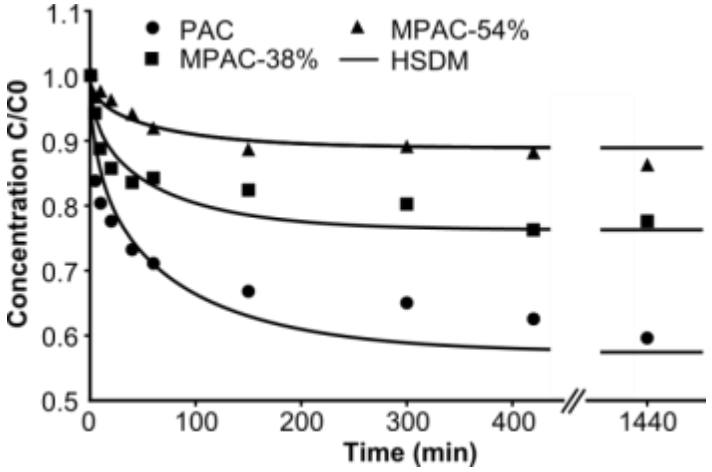

Figure 4.7 : Kinetic experimental data and HSDM model with diffusion coefficients of $0.91 \cdot 10^{-14}$ m²/s (PAC), $1.21 \cdot 10^{-14}$ m²/s (MPAC-38%) and $1.18 \cdot 10^{-14}$ m²/s (MPAC-54%). The root mean squared error RMSE is highest for PAC (0.170), and lower for MPAC-38% (0.107) and MPAC-54% (0.055).

4.3.4 Adsorption selectivity

$SUVA_{254}$ indices for prepared SR-NOM solutions were high (3.73 ± 0.21 L/mg/m) as SR-NOM is primarily composed of aromatic humic acid (Averett and Geological 1994). Evaluating selectivity for the aromatic NOM fraction is thus difficult and changes in the ratio UVA_{254} / DOC in the remaining liquid become only detectable if both removals of the aromatic NOM fraction are much higher than that of aliphatic NOM and removals of NOM are important. For NOM loadings < 50 mg DOC/g adsorbent, $SUVA_{254}$ decreased by 10 % to 50 % after 24 h adsorption on PAC and MPAC indicating preferred adsorption of aromatic NOM for all adsorbents (Figure A-4 in the SI). Differences between the $SUVA_{254}$ indices of the three MPAC compared to PAC were not significant (p-values 0.09 – 0.24). In tests with pure IONP the $SUVA_{254}$ index did not change. The results show that IONP do not change the selectivity of the carbon matrix for aromatic NOM.

HPSEC/UV chromatograms of SR-NOM before and after 24 h adsorption experiments with PAC, MPAC-38%, and MPAC-54% showed that both PAC and MPAC adsorbed preferably the low molecular weight fraction (Figure 4.8). To roughly quantify the differences between the adsorbents, the area under the HPSEC/UV curves between 40 and 50 minutes retention time were integrated resulting in approximately 10 % and 30 % higher NOM quantity adsorbed on PAC

compared to MPAC-38% and MPAC-54% respectively which results from the different PAC mass fraction in the adsorbents.

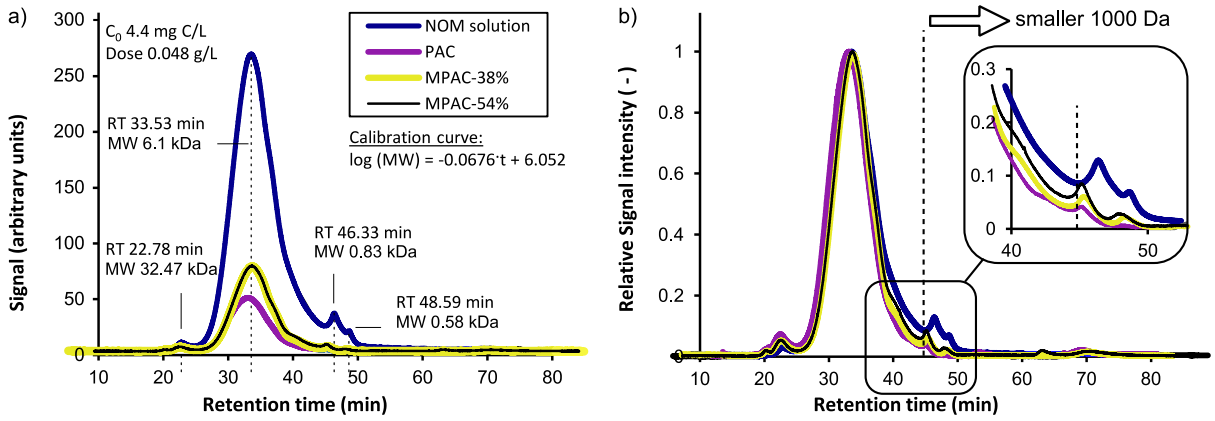

Figure 4.8 : a) Absolute HPSEC/UV chromatograms of SR-NOM remaining in solution after 24h adsorption tests with a dose of 0.048 g/L of PAC and MPAC. Retention times were converted into molecular weight (daltons) with the help of a polystyrene sulfonate standard calibration curve. b) Normalized SR-NOM chromatograms were calculated as the ratio absolute / maximal measured signal intensity. PAC, MPAC-38% and MPAC-54% eliminate over-proportionally the small aromatic NOM fraction from the SR-NOM solution. The detail of the low molecular weight fraction shows higher adsorption on PAC compared to MPAC-38% and MPAC-54%.

4.4 Discussion

Understanding the impact of IONP in MPAC on NOM adsorption requires a thorough analysis of the IONP mass fraction in the composite material coupled to a detailed analysis of the pore size distribution. While the benefits of magnetic IONP on PAC for NOM removal were unclear in previous studies - they were reported to either enhance (Park et al. 2015) or reduce (Zahoor 2014) adsorption capacities - our results indicate that the adsorption capacity is reduced proportionally to the mass fraction of PAC in the composite due to the relatively low adsorption capacity of IONP for NOM compared to PAC. Above the critical mass fraction of 38 %, the mesopores in the carbon matrix were blocked leading to a disproportional reduction in sorption capacity. However, the adsorption rate of NOM on MPAC was not statistically different from bare PAC.

4.4.1 Adsorption capacity of IONP

Contrary to previous adsorption studies, we analyzed the adsorption capacity of pure IONP and PAC separately and compared the values to the adsorption capacity of the composite material MPAC at different IONP mass fractions. The adsorption capacity of our maghemite IONP (8 mg DOC/g or 0.12 mg DOC/m²) is similar to the adsorption capacity of hematite (0.18 mg C/m² with Suwannee River fulvic acid and Georgetown NOM) (Gu et al. 1994) and slightly higher than the adsorption capacity of magnetite and goethite particles (2.6 and 4.05 mg DOC/g respectively with standard humic acid) (Rahman et al. 2013). The low affinity of maghemite and magnetite IONP for organic molecules was also confirmed in a study with phenantrene and phenol on MPAC produced with two different commercial PAC (Han et al. 2015). The authors found that adsorption capacities for both molecules on MPAC were solely proportional to the PAC mass content (ca. 60 %) while their IONP did not contribute to the adsorption of the tested compounds. Much higher NOM adsorption capacities were recorded in a study by Kang and Choo (2010) for the iron oxide ferrihydrite (ca. 50 mg DOC/g ferrihydrite or 0.4 mg DOC/m² ferrihydrite) which was found to adsorb much larger quantities than PAC (10 mg DOC/g PAC or 0.03 mg DOC/m² PAC). There are two reasons for their results. First, their solid concentration of NOM on PAC was normalized by the total PAC surface area of 1255 m²/g and not the accessible surface area (e.g. using pores > 1 nm) – which leads to very low NOM solid concentrations for PAC. Secondly, the iron oxide ferrihydrite has a lower degree of crystallinity compared to other iron oxides such as maghemite, hematite, goethite and magnetite, leading to a higher specific surface area for adsorption (Cornell and Schwertmann 2003). Choo and Kang (2003) found micron sized ferrihydrite particles to outperform goethite and hematite for the adsorption of DOC from wastewater (approx. 5 mg DOC/g hematite or goethite vs. 12 mg DOC/g ferrihydrite as calculated from provided data) and also related their findings to the low crystalline structure of ferrihydrite. While ferrihydrite might be the iron oxide of choice for PAC/iron oxide adsorbents with regard to efficient NOM removal, one has to keep in mind that only the iron oxides maghemite and magnetite exhibit sufficiently high magnetization allowing for magnetic separation (Cornell and Schwertmann 2003) and are thus suitable for the application in MPAC. In terms of preferential adsorption, pure IONP did not change the $SUVA_{254}$ index due to the low NOM adsorption capacity. Consequently, they also did not impact the $SUVA_{254}$ index of the composite material: both PAC and MPAC preferentially adsorbed the aromatic fraction of NOM

and thus no differences in the $SUVA_{254}$ index were observed in our study. Similar results were reported by Kim et al. (2013) who compared NOM adsorption (SR-NOM as well as NOM from surface water) on magnetite impregnated wood and coal based PAC to bare PAC. With respect to molecular size, our measurements showed that both PAC and MPAC preferably adsorbed the low molecular weight fraction of NOM. As the PAC used as base material during our study was a microporous PAC the result are consistent with the literature where NOM molecules adsorbed in pores of similar diameter (Newcombe et al. 1997). Between adsorbents, a slightly higher adsorption of the low molecular weight NOM was observed on PAC compared to MPAC which results from the lower mass fraction of PAC in MPAC. Also other studies with magnetite impregnated and iron impregnated PAC did not see differences between SEC chromatograms of modified and bare PAC (Cheng et al. 2005, Kim et al. 2013).

4.4.2 Reduction of mesopores in PAC

Our EDS and pore size distribution results show that small IONP form inside the micropore structure of PAC and that 17 nm sized spherical IONP cover the outside of PAC particles with an irregular crust or agglomerates of IONP. While the former phenomenon leads to the reduction of microporosity, the latter also partly block the mesopores of the carbon matrix in MPAC. It is important to distinguish between mesoporosity that is added due to the pore volume in the IONP crust and blocked mesopores in the carbon matrix that lead to a reduction of the adsorption capacity for NOM. However, this reduction of adsorption sites in the mesopores becomes dominant only at high IONP mass fraction as could be seen for our sample MPAC-54% when normalizing the NOM solid concentration by the PAC mass fraction. At lower IONP mass fraction the effect is not statistically significant and the observed reductions in adsorption capacity are mainly related to the reduction of the PAC mass fraction in MPAC. The added mass of IONP cannot compensate for the loss of adsorption sites in PAC as their adsorption capacity is an order of magnitude lower, even when compared based on available surface area. Reduced surface area or pore volume after impregnation of PAC with a mass fraction of an estimated 20 % maghemite and goethite IONP has also been reported by Zahoor (2014). The reduced adsorption capacity of their MPAC (20 % lower than PAC) was attributed to the loss of the micropore volume. More likely, the loss resulted from the reduced PAC mass fraction (20 %). Most studies on NOM adsorption on MPAC composite materials lack a thorough analysis of the IONP mass

fraction (Anzai et al. 2016, Kim et al. 2013, Kondo et al. 2010, Park et al. 2015, Zahoor 2014) which makes it difficult to understand the NOM adsorption behaviour. It is our intention to raise awareness for the different contribution of PAC and IONP to the adsorption of NOM. Our results show that comparing PAC and MPAC on the basis of the total mass of adsorbent or the total pore volumes is not sufficient to elucidate the IONP effects. A detailed description of pore size distributions, a separate evaluation of adsorption capacities of IONP and PAC and knowledge about the molecular size of the adsorbate are necessary to compare PAC and MPAC adsorbents. In our study, a maximum IONP mass fraction existed below which the adsorption capacity was essentially proportional to the PAC mass fraction in MPAC. This information is important for practical considerations such as MPAC production costs. Also, the mass fraction of IONP has to be chosen carefully considering the trade-off between the remaining NOM adsorption capacity and the magnetic separability.

4.4.3 Adsorption kinetics

In our experiments, the rate of adsorption remained similar in PAC and MPAC despite the high mass fraction of IONP. Marginally higher diffusion coefficients for MPAC compared to PAC had no tangible influence on the adsorption performance curves. Diffusion of NOM molecules from the PAC surface towards the inner core (as is described by the HSDM) was thus not impacted by the presence of IONP. Few authors studied NOM adsorption kinetics on MPAC (Anzai et al. 2016, Kim et al. 2013, Zahoor 2014) and to the best of our knowledge, only Zahoor (2014) fitted an adsorption kinetic model to data obtained with humic acids (Sigma Aldrich) and an MPAC containing goethite and maghemite IONP (with estimated mass fraction of 20 %). They found a good fit to a pseudo-second-order kinetic model and much higher rate constants for MPAC ($1.30 \cdot 10^{-2}$ g/mg/min) than PAC ($7.50 \cdot 10^{-4}$ g/mg/min). Results from our fit to a pseudo-second order model also revealed higher rate constants for MPAC than PAC but differences were marginal. It also has to be considered that rate constants are not physical parameters describing the diffusion process dominating adsorption (Worch 2012). They are empirical fitting parameters which change with the data normalization (e.g. normalizing to the PAC mass fraction). Therefore, comparisons between rate constants should be made after normalizing the data for the PAC mass fraction. In our study, the differences between the rate constants were smaller when the pseudo-second order model was fitted to the data expressed as mg DOC/g PAC (Table A-3 in the SI).

4.4.4 Practical implications

Improving the generally low NOM adsorption capacities of bare PAC by depositing magnetic IONP is ineffective due to their low affinity for NOM molecules. At IONP mass fractions below 54 % the necessary MPAC dose for NOM removal is proportional to its PAC content which implies higher doses of the composite material compared to bare PAC and thus slightly overall higher costs considering (i) the unit costs of iron salts and caustic soda and (ii) the energy cost related to MPAC synthesis. The advantage of using MPAC for sorbing NOM during drinking water production arises therefore only from its magnetic separability. In a drinking water treatment process, MPAC should therefore be applied in a polishing step for settled water (after coagulation-flocculation) to remove residual NOM. Its magnetic properties would allow recycling it in the reactor in order to fully exhaust its sorption capacities. The magnetic separability would also allow its application in a biological PAC reactor as proposed in our previous study (Lompe et al. 2016). In this combined adsorption/biodegradation process MPAC acts simultaneously as an adsorbent and biomass support in a reactor with high PAC concentration and age followed by a magnetic separation step and membrane filtration.

4.5 Conclusions

Concerning our initial research question – do magnetic IONP on PAC improve or reduce the adsorption capacity of PAC for NOM? – our study showed that maghemite IONP do not contribute significantly to the adsorption of NOM itself and reduce the adsorption capacity of MPAC by blocking the mesopores of the carbon matrix. However, this phenomenon is only significant for high IONP mass loading and MPAC could still be of use in a variety of water-treatment applications. If NOM adsorption is the targeted water pollutant and a magnetic PAC is desired, a highly mesoporous PAC and a low IONP mass fraction should be chosen during MPAC synthesis to reduce the negative impact of IONP on the high adsorption capacity of PAC. In summary, the following conclusions were drawn from this work:

- A thorough analysis of the pore size distribution linked to the mass fraction of IONP in the composite is of paramount importance to understand adsorption capacity changes of MPAC,

- IONP reduced the micropore and mesopore volume of the carbon matrix while adding mesopore volume in the voids of the IONP crust,
- IONP are not uniformly covering PAC particles; they form clusters and patches of IONP on the PAC surface and are also found inside the carbon matrix of MPAC,
- IONP contribute little to NOM adsorption due to their lower adsorption capacity per area compared to PAC,
- IONP block mesopores in the carbon matrix and thus reduce the NOM adsorption capacity of MPAC. This effect became important only for the highest IONP mass fractions investigated (54 %),
- The diffusion coefficient D_s for NOM was not influenced by the presence of nanoparticles on MPAC,
- Adsorption on MPAC and PAC targeted the same NOM fractions regarding aromatic content and molecule size.

ACKNOWLEDGEMENTS

The authors are thankful for the technical support of Jacinthe Mailly, Julie Philibert, Mireille Blais and Yves Fontaine and the fruitful discussions with Christoph Reinhardt and Dieter Lompe. This work was completed at the Industrial-NSERC Chair in Drinking Water of Polytechnique Montréal with the financial support of its partners, namely the City of Montreal, Veolia Water Technologies Canada Inc., the City of Laval and the City of Repentigny.

CHAPTER 5 ARTICLE 2 - REMOVAL OF MICROPOLLUTANTS BY FRESH AND COLONIZED MAGNETIC POWDERED ACTIVATED CARBON

In this study, we present the adsorption properties of fresh and colonized magnetic activated carbons for 9 organic MP. We discriminate the relative contributions of PAC and maghemite IONP in the composite material with respect to isotherm and sorption kinetics. We were able to show that MP removal is achieved primarily by adsorption on PAC - not IONP. Aged adsorbents (both regular and magnetic) exhibited a 10 fold lower but still considerable residual MP adsorption capacity. This chapter was submitted as a research paper to the *Journal of Hazardous Materials* in 2018.

REMOVAL OF MICROPOLLUTANTS BY FRESH AND COLONIZED MAGNETIC POWDERED ACTIVATED CARBON

Kim M. Lompe[a], Sung Vo Duy[b], Sigrid Peldszus[c], Sébastien Sauvé[b], Benoit Barbeau[a]*

[a]NSERC Industrial Chair on Drinking Water, Department of Civil, Geological and Mining Engineering, Polytechnique Montréal, P.O. Box 6079, Downtown Station, Montreal, Qc, Canada

[b] Department of Chemistry, Université de Montréal, Montreal, Qc, Canada

[c] NSERC Industrial Research Chair in Water Treatment, Department of Civil & Environmental Engineering, University of Waterloo, On, Canada

* corresponding author. Tel: +1 514 340-4711 ext. 2983.

E-mail: kim-maren.lompe@polymtl.ca (Kim Maren Lompe)

ABSTRACT

This study evaluated the adsorption capacity and rate constants for 9 micropollutants (MP) on fresh and aged magnetic powdered activated carbon (MPAC) as a magnetically separable alternative to conventional PAC for drinking water treatment. MPAC with mass fractions of 10 %, 38 % and 54 % maghemite nanoparticles were compared to bare PAC and pure maghemite in batch adsorption experiments. Pure maghemite alone did not adsorb significant amounts of MP and when normalized to PAC content, no significant differences of MP adsorption between MPAC and PAC were observed. Freundlich constants K_F (normalized to PAC content) ranged

between 2.3 – 37 µg/mg $(L/\mu g)^{1/n}$ for all MP and adsorbents. Pseudo-second order rate constants for MP decreased with increasing maghemite content ranging between 0.2 to 2.7 mg/µg/min for bare PAC and 0.02 – 2.19 mg/µg/min for MPAC. Residual adsorption capacities of 90-days old colonized adsorbents were 10 times lower than for fresh adsorbent. At typical concentrations of 3.5 g colonized adsorbent/L found inside reactors, kinetics were still fast and removals of all MP except sulfamethoxazole exceeded 90% within 5 minutes.

KEYWORDS

Magnetic activated carbon, IONP, micropollutants, bioreactor, drinking water

5.1 Introduction

Contaminants of anthropogenic origin such as pesticides, herbicides, and pharmaceutical residues enter drinking water sources due to runoffs or as wastewater effluents. Although they are generally found at trace levels, many of these so-called micropollutants (MP) are considered as a potential risk for human health and the ecosystems. The list of regulated MP in North America remains limited considering the number of molecules found in the environment. However, the USEPA added hormones, pesticides, insecticides, fungicides and pharmaceuticals to their contaminant candidate list (CCL) for future regulation in drinking water (EPA 2016). In its most recent version (CCL-4) it includes 55 MP.

Among available drinking water treatment processes, powdered activated carbon (PAC) is one of the most common approaches to deal with MP, as it efficiently removes a wide range of organic MP via adsorption. However, the short contact times typically prevailing within water treatment processes do not allow to fully exhaust the PAC adsorption capacity (Kim et al. 2014). In order to address this limitation, magnetic powdered activated carbons (MPAC) have repeatedly been proposed as easily separable and reusable adsorbents (Bastami and Entezari 2012, Castro et al. 2009, Han et al. 2015, Lompe et al. 2017, Oliveira et al. 2002). MPAC are composite materials combining the adsorption capacity of PAC with magnetic properties of iron oxide nanoparticles (IONP). The magnetic IONP (mainly maghemite (Fe_2O_3) and magnetite (Fe_3O_4)) allow for easy magnetic separation of MPAC from water using a magnetic field (Anzai et al. 2016, Borghi and Fabbri 2014). Previous adsorption studies have shown the suitability of novel magnetic adsorbents for a range of MP such as bisphenol-A (endocrine disruptor) (Koduru et al. 2016,

Nakahira et al. 2006, Nakahira et al. 2007, Park et al. 2015), atrazine (herbicide) (Castro et al. 2009), imidacloprid (insecticide) (Zahoor and Mahramonlioglu 2011), ciprofloxacin (antibiotic) (Shi et al. 2013), carbamazepine (anti-epileptic drug) (Baghdadi et al. 2016), and naproxen (anti-inflammatory) (Ilbay et al. 2015). Compared to PAC most authors found lower adsorption capacities on MPAC, with bisphenol-A being an exception (Park et al. 2015). The reduced adsorption capacities are mostly attributed to IONP occupying or blocking relevant adsorption sites on PAC, although this phenomenon is more probably linked to the reduced mass fraction of PAC in the composite. A systematic study evaluating the contributions of IONP and PAC separately and comparing the adsorption capacities and kinetics normalized to PAC mass content is missing so far and will help to optimize the adsorbent regarding magnetic separation while minimizing interference on sorption capacity. In natural waters natural organic matter (NOM) reduces the removal efficiency of AC for MP. The effects of NOM on MP adsorption using MPAC are not yet well understood. Most of the cited studies above were carried out in pure water. Park et al. (2015) found that NOM improved BPA removal on MPAC due to the affinity of NOM for IONP surface groups and the molecular coordination between NOM and BPA. In contrast, an adsorption study carried out for different antibiotics and a chitosan-magnetite-PAC composite showed only negligible decrease of adsorption performance (Ma et al. 2017b). More systematic studies are needed to understand the interactions of competition between NOM and MP on MPAC.

Also, the effect of MPAC aging on MP removal capacities has not yet been evaluated. As MPAC offers the opportunity to work at higher adsorbent age (returning MPAC into the process), the residual MP adsorption capacity after NOM preloading or biofilm formation are crucial for the application. Stoquart et al. (2016) have shown that aged PAC exhibits a significant residual adsorption capacity for MP when operating a steady-state adsorption/membrane reactor at constant PAC age of up to 60 days. In our previous study, we have shown the suitability of MPAC as adsorbent and support for biomass in pilot-scale bioreactors used for DOC and ammonia removal (Lompe et al. 2016).

The overall objective of the present study is to demonstrate the effectiveness of fresh and colonized MPAC for the removal of MP in natural waters. MPAC performances were tested for both virgin and colonized materials from bioreactors operated for 90 days. Three MPAC containing IONP mass fractions of 10 %, 38 % and 54 % maghemite IONP as well as pure IONP

were prepared and compared through adsorption isotherms and kinetic studies with hormones, pharmaceuticals and pesticides. Hence, the present study aimed to address three important research questions: i) how does IONP content of MPAC influence their adsorption capacity for MP? ii) what is the role of NOM in MP adsorption on MPAC? and iii) is there a significant residual MP adsorption capacity on 90-days aged MPAC?

5.2 Materials and Methods

5.2.1 Water matrix

A coal-based PAC (AquaSorb® CB1-MW by Jacobi) was washed with demineralized water to reduce its basicity below pH 8 and dried at 105°C before serving as adsorbent and as the base material for MPAC synthesis. MPAC was prepared by an alkaline co-precipitation process as proposed by Oliveira et al. (2002) $FeCl_3$-$6H_2O$ and $FeSO_4$-$7H_2O$ solutions (50 mL each, molar ratio 1:2) were injected into a stirred (700 rpm) deoxygenized carbon suspension (containing between 2 to 10 g of PAC in 150 mL of ultra-pure water) while the temperature was maintained at 70°C. A 5 M NaOH solution was added drop-wise to precipitate the iron oxide. Pure IONP and three different MPAC with mass fractions of 10%, 38% and 54% IONP were prepared (hereafter referred to as MPAC-10%, MPAC-38% and MPAC-54%). The IONP mainly consisted of maghemite and had an average particle size of 17 nm, as determined by X-ray diffraction (XRD) analysis. The adsorbents were superparamagnetic and exhibited high enough saturation magnetization to be magnetically separable in a high gradient magnetic separator (Anzai et al. 2016). The particle size distribution of PAC did not increase during MPAC synthesis due to the high density of maghemite (5.0 g/cm3) compared to PAC (apparent density of 0.4 g/cm3) (Table 5.1).

Colonized PAC and MPAC were obtained from 1-L bioreactors described in Lompe et al. (2016) Influent water was de-chlorinated tap water amended with nutrients (0.3 mg C/L added as acetate, 60 mg N/L as NH_4Cl and 3 μg P/L as K_2HPO_4). The bioreactors were operated for 90 days at 22^{o}C (no purge or adsorbent replacement) using an equivalent PAC concentration of 10 g PAC/L. This strategy (equivalent PAC concentration rather than equivalent MPAC concentration) was selected to develop equal amount of biomass per adsorbent particle. The latter were shown to be colonized with heterotrophic and nitrifying bacteria at the end of the study

(48.2 mg C/cm^3) and the bioreactors reached stable dissolved organic carbon (DOC) removal of 20 - 30 % and full nitrification. PAC and MPAC were recovered from the reactors via filtration through an 8-µm paper filter (Grade 40 Whatman) and used immediately for adsorption experiments. Dry weights of the collected filter cakes were analyzed in triplicate according to *Standard Methods* (2540-B, APHA 2012). Adsorption results are reported per mass of dry weight.

5.2.2 Micropollutants and water matrices

Nine MP were selected for this study to provide a wide range of usage and chemical properties (Table 5.2). Native standards of the 9 MP were purchased from Sigma Aldrich (St. Louis, MO, USA) with chemical purity ≥ 99%. Individual stock solutions were prepared in HPLC grade methanol (MeOH) purchased from Fisher Scientific (Whitby, ON, Canada) at 1000 mg L^{-1}. A mixture was prepared in advance and evaporated to dryness using a gentle N_2 stream and mild heating (40 °C). HPLC-grade water was then added to obtain stock solutions in water of 1 mg/L or 10 mg/L for each compound. For isotherm and kinetic experiments on virgin IONP and MPAC (section 5.3.1 and 0), Montreal tap water was used (pH 7.9, DOC 2.0 ± 0.02 mg/L standard deviation). Experiments on virgin PAC and MPAC with different background NOM concentrations (section 5.3.3) were carried out with Montreal tap water and surface water from the Des Mille-Îles River (pH 7.61, DOC 6.25 ± 0.03 mg/L). These waters were filtered through 0.45 µm (PALL Supor450) PES filters and kept at 4 °C until use. As a reference condition, ultra-pure water (18 mS/cm, DOC 0.03 mg/L ± 0.01 mg/L) was buffered at pH 7.0 and adjusted to an ionic strength of 3 mM (NaCl). Experiments on colonized PAC (section 5.3.4) were carried out using the influent water of the bioreactors. The water matrices for all isotherm adsorption experiments were spiked with the MP mixture to obtain an initial concentration of 500 µg/L of each compound. Kinetic experiments were performed at a spike level of 10 µg/L. In all cases, adsorption performance calculations were based on the actual initial and final MP measurements and not the theoretical dissolved concentrations. During the experiments, no significant loss of MP through volatilization or adsorption on glassware and caps was observed (standard deviations of all MP in the 24 h controls were < 1.5 µg/L in all experiments with Co = 10 µg/L and < 30 µg/L in experiments with Co = 500 µg/L).

5.2.3 Adsorption experiments

Adsorption isotherms for non-colonized and colonized adsorbents were recorded using the bottle point technique (Worch 2012) in flasks filled with 200 mL solution and closed with aluminum foil and parafilm. The flasks were shaken on an orbital shaker (Innova 2300, Brunswick Scientific) at 250 rpm and room temperature for 12-24 hours. All isotherm experiments were spiked at 500 µg/L of each MP and seven adsorbent doses were used spanning from 0.0005 to 0.54 g/L of non-colonized adsorbents and from 0.005 to 5 g/L for isotherms on colonized adsorbents. Colonized adsorbents were added as mass of known humidity for high adsorbent concentrations (5 g/L and 0.5 g/L) and pipetted as suspensions for lower concentrations (0.1; 0.05; 0.025 and 0.005 g/L). Five duplicate bottles containing PAC/MPAC and the spiked matrix were chosen on a random basis and added to the setup to evaluate the experimental error. Negative blanks containing ultra-pure water and non-spiked water matrix, and positive blanks containing spiked MP solution without adsorbent were sampled at the beginning and after 24 hours of the assay to check for background MP concentration and to evaluate the loss of MP over 24 hours. ***Kinetic tests on non-colonized adsorbents*** were carried out using the bottle-point technique with 10 mg/L of adsorbent and an initial concentration of 10 µg/L in 125 mL serum bottles equipped with *Teflon* lined septa and crimp caps. Dry adsorbents were pre-wetted with 10 mL of ultra-pure water 24 h before the experiment. The bottles were filled with 100 mL of spiked water matrix to start the experiment and shaken at 200 rpm. ***Kinetic tests on colonized adsorbents*** were carried out in 1 L beakers on a jar tester at 200 rpm. Five grams (wet weight) of PAC and MPAC filter cakes were added to the agitated MP solution at time zero. Samples (10 mL) were taken from the 500 mL PAC suspension at increasing contact times (1, 5, 10, 30, 60 min and 24 h). In all adsorption experiments, samples were immediately filtered through 0.3 µm glass fiber syringe filters (Sterlitech GF-75) to separate PAC from water. The samples were acidified with 50 µL concentrated formic acid (purity ≥ 95%) purchased from Sigma Aldrich (St Louis, MO, USA) and stored in 10 mL amber glass vials at 4°C until analysis the next day. The vials had been previously washed with concentrated HCl, and combusted at 500°C to remove impurities.

5.2.4 Analytical methods

The samples were analyzed by on-line solid phase extraction coupled to ultra-high performance liquid chromatography atmospheric pressure chemical ionization tandem mass spectrometry (on-line SPE – UHPLC-APCI-MS/MS). Briefly, the instrumental system consisted of an HTC thermopal autosampler (CTC analytics AG, Zwingen, Switzerland) with a 1 mL loop, and a dual switching-column array. An Accela 600 quaternary pump (Thermo Finnigan, San Jose, CA) was used for the sample loading step onto an on-line Hypersil Gold aQ C_{18} column (20 mm x 2.1 mm, 12 µm particle size). The elution step was achieved using an Accela 1250 quaternary pump (Thermo Finnigan, San Jose, CA) and chromatographic separation performed with a Hypersil Gold column C18 (100 mm x 2.1 mm, 1.9 µm particle size) kept at 55 °C in a thermostated column compartment. A TSQ Quantiva triple-quadropole Mass Spectrometer (Thermo Fisher Scientific, Waltham, MA) with an atmospheric pressure chemical ionisation (APCI) source was used for detection and quantification. The mass spectrometer was operated in selected reaction monitoring (SRM) mode and ionization achieved in positive mode. The method has been described in detail in Morissette M.F. et al. (2015).

5.3 Results and discussion

5.3.1 MP removal on pure maghemite IONP

After 24 h contact time, pure maghemite IONP (dosed at 0.005 – 1.0 g/L) did not adsorb significant amounts ($p > 0.05$) of any of the nine MP spiked in tap water at a concentration of 10 µg/L (Figure 5.1). According to Gu et al. (1994) the hydroxyl moieties found on iron oxides are the functional groups that can interact with the functional groups of organic MP. Rakshit et al. (2013) and Gu et al. (1994) found surface complexation between the iron oxide surface functional groups and the ones of the MP ciprofloxacin as the dominant adsorption mechanism. Although the organic MP tested during our study all varied with respect to functional groups, molecular charge, hydrophobicity and molecular weight (Table 5.2), none of these molecules showed increased affinity to IONP under the tested conditions. Similar results were observed by Shi et al. (2013) who measured 20 times lower adsorption capacities of magnetite IONP (2.62 µg/mg) compared to PAC (48 µg/mg) for the antibiotic ciprofloxacin.

Table 5.1 : Adsorbent properties.

Material	Mass fraction Fe_2O_3[a] %	Saturation magnetization[b] m^2A/kg	pHpzc[c]	Surface area[d] m^2/g	Pore volume[d] Micro mL/g	Meso mL/g	Total mL/g	Mean particle diameter[e] µm
PAC (coal based)	0	0	7.5	1256	0.39	0.15	0.54	23
MPAC-10%	10	5.2	8.6	783	0.24	0.17	0.41	-
MPAC-38%	38	20.1	7.3	748	0.25	0.38	0.63	-
MPAC-54%	54	30.3	7.0	433	0.18	0.55	0.72	23
Fe_2O_3 nanoparticles	100	57.8	-	64	-	-	-	0.017 (17 nm)

[a] Maghemite mass fractions determined from saturation magnetization values and incineration tests, [b] measured with vibrating sample magnetometer, [c] pHpzc : pH at point of zero charge, [d] N_2 adsorption isotherms (NLDFT method) using a Quantachrome Autosorb 1MP, [e] determined in scanning electron microscope measurements and a Mastersizer 3000 (Malvern Instruments Ltd.)

Table 5.2 : Micropollutants, initially spiked concentrations and detection limits.

Compound	Application	MW[a] (g/mol)	Hydro -phobic (+) -philic (-)[b]	Charge at pH 7[c]	Solubility[d] (mg/L)	pKa[e]	$logK_{ow}$[f]	Initial spiked concentrations (µg/L) Colonized adsorbents (bioreactor water matrix) Kinetics	Isotherms	Virgin adsorbents (in tap water) Kinetics	Isotherms	LOD[g] (ng/L)
Diclofenac (DCF)	Anti-inflammatory	296.2	+	-	2.37	4.15	4.51	1.32	470	10.6	352	10
Fluoxetine (FLUO)	Antidepressant	309.3	+	+	50.0	10.15	4.05	10.2	576	-	-	5
Estradiol (E2)	Steroid, hormone	272.4	+	0	3.6	10.4	4.01	4.23	1079	11.5	615	10
Norethindrone (NOR)	Contraceptive	298.4	+	0	7.04	13.09	2.97	5.95	524	11.6	613	10
Atrazine (ATZ)	Herbicide	215.1	+	0	34.7	1.6	2.61	8.34	469	9.12	200	2
Carbamazepine (CBZ)	Mood stabilizer	236.3	+	0	18.0	2.3/14	2.45	7.82	466	10.9	570	2
Deethylatrazine (DEA)	Atrazine metabolite	187.6	-	0	3200	1.4	1.51	8.17	502	9.34	188	10
Sulfamethoxazole (SMX)	Antibiotic	253.3	-	-	610	1.6/5.7	0.89	6.43	509	10.3	518	10
Caffeine (CAF)	Stimulant	194.2	-	0	21600	14	-0.07	20.6	517	10.8	411	10

[a] MW: molecular weight (PubChem 2017),[b] hydrophilic for $LogK_{ow} < 2$, [c] neutral (0), positive (+), negative (-), calculator plugins were used for structure property prediction and calculation, Marvin 16.0, 2016, ChemAxon (http://www.chemaxon.com), [d] solubility at 25 – 27 °C (PubChem 2017) ,[e] retrieved from PubChem 2017 or calculated using Marvin 16.0, 2016, ChemAxon (http://www.chemaxon.com), [f] Octanol-water partition coefficient (PubChem 2017), [g] LOD: limit of detection, determined as the concentration giving a signal to noise ratio of S/N = 3.

5.3.2 MP removal by virgin PAC and MPAC

Maximum adsorption capacities on PAC and MPAC for all pollutants ranged between 1.43 ± 1.75 and 80.7 ± 11.2 µg/mg of adsorbent with the two hormones (E2 and NOR) being the most adsorbable compounds (Figure B-1 a). The lowest affinity for adsorption on either PAC or MPAC was observed for the pesticide ATZ and its metabolite DEA. ATZ and DEA were also the least removed compounds among 10 pollutants in an adsorption study with virgin and colonized PAC carried out by Stoquart et al. (2016) The Freundlich isotherm model was fitted to the data, where the Freundlich constant K_F characterizes the strength of adsorption (Worch 2012), and is therefore often used to characterize adsorption capacities if the Freundlich parameters 1/n are similar. The Freundlich parameter *1/n*, as a measure for adsorption affinity, is < 1 (0.1 - 0.26) for all pollutants and adsorbents which characterizes an isotherm with a concave shape and thus high sorption affinity of the pollutants on PAC and MPAC (i.e. high MP loadings at low concentrations). K_F values for all MP decreased with increasing IONP mass fraction (Figure 5.2 a). The differences between all adsorbents are significant with p-values <0.035 in paired t-tests. The adsorption capacities q_e were subsequently normalized to the mass fraction of PAC (µg MP/mg PAC) instead of total adsorbent mass to account for the different mass fraction of adsorbent in the composite material. The Freundlich isotherm was then refitted to the normalized data and resulted in a high quality of fit ($R^2 > 0.98$, Table B-1 a). K_F values ranged between 2.46 ± 0.21 (DEA) and 28.9 ± 6.5 (E2) (µg/mg PAC)$(L/\mu g)^{1/n}$ (Figure 5.2 b) and Table B-1 a). The values are in the typical range for MP adsorption on MPAC (Table B-2). An ANOVA, carried out on the Freundlich constants K_F of PAC and MPAC, showed that adsorbent type was not statistically significant (p = 0.94). Hence, normalizing the adsorption data by PAC content reveals that lower adsorption capacities on MPAC compared to PAC are mostly due to the lower PAC content in these adsorbents. Although IONP do not contribute to the adsorption of MP, their presence does not lead to a loss of adsorption sites on PAC even at mass fractions as high as 54%. This makes MPAC an adsorbent that is easy to customize with respect to its IONP content and ergo its magnetic properties.

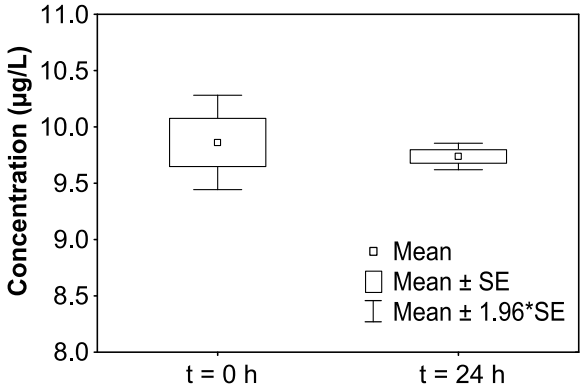

Figure 5.1 : Differences between concentration of all 9 MP before (0 h) and after (24 h) adsorption on 0.005 – 1 g IONP/L are not statistically significant (p = 0.78). SE: standard error.

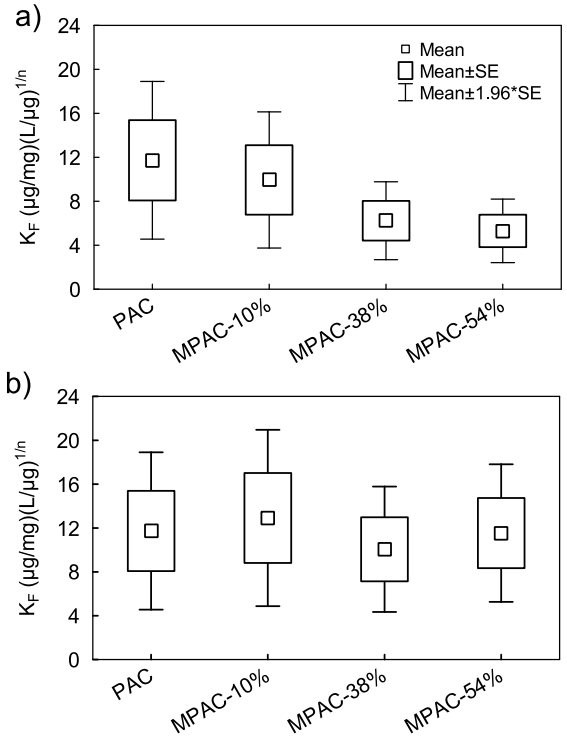

Figure 5.2 : Freundlich constants K_F adsorbent for non-colonized PAC and MPAC expressed as µg pollutant a) per total mass of adsorbent and b) per mass of PAC.

.

The K_F values for PAC and MPAC were best correlated with the solubility of non-charged MP (Figure 5.3): low solubility led to higher K_F values. This is expected as the adsorbability of organic substances onto PAC increases with decreasing solubility (i.e. substance is more hydrophobic) (Worch 2012). Negatively charged DCF and SMX as well as hydrophilic MP such as CAF and DEA had low K_F values. The low adsorbability of DCF and SMX can result from repulsive forces between negative electrostatic surface charges of the adsorbent surface (pH of the water matrix > pHpzc of the adsorbents) and the negative charge of the MP molecules (Edzwald 2011). As for hydrophilic CAF and DEA, hydrophobic interactions between MP and the adsorbent surface are known as the main mechanism for the removal of organic MP on PAC (Ternes and Joss 2006).

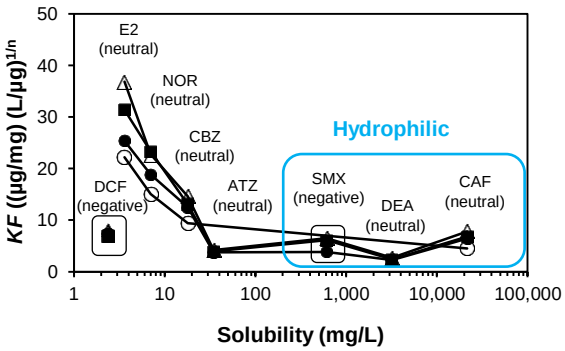

Figure 5.3 : Freundlich K_F-values dependence on MP solubility and charge.

Adsorption kinetics on all non-colonized adsorbents, normalized to PAC content, fitted well a pseudo-second order kinetic model (Ho and McKay 1998). Under the studied conditions (10 mg adsorbent/L and Co = 10 µg MP/L) equilibrium was achieved after a maximum of 60 min on pure PAC and after 2 – 6 hours on MPAC-10%, MPAC-38% and MPAC-54% (Figure B-2 a). Kinetic constants k_2 varied between 0.23 and 3.65 mg/(µg min) for PAC with NOR, CBZ and E2 showing the highest adsorption rates (Figure 5.4). Values of k_2 for the MPAC adsorbents ranged between 0.01 – 0.19 mg/(µg min) (Table B-3 a). These values are in a similar range as results for k_2 values reported for adsorption of diverse MP on MPAC materials in the literature (Table B-2). IONP on the PAC surface and/or reduced PAC content slowed down adsorption kinetics and rate constants were up to two orders of magnitude smaller compared to PAC. Yet, MP removals of > 50 % were achieved in less than 30 minutes on all adsorbents, except MPAC-54% (Figure B-2 a).

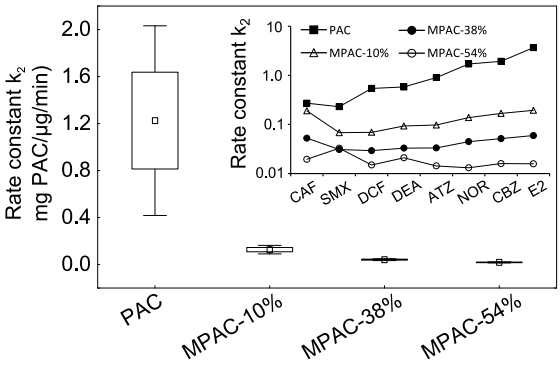

Figure 5.4 : Kinetic constants of the pseudo-second order kinetic model for all MP regrouped by adsorbent type for data (0 – 24 h) normalized to PAC content. Inset (logarithmic scale) shows the kinetic rate constants for each adsorbent grouped by pollutant.

5.3.3 Influence of NOM

Equilibrium adsorption experiments (adsorbent dose of 10 mg adsorbent/L and initial MP concentrations of 10 ± 0.76 µg/L) were carried out with waters containing 0.03 ± 0.01 mg C/L (ultra-pure water), 2.0 ± 0.02 mg C/L (tap water) or 6.25 ± 0.03 mg C/L (raw water). NOM is known as a competitor for MP adsorption on bare PAC (Worch 2012) but has also been discussed in the literature as a promoter for MP adsorption on MPAC in two studies about BPA removal (Koduru et al. 2016, Park et al. 2015). In this study, NOM molecules were competing with MP for adsorption sites on PAC and MPAC: Loadings were significantly lower ($p < 0.005$) in raw water containing a high NOM concentration (6.25 mg DOC/L) compared to tap (1.88 mg DOC/L) and ultra-pure water (0.03 mg DOC). Differences between tap and ultra-pure water loadings were not significant ($p = 0.09$) (s. Figure 5.5). No further insights were gained analyzing NOM concerning its aromatic fraction measured by the $SUVA_{254}$ index (UV_{254} absorbance divided by the DOC) (Weishaar et al. 2003) with values of 1.0, 3.3 and 4.16 L/mg/m for tap, raw and ultra-pure water respectively. The competitive low molecular weight fraction of NOM (assumed as < 500 Da and calculated with LC-OCD analysis, Figure B-3) was similar in tap and raw water with values of 277 and 333 µg DOC/L (ultra-pure water: 24 µg/L) and not correlated to MP adsorption ($R^2 = 0.10$).

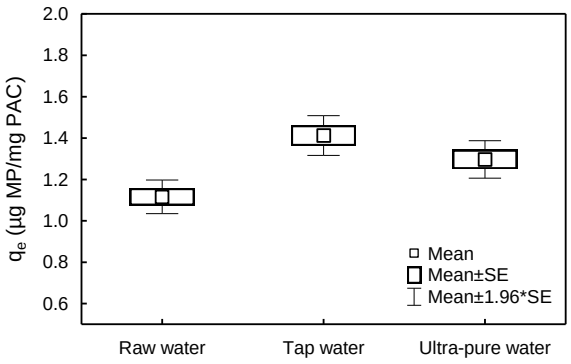

Figure 5.5 : Normalized MP solid concentrations obtained with the 4 adsorbents in different water types. Whiskers represent the 95 % confidence interval and variation is due to the variation in duplicates and between adsorbent types.

5.3.4 The influence of biofilm formation on MP removal

In order to evaluate the residual adsorption capacity of colonized PAC and MPAC for peak events of MP, adsorption isotherms and kinetics were measured on adsorbents aged for 90 days in bioreactors. The colonized adsorbents were characterized by similar amounts of active heterotrophic biomass (48 – 57 µg C/cm³) that had developed on the adsorbents (no statistically significant difference between PAC and MPAC with a p-value of 0.89) and biofilms were visible on the surface of all 4 materials (Lompe et al. 2016). As the current study was carried out for a 24 h period without suppressed microbial activity, biodegradation might have contributed to the reduction of MP during the adsorption isotherm experiments. However, working at a high initial concentration (500 µg/L of each adsorbent) and a mixture of many MP including antibiotics such as SMX without acclimation of the biomass makes biodegradation an unlikely mechanism. Tests with colonized PAC (a pilot plant operated as a CSTR with constant PAC age of 60 days) and an abiotic control carried out by Stoquart et al. (2016) with a mix of 10 MP dosed at a concentration < 10 µg/L showed no significant effect of biodegradation on adsorption results. The mechanism of MP elimination is therefore considered to be dominantly adsorption in this study. To compare results between adsorbents, MP solid concentrations were normalized to the PAC content of the adsorbents (µg MP/mg PAC) as IONP did not contribute to the adsorption of MP. The isotherm data from colonized adsorbents fitted best the Freundlich adsorption model with K_F values (as a measure of adsorption capacity) ranging between 0.05 ± 0.02 (SMX) and 3.29 ± 0.49 (E2) $(\mu g/mg)(L/\mu g)^{1/n}$. Compared to non-colonized adsorbents, the K_F values for the 8 tested MP had

decreased in average tenfold (Figure 5.6). Lebeau et al. (1999) observed that K_F values decreased by factor 3 – 6 when comparing fresh and aged PAC with an average age of 62 days in ultra-pure and natural waters. Besides the diffusion barrier formed by the biofilm itself, aged adsorbents show lower adsorption capacity for MP due to exhausted adsorption sites as a consequence of the pre-loading with NOM and other molecules (Çeçen and Aktas 2012). During the 90 days aging period of the adsorbents in this study, DOC adsorption capacity was exhausted (Figure B-4) and biofilms as well as mineral precipitates (silicium and calcium) were observed on the adsorbent surface using an environmental scanning electron microscope (SEM) Quanta 200 FEG with X-ray microanalysis (Figure B-5). Concerning the parameter *1/n*, Lebeau et al. (1999) observed that values were independent of PAC age. In our experiments, *1/n* values were up to 3 times higher on colonized adsorbents compared to fresh adsorbents.

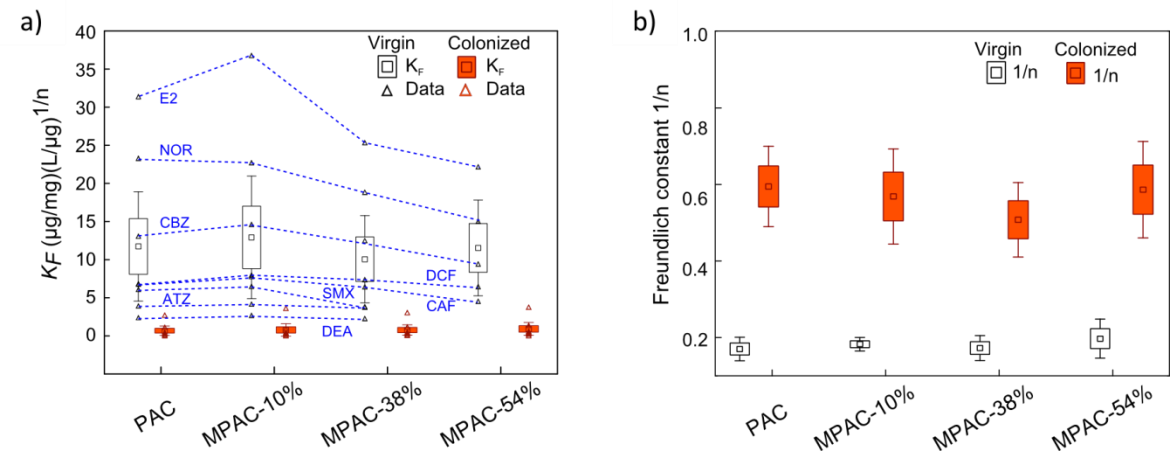

Figure 5.6 : a) Freundlich parameters K_F and b) 1/*n* for MP adsorption on virgin and colonized adsorbents with data normalized to PAC content. Boxes represent standard errors and whiskers the 95 % confidence interval (1.96 x standard error) while the dotted blue lines provide the specific values for individual MP.

To simulate a scenario resembling a typical MP peak event, adsorption kinetics were recorded with low MP initial concentrations of 8.11 ± 5.35 µg/L of each MP. Adsorbent doses of 3.93 ± 0.49 g (dry weight)/L were chosen to represent typical operation conditions of a hybrid PAC-membrane reactor in adsorption/biodegradation mode where PAC concentrations inside the reactor of 1-40 g PAC/L have been reported (Stoquart et al. 2012). The removal kinetics of all MP were fast on PAC and MPAC (Figure B-2 b) and equilibrium was reached for all compounds after a 5 min contact time except for SMX (30 - 60 min). The removal of MP was dependent on

the mass fraction of IONP in the composite. While after only 1 minute all MP were reduced by > 80 % with regular colonized PAC, the colonized composite materials achieved only > 60 % (MPAC-10%), > 40 % (MPAC-38%) and > 17 % (MPAC-54%). As with non-colonized adsorbents, the pseudo-second order kinetic model fitted best the kinetic data (Table B-3 b).

5.3.5 Implications for water treatment

In this study we showed that IONP in MPAC did not contribute to the adsorption of 9 MP representing pharmaceuticals, herbicides and hormones with different properties. Normalizing adsorption capacities to the PAC content in MPAC revealed that IONP did not reduce the intrinsic adsorption sites of the PAC matrix. This shows that MPAC produced via co-precipitation can be customized with respect to its magnetic properties without compromising its adsorption capacity beyond the reduction expected for lower PAC contents. Adsorption capacities for MP on MPAC with a mass fraction of 10 % were not significantly different to PAC while magnetization saturation was high enough for separation. As for PAC, NOM competes with MP for adsorption sites on MPAC. The application of MPAC should consequently be considered as a polishing step after NOM removing treatment steps such as coagulation-flocculation. A residual adsorption capacity for MP exists even for a high adsorbent age of 90 days which makes MPAC a promising adsorbent in a mixed adsorption/biodegradation process.

ACKNOWLEDGEMENTS

The authors are thankful for the technical support of Jacinthe Mailly, Julie Philibert, Mireille Blais, Yves Fontaine and Lin Shen. This work was completed at the Industrial-NSERC Chair in Drinking Water of Polytechnique Montréal with the financial support of its partners, namely the City of Montreal, Veolia Water Technologies Canada Inc., and the City of Laval. All experiments were completed at CREDEAU laboratories, a research infrastructure supported by the Canadian Foundation for Innovation (CFI). LC-OCD measurements were performed at the NSERC IRC in Water Treatment at the University of Waterloo.

CHAPTER 6 ARTICLE 3 - PERFORMANCE OF BIOLOGICAL MAGNETIC POWDERED ACTIVATED CARBON FOR DRINKING WATER PURIFICATION

The purpose of this study was to evaluate MPAC as an adsorbent for the biological hybrid membrane process for which a solid-liquid separation step would help to avoid membrane fouling issues resulting from colonized PAC. We evaluated the presence of IONP within biological reactors and the composite stability. For this purpose we aged MPAC with different IONP content in small bioreactors for over 90 days while monitoring DOC and ammonia removals. Our results suggest that IONP neither inhibit biological growth or DOC and ammonia biological removals nor contribute to significant adsorption of these compounds. The stability of the composite seems to be crucial for industrial applications. This chapter was published as a research article in the journal *Water Research* in 2016.

PERFORMANCE OF BIOLOGICAL MAGNETIC POWDERED ACTIVATED CARBON FOR DRINKING WATER PURIFICATION

Kim Maren Lompe[a*], *David Menard*[b], *Benoit Barbeau*[a]

[a]NSERC Industrial Chair on Drinking Water, Department of Civil, Geological and Mining Engineering, Polytechnique Montreal, P.O. Box 6079, Downtown Station, Montreal, QC, Canada

[b] Department of Engineering Physics, Polytechnique Montreal, Montreal, Qc, Canada

***** corresponding author. Tel: +1 514 340-4711 ext. 2983.

E-mail: kim-maren.lompe@polymtl.ca (Kim Maren Lompe)

ABSTRACT

Combining the high adsorption capacity of powdered activated carbon (PAC) with magnetic properties of iron oxide nanoparticles (NPs) leads to a promising composite material, magnetic PAC or MPAC, which can be separated from water using magnetic separators. We propose MPAC as an alternative adsorbent in the biological hybrid membrane process and demonstrate

that PAC covered with magnetic NPs is suitable as growth support for heterotrophic and nitrifying bacteria. MPAC with mass fractions of 0; 23; 38 and 54 % maghemite was colonized in small bioreactors for over 90 days. Although the bacterial community composition (16s rRNA analysis) was different on MPAC compared to PAC, NPs neither inhibited dissolved organic carbon and ammonia biological removals nor contributed to significant adsorption of these compounds. The same amount of active heterotrophic biomass (48 µg C/cm³) developed on MPAC with a mass fraction of 54 % NPs as on the non-magnetic PAC control. While X-ray diffraction confirmed that size and type of iron oxides did not change over the study period, a loss in magnetization between 10 % and 34 % was recorded.

KEYWORDS

Iron oxide nanoparticles, magnetic powdered activated carbon, heterotrophic biomass, biological treatment, hybrid membrane process

6.1 Introduction

Magnetic PACs (MPAC) are composite materials made of a non-magnetic structure such as PAC and magnetic labels such as nano-scale iron oxides (mainly maghemite (γ-Fe_2O_3) and magnetite (Fe_3O_4)) which are responsible for the magnetic behaviour of the composite (Oliveira et al. 2002). These novel adsorbents have gained attention in the drinking water community due to their good magnetic separability on the one hand as well as their promising adsorption properties for drinking water contaminants on the other hand. So far, these composite materials have been applied in pure adsorption studies at lab-scale, e.g. as adsorbent for natural organic matter (Kondo et al. 2010, Park et al. 2015) or against contaminants of emerging interest such as herbicides (Castro et al. 2009), insecticides (Zahoor and Mahramonlioglu 2011) and pharmaceuticals (Shi et al. 2013).

Recently, Zahoor (2014) proposed MPAC as an alternative to the use of PAC in the hybrid membrane process (HMP) which combines a high concentration PAC contactor (1 to 40 g/L) with low pressure membranes. In these processes PAC removes adsorbable dissolved contaminants such as taste and odour compounds or organic micropollutants, whereas the membrane removes particulate contaminants such as *Cryptosporidium* or other protozoan pathogens (Lebeau et al. 1998, Stoquart et al. 2012). When HMPs operate with PAC age > 20 to

30 days, heterotrophic and nitrifying bacteria colonize the PAC particles, allowing for removal of not only adsorbable, but also biodegradable dissolved contaminants such as biodegradable DOC (BDOC) and ammonia (Leveillé et al. 2013, Markarian et al. 2010, Stoquart et al. 2014a, Stoquart et al. 2014b) Although HMPs with PAC age < 7 days exist in full scale processes, such as the CRYSTAL® and Opaline™ S, abrasion and severe membrane fouling resulting from the direct contact of the immersed membranes with highly concentrated and colonized PAC have limited so far the industrial application of biologically working HMPs (Leveillé et al. 2013, Stoquart et al. 2012). Alternatively, Zahoor (2014) tested an adsorption/ultrafiltration hybrid process at lab-scale where problems related to cake formation and membrane fouling where avoided using magnetic separation to provide a low-particle membrane feed. Other advantages of MPAC over PAC arise from their ease of separation. For one, it is possible to recirculate the adsorbent back into the contactor in order to maintain a high adsorbent age which translates into more efficient carbon usage (i.e. higher exhaustion) before disposal. Finally, high MPAC age offers the opportunity to operate HMPs in biological mode.

However, applying MPAC in the HMP in mixed adsorption/biodegradation raises the question if nano-size iron oxides on the surface of PAC are deleterious to biological activity. To the best of our knowledge, such evaluation has not yet been carried on and little is known about the effects of iron oxide NPs on heterotrophic and nitrifying microorganisms. In contrast to larger particles, iron oxide NPs below a critical size of 30 nm (Auffan et al. 2009) are highly reactive at their surface and have been shown to interact with the membrane of bacterial cells (Auffan et al. 2008, Luyts et al. 2013). When *E. coli* bacteria were incubated with 100 mg/L of magnetite and maghemite NPs, the latter were observed to attach to the cell membranes (Auffan et al. 2008) and cell damage resulting from oxidative stress was identified as a possible mechanism of toxicity (Auffan et al. 2009). Oxidative stress can result from the disturbance of the cell's electron or ionic transport chains by reactive oxygen species (ROS) that form via redox transformations and dissolution of the atoms at the surface of the NPs (Auffan et al. 2008, Auffan et al. 2010). Low to moderate cytotoxicity was observed towards pure culture of planktonic bacteria such as *E. coli* (Auffan et al. 2008, Hu et al. 2009) and *Ps. aeruginosa* (Kafayati et al. 2013) at concentrations exceeding 500 to 700 mg/L Fe_3O_4 or Fe_2O_3 NPs. Arakha et al. (2015) observed antimicrobial effects of magnetite NPs towards *E. coli* and *B. subtilis* even at 50 µM (11.6 mg/L). Microcosm tests on soil bacterial communities carried out by He et al. (2011) and Vittori Antisari et al.

(2013) with 0.14 to 1260 mg/kg Fe_3O_4 NPs (10 to 50 nm) showed no or low inhibitory effects, a result which may be explained by the formation of extracellular polymeric substance (EPS) and other protection strategies of sessile bacteria. Although the literature indicates lower cytotoxicity of magnetic NPs compared to other metal NPs such as elemental Ag, Zn and Cu or metal oxide such as TiO_2, ZnO, CuO or NiO (Dinesh et al. 2012, Wang et al. 2010), additional studies are necessary to determine the applicability of MPAC in biological reactors for drinking water treatment.

Another aspect to consider is the long-term stability of magnetic adsorbents which is crucial for industrial applications where changes in magnetization or dissolution of iron oxide NPs are not desired. Auffan et al. (2008) found that magnetite NPs were subjected to structural modifications especially in the presence of bacteria. The surface of magnetite NPs was entirely oxidized to a more stable iron species resembling maghemite. According to Mohan et al. (2011) magnetite NPs are generally not very stable at ambient conditions and can easily be oxidized to maghemite. This phenomenon is related to the high mobility of electrons within the Fe(II)/Fe(III) structure of magnetite and the release of Fe(II) ions into solution (Auffan et al. 2008). As maghemite is a ferrimagnet with similar magnetic properties as magnetite (Cornell and Schwertmann 2003), oxidation should not lead to a loss of magnetization and is therefore no constraint for MPAC applications. While Lee et al. (2005) reported a decrease of nearly 50 % in saturation magnetization of their magnetic adsorbent after 5 months, Safarik et al. (2013) observed a stable magnetic response of different magnetic adsorbents containing magnetite after several months. Yang et al. (2008) also confirmed magnetic stability of a rice husk based magnetic carbon that was stirred in water for 2 months. Dissolution of iron oxide NPs is pH dependent and was studied by Zahoor and Mahramonlioglu (2011) in a range of pH 1 to 8. Dissolution occurred below pH 4.8 leading to a loss of iron content in MPAC. With typical pH values between 6 and 8 in drinking water treatment processes, dissolution of magnetic NPs is therefore not expected.

While previous studies on MPACs focussed solely on the adsorption properties of MPACs, this study was designed to evaluate its performances both as an adsorbent and as a support for biological growth for its application within the HMP. The research question of this study can be stated as follows: Do iron oxide NPs on the PAC surface prevent biological growth or inhibit activity of heterotrophic and nitrifying bacteria?

Five small bioreactors containing MPACs with increasing iron oxide mass fractions (0 %, 23 %, 38 % and 54 %) were fed for 90 days with nutrient enriched, de-chlorinated tap water. DOC and ammonia removals were monitored weekly whereas active heterotrophic biomass and the composition of the bacterial population were only measured at the end of the study. The originality of this project lies in (i) the application of a magnetic adsorbent in a mixed adsorption/biological drinking water treatment process, (ii) the systematic evaluation of the impact of iron oxide NPs content on biomass development and (iii) the evaluation of the potential degradation of the magnetic adsorbent in a biological process.

6.2 Materials and Methods

6.2.1 Magnetic powdered activated carbon

Commercially available Aquasorb® MP23 (Jacobi, formerly Picahydro MP23 from PICA^{TM}) was used in the colonization assay and as a base material for MPAC preparation. This mineral based PAC with an iodine number of 900 mg/g and a median volume diameter of 15 to 35 µm was washed and dried before usage to reduce its basicity below pH 8.0. This carbon has been chosen among others in adsorption pretests for its good DOC removal from the water matrix used during this study (data not shown).

MPAC was prepared by an alkaline co-precipitation process as proposed by Oliveira et al. (2012) and then characterized for its physico-chemical properties (Table 6.1). Three different MPACs with mass fractions of 23 %, 38 % and 54 % iron oxide NPs were prepared (hereafter referred to as MPAC-23%, MPAC-38% and MPAC-54%). The NPs on the PAC surface mainly consisted of maghemite and had an average particle size of 17 nm, as determined by X-ray diffraction (XRD) analysis, using the Scherrer formula for the average crystallite diameter. According to the NP mass fraction, the apparent density of the magnetic adsorbents varied between 0.40 g/cm³ and 0.79 g/cm³.

Table 6.1 : Characteristics of the PAC and MPAC adsorbents.

Parameters	Units	PAC	MPAC	Methods
Commercial name		Picahydro MP23 (mineral base)		N.A.
Iron oxide mass fraction	%	0	23%; 38% and 54%	Thermo-gravimetric analysis
Type of iron oxide	N.A.	N.A.	Maghemite	XRD, D5000 Bruker, Sol-X detector, Co Kα
Porosity (Total)	cm^3/g	0.54	0.41; 0.63; 0.72	BET Isotherm (Quantachrome Autosorb 1MP)
Surface area	m^2/g	769	521; 575; 417	
Magnetization saturation	m^2A/kg	N.A.	5.20; 20.1; 30.3 (57.8 pure NP)	Vibrating sample magnetometer (VSM)
Remanent magnetization	m^2A/kg	N.A.	0.56; 0.13; 0.22 (0.32 pure NP)	
Type of magnetic behaviour	N.A.	N.A.	Superparamagnetic	
Bulk density	g/cm^3	0.40	0.51; 0.62; 0.79	Calculated & technical info. provided by Pica™

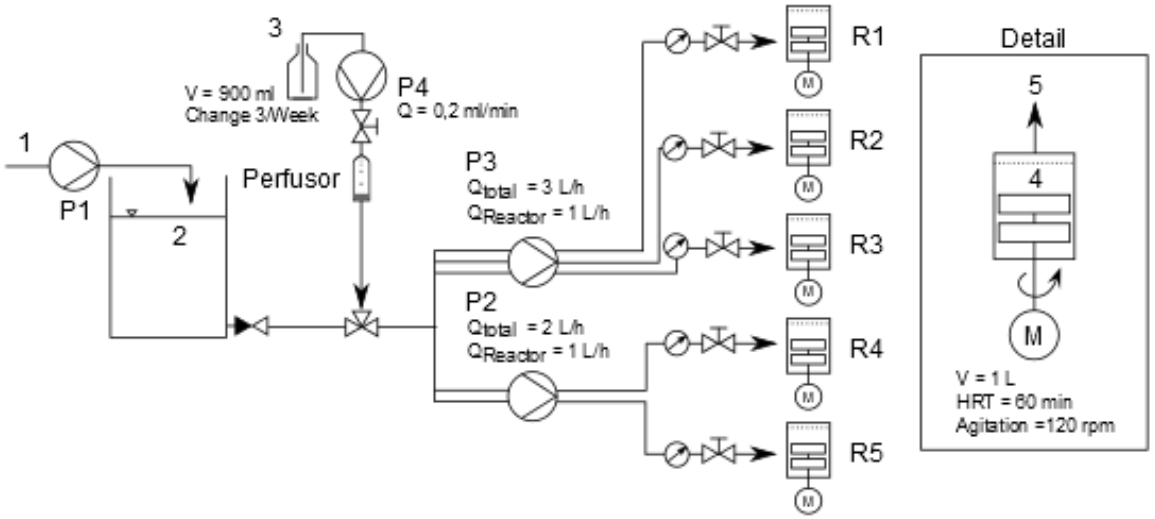

Figure 6.1 : Schematic of the bioreactor setup. 1: Influent dechlorinated tap water; 2: Reservoir (1.7 m^3) for temperature adjustment; 3: Nutrient reservoir (autoclaved); 4: bioreactor with 10 µm nylon mesh strainer and agitator; 5: Effluent water.

6.2.2 Colonization study

Five PAC/MPAC bioreactors with a volume of 1 L each were equipped with blade stirrers (120 rpm) to prevent settling of the adsorbents. For the current study, magnetic separation of the MPAC was not performed. Instead, the adsorbents were kept in the reactor using a 10 µm nylon mesh strainer located on the effluent (at the top of the reactors, s. Figure 6.1). Increasing pressure of the reactors due to blockage of the strainer required regular opening of the reactors and manual cleaning every 2 days. The reactors were fed continuously at a flow rate of 1 L/h (HRT = 1 h) for 43 days which was subsequently decreased to 0.25 L/h (HRT = 5 h) for a period of 35 days once the pilot operated in biological mode in order to reduce maintenance time. Two weeks before the end of the study, the flow rate was again increased to 0.5 L/h (HRT = 2 h).

Table 6.2 : Pilot influent characteristics.

Parameters	Units	Average Values (+/- std dev.)
DOC (natural)	mg/L	2.20 ± 0.14
BDOC (natural)	mg/L	0.30 ± 0.12
UVA_{254}	cm^{-1}	0.022 ± 0.003
NH_4^+-N (natural)	mg/L	< 0.005 (detection limit)
Chlorine	mg Cl_2/L	< 0.01 (detection limit)
Alkalinity	mg $CaCO_3$/L	86
Hardness (total)	mg $CaCO_3$/L	134
pH		8.0 ± 0.06
Temperature	°C	22 ± 0.28
Spiked Acetate	mg C/L	0.31 ± 0.14
Spiked Ammonia	mg N/L	0.06 ± 0.06 (peak doses up to 0.2 due to problems with the dosage pump)
Spiked Phosphate	mg P/L	0.003 (not measured)

The influent water (dechlorinated tap water from the city of Montreal) exhibited an average DOC and BDOC of 2.2 mg C/L and 0.3 mg C/L, respectively. To promote the growth of heterotrophic and nitrifying bacteria, this matrix was amended with a nutrient solution by adding low concentrations of acetate (0.3 mg C/L) as carbon source as well as NH_4Cl (60 µg N/L) and

K_2HPO_4 (3 µg P/L) as nitrogen and phosphate sources to yield a C:N:P ratio of 100:20:1. The water temperature and the pH remained constant at 22 ± 0.5°C and 8.0 ± 0.1, respectively.

Two reactors contained 10 g/L of unmodified PAC (control reactors) whereas the remaining three reactors contained MPAC with increasing percentage of iron oxide. The concentration of MPAC in all reactors was adjusted to correspond to an equivalent PAC concentration of 10 g/L which involves adding higher mass concentrations of the MPACs with higher iron oxide content, to compensate for the density differences. Working with the same concentration of PAC in each reactor was chosen to facilitate the evaluation of biomass development as a function of NP concentration. It also simplified the analysis of adsorption performance. Finally, one has to keep in mind that the volume of MPAC does not significantly change when covered by iron oxides, even for a high load of NPs (due to the high density of iron oxide compared to PAC). Therefore, it was not expected that the surface for colonization on the MPAC was significantly increased by the presence of iron oxides.

6.2.3 Analytical methods

DOC samples of the pilot's influent and effluent were collected twice per week and filtered through 0.45 µm PES filters (Pall Supor® -450), previously rinsed with 1 L of Milli-Q water. DOC was analyzed in duplicate with a TOC meter (Sievers 5310 C). The limit of detection of this method is 0.07 mg C/L and the limit of quantification is 0.15 mg C/L. The UV absorbance (UVA_{254}) of the filtered sample was measured with a UV spectrophotometer. BDOC was measured only once in triplicate to confirm the BDOC concentration of Montreal's tap water (i.e. the influent) using the method developed by Servais et al. (1989) modified as described in Markarian et al. (2010) (detection limit 0.12 mg C/L). Ammonia nitrogen (measured as N) in the pilot's influent and effluent was measured once per week and analyzed in triplicate using the indophenol method #T90-015 (AFNOR 1990) with a detection limit of 5 µg N/L. Furthermore, turbidity, dissolved and total iron were measured on a weekly basis. A summary of the applied analytical method can be found in Table 6.4.

6.2.4 Quantification of biomass on PAC and MPAC particles

Colonized PAC and MPAC suspensions were recovered from the bioreactors at the end of the study (95 days) and filtered immediately through an 8 µm paper filter (Grade 40, Whatman®) to

retain a dense cake of PAC or MPAC. The humidity of the filter cake was analyzed according to the standard method 2540 B (APHA 2012). The density of the wet filter cake was measured in triplicate by weighing a known volume of the cake material.

The active heterotrophic biomass was analyzed the same day using the potential glucose activity technique (Servais et al. 1991). This method was previously tested on PAC (Stoquart et al. 2014a) and consists of measuring the maximal heterotrophic activity derived from the formation of $^{14}CO_2$ (detected by liquid scintillation) produced by the respiration of radio labelled glucose. All samples were prepared as triplicates and the amount of respired glucose converted to bacterial biomass with a conversion factor of 1.1 µg C of bacterial biomass per nanomole glucose respired per hour. Bacterial biomass, expressed as µg C, was converted to concentration by assuming $2.16 \cdot 10^{-8}$ µg C per bacterium (Servais et al. 1991).

6.2.5 Bacterial community analysis

Upon sample collection from the reactors, biomass was extracted from the recovered adsorbents using a method developed by Camper et al. (1985). A known quantity of humid PAC or MPAC was homogenized in a sterilized blender (Waring Laboratory Science, model 7012s) at 16,900 rpm and 4°C with a mixture containing 10^{-6} M Zwittergent, 10^{-3} M EGTA (ethylene glycol-bis-(β-aminoethyl ether)-N,N,N', N'-tetraacetic acid), 0.01 M Tris buffer (pH 7) and 0.1 % peptone. The suspension was first filtered through an 8 µm sterile filter (SCWP04700, Millipore) to separate PAC from the suspension of bacterial cells, then concentrated on a 0.45 µm sterile filter (HAWG047S6, Millipore) and finally stored in sterile DNA extraction tubes at -25°C until extraction. DNA extraction was performed directly on the filters using a bead beating method followed by ammonium acetate precipitation and ethanol washes as described by Bédard et al. (2014). Extracted DNA was sent to Research & Testing Laboratory LLC (Texas) for the microbial diversity analysis. MiSeq (Illumina) next generation sequencing technology was chosen using primers 515F (5'-GTGCCAGCMGCCGCGGTAA-3') and 806R (5'-GGACTACHVGGGTWTCTAAT-3') targeting the V4 region of the bacterial and archae 16s rRNA gene. Sequences were de-noised, quality checked and aligned against an in-house database as well as the Silva Bacteria reference database. With higher resolution on the class level, the in-house database results are presented.

Table 6.3 : PAC and MPAC concentrations in the bioreactors.

Parameters	Units	R 1	R 2 (duplicate)	R 3	R 4	R 5
Adsorbent type		PAC	PAC	MPAC-23%	MPAC-38%	MPAC-54%
Fe_3O_4 mass fraction	%	0	0	23	38	54
PAC mass fraction	%	100	100	77	62	46
Mass PAC	g	10	10	10	10	10
Mass NPs	g NPs	0	0	3.00	6.13	11.74
Concentration of adsorbent	g/L	10	10	13.00	16.13	21.74

6.2.6 Imaging biofilm and bacteria on PAC and MPAC

Biofilm on colonized PAC and MPAC samples was imaged using an environmental scanning electron microscope (SEM) Quanta 200 FEG. Samples were taken 2 hours prior to analysis letting water evaporate under the fume hood. Once every two weeks, colonization on PAC and MPAC was qualitatively monitored by fluorescence microscopy using the viable/dead Baclight™ staining kit (Boulos et al. 1999).

6.2.7 Analyzing MPAC stability

Magnetic properties of colonized PAC and MPAC samples, dried at 105°C, were analyzed and compared to the values of the non-colonized material. The type of iron oxide and crystal size of the NPs in dried samples of MPAC-54% before and after colonization were evaluated using XRD (specification see Table 6.1).

6.2.8 Statistical analysis

The statistical significance of differences between the adsorbent types concerning DOC, UVA_{254} and ammonia removals as well as biomass development were evaluated using paired t-tests for independent samples performed in Statistica version 12 (StatSoft Inc., USA).

Table 6.4 : Analytical methods.

Parameter	Description	Reference
DOC	UV/Persulfate oxidation method with a TOC meter (5310 C). Samples are filtered through 0.45 µm PALL Supor450 PES filters, duplicate analysis	Standard Methods APHA 2012, 5310-C
BDOC	DOC sample (filtered) incubated with indigenous bacteria in pre-filtered raw water and nutrients for 30 days in the dark, triplicate analysis	Servais et al. (1989)
$N\text{-}NH_4$	Indophenol colorimetric method, triplicate	AFNOR 1990, NF T 90-015
$N\text{-}NO_3$ and $N\text{-}NO_2$	Colorimetric method. Detection of the nitrite-complex at 540 nm with a UV spectrometer. Nitrate reduction by shaking with cadmium, triplicate analysis	Jones (1984)
UVA_{254}	Detection at 254 nm with a UV spectrometer. Sample pre-filtered through 0.45 µm PALL Supor450 PES filters, duplicate analysis	Standard Methods APHA 2012, 5910B
Alkalinity	Titration method, duplicate analysis	Standard Methods APHA 2012, 2320B
Turbidity	Nephelometric method, Hach turbidimeter, model 2100 An, triplicate analysis	Standard Methods APHA 2012, 2130B
Fe-total	ICP-OES, model iCAP 6000	Adapted from EPA 200.7 and CEAEQ Ma. 203-Mét. 3.2
Fe-dissolved	ICP-OES, model iCAP 6000. Sample pre-filtered through 0.45 µm PALL Supor450 PES filters	
Humidity of the filter cake	Drying known mass of wet filter cake at 105°C, duplicate analysis	Standard Methods APHA 2012, 2540 B
Heterotrophic active biomass	Potential glucose respiration (PGR) using radio labelled glucose, triplicate analysis	Servais et al. (1991)
Detaching biomass from PAC particles	Separating biomass from particles with a blender at 16,900 rpm	Camper et al. (1985)
Live/dead bacteria visualization	Epifluorescence microscopy using Baclight™ staining kit	Boulos et al. (1999)
Extracting DNA	Bead beating method followed by ammonium acetate precipitation and ethanol washes	Bédard et al. (2014)
Gene amplification	Primers 28F – 388R and 515F – 806R for the bacterial and archae 16S rRNA gene	Research & Testing Laboratory LLC (Texas)
16s rRNA gene analysis	MiSeq (Illumina) next generation sequencing technology with Silva Bacteria database	Research & Testing Laboratory LLC (Texas)

6.3 Results

6.3.1 Removal of organic matter

The average DOC in the pilot feed water was 2.56 ± 0.25 mg C/L (standard deviation) and was composed of 2.20 ± 0.14 mg C/L of natural DOC (86 % of the DOC) and of 0.35 ± 0.21 mg C/L of easily biodegradable/poorly adsorbable acetate (14 %). DOC removals in the five bioreactors are presented as a function of the carbon usage rate (CUR = L of treated water per g of activated carbon inside the reactor) (Figure 6.2). At the beginning of the study (first measurement after 4 days of operation) 60 % of the inlet DOC was removed via adsorption by un-colonized PAC and MPAC. The residual fraction of 40 % of the incoming DOC is most likely composed of poorly adsorbable DOC from the tap water (Saint Lawrence River treated with direct filtration) as well as acetate which has a low affinity for activated carbon (data not shown).

For all five reactors, the removal capacity of the adsorbents decreased slowly with increasing CUR. Removals of 20 to 30 % were achieved under steady state which was reached after 72 L/g of PAC (after approx. 40 days). This performance was maintained over the following month of operation. Four data points at the end of the study show removals as high as 50 %. However, this performance was related to a problem with the dosing pump that resulted in acetate concentrations in the feed water reaching as high as 1.4 mg C/L for a short period. At the reactor outlets, the usual concentration of 1.8 mg C/L was measured indicating that acetate was eliminated completely via biodegradation explaining the higher measured performances.

A one-way ANOVA performed on magnetic adsorbents and PAC confirms that DOC removal is neither enhanced nor reduced by the iron oxides on MPAC (p-value = 0.72). In addition, no difference in the time evolution was observed between MPAC and PAC as all reactors attain the steady state after 72 L/g (or 40 days).

The UVA_{254} found in the feed water was low (on average 0.022 cm^{-1}). The dosage of acetate does not increase this value as UV light at 254 nm is absorbed mainly by natural organic carbon with an aromatic structure or compounds that have a conjugated C=C double bond Edzwald (2011). Similar to DOC removals, UVA_{254} was removed up to 60 % to 70 % in the beginning and then decreased steadily until it stabilized at 30 % to 35 % removal after approx. 35 to 40 days (CUR of 65 to 72 L/g). UVA_{254} removal is not affected by the adsorbents' iron oxide content as paired t-

tests comparing reactors containing PAC and MPAC showed no significant differences (all p-values > 0.05). In general, UVA_{254} removals were slightly higher than DOC removals, which is concordant with results from previous studies (Markarian et al. 2010, Oh et al. 2007) and is explained by the selective adsorption of these components on activated carbon.

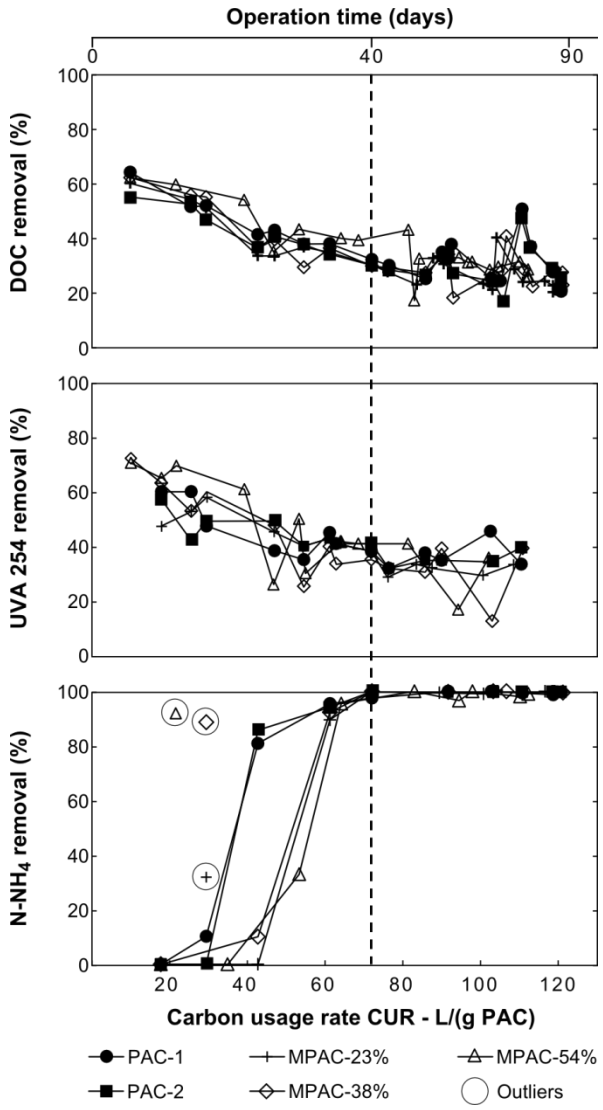

Figure 6.2 : Removals of : DOC, UVA_{254} and $N\text{-}NH_4$ in 5 bioreactors with 10g/L of PAC and variable iron oxide content. The dashed line represents the beginning of the steady state after approx. 40 days.

6.3.2 Removal of ammonia

It has been shown that PAC (5 to 10 g/L) can partially adsorb ammonia (Stoquart et al. 2014b), but the adsorption capacity for ammonia is low due to the non-polar surface that is not attractive for polar molecules such as ammonia (Halim et al. 2010). Consequently, as expected, ammonia nitrogen (60 µg N/L) was not removed in any of the five reactors at the beginning of the study at which time adsorption was the only removal mechanism. The first sample was collected after one week of operation which was sufficient to exhaust the ammonia adsorption capacity of all the sorbents under investigation. The first recorded ammonia removal started after approx. 20 days (or 18 L/g) in reactors R1 and R2 that contained non-modified PAC and reached 100 % removal after approx. 33 days (70 L/g). In the three reactors containing MPAC ammonia removal started 6 days later but also reached complete removal after 33 days. During a short period of 12 days at the end of the study (data not shown) the ammonia dosage was accidentally too high and inlet concentrations as high as 150 to 200 µg N/L were fed to the reactors. However, in spite of the much higher inlet concentration, ammonia removal remained at 100 % in all 5 reactors.

Nitrate and nitrite were analyzed on five occasions in the last two months of operation in order to confirm the presence of nitrifying bacteria. Nitrate was present in the feed water at a concentration of 0.30 ± 0.05 mg N-NO_3/L whereas nitrite was not detected (< 0.5 µg N/L). In the pilot's effluent, nitrate was on average higher than the inlet concentration (0.37 ± 0.05 mg N/L vs. 0.30 ± 0.05 mg N/L, $p = 0.002$) whereas nitrite remained low and close to the detection limit (0.5 µg N/L). Therefore, we can conclude that nitrification was the most likely ammonia removal mechanism within the reactors.

6.3.3 Bacterial biomass density in the bioreactors

Bacterial biomass was measured as respired nmole of glucose per gram of wet filter cake at the end of the study. Due to the different densities of the adsorbents resulting from the different magnetic NP loads, an adsorbent mass-based comparison is misleading. The respiration values were expressed therefore per volume of adsorbent. As the five reactors were operated with the same adsorbent concentration in terms of PAC content (10 g/L, *cf.* Table 6.3) and given that the volume of MPAC particles is barely higher than that of PAC, each reactor contained the same number of adsorbent particles which served as support for bacterial growth. Previous studies have

shown that biomass density on PAC is a function of nutrient limitation and available support area for colonization (Markarian et al. 2010, Stoquart et al. 2014a). As equal support area and nutrient availability were presumably maintained in each reactor, any difference in biomass activities would be the result of the inhibitory effect of iron oxide NPs. To enable comparison with the scientific literature PGR values expressed as nmole glucose/cm^3 of adsorbent and were further converted to µg of bacterial carbon per volume of adsorbent (µg C/cm^3) for each adsorbent type (see methods section). Heterotrophic bacterial activities (Figure 6.3) were found to be in the range of 48 to 57 µg C/cm^3. Comparing unmodified PAC to MPAC containing the highest mass fraction of magnetic NPs (54 %) reveals that the active heterotrophic biomass was not statistically different between the two materials ($p = 0.89$). Therefore, the presence of iron oxides did not significantly inhibit heterotrophic biomass activity.

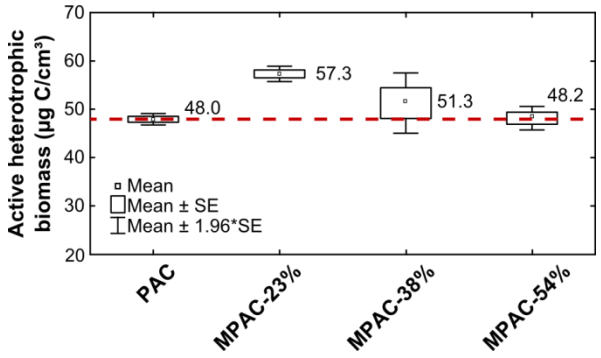

Figure 6.3 : PGR rates and measured active heterotrophic biomass on PAC and MPAC expressed as µg C/cm^3 adsorbent.

6.3.4 Visualizing colonisation on MPAC

Images were taken with the environmental SEM to document surface characteristics of (i) non-modified PAC, (ii) virgin MPAC-54% and (iii) MPAC-54% after 95 days of use. Magnetic NPs on the carbon surface form a spongy crust (Figure 6.4 b) which was covered by biofilm at the end of the 3 months study (Figure 6.4 c). Green-fluorescent bacteria (i.e. viable as defined with this technique) were detected on both PAC and MPAC particles in Baclight™ tests. Bacteria were visible as light dots on the particles' surface (Figure 6.4 d). No qualitative differences were observed between colonized PAC and MPACs (data not shown).

6.3.5 Analysis of the bacterial community

The different bacterial communities found on the five colonized PAC and MPAC samples are presented with respect to the taxonomic class level (Figure 6.5). The number of analyzed sequences varied between 9,291 and 21,923, but was normalized to approx. 9,100 - 9,600 in each sample. The number of identified operational taxonomic units (OTUs) (sequences sharing >97 % identity) are a measure of community richness. PAC-1, PAC-2, MPAC-23% and MPAC-54% are in the same range with 67 to 96 OTUs while the richness of MPAC-38% is distinctively lower (11 OTUs). Also, 46 % of all sequences of MPAC-38% belong to unclassified *Cyanobacteria* and this sample was therefore not used for further interpretation. *Betaproteobacteria* was the major group (74 to 85 %) in samples PAC-1, PAC-2 and MPAC-23% followed by *Alphaproteobacteria* (7 to 12 %). These samples form a group of very similar communities (Figure 6.5). Sample MPAC-54% is distinctively different from the first three samples showing only 11 % *Betaproteobacteria*, but 50 % *Alphaproteobacteria* and 33 % *Proteobacteria* of unknown class. On the genus level of *Betaproteobacteria* mainly *Variovorax* from the family *Comamonadaceae* were found. *Alphaproteobacteria* were mainly related to the genera Sphingomonas and *Afipia*. These genera have previously been found in BAC filters (Magic-Knezev et al. 2009, Niemi et al. 2009).

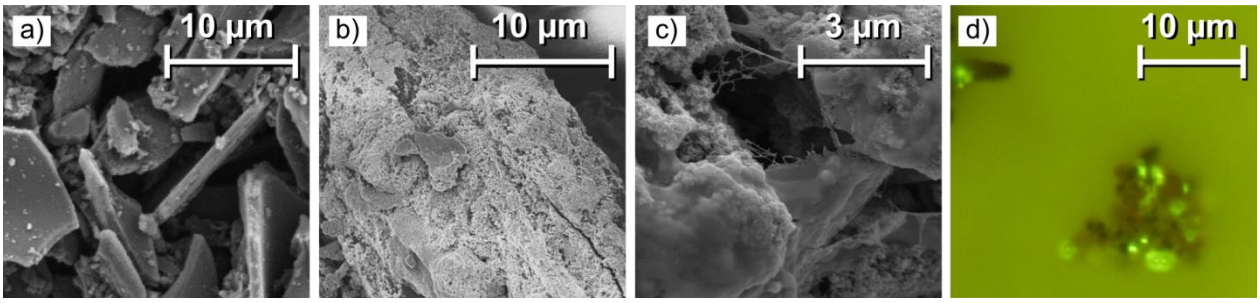

Figure 6.4 : SEM images of (a) virgin PAC, (b) virgin MPAC-54%, (c) 95 days old colonized MPAC-54% and (d) Baclight™ image of living/dead bacteria on MPAC-54% (cells with intact membranes are green).

Table 6.5 : Number of analyzed sequences and OTUs.

Sample	No. of sequences	No. of OTUs
PAC-1	9097	90
PAC-2	9287	88
MPAC-23%	9247	96
MPAC-38%	9593	11
MPAC-54%	9159	67

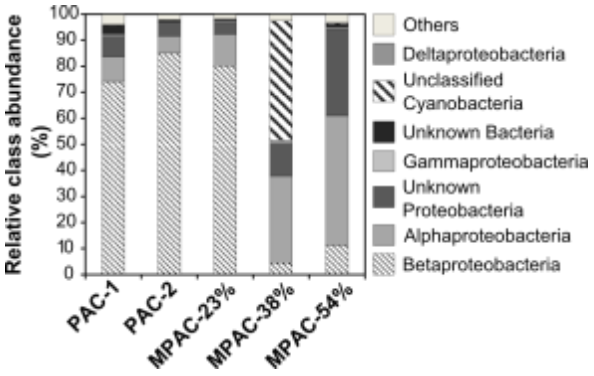

Figure 6.5 : Relative abundance of bacterial classes in biomass extracted from PAC and MPAC samples.

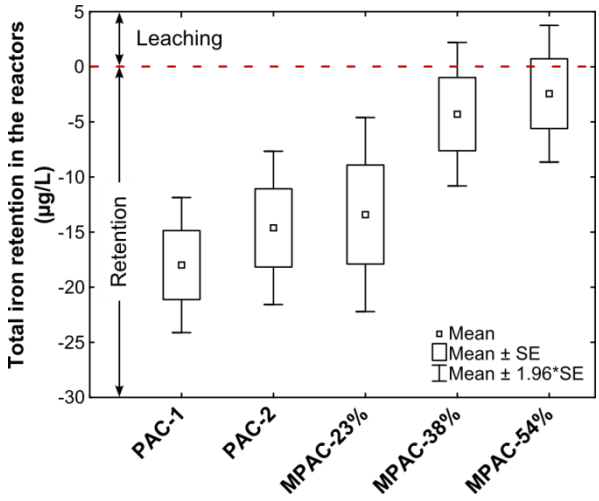

Figure 6.6 : Total iron retentions (calculated as the difference between outlet and inlet) over the whole study period of > 90 days. N = 120 samples per reactor.

6.3.6 Stability of the magnetic adsorbent

The stability of the magnetic coating of MPAC was assessed by performing routine iron monitoring of the reactors influent and effluent. Iron analysis (ICP-OES, see Table 6.4) of the feed water revealed low total iron concentrations (10 to 50 µg/L) and negligible dissolved iron concentrations (< 10 µg/L = LOD). Dissolved iron concentrations in the reactor outlet were < LOD. Figure 6.6 presents the net removals of total iron over the entire study period for each reactor. Reactors containing unmodified PAC or MPAC with low NP load such as MPAC-23% always showed lower effluent than influent concentrations and were thus providing a net removal of iron across the process. On the other hand, the reactors MPAC-38% and MPAC-54% had a neutral impact on iron release (i.e. no release and no retention, $p = 0.14$). Compared to the

unmodified PACs, MPAC-54% (the material with the highest iron oxide content) released only 6.8 mg (0.08 % of the initial iron content in this reactor) over the 95 days of operation based on the measured total iron concentration.

After 90 days of operation, magnetic saturation values were reduced by 10.1 % (MPAC-54%), 17.5 % (MPAC-38%) and 34.6 % (MPAC-23%) compared to the values before colonization (Figure 6.7). XRD analysis of the dried samples did not show any change of the iron oxide type on MPAC. The predominant phase was maghemite before and after colonization with major diffraction peaks at d_{hkl} values of 0.2509 nm, 0.1475 nm, 0.2955 nm and 0.1607 nm which are close to literature values for maghemite with 0.2514 nm (313), 0.1474 nm (440), 0.2950 nm (220), and 0.1604 nm (513) respectively. The mean diameter of the NPs remained identical (13 to 17 nm). However, the percentage of amorphous versus crystalline phase in MPAC-54% increased slightly from 57 % to 63 % indicating the loss of roughly 10 % iron oxides from the structure, a value comparable to the decrease in magnetic saturation measured for this sample.

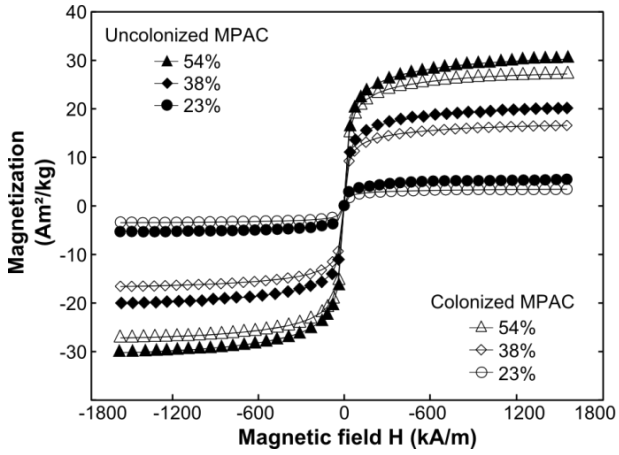

Figure 6.7 : Magnetization of MPAC before and after 90 days aging period.

6.4 Discussion

6.4.1 DOC removals

Despite a mass fraction of up to 54 % of NPs, adsorption of DOC on un-colonized MPAC was neither reduced nor enhanced compared to PAC at the beginning of the study. DOC removals of 60 % or higher are typical for reactors operated with a PAC age < 7 days (Leveillé et al. 2013, Stoquart et al. 2012). In contrast, Park et al. (2015) found higher adsorption capacity on PAC

impregnated with magnetite NPs (16 mg Fe/g PAC) compared to PAC (Freundlich constants K_F of 6.23 L/g and 0.08 L/g respectively). However, they report adsorption capacities after 200 min whereas our first sample was taken after 4 days and thus the initial higher adsorption of NOM on iron oxides was likely to be levelled due to the slower adsorption kinetics on PAC compared to MPAC (Park et al. 2015). As to performances in biological mode, this study offers several evidences that the growth of heterotrophic biomass was not negatively impacted by the NPs on MPAC. DOC removals showed the typical transition from a purely adsorptive mode to a mostly biological process for all 5 bioreactors: the decrease in DOC removal from 60 % to a constant removal of 20 to 30 % after approx. 40 days. Although no BDOC samples from the pilot's effluent are available in our study, the stabilization of DOC data confirms steady-state operation of a biological process (Çeçen and Aktas 2012, Velten et al. 2007). According to Stoquart et al. (2012) PAC older than 20 to 30 days is fully colonized and accounts for 20 % DOC removal or more. Markarian et al. (2010) confirm the contribution of biodegradation on PAC > 20 days. While PAC age increased, they observed decreasing DOC removals and increasing BDOC removals that stabilized at 30 % to 32 % in reactors containing 5 g/L of PAC and 40 % to 45 % removal in reactors containing 25 g/L of PAC. Furthermore, biomass development was favoured in our study by the warm influent water (22°C) and the dosage of acetate as an easily biodegradable carbon source. The observed plateau of 20 % to 30 % DOC removal in the reactors corresponds therefore most likely to the biodegradable fraction of DOC in the feed water (ca. 12 % natural BDOC in Montreal's tap water and 14 % BDOC as non-adsorbable acetate). Mass fractions of 23 % to 54 % iron oxide NPs in MPAC thus neither reduced adsorption and biodegradation of DOC nor altered the temporal development of heterotrophic biomass as biodegradation started in all 5 reactors at the same time.

PGR measurements confirmed the presence of active heterotrophic biomass on all PAC and MPAC samples. The values from our study (48 to 57 µg C/cm³) are similar to measurements of active heterotrophic biomass in PAC and GAC studies. In a HMP study with constant PAC age (60 days), 10 g PAC/L, a 69 min HRT and similar influent water quality, Stoquart et al. (2014a) measured active heterotrophic biomass equivalent to 110 nmole glucose/(g_{dw}*h) which corresponds to 43.9 µg C/cm³. The slightly higher biomass concentration in our study could be related to a) the higher operation temperature (22°C in PAC/MPAC study vs. 16°C in the HMP study), b) the higher PAC and MPAC age (90 days vs 60 days in the HMP study) and c) the

presence of easily available acetate as substrate. Comparing biomass in a PAC reactor to measurements on biological GAC filters is more difficult as biomass densities in fixed beds are not only a function of temperature, substrate availability, carbon type and age but also dependent on filter depth and backwash frequency/type (Velten et al. 2011). Velten et al. (2011) measured 1.8 x 10^{15} cells/m³ in a GAC filter fed with pre-ozonated surface water (1.1±0.14 mg DOC/L; 7°C; empty bed contact time 15.8 min). With an average bacterial carbon content of $2x10^{-14}$ g C/cell (Servais et al. 1991) and their filter bed volume (1.47 m³) as an approximation for the media volume one can transform their results to an average biomass density of 38.9 µg C/cm³. Similar results were obtained applying the PGR method on a GAC sample from the surface of a biological dual media BAC/sand filter (influent DOC= 3.0 mg C/L; empty bed contact time 20 to 30 min) by Stoquart et al. (2014a). They compared active heterotrophic biomass from their above-mentioned PAC reactor to the BAC filter and found lower values in the BAC samples (average 38.6 µgC/cm³). Although the biomass densities measured in our pilot study were higher than the literature values for PAC and GAC, they were very similar in our PAC and MPAC reactors (PAC-1: 48 µg C/cm³; MPAC-54%: 48.2 µg C/cm³) showing that NPs in MPAC did not inhibit the proliferation of active heterotrophic bacteria.

6.4.2 Ammonia removal

The complete ammonia removal we observed in all bioreactors after 40 days of operation is an indicator of the presence of nitrifying bacteria. This was confirmed by the increase of nitrate in the effluent, closing the reactors' nitrogen mass balance. According to Stoquart et al. (2014b) complete ammonia removal by PAC can only be attained in the presence of nitrifying biomass. Nitrifying bacteria developed six days later on all MPACs compared to PAC indicating initial inhibition of colonization. The impact of NPs on nitrifying bacteria has not been extensively investigated at this point. A study on short and long-term effects of magnetic NPs on nitrifying bacteria in an activated sludge waste water treatment process showed a decrease of nitrate removal performance at loads of 50 mg/L magnetite NPs during the first days of the long-term experiment followed by an adaptation and even an increase in nitrogen removal compared to the control system Ni et al. (2013). In different toxicity studies bacteria were observed to adapt to NPs via self-protection mechanisms such as altering membrane lipid composition, membrane fluidity or the production of extracellular proteins (Dinesh et al. 2012). The delayed proliferation

of nitrifying bacteria in our study could be related to such bacterial protection strategies. With regard to the observed differences in bacterial community composition a shift in the nitrifying population might also be a possible explanation. However, the low taxonomic depth of the 16s rRNA gene sequencing did not allow for the identification of nitrifying species in our study.

6.4.3 Bacterial community composition

The 16s rRNA gene analysis revealed differences in bacterial community structures between adsorbents with no or little iron oxide NPs and MPAC-54% containing high amounts. PAC-1, PAC-2 and MPAC-23% had a very similar bacterial community composed mainly of *Betaproteobacteria* (74 to 85 %) and to a lower extent *Alphaproteobacteria* (7 to 12 %). *Betaproteobacteria* was also the dominant group (68 %) in a 16s rRNA gene analysis of the biofilm community in GAC filters treating ground or surface water (Magic-Knezev et al. 2009), and in a GAC pilot plant fed with lake water (Niemi et al. 2009). Our reactor containing a high quantity of iron oxide NPs (MPAC-54%) had a community structure dominated by *Alphaproteobacteria* (50 %). They were also the dominant population in a pilot study of a carbon-sand dual media filter by Feng et al. (2013). The composition of bacterial communities in biofilms depends on a variety of parameters such as substrate type and availability, presence of oxygen, biofilm age and environmental stress factors. With the same influent water quality and growth surface available in each of our five bioreactors, the different dominant populations on PAC and MPAC may indicate the importance of surface and material properties that could favour one population over another. Despite the presence of different dominant populations in our reactors, the treatment performance was the same in all bioreactors.

6.4.4 Stability of iron oxide NPs

The analysis of magnetic properties and XRD indicate that the magnetic adsorbents had changed over the 90 days aging process. Although the type of iron oxide did not change (maghemite), the decrease of the crystalline phase and saturation magnetization suggest a loss of iron oxides. Shear forces in the continuously agitated reactors at 120 rpm might have led to abrasion and the subsequent exportation of small iron oxide particles. Yet, these findings contradict the weekly monitoring results of total iron that show marginal iron exportation from the reactors (0.08 % of the iron content). A possible undocumented exportation probably occurred during the routine

cleaning of the 10 µm nylon mesh. The material removed from the mesh during this procedure was transferred back into the reactors to reduce adsorbent losses. However, fine material was removed under running water applying vigorous scrubbing which might have represented a sink of fine iron oxides.

6.5 Conclusions

Previous studies on iron oxide-PAC composite materials focussed solely on the adsorption properties at lab-scale of various contaminants and dyes. In our study we evaluated its performances both as an adsorbent and as a support for biological growth with respect to an application in a drinking water treatment process. The following conclusions were drawn:

- Iron oxide NPs on PAC did not influence the DOC and ammonia elimination performance in the bioreactors.
- The same quantity of active heterotrophic biomass developed on both PAC and MPAC even at high NP loads.
- While the slightly slower onset of nitrification (6 days) in reactors containing MPACs might be an indicator for their initial inhibition, full nitrification was observed after 40 days on all adsorbent types.
- Bacterial community composition was influenced by the presence of iron oxide NPs but did not impact the overall treatment performance.
- The iron oxide remained stable over the 95-day operation period, however, lower magnetic saturation points at losses of iron oxide from the MPAC structure that might be related to abrasion.

From an operational point of view the material resistance to abrasion might play a crucial role for process design and should be the topic of further research.

ACKNOWLEDGEMENTS

The authors are thankful for the technical support of Jacinthe Mailly, Julie Philibert, Mireille Blais, Yves Fontaine, Mélanie Rivard, and our intern Sarah Nambukarawasam. This work was completed at the Industrial-NSERC Chair in Drinking Water of Polytechnique Montréal with the financial support of its partners, namely the City of Montreal, Veolia Water Technologies Canada Inc. and the City of Laval.

CHAPTER 7 SEPARABILITY OF MPAC – CHALLENGES AND LIMITS

7.1 Introduction to magnetic separation for MPAC in water treatment

As discussed previously (Chapter 2.3.3), separating MPAC - a composite combining the diamagnetic carbon matrix with superparamagnetic IONP – requires high gradients and/or high magnetic field strength. These requirements are met by high gradient magnetic separators (HGMS). Kondo et al. (2010) and Okamoto et al. (2011) tested a superconducting HGMS consisting of a 7 mm wide and 600 mm long filter tube filled with stainless steel wool (8 – 13 % volume filling) surrounded by a superconducting magnet. With a magnetic field strength of 2 T, nearly 90 % removal of MPAC (6.43 – 17.6 Am^2/kg) was achieved after filtering a 50 or 100 mg MPAC/L suspensions at a flow rate of 2.31 L/min (flow velocity of 3600 m/h). Both authors note that the smallest particle fraction was exported from the separator. Anzai et al. (2016) tested a HGMS consisting of a rotary magnetic drum with permanent magnets (0.5 T) wrapped in stainless steel fibres. The filter length (contact length on the drum) was 85 mm and the flow rate was varied between 230 and 1200 mL/min. Separation efficiency for MPAC with a saturation magnetization of 6.3 – 10.2 Am^2/kg depended strongly on the flow rate. After filtration of 2 L of a 100 mg MPAC/L suspension separation efficiencies of 92 – 95 % were achieved at 230 mL/min which decreased to 70 – 85 % at 1200 mL/min depending on the IONP content of MPAC. A HGMS using a superconducting magnet has been commercialized by MS-Engineering Co., LTD in Japan to separate fine MPAC from water (volume fraction of 25 – 35 % magnetite, MPAC diameter 40 – 50 nm, aggregate size 1 - 3µm). Their system is able to treat 500 – 2000 m^3/day, separation efficiencies are not reported (MS-Engineering 2006). A downside of these HGMS systems is the need for power supply and the big footprint due to the electromagnets or superconducting magnets used to produce high magnetic fields.

Separators using permanent magnets for the separation of MPAC are less common Borghi and Fabbri (2014) proposed a high gradient magnetic separator using permanent magnets producing a homogeneous and relatively low external magnetic field (0.5 T) to separate MPAC (obtained from MS-Engineering Co., LTD). For their lab-scale separator, the high gradient was obtained using a 210 mm long filter element with a 37 x 23 mm cross-section filled with stainless steel spheres of 3 mm diameter. A suspension containing 0.5 g MPAC/L was continuously circulated

through the separator with a flow velocity of 1.3 m/s and a flow rate of 240 mL/s. After 20 min of filtration cycles 99 % removal of MPAC (97 % after 10 min) was achieved. The authors point out that the advantage of the sphere-filled filter over a steel-wool filter as tested in a previous study (Borghi et al. 2011) was the higher filling factor (55%), the insensibility to the local direction of the external magnetic field and the easier handling concerning cleaning and assembling (Borghi and Fabbri 2014). However, no data is presented concerning the backwash technique or efficiency of the sphere filter. According to Borghi (2014) progressive clogging of the filter occurred which reduced the filtration efficiency and lead to frequent washing or replacing of the metal spheres. This might limit the application of the sphere filter for large-scale applications.

In this exploratory study we used a permanent magnet operated HGMS filled with a coarse steel wool at three different packing densities to separate MPAC with maghemite mass fractions of 10 %, 38 % and 54 %. A setup using a permanent magnet was designed to avoid power consumption which leads to higher operating costs. A coarse steel wool was chosen to allow for easy backwash of the filter column and to reduce head losses during filtration cycles. The objective was to identify the separator's limitations regarding (i) flow rate, (ii) MPAC concentration, (iii) matrix packing density and (iv) maghemite content in MPAC.

7.2 Material and methods

7.2.1 Magnetic powdered activated carbon

Three MPAC with maghemite IONP mass fractions of 10 %, 38 % and 54 % were produced via a co-precipitation process as described previously (Chapter 4). The nanoparticles in MPAC show spherical shape and are homogeneous in size (average diameter of 17 nm). The composite material exhibits superparamagnetic behaviour with remanent magnetization ranging between 0.13-0.56 Am²/kg and saturation magnetizations of 5.20, 20.1 and 30.3 Am² /kg for MPAC-10%, MPAC-38% and MPAC-54% respectively (s. Table 7.1). All three MPAC particles have the same particle size distribution with a d_{50} of 23 µm and prior to the separation tests, all MPAC powders were sieved (< 100 µm) to eliminate agglomerates. The particle size distribution by number shows that 50 % of all particles are < 3 µm (Figure C-3).

Table 7.1 : MPAC properties.

Adsorbent	Fe_2O_3 mass fraction (%)	Bulk density (g/mL)	Wet particle density (g/cm^3)	M_s [a] (Am^2/kg)	M_r [b] (Am^2/kg)	d_{min}	d_{max}	d_{10} (µm)	d_{50}	d_{75}
MPAC-10%	10	0.51	1.957	5.20	0.56					
MPAC-38%	38	0.62	2.228	20.1	0.13	0.77	100	6	23	49
MPAC-54%	54	0.79	2.613	30.3	0.22					

[a] saturation magnetization , [b] remanent magnetization

7.2.2 Magnetic Separator and setup

The magnetic separator consisted of two squared rare-earth magnets ($Nd_2Fe_{14}B$, grade N42) mounted in parallel in a Plexiglas casing to provide a relatively uniform magnetic field to magnetize the wire filter element (Figure 7.1). The filter bed was formed by ferromagnetic stainless steel wool in glass tubes of 1 cm diameter. Three filter beds were prepared with different wool packing densities (Table 7.2). The individual wool fibres were flat strings of rectangular cross-section (Figure 7.2). The role of the external magnets was to magnetize the steel wool which then provided the magnetic field gradients inside the column. For the experiments, a suspension of 2 L MPAC was pumped through the filter element at different flow rates and particle concentrations. During filtration, the particles were magnetized by (i) the external field and (ii) the field of the stainless steel fibres to be captured in the filter bed.

The suspensions of MPAC-10%, MPAC-38% and MPAC-54% were prepared at equivalent PAC concentration (2.5, 25 and 250 mg PAC/L) to obtain suspensions with equal particle numbers. Working at equivalent PAC concentration (instead of equivalent adsorbent concentration) was necessary as the densities of MPAC vary according to their IONP content. All suspensions were stirred at 200 rpm to keep MPAC in suspensions during the experiment. Samples were collected every 1 or 2 minutes in 40 mL vials at the outlet of the separator and analyzed using a UV spectrometer at 850 nm. Particle concentrations were obtained based on mg PAC/L with the help of a calibration curve relating MPAC concentration to UV absorbance.

Separation efficiency was calculated as:

$$E(t) = \frac{m_r\,(t)}{m_f\,(t)} \cdot 100\%\,, \qquad \text{Eq. 7.1}$$

where m_r is the mass retained in the separator and m_f is the mass that is fed into the separator.

Table 7.2 : Characteristics of the separator.

Separator data		Units
Material	$Nd_2Fe_{14}B$, grade N42	
Magnet dimensions L x W x H	5 x 5 x 1	cm
Remanent magnetization B_r	1.32	T
Coercive field H_c	1170	kA/m
Maximum energy product BH_{max}	3342.4	Mega A/m
Filter width	1	cm
Filter length	7	cm
Stainless wool filling	0.1, 0.15 and 0.2	g/cm³
Stainless steel fibre cross section	30 x 300	µm
Filter porosity	0.97, 0.98 and 0.99	

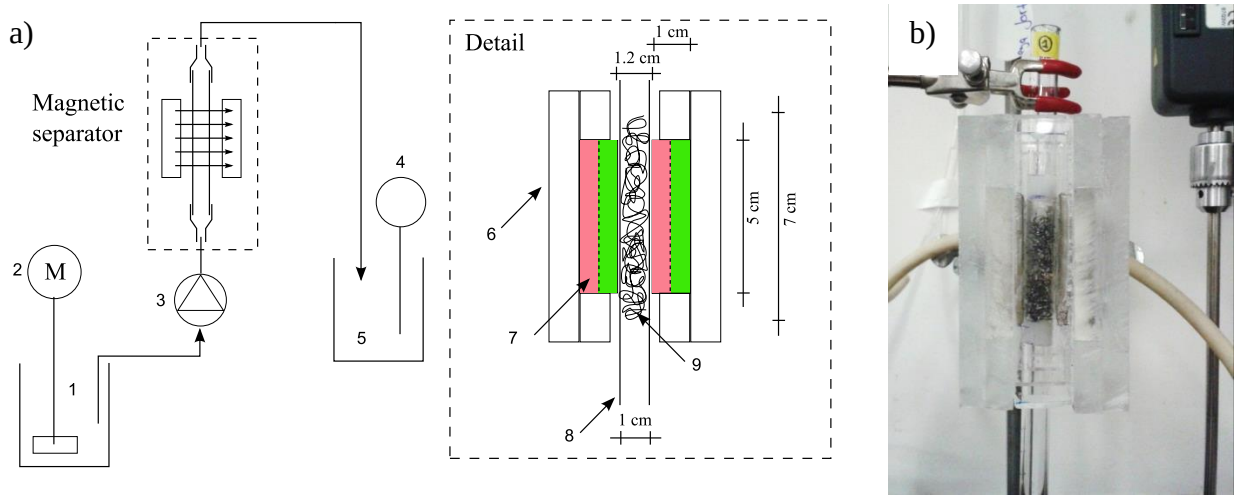

Figure 7.1 : a) Schematic of the magnetic separation setup : (1) carbon contactor 2 L, (2) stirrer 200 rpm, (3) peristaltic pump 6 – 600 rpm, (4) UV-spectrometer analysis 850 nm, (5) clean water tank, (6) Plexiglas casing for magnets, (7) magnet, (8) glass tube Ø 1 cm, (9) stainless steel packing. b) Picture of the separator.

7.2.3 Experimental plan and statistical analysis

The parameters IONP content, MPAC concentration, packing density of the steel wool and flow rate were tested at two or three levels (Table 7.3 and Figure 7.2) to identify their relative importance with respect to the separation efficiency. A general linear model was carried out to explore main effects and interactions among the factors (Statistica 12, StatSoft Inc., USA).

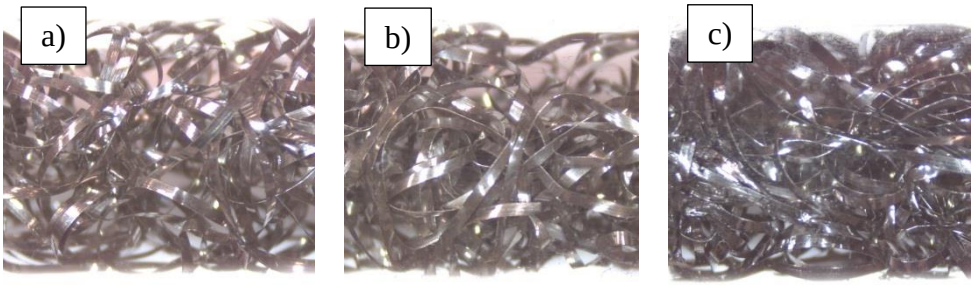

Figure 7.2 : Packing densities of a) 0.1 g/cm³, b) 0.15 g/cm³ and c) 0.2 g/cm of stainless steel wool in the separator.

Table 7.3 : Experimental conditions for the separation tests.

Factors	Level			Unit
MPAC type	10	38	50	% IONP
MPAC concentration	2.5	25	250	mg PAC/L
Packing density separator	0.1	0.15	0.2	g/cm³
Flow rate	200		470	mL/min

7.3 Results and discussion

7.3.1 Magnetic separator characterization

The flux density and field lines of the magnetic field between both permanent magnets were modelled for the chosen parallel arrangement using the software Quickfield (student version, © Tera Analysis Ltd) (Figure 7.3). The model confirmed a uniform field of about 0.6 T in the gap between both magnets (parallel field lines), in absence of a steel wool filter. It also showed that

the flux density is highest at the corners of the magnets which points at increased particle capture in this area due to the edge effect[4] which might lead to early clogging of the filter.

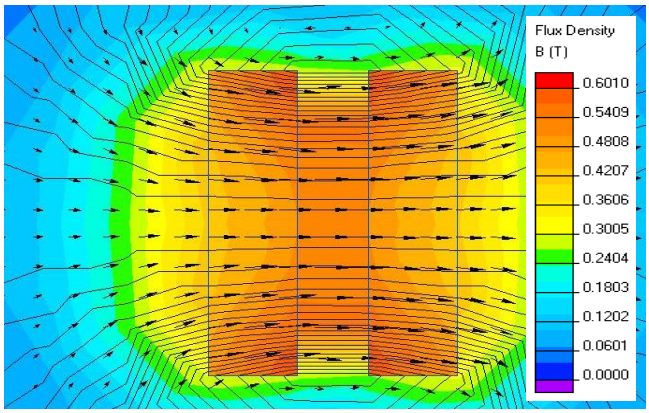

Figure 7.3 : Flux density and field lines for the permanent magnet setup without the steel wool in the gap.

7.3.2 Separation efficiencies under different operation conditions

In total 13 experiments were carried varying the parameters MPAC type, MPAC concentration, flow rate and steel wool packing. The results are summarized in Table 7.4 and Figure 7.5. In the following, the relative importance of the parameters is discussed with respect to the separator limitations, particle breakthrough and filter backwashing.

7.3.2.1 **Flow velocity**

Operating the magnetic filter with MPAC-54% at doses between 9 – 25 mg PAC/L and a flow rate of 200 mL/min (velocity 0.04 m/s) showed separation efficiencies of 94 – 97% (Table 7.4). The ***flow velocity*** was thus low enough to generate only weak ***drag forces*** which were outweighed by the magnetic force in the filter bed. According to the drag equation (Eq. 2.17) the drag force is proportional to the flow velocity. Increasing the flow rate to 470 mL/min (flow velocity of 0.1 m/s) increases the drag force by factor 2.5. Under these conditions, the magnetic filter was not able to retain the MPAC-54% particles despite their high magnetization saturation (Figure 7.5 a). The drag force is also dependent on the particle diameter with bigger particles

[4]This effect results from the lower quantity of dipole magnets at the corners compared to the center of the material where magnetic dipoles partially cancel each other as they are oriented in antiparallel fashion.

being the most affected by the increase in flow velocity (Figure 7.4). Concerning the magnetic force, particles with smaller diameter have a lower volume magnetization and are thus expected to be more difficult to capture. In this study, the exported particles were not analyzed concerning their particle size distribution. In future studies, however, the determination of a critical particle diameter could be a valuable contribution to optimize the efficiency of the separator.

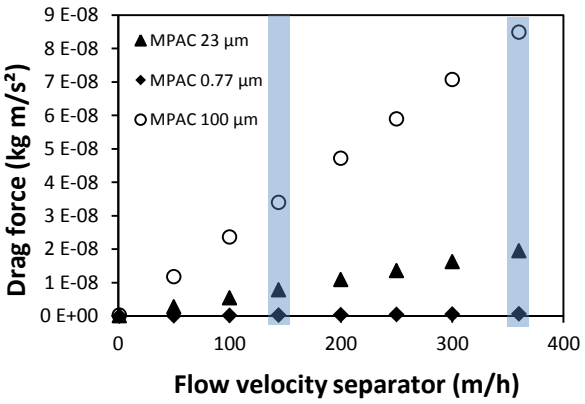

Figure 7.4 : Drag force calculated as a function of the particle diameter and flow velocity. Highlighted zones are the tested flow velocities in the magnetic separator of 144 m/h and 360 m/h.

Table 7.4 : Experiments and separation efficiency.

MPAC	PAC conc. mg/L	Flow rate mL/min	Density g/cm³	Separation efficiency (%)
MPAC-50%	24.5	200	0.15	0.97
MPAC-50%	24.3	200	0.10	0.96
MPAC-50%	9.00	200	0.10	0.94
MPAC-38%	25.0	200	0.15	0.91
MPAC-38%	257	200	0.15	0.88
MPAC-50%	231	200	0.15	0.86
MPAC-50%	2.60	200	0.15	0.85
MPAC-50%	23.4	470	0.20	0.81
MPAC-50%	23.4	470	0.15	0.73
MPAC-10%	25.1	200	0.15	0.71
MPAC-50%	24.6	470	0.10	0.67
MPAC-10%	233	200	0.15	0.62
Experiments without magnetic field :				
MPAC-50%	23.1	200	0.15	0.30
MPAC-50%	24.1	200	0.20	0.27

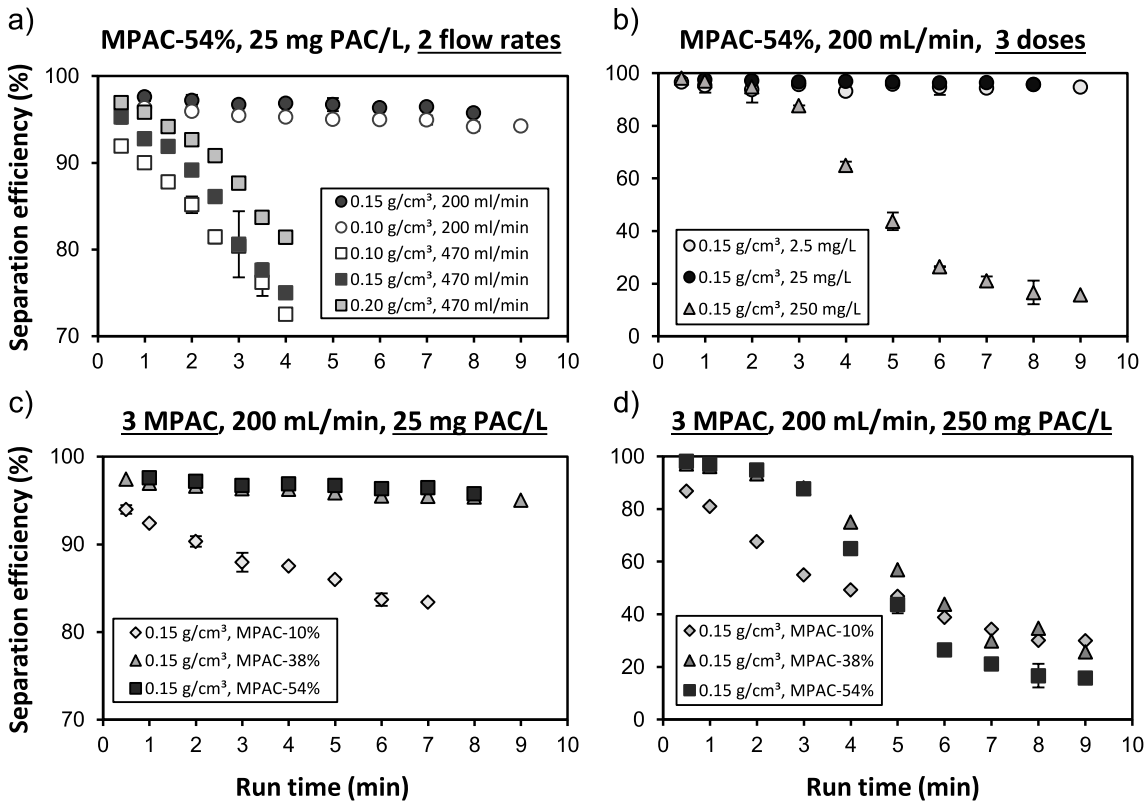

Figure 7.5 : Separation test results for filtration of 2 L of MPAC suspensions.

7.3.2.2 **Particle breakthrough**

Filters are usually operated until either breakthrough occurs or the limiting ***head loss*** in the filter bed is reached. In this study, a small head loss of 4 – 6 cm was observed only at high particle concentrations of 250 mg PAC/L (data not shown). Breakthrough is dependent on the ***number of particles*** that can be retained throughout the filter depth. At the lower concentration of 25 mg PAC/L no breakthrough was observed during the filter operation time (Figure 7.5 b). Yet, by increasing the particle concentration from 25 mg PAC/L to 250 mg PAC/L, the particle breakthrough was observed after only 2 – 3 min of filtration time (Figure 7.5 b). The mass of particles retained in the filter before breakthrough (roughly 175 mg PAC) under these conditions (flow rate of 200 mL/min and a filter packing of 0.15 g/cm³) represents the filter capacity. In case of the suspension containing only 25 mg PAC/L, the total particle mass retained in the filter was by factor 2.3 lower (75 mg) which explains why no breakthrough was observed.

When comparing the volume of the captured particles with the available volume in the wire filter, it became obvious that the wire filter was not completely occupied when breakthrough occurred. Indeed, the volume of the captured particles represented only about 10 % of the available void volume in the steel wool filters. As a measure to increase the number of particles to be captured in the filter bed, the steel wool packing density was increased. It was hypothesized that enlarging the magnetic surface would increase the probability of a particle to encounter a magnetized wire and thus to get captured. However, increasing the packing density from 0.1 to 0.15 and then 0.2 g/cm³ did not prevent the breakthrough of MPAC-54% particles at high flow velocity (Figure 7.5 a). This was probably related to the higher flow velocity (and thus higher drag force) in smaller voids of the more densely packed steel wool.

During the experiments, it was also visible that the distribution of captured particles was not homogeneous throughout the filter bed. As the external magnetic field was strongest at the edges of the magnets (Figure 7.3), the retention of MPAC took place predominantly in the area of the filter inlet. Another measure to increase the capacity of the wire filter, is thus to change the inlet design of the filter. The parallel arrangement of the magnets could easily be changed towards a design with a wider gap between the magnets at the bottom of the filter (e.g. by an angle of 5°-10°). The strong external magnetic field at the filter inlet would decrease which could lead to a better transport of the particles deeper into the wire filter.

7.3.2.3 **IONP content in MPAC**

Another set of experiments explored the influence of IONP mass fraction on separation efficiency at low and high particle concentration. In both cases, differences were small between separating efficiencies of MPAC-54% and MPAC-38% (though significant with p-values > 0.015) while MPAC-10% had too low IONP content to be retained in the filter column (s. Figure 7.5 c and d).

7.3.2.4 **Parameter interactions**

Main effects and interactions that govern MPAC removal in the magnetic wire filter were consequently analyzed using a general linear model with the factors MPAC concentration (C), MPAC type (MPAC), wire filter density (DENSITY) and flow rate (Q). Ideally, full breakthrough curves would have been registered for all test conditions. Yet, the large differences in concentration and flow velocity and the limited volume filtered (2 L) did not allow a

comparing breakthrough times. Instead, the separation efficiency E in the first 4 min filtration time was analyzed which allows comparing all data sets (Table 7.4). To stabilize the variance, the MPAC concentration with levels 2.5, 25 and 250 mg PAC/L was log-transformed (log(C)) and the square root of the flow rate was used (SQRT(Q)). The results of this model indicated that no linear relation between separation efficiency exists at low levels (2.5 and 25 mg/L) vs. high level (250 mg/L) within the observed filtration time. Consequently the factor was transformed into the categorical factor with levels "low" and "high". The resulting model (E = f(SQRT(Q), MPAC, log(C), Density) without interactions returned the flow rate Q and the MPAC type as only significant predictors for the separation efficiency E (p-values of 0.002 and 0.004 respectively). Interactions of these factors were not significant. These results confirmed the observations discussed previously where the steel wool packing density had little influence on the separation efficiency. Also the MPAC concentration did not influence the separation efficiency significantly as the number of particles impact only the filter runtime, not the separation efficiency.

7.3.2.5 **Filter backwash**

Backwashing the filter was carried out by simply removing the magnetic field (pulling the separator column out of the magnetic setup) and rinsing the column using a standard laboratory washing bottle. Separation of the particles from the wire filter was easy due to the low remanent magnetization of the steel wool fibres and the superparamagnetic behaviour of the MPAC particles.

7.4 Conclusions and recommendations for future work

This exploratory study has shown that the tested separator consisting of permanent magnets and a wire filter bed allowed separating typical adsorbent dosages for drinking water treatment of 2.5 - 25 mg PAC/L of > 90% at flow rates of 200 mL/min (flow velocity of 144 m/h) for both MPAC-54% and MPAC-38%. While MPAC-10% did not contain enough IONP to be efficiently separated under the tested conditions, separation efficiencies were similar for both MPAC-54% and MPAC-38%. These findings are interesting not only with respect to MPAC separation but also with respect to their function as adsorbents. Our previous studies have shown that e.g. NOM adsorption capacity of MPAC containing up to 54% IONP is reduced to a higher degree than expected from their PAC content. Being able to use MPAC containing 38% IONP for both

efficient contaminant adsorption and separation is thus promising. For future applications, MPAC could be produced with an IONP content matching the requirements of the specific magnetic separator design.

Furthermore, this exploratory study has shown that the flow velocity was the most important operation parameter. An increase of the flow velocity by factor 2.5 resulted in a drag force that was too high to retain any of the tested MPAC magnetically in the filter bed. In future studies, additional flow rates between 200 – 470 mL/min should be tested to identify optimal flow rates.

To increase the filter capacity, the design of the separator can also be modified. Changing from a parallel layout of the magnets to a slightly larger opening at the bottom (e.g. 5°), could help to avoid the edge effect and thus the over-proportional accumulation of particles at the separator inlet.

Future studies should include the development of a computer model combining the magnetic field and the flow field in the separator column in order to (i) explore scale up options and to (ii) help identifying optimum operation conditions.

In preparation of the laboratory study presented in this chapter, a simple magnetic separator channel (without steel wool) in the shape of a lamella clarifier had been modelled (presented in APPENDIX C). Lamella clarifiers are typically used in drinking water treatment for the gravity separation of flocks. The model allowed identifying maximum flow rates and the influence of particle size distributions on separation efficiency. It also became clear that steel wool or other filling materials are indispensable to create the high gradient necessary for magnetic separation of MPAC. Yet, due to the irregular wire structure in the separator column, the magnetic force can only be calculated using a finite element model which was beyond the scope of this project.

CHAPTER 8 GENERAL DISCUSSION

This chapter underlines the main findings from this project with respect to the initial research objectives and hypotheses. The general objective was to evaluate a magnetically separable PAC as an alternative adsorbent for drinking water treatment. The specific focus was on its suitability as an adsorbent and growth support for heterotrophic and nitrifying bacteria in a biological process. The project was structured in four thematic blocks (Figure 8.1). First, MPAC was prepared and characterized to set the basis for the design and interpretation of the subsequent experiments. Second, the interactions between IONP, PAC and typical drinking water contaminants were identified with the help of isotherm and kinetic experiments. The next step was to understand how IONP on MPAC influence heterotrophic and nitrifying bacteria and if the composite material remains stable during the long-term application. Finally, magnetic separation was tested with a magnetic separator based on permanent magnets to explore an alternative to high-energy consuming high gradient magnetic separators with electromagnets. Recommendations for the preparation and application of MPAC for drinking water treatment will be given in the conclusions and recommendation chapter.

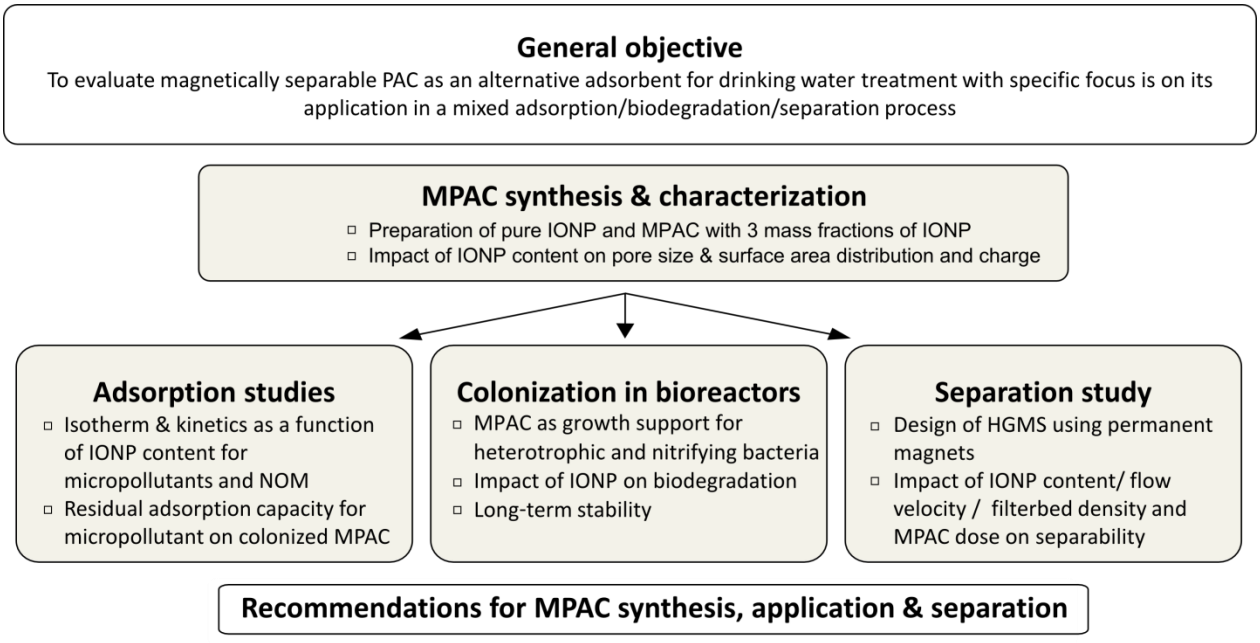

Figure 8.1 : Structure of the research project.

8.1 How does the IONP content change the adsorption properties?

8.1.1 IONP location in MPAC

One of the objectives of this project was to understand the relation between IONP content in MPAC and the adsorption properties for water contaminants NOM and MP. Our main critique of anterior studies is the lack of characterization of PAC before and after magnetization and the missing distinction between adsorption sites on PAC and IONP (Chapter 2).

The designed co-precipitation reactor enabled us to produce batches of consistent adsorbent characteristics. When choosing a different synthesis protocol, reactor and PAC type, the nature of IONP will vary as will the location of IONP in MPAC depending on the size of IONP and the pore size distribution of the PAC source. This variability makes it difficult to compare adsorption results between studies if no thorough material analysis is provided. One of our contributions in this project is to provide a full characterization of the adsorbent in terms of IONP location and changes in pore size and surface area distribution. One limitation of our study was to focus on only one PAC as base material for the preparation of MPAC. If the optimization of MPAC for the adsorption of a specific contaminant is the objective, a range of PAC types with different pore size distributions should be tested as MPAC templates. Instead, in this project, we opted to first choose an optimal PAC for the adsorption of our target pollutants MP and NOM, followed by its magnetization and characterization. The chosen PAC was a mineral-base microporous PAC that is certified for drinking water applications (NSF60).

In our study, spherical maghemite IONP prepared via co-precipitation had an average diameter of 17 nm and were mostly scattered on the surface of PAC where they formed an irregular spongy crust. To a smaller degree, IONP were also found inside the PAC matrix. Analyzing the pore volume distribution of the prepared MPAC showed that the primary and secondary micropore volume decreased with increasing IONP mass fraction, whereas the mesopore volume increased. The decrease in micropore volume can be explained with (i) mostly the decrease in PAC content and (ii) partially the blockage of micropores (Ø < 2 nm) by IONP. The micropore volume was in average 10 % lower than expected with respect to the PAC content. The change in mesopore volume was related to a combination of two overlaying effects (i) an increase in pore volume due to the voids formed between IONP on the PAC surface and (ii) the blockage of mesopores at

IONP mass fractions of 54 % (Chapter 4). Understanding the origin and nature of the measured pore volumes, the mass fraction of IONP and their adsorption capacities was essential for the interpretation of the subsequent NOM and MP adsorption data.

In previous studies the loss of adsorption capacity of MPAC compared to PAC has been related to blocked or occupied adsorption sites in PAC, simply because lower pore volumes were measured after magnetization (Chapter 2). Contrary to previous research we could demonstrate in Chapter 4 and Chapter 5 that (i) IONP did not contribute to NOM or MP adsorption, (ii) the size of the target pollutant, the pore size distribution of PAC and the IONP content determine the loss of adsorption capacity in PAC and (iii) reduced adsorption capacity of MPAC for NOM and MP is mostly proportional to the PAC content.

8.1.2 Adsorption of NOM on MPAC

PAC impregnated with iron oxides has repeatedly been proposed as an enhanced adsorbent for the removal of NOM. The results in Chapter 4, however, demonstrated that maghemite IONP did not contribute significantly to the adsorption of NOM (Suwannee River NOM). Our results from Chapter 6 are in line with findings from Chapter 4, where PAC and three MPAC with increasing IONP mass fractions had been used in stirred continuously fed reactors for 90 days. Dosed at equivalent PAC mass fraction, removal of DOC during the adsorption phase was not significantly different between PAC and MPAC. The water in that study was Montreal's dechlorinated tap water where adsorbable DOC was composed of NOM from the Saint Lawrence River. Contrary to many other studies, we also analyzed the adsorption capacity of pure IONP and PAC separately and compared the values to the adsorption capacity of the composite material MPAC at different IONP mass fractions. The adsorption capacity of our maghemite IONP for Suwannee River NOM (measured as DOC) was low with only 8 mg/g or 0.12 mg/m². These results are in line with studies on pure IONP and their potential to bind NOM in natural ecosystems such as demonstrated for hematite (0.18 mg/m² with Suwannee River fulvic acid and Georgetown NOM) (Gu et al. 1994), magnetite and goethite particles (2.6 and 4.1 mg/g respectively with standard humic acids) (Rahman et al. 2013). According to the literature, the iron oxide ferrihydrate is a far better NOM adsorbent and could be chosen to enhance NOM adsorption on PAC (Choo and Kang 2003). This iron oxide has a lower degree of crystallinity compared to the highly ordered maghemite, magnetite, goethite or hematite and thus exhibits a larger surface area per weight

(Cornell and Schwertmann 2003). However, one has to keep in mind that only the iron oxides maghemite and magnetite show sufficiently high magnetization that allow for magnetic separation (Cornell and Schwertmann 2003) and are thus suitable for the application in MPAC.

Another finding from Chapter 4 was that maghemite IONP did not change the selectivity of MPAC for certain NOM fractions. Both, PAC and IONP adsorb mostly the aromatic and low molecular weight fraction of NOM. It has to be considered, though, that the NOM tested in this study was Suwannee River NOM. This NOM is a well-characterized mixture which is often used to evaluate adsorption properties. However, it is constituted dominantly of large humic acids and only low fractions of low molecular weight molecules such as ketones and amino sugars or monoprotic organic acids. As the NOM composition varies widely according to the source, the selectivity of MPAC might be more or less pronounced in other water matrices.

Due to their size NOM molecules adsorb mostly in the mesopores of PAC. While the mesopore volume of MPAC was higher than that in PAC, this additional mesopore volume was formed by the IONP voids and thus did not contribute to NOM adsorption. Normalizing the adsorption capacity of MPAC to the PAC content confirmed that IONP did not contribute to NOM adsorption. It became also clear that IONP did not block NOM adsorption sites in the PAC matrix below a mass fraction of 54 % IONP.

Diffusion of NOM molecules from the PAC surface towards the inner core of the adsorbent particle (as is described by the HSDM) was not impacted by the presence of IONP and diffusion coefficients were very similar between PAC and MPAC. Part of the reason might be that the surface of PAC was not covered homogeneously by a thick crust of IONP but rather irregularly by IONP patches. The mesopores were only blocked at a mass fraction of 54 % and the pores formed by IONP were in the mesopore range and thus accessible for NOM.

In summary, improving the generally low NOM adsorption capacities of bare PAC by depositing magnetic IONP is ineffective due to their low affinity for NOM molecules to IONP. Above the critical mass fraction of 38 %, the mesopores in the carbon matrix were blocked leading to a disproportional reduction in sorption capacity. For lower IONP mass fractions, adsorption capacity of MPAC is reduced proportionally to the mass fraction of PAC in the composite. For drinking water applications, this implies higher doses of the composite material compared to bare PAC. The advantage of using MPAC for removing NOM arises therefore only from its magnetic

separability and MPAC should ideally be applied in a polishing step for settled water (after coagulation-flocculation) to remove residual NOM and/or micropollutants. This strategy will limit the MPAC dose to apply.

8.1.3 Adsorption of MP on fresh and colonized MPAC and PAC

MPAC has been proposed by various authors to replace PAC as easily separable adsorbents for micropollutants (Bastami and Entezari 2012, Castro et al. 2009, Han et al. 2015, Oliveira et al. 2002). Compared to PAC most authors found lower MP adsorption capacities on MPAC. The reduced adsorption capacities were mostly attributed to IONP occupying or blocking relevant adsorption sites on PAC although a thorough analysis of the IONP content and pore size and surface distribution was mostly lacking. A systematic study evaluating the contributions of IONP and PAC separately and comparing the adsorption capacities and kinetics normalized to PAC mass content was missing so far and is the contribution of this study.

The nine organic MP tested during our study, presented in Chapter 5, were selected to provide a wide range of usage and chemical properties (Table 5.2). They varied with respect to their functional groups, molecular charge, hydrophobicity and molecular weight. In tests with pure IONP, none of these molecules were adsorbed in significant amounts. Similar results were observed by Shi et al. (2013) who measured 20 times lower adsorption capacities of pure magnetite IONP (2.62 µg/mg) compared to PAC (48 µg/mg) for the antibiotic ciprofloxacin. Consequently, PAC was the only active ingredient for organic MP removal in MPAC. Normalizing adsorption data by PAC content confirmed that lower adsorption capacities on MPAC compared to PAC were mostly due to the lower PAC content in these adsorbents. Although IONP did not contribute to the adsorption of MP, their presence did not lead to a relevant loss of adsorption sites on PAC even at mass fractions as high as 54%. Among the tested MP, two hormones (estradiol and norethindrone) were the most adsorbable compounds whereas atrazine and deethylatrazine were the least adsorbable compounds. Atrazine and deethylatrazine were also the least removed compounds among 10 pollutants in an adsorption study with virgin and colonized PAC carried out by Stoquart et al. (2016). The adsorbability was best correlated with the solubility of non-charged MP. This is supported by literature as the adsorbability of organic substances onto PAC increases with decreasing solubility (i.e. the substance is more hydrophobic) (Worch 2012).

Regarding adsorption kinetics, MP removal of > 50 % were achieved in less than 30 minutes on all adsorbents, except MPAC-54%. However, in contrast to slower NOM kinetics, the rate constants of the much faster MP kinetics were negatively affected by the presence of IONP. The second-order rate constants of MP were up to two orders of magnitude smaller on MPAC compared to PAC due to the reduced micropore volume in MPAC. Under the studied conditions, equilibrium was achieved after a maximum of 60 min on pure PAC and after 2 – 6 hours on MPAC-10%, MPAC-38% and MPAC-54%.

In this project, we suggested MPAC for the first time as an adsorbent and growth support for the biological hybrid membrane process. One of the questions was if colonized MPAC has a residual adsorption capacity for MP. Our results in Chapter 5 demonstrated that the Freundlich coefficient K_F as a measure for the MP adsorption capacities on colonized MPAC and PAC were greatly reduced. This was expected due to (i) exhausted adsorption sites due to pre-loading with NOM and (ii) the formation of a biofilm as additional diffusion barrier. We observed in average tenfold lower adsorption capacities on colonized adsorbents (PAC as well as MPAC) compared to fresh adsorbents. This is lower than reported in the literature where Lebeau et al. (1999) observed that K_F values decreased by factor 3 – 6 when comparing fresh and aged PAC with an average age of 62 days (with constant adsorbent replacement) in ultra-pure and natural waters. However, in contrast to their study, our bioreactors were operated 30 days longer and without adsorbent replacement. The measured residual adsorption capacities in our study are thus true residual capacities of aged adsorbents, which are expected to be lower.

Kinetic experiments with colonized PAC and MPAC were recorded with MP concentrations of 8.11 ± 5.35 µg/L of each MP. Adsorbent doses of 3.93 ± 0.49 g (dry weight)/L were chosen to represent typical operation conditions of a hybrid PAC-membrane reactor in adsorption/ biodegradation mode where PAC concentrations inside the reactor of 1-40 g PAC/L have been reported (Stoquart et al. 2012). With high adsorbent concentrations, kinetics of all MP were fast on colonized PAC and MPAC and equilibrium was reached for all compounds after a 5 min contact time except for SMX (30 - 60 min).

It would have been interesting to measure the capacity of colonized materials to biodegrade the pollutants during the long-term adsorption biodegradation study. However, dosing MP during our long-term adsorption/biodegradation study presented in Chapter 6 was not an option due to the

reactors materials (PVC containers and plastic tubing) that we considered being a potential MP sink. Instead, we opted for adsorption studies on fully colonized MPAC and PAC at the end of the colonization study. During this study, however, biodegradation was not expected to contribute significantly to the removal of the tested compounds. Although similar amounts of active heterotrophic biomass (48 – 57 µg C/cm³) had developed on all adsorbents and microbial activity was not suppressed during the adsorption study, biodegradation was an unlikely mechanism due to (i) the high initial concentration (500 µg/L of each adsorbent during isotherm experiments), (ii) the fact that the mixture of MP included antibiotics, and (iii) because the biomass was not previously acclimatized to the mixture of MP.

8.1.4 MPAC vs. PAC in the bioreactor

An important finding in Chapter 6 is the compatibility of IONP on MPAC with heterotrophic and nitrifying bacteria. As discussed in Chapter 2, IONP have a cytotoxic potential related to their nano-size and the formation of reactive oxygen species on their surface that can be deleterious to bacterial cells. Studies with IONP suspensions and pure cultures of planktonic bacteria, waste water biofilms or soil bacteria have shown only low to moderate inhibitory effects and in some cases IONP were stimulating bacterial activity (Chapter 2.7.2). So far, interactions between IONP and environmental bacteria were studied using exclusively IONP suspensions. In this project, we demonstrated for the first time the suitability of PAC covered with IONP as a growth support for bacteria in a biological drinking water process.

As described in Chapter 6, visual evidences confirmed colonization qualitatively on adsorbents without IONP (regular PAC) and on MPAC with increasing IONP mass fractions of 10 %, 38 % and 54 %. ESEM images corroborated the presence of biofilm on the IONP covered surface of MPAC and Baclight™ tests revealed that bacteria were mostly viable (based on membrane integrity) on both colonized PAC and MPAC.

Results presented in Chapter 6 further supported the hypotheses that IONP content in MPAC was uncritical for the colonization with heterotrophic bacteria. In the bioreactors DOC removals of 20 – 30 % were achieved in all reactors containing PAC or MPAC with 10 %, 38 % and 54 % IONP once the adsorption capacity was exhausted and biodegradation dominated the process. PGR measurements confirmed the presence of active heterotrophic biomass on all PAC and MPAC samples. No significant differences were found between regular colonized PAC (48 µg C/cm³)

and MPAC (48.2 µg C/cm³) containing a mass fraction of 54 % IONP. The values from our study were comparable to measurements of active heterotrophic biomass in PAC and GAC studies. In a HMP study with constant PAC age (60 days) and adsorbent replacement, 10 g PAC/L, a 69 min HRT and similar influent water quality, Stoquart et al. (2014a) measured active heterotrophic biomass of 43.9 µg C/cm³. In the same study, active heterotrophic biomass in a BAC filter showed on average 38.6 µg C/cm³. The biomass concentration in our study are thus slightly higher which could be related to (i) the higher operation temperature (22°C in PAC/MPAC study vs. 16°C in the HMP study), (ii) the higher PAC and MPAC age (90 days vs. PAC with an average PAC age of 60 days in the HMP study) and (iii) the presence of easily available acetate as substrate.

With regard to nitrification, results in Chapter 6 demonstrated that complete ammonia removal was established in all bioreactors after 40 days of operation. Ammonia removal was accompanied by an increase of nitrate in the effluent, closing the reactors' nitrogen mass balance. This is an indicator for the presence of nitrifying bacteria. Nevertheless, monitoring of ammonia and nitrite revealed that IONP delayed the development of nitrifying bacteria on all MPAC adsorbents for 6 days compared to regular PAC. Studies with suspended magnetite IONP and activated waste water sludge also found initial inhibition of nitrifying bacteria followed by a recovery and even increase of nitrification after several days (Chapter 2.7.2). In several toxicity studies bacteria were observed to adapt to IONP via self-protection mechanisms such as altering membrane lipid composition, membrane fluidity or the production of extracellular proteins (Dinesh et al. 2012). The delayed proliferation of nitrifying bacteria in our study could have been related to the time required for developing such bacterial protection strategies.

Previous studies with suspended magnetic IONP have shown changes in bacterial communities of activated sludge and soil bacteria (Chapter 2.7.2). This is supported by findings from our study, where the 16s rRNA gene analysis revealed differences in bacterial community structures between adsorbents with no or little IONP and MPAC-54% containing high amounts. While regular colonized PAC and MPAC-10% had a very similar bacterial community composed mainly of *Betaproteobacteria* (74 to 85 %) and to a lower extent *Alphaproteobacteria* (7 to 12 %), MPAC-54% had a community structure dominated by *Alphaproteobacteria* (50 %). The composition of bacterial communities in biofilms depends on a variety of parameters such as substrate type and availability, presence of oxygen, biofilm age and environmental stress factors.

As the influent water quality in each of our five bioreactors was identical, the different dominant populations on PAC and MPAC may indicate the importance of IONP related changes in surface and material properties. With regard to the observed differences in the development of nitrifying bacteria in reactors containing MPAC, a community shift might also be a possible explanation. However, the low taxonomic depth of the 16s rRNA gene sequencing results did not allow for the identification of nitrifying species in our study. Future studies should target more specifically the AmoA genes (the active site polypeptide of the ammonia monooxygenase) that are characteristic for ammonia oxidizing bacteria.

8.2 Stability of MPAC in long-term applications

Proposing MPAC for long-term applications in water treatment requires a discussion about the composite's mechanical strength and magnetic stability. While some studies report magnetic stability of magnetic properties of MPAC in water (Safarik et al. 2013, Yang et al. 2008), stability has not been investigated under real operating conditions. As presented in Chapter 6, we tested MAPC stability during a 90-day colonization study in continuously stirred flow-through reactors (Blade stirrer, 120 rpm). Results of XRD analysis before and after the aging period indicated that the type of iron oxide had not changed (maghemite). However, a decrease in magnetization saturation by 10 – 30 % and an increase in the amorphous signal during XRD suggested a loss of iron oxides, resulting most likely from shear forces in the continuously agitated reactors. The particles are rubbing against each other in the highly concentrated suspension (10 g/L) and the nylon mesh strainer on the top of the reactor might have acted as an abrasive surface. The fact that MPAC is somewhat sensitive to attrition was confirmed during the experiments presented in Chapter 4. Pre-tests had shown the vulnerability of the composite materials to shear forces caused by particles rubbing against each other during vigorous shaking on a linear shaker at 200 rpm for > 24 h. The decomposition of MPAC was more pronounced at higher mass fractions of IONP due to the higher density of the material. Higher IONP content leads to a higher density of the material - which will then require more vigorous stirring to keep the particles in suspension. Also one has to keep in mind that the results presented in Chapter 6 are obtained from reactors without adsorbent replacement (purge). If operated as a CSTR with a continuous adsorbent replacement stream and constant adsorbent age, the loss of magnetization would be balanced by fresh MPAC added to the reactor. These results show that choosing the

reactor design, operation conditions and IONP content in MPAC are crucial for the stability of the composite material.

8.3 Is there an optimum mass fraction IONP/PAC?

The short answer to this question is – as so often: it depends! However, results of this study can be used to give some more precise advice. In general, IONP content has to be optimized with regard to (i) the target contaminant, (ii) the process design and (iii) the type (strength and gradient) of the magnetic separator. While the literature agrees on the improved adsorption of metal ions on MPAC compared to PAC, our results presented in Chapter 4 and 5 clearly showed that ***IONP do not contribute to the adsorption of MP and NOM***. Consequently, adsorption capacity for these compounds is inversely proportional to the IONP content or lower. In Chapter 4, we presented data showing that only at an IONP mass fraction of 54 %, intrinsic mesopores of PAC were blocked for NOM adsorption, below this mass fraction, adsorption capacity depended on the PAC content. In the case of the much smaller MP, no such limitation was observed at high IONP mass fractions of 54 %. In terms of NOM adsorption kinetics, which are slower than MP adsorption kinetics, the presence of IONP did not change rate constants or diffusion coefficients. MP rate constants, on the other hand, decreased significantly for MPAC compared to PAC due to the reduced micropore volume. For the adsorption of MP and NOM, a lower IONP mass fraction is thus recommended to have the highest amount of the active adsorbent PAC in the composite.

In terms of ***biological growth*** results from Chapter 6 have shown that the presence of IONP does not limit the application of MPAC in the bioreactor. Although the bacterial communities were different on the magnetic adsorbents and nitrification was delayed on MPAC, IONP did not impact the biodegradation of DOC. Also, full nitrification was achieved by all colonized adsorbents once steady state was reached.

When collating data from the stability study and the adsorption studies presented in Chapter 4 and 6, it becomes obvious that MPAC is less ***resistant to attrition*** than PAC and that higher agitation rates are necessary to keep MPAC in suspension due to higher densities of the adsorbent. As density is a function of IONP content, MPAC with a lower mass fraction of IONP should be preferred for long-term applications of MPAC.

In Chapter 7 we observed that a mass fraction of 10 % is too low for efficient ***magnetic separation*** with the proposed separator design. MPAC with 38 % and 54 % IONP were held back in the stainless steel matrix at 2.5 times higher velocity compared to MPAC containing only 10 % IONP. The study also showed that no beneficial effect was obtained by further increasing the IONP content from 38 % to 54 %.

To ensure high enough magnetization and at the same time high PAC content and low density, the IONP content should be higher than 10 % but lower than 38 %. Ultimately, the IONP mass fraction of MPAC has to be adjusted depending on the desired design and strength of the magnetic separator. The study has also shown that MPAC can be produced with any desired IONP content and is thus easy to customize it for the final application.

8.4 Cost vs. benefits

8.4.1 Unit costs of MPAC

The unit costs of MPAC arise from the cost of PAC, the cost of iron salts and sodium hydroxide as well as the energy costs to stir and heat the reactor. In this project we chose a widely used co-precipitation method described in Chapter 4 where ferrous and ferric iron were combined in the molar ratio 1:2 and in the form of the iron salts $FeCl_3$ and $FeSO_4$. Furthermore, sodium hydroxide solution is added to precipitate the solid iron phase. As the adsorbent base material we chose a commercial PAC that is certified for the use in drinking water. Unit costs for MPAC were estimated based on prices for bulk orders of $FeCl_3$, $FeSO_4$ and NaOH (10,000 metric tonnes) in the market of Quebec (APPENDIX D). The price of iron salts and sodium hydroxide are a function of many factors such as the region (country/province), the delivery type (truck/train/tanks), product purity, raw materials, fluctuation of demand and order format. Cost estimations in this chapter should therefore be considered as being rough estimates. Additional costs would arise from the synthesis process of MPAC. In this study, the best quality of MPAC was achieved when working at 70°C and while stirring at 700 rpm. The power for heating and stirring to produce 1 kg of MPAC make up for less than 7 % of the total costs as calculated with current electricity costs in Quebec with 0.08 $/kWh (APPENDIX D). Ultimately, however, the price for energy will depend on the exact process design.

The calculated unit price for IONP is higher than the price of PAC (4.45 $/kg vs. 2.5 $/kg respectively) which means that the price of MPAC increases with increasing IONP content and decreasing PAC content (Figure 8.2). The price of the composite material increases by 0.02 $ per additional percent of IONP. Depending on the mass fraction of IONP in MPAC, more MPAC has to be dosed in the water treatment process to compensate for the lower PAC content. For example, if MPAC is produced with a mass fraction of 20 % IONP, the additional costs compared to PAC arise from the 20 % IONP in the composite and the 20 % higher mass of MPAC that has to be dosed. A small exemplary calculation is given in the APPENDIX D. If only the unit chemical costs were to be considered, a water works that wants to replace a 10 mg/L dose of PAC by MPAC with 20 % IONP, an equivalent of 12.5 mg/L have to be dosed to compensate for the IONP in the composite. The replacement would entail 18 % higher costs compared to the dosage of PAC (12.5 mg MPAC/L at a price of 2.96 $/kg MPAC instead of 10 mg/L of PAC at the price of 2.5 $/kg).

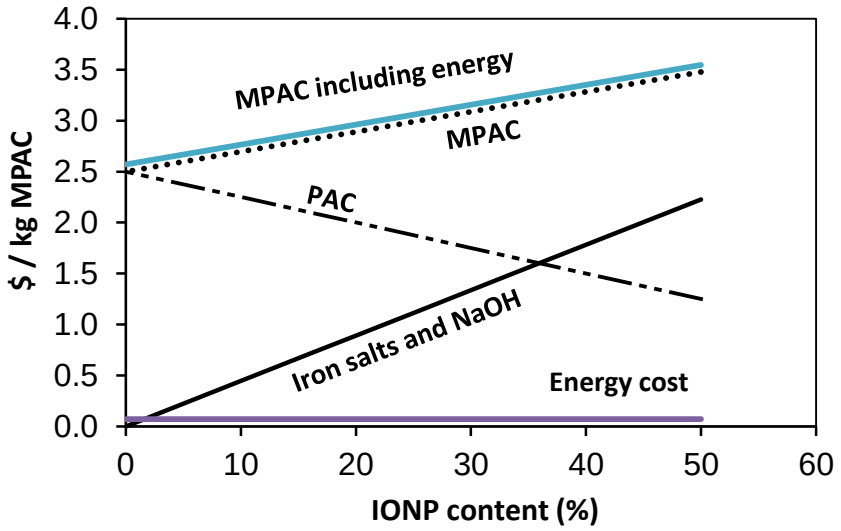

Figure 8.2: Unit costs of raw materials for the preparation of MPAC calculated for metric tons of aqueous salt solutions with 330 $/t (NaOH, 50 %), 180 $/t (FeSO4, 18 %), 140 $/t (FeCl3, 13.8 %) and Energy costs of 0.08 $/kWh.

8.4.2 Scale-up and costs of the magnetic separator

In this project, a small lab-scale separator was designed to explore (i) the influence of the flow rate, IONP content, MPAC concentration and the packing density of the filter medium and (ii) to

test a filter design that uses permanent magnets instead of electromagnets. Estimating costs of adequate magnetic separators for large-scale applications requires i.a. the knowledge about the maximum possible dimensions of the filter to achieve satisfying filtration efficiencies. With our lab-scale test filter we treated water at flow rates of only 200 and 470 mL/min which, in a 1 cm diameter column resulted in flow velocities of 0.04 m/s (144 m/h) and 0.1 m/s (360 m/h) respectively. Such applied velocities are in the range of what would be expected for the design of industrial micro-strainers of 50-500 µm.

To treat a high drinking water flow, the column diameter would have to be increased in size and/or multiple separators would have to be operated in parallel. The limitation of the scale-up is related to the creation of a strong uniform magnetic field with permanent magnets to magnetize the matrix loaded filter column with a large diameter. A mathematical model of the magnetic filter could help to find the maximum column diameter feasible to achieve the necessary magnetization of the filter matrix in the column center; however, scale-up calculations were not within the scope of this project.

Nevertheless, some estimation can be made based on a previous study published by Borghi (2014). Her design consisted of a column filled with small stainless steel spheres and permanent magnets arranged to provide the external homogeneous magnetic field. A column diameter of up to 30 cm and a column length of 120 cm were considered a feasible setup. A magnetic field strength of nearly 0.5 T would be achievable in the centre of such a column. Among different magnets (Sm-Co and Nd-Fe-B), a coated neodymium magnet of medium grade (N33 EH, remanence of 1 T) was considered the most economic choice. For the magnets in their setup with a 15-cm column diameter – able to treat 15 m^3/h (equivalent to 849 m/h) - they received a rough price estimate of 217 k€ from a single company in 2012. While this cost seems high, one has to keep in mind that costs can vary largely among suppliers and that they depend on multiple factors such as the availability of rare earth raw materials and the demand for magnets in other industries. Compared to existing technologies that require electromagnets such as the CoMag, the BioMag, the Hitachi Ballast and the MS-Engineering HGMS process, the advantages of a layout using permanent magnets are that no power supply is required and that the footprint is lower. In general, investment and operating costs can only be determined in the frame of a specific project planning. Nevertheless, this preliminary estimate indicates that such process might be best applicable for low flow applications.

8.4.3 Benefits of using MPAC

Ultimately, the higher product costs of MPAC and the magnetic separator have to be outweighed against the benefits of replacing PAC by MPAC. The benefits of using MPAC instead of PAC arise from its magnetic separability and thus its reusability. Being able to separate MPAC from water, opens the door for its reuse in order to work at higher adsorbent age. Several scenarios for MPAC applications are imaginable:

(i) In pure adsorption processes PAC is usually dosed at low concentration and contact times are low (minutes) e.g. for taste and odor removal. In these conditions, PAC is usually discarded before its adsorption capacity is exhausted. Working with MPAC instead of PAC would allow returning the adsorbent into the PAC reactor until its adsorption capacity is fully exhausted. This would further reduce the amount of virgin MPAC necessary which might reduce or balance the additional costs of MPAC. While re-activation and re-use of GAC is already done to save costs, PAC is usually discarded with the sludge from the coagulation-flocculation step. As MPAC can be recovered, regeneration or reactivation of MPAC could further reduce costs. Regeneration of MPAC has been tested by Kondo et al. (2010), Shi et al. (2013) and Do et al. (2011) by desorbing, incinerating or oxidizing the adsorbed contaminants. More tests are necessary to evaluate regeneration of MPAC and the adsorption properties of regenerated MPAC. Regeneration and re-use of MPAC would further lead to a more sustainable process as the solid fraction in the sludge decreases and thus less solid residual disposal is required.

(ii) In adsorption reactors with high PAC concentration and higher adsorbent age (< 30 d), membranes are usually used to keep PAC in the reactor. Membranes that are in direct contact with PAC have lower lifetimes due to abrasion and clogging issues. Replacing PAC by MPAC solves this problem as MPAC can be removed ahead of the membrane via magnetic separation. A feed flow with low PAC particles is expected to extend the membrane lifetime.

(iii) In combined adsorption/biodegradation reactors with high PAC concentration and high adsorbent age (> 30 d) PAC is at the same time adsorbent and growth support. A biologically working PAC reactor is promising as biodegradation of DOC and ammonia can be achieved and PAC consumption is lower due to the high adsorbent age. Biological PAC reactors have successfully been investigated for drinking water treatment in combination with low-pressure membranes that serve as a barrier for PAC particles and particulate pathogens (Stoquart et al.

2012). So far, the biological PAC-membrane hybrid reactor has not been commercialized as contacting colonized PAC with membranes leads to fouling and clogging issues. Using MPAC instead of PAC solves this problem. As demonstrated in this project, MPAC can be readily colonized to achieve biological DOC and ammonia removal. A magnetic separation step between the PAC reactor and the membrane allows for recycling the adsorbent back into the contactor. Thus the desired PAC age can be achieved while providing a mostly particle free feed flow to the membrane. As magnetic separation is a purely physical separation step, the need for chemicals such as coagulants and flocculation aids become no longer necessary.

(iv) The trend in PAC application is to reduce the particle diameter to 0.1 – 1 µm (Partlan et al. 2016) as so called super-fine PAC or S-PAC. On the one hand, with decreasing diameters, adsorption kinetics increase which is a clear advantage of this product. On the other hand, S-PAC is even more difficult to remove from water and it is thus usually combined with membranes to avoid the export of these fines. Magnetizing S-PAC makes it possible to remove this product with the help of a magnetic separator. As shown in Chapter 7, very fine magnetic PAC with diameters of 40 – 50 nm (aggregate size 1 - 3µm) has already been commercialized in Japan and a HGMS is able to separate it from water.

(v) Thinking outside the drinking water application, MPAC clearly has potential to be applied in industrial applications, where the adsorbate has a high market value making separation lucrative. Also the design flows are lower than in municipal applications. Indeed, most MPAC or other magnetic adsorbents (magnetic nanotubes, etc.) have been proposed for applications like removing dyes or recover gold or other metals as discussed in Chapter 2.6.

In summary, the unit costs of MPAC are higher (approx. 20 % for an IONP content of 25%) compared to the use of PAC. Additional costs arise from the magnetic separation unit. Magnetic separators that use permanent magnets instead of electromagnets would allow cutting the operating costs as no electricity is required to create the magnetic field. Although multiple benefits arise of using MPAC instead of PAC, the advantage is most clearly for the combined adsorption/biodegradation PAC reactor coupled to a low-pressure membrane (HMP) with high PAC age and concentration. While this process has seen no industrial application so far, MPAC combined with a magnetic separator could solve the separation issue without compromising the biological activity or adsorption properties.

CHAPTER 9 CONCLUSIONS AND RECOMMENDATIONS

9.1 Main findings – MPAC in drinking water treatment

This research project sought to evaluate magnetically separable PAC as an alternative adsorbent for drinking water treatment with specific focus on its application in a mixed adsorption/biodegradation/separation process. In this chapter, the findings with regards to the initial research questions are summarized. The initial questions were: How does increasing mass fractions of IONP in MPAC change the pore size and surface area distribution of the adsorbent? Do magnetic IONP on PAC improve or reduce its NOM adsorption capacity? How does the IONP content of MPAC influence their adsorption capacity for micropollutants? Is the same quantity and activity of heterotrophic and nitrifying biomass developing on MPAC with increasing IONP content as on regular PAC or are IONP inhibiting growth and reduce activity? Is there a significant residual MP adsorption capacity on 90-days aged MPAC? Do agitation and colonization of MPAC change its magnetic properties over time? Which IONP mass fraction in MPAC is necessary for efficient separation in a magnetic separator?

The following conclusions were reached regarding the influence of IONP mass fraction in MPAC on pore size and surface area distribution:

- IONP prepared via the co-precipitation method were not uniformly covering the microporous PAC particles; they formed porous clusters and patches of IONP mainly on the PAC surface but were also found inside the carbon matrix of MPAC,
- IONP reduced the primary and secondary micropore volume mostly proportional to the PAC content while the mesopore volume of the composite material was increased compared to PAC due to added volume that is formed in the voids of the IONP crust.

Changes in pore size distribution and surface area as a consequence of IONP deposition depend on the size of IONP and the initial properties of PAC. This research highlighted that measured pore volumes of the composite material have to be used carefully when interpreting adsorption results. Pore volumes and surface area are blocked and produced during the co-precipitation process and their contribution to - or reduction of – adsorption capacity depends on the adsorption capacity of IONP for the target pollutant.

Concerning our research question – do magnetic IONP on PAC improve or reduce the adsorption capacity of PAC for NOM? – our study showed that maghemite IONP do not contribute significantly to the adsorption of NOM itself and reduce the adsorption capacity of MPAC by blocking the mesopores of the carbon matrix. However, this phenomenon is only significant for high IONP mass loading and MPAC could still be of use in a variety of water-treatment applications. If NOM adsorption is the targeted water pollutant and a magnetic PAC is desired, a highly mesoporous PAC with low IONP mass fraction should be chosen to obtain a higher adsorption capacity for NOM. In summary, the following conclusions were drawn:

- IONP contribute little to NOM adsorption due to their lower adsorption capacity per area compared to PAC,
- IONP block mesopores in the carbon matrix and thus reduce the NOM adsorption capacity of MPAC. This effect became important only for the highest IONP mass fractions investigated (54 %),
- The diffusion coefficient D_s for NOM was not influenced by the presence of IONP,
- Adsorption by MPAC and PAC targeted the same NOM fractions regarding aromatic content and molecule size.

Concerning the adsorption of organic MP on MPAC, we showed that IONP did not contribute to the adsorption of the tested pharmaceuticals, herbicides and hormones with different properties. Normalizing adsorption capacities to the PAC content revealed that the adsorption capacity was mostly proportional to the PAC content in MPAC. This shows that MPAC produced via co-precipitation can be customized with respect to its magnetic properties without compromising its adsorption capacity beyond the reduction expected for lower PAC contents. NOM competes with MP for adsorption sites on MPAC and the application of MPAC should consequently be considered as a polishing step after NOM removing treatment steps such as coagulation-flocculation. In summary we conclude:

- IONP did not adsorb significant amounts of any of the tested organic MP of different charge, size, and hydrophobicity.
- Adsorption capacity of MPAC for MP was proportional to the PAC content in MPAC.
- A residual but tenfold lower adsorption capacity for MP exists even for aged MPAC (90 days) that are colonized and covered with biofilm.

Concerning the question as if MPAC can be used in long-term applications in adsorption/biodegradation reactors, we found that:

- IONP on PAC did not influence the DOC and ammonia elimination performance in the bioreactors once steady state was reached.
- The same quantity of active heterotrophic biomass developed on both PAC and MPAC even at high IONP loads.
- While the slightly slower onset of nitrification (6 days) in reactors containing MPAC might be an indicator for their initial inhibition, full nitrification was observed after 40 days on all adsorbent types.
- Bacterial community composition changed from mostly *Betaproteobacteria* to dominantly *Alphaproteobacteria* in the presence of IONP but did not impact the overall treatment performance.

The evaluation of MPAC before and after the colonization study in continuously stirred bioreactors allowed us to conclude on the stability of the magnetic adsorbents. The results corroborated findings from our adsorption studies where MPAC was often vigorously shaken. The following conclusions were drawn:

- Maghemite IONP were stable over the 95 day bioreactor study as confirmed by XRD.
- Saturation magnetization values were 10 – 30 % for aged adsorbents which points at losses of iron oxide from the MPAC structure. This might be related to the attrition between particles in the highly concentrated reactors (10 g/L) and high stirring speeds (120 rpm) necessary to keep heavier adsorbents in suspension.
- From an operational point of view the materials low resistance to abrasion might play a crucial role for process design and should be the topic of further research.

Separation tests with a lab-scale magnetic filter column have demonstrated the separability of MPAC in a magnetic field produced by permanent magnets of medium grade. A setup with a permanent magnet was designed as compared to an electro magnet to reduce investment and operating costs for future applications in drinking water treatment. Varying the operation parameters allowed the following conclusions:

- MPAC containing only 10 % IONP was not efficiently separated with the tested device even at low flow velocity of 0.04 m/s.

- No additional benefit regarding separation was achieved by increasing the IONP content from 38 % to 54 %, both were equally well separated by the device.
- As the drag force is directly proportional to the flow velocity, increasing the flow velocity reduces the separation efficiency of the magnetic separator. MPAC with 38 % and 54 % IONP were separated at 0.04 m/s (200 mL/min) by over 90 %.

Overall, this project has shown that MPAC can be used as an alternative adsorbent and growth support to replace PAC in processes where PAC separation is currently a limitation. MPAC can be separated in a magnetic field without losing its adsorption capacity beyond the reduction in PAC content. IONP did neither hinder the growth of heterotrophic and nitrifying bacteria nor did they significantly contribute to or hinder the adsorption of NOM or MP. Specifically the combined adsorption/biodegradation process could be an application for MPAC. In this process, where PAC particles serve at the same time as adsorbent and growth support for heterotrophic and nitrifying bacteria and a low-pressure membrane removes particulate contaminants such as parasites, the lack of a physical separation step hindered its application at industrial scale so far.

9.2 Future work

During this project, new questions came up as well as ideas for future research venues. It would be interesting to:

- Test MPAC as an adsorbent for taste & odour metabolites such as geosmin and MIB. A pre-test comparing the performance of MPAC containing 54 % IONP and regular PAC has been carried out as a side-project with promising results (APPENDIX E).
- Further tests with a magnetic separator device and a model combining magnetic and hydrodynamic forces in the stainless steel wool filter would help to identify optimum operation parameters and possible scale-up scenarios.
- Reactivation or regeneration of MPAC could further enhance its potential as a sustainable adsorbent. Combined with easily separation from water or sludge opens the doors for longer adsorbent life-times. To the author’s knowledge fewer than 5 publications have tested regeneration so far and results do not yet target typical drinking water contaminants.

BIBLIOGRAPHY

Ai, L. and Jiang, J., 2010. Fast removal of organic dyes from aqueous solutions by AC/ ferrospinel composite. Desalination 262(1-3), 134-140.

Ai, L., Zhang, C. and Chen, Z., 2011a. Removal of methylene blue from aqueous solution by a solvothermal-synthesized graphene/magnetite composite. Journal of Hazardous Materials 192(3), 1515-1524.

Ai, L., Zhang, C., Liao, F., Wang, Y., Li, M., Meng, L. and Jiang, J., 2011b. Removal of methylene blue from aqueous solution with magnetite loaded multi-wall carbon nanotube: kinetic, isotherm and mechanism analysis. Journal of Hazardous Materials 198, 282-290.

Ambashta, R.D. and Sillanpaa, M., 2010. Water purification using magnetic assistance: a review. Journal of Hazardous Materials 180(1-3), 38-49.

American Public Health Association (APHA), American Water Works Association (AWWA) and Water Environment Federation (WEF), 2012. Standard methods for the examination of water and wastewater, American Public Health Association, Washington, D.C.

Andreu, J.S., Barbero, P., Camacho, J. and Faraudo, J., 2012. Simulation of magnetophoretic separation processes in dispersions of superparamagnetic nanoparticles in the noncooperative regime. Journal of Nanomaterials 2012, 1-10.

Anzai, T., Matsuura, Y., Sugawara, T. and Miura, O., 2016. Removal of humic acid in water by rice hull magnetic activated carbon and magnetic separation. Ieee Transactions on Applied Superconductivity 26(4).

Arakha, M., Pal, S., Samantarrai, D., Panigrahi, T.K., Mallick, B.C., Pramanik, K., Mallick, B. and Jha, S., 2015. Antimicrobial activity of iron oxide nanoparticle upon modulation of nanoparticle-bacteria interface. Scientific Reports 5, 14813.

Arora, S., Rajwade, J.M. and Paknikar, K.M., 2012. Nanotoxicology and in vitro studies: the need of the hour. Toxicology and applied pharmacology 258(2), 151-165.

Association Française de Normalisation (AFNOR), 1990. Ammonia dosage by indophenol colorimetric method (Method #T90-015). Recueil des normes françaises: eaux méthodes d'essais (Fourth Edition), p. 736, La Défense. Agence Français de Normalisation, Paris, France.

Athar, M. and Vohora, S.B. (eds), 2001. Heavy metals and environment, New Age International (P), New Delhi, India.

Auffan, M., Achouak, W., Rose, J., Roncato, M.A., Chaneac, C., Waite, D.T., Masion, A., Woicik, J.C., Wiesner, M.R. and Bottero, J.Y., 2008. Relation between the redox state

of iron-based nanoparticles and their cytotoxicity toward *Escherichia coli*. Environmental Science & Technology 42(17), 6730-6735.

Auffan, M., Rose, J., Bottero, J.Y., Lowry, G.V., Jolivet, J.P. and Wiesner, M.R., 2009. Towards a definition of inorganic nanoparticles from an environmental, health and safety perspective. Nature Nanotechnology 4(10), 634-641.

Auffan, M., Bottero, J.Y., Chaneac, C. and Rose, J., 2010. Inorganic manufactured nanoparticles: How their physicochemical properties influence their biological effects in aqueous environments. Nanomedicine 5(6), 999-1007.

Averett, R.C. and Geological, S., 1994. Humic substances in the Suwannee River, Georgia : Interactions, properties, and proposed structures, U.S. Geological Survey, Denver, CO, USA.

Baalousha, M., Manciulea, A., Cumberland, S., Kendall, K. and Lead, J.R., 2008. Aggregation and surface properties of iron oxide nanoparticles: Influence of pH and natural organic matter. Environmental Toxicology and Chemistry 27(9), 1875–1882.

Baghdadi, M., Ghaffari, E. and Aminzadeh, B., 2016. Removal of carbamazepine from municipal wastewater effluent using optimally synthesized magnetic activated carbon: Adsorption and sedimentation kinetic studies. Journal of Environmental Chemical Engineering 4, 3309–3321.

Bansal, R.C. and Meenakshi, G., 2005. Activated carbon adsorption, Taylor & Francis, Boca Raton, FL, USA.

Barceló, D. (ed) 2012. The Handbook of Environmental Chemistry, Springer-Verlag Berlin Heidelberg, Germany.

Bastami, T.R. and Entezari, M.H., 2012. Activated carbon from carrot dross combined with magnetite nanoparticles for the efficient removal of p-nitrophenol from aqueous solution. Chemical Engineering Journal 210, 510-519.

Bédard, E., Charron, D., Lalancette, C., Déziel, E. and Prévost, M., 2014. Recovery of *Pseudomonas aeruginosa* culturability following copper- and chlorine-induced stress. FEMS Microbiology Letters 356(2), 226-234.

Borcherding, J., Baltrusaitis, J., Chen, H., Stebounova, L., Wu, C.M., Rubasinghege, G., Mudunkotuwa, I.A., Caraballo, J.C., Zabner, J., Grassian, V.H. and Comellas, A.P., 2014. Iron oxide nanoparticles induce Pseudomonas aeruginosa growth, induce biofilm formation, and inhibit antimicrobial peptide function. Environmental Science Nano 1, 123-132.

Borghi, C.C., Fabbri, M., Fiorini, M., Mancini, M. and Ribani, P.L., 2011. Magnetic removal of surfactants from wastewater using micrometric iron oxide powders. Separation and Purification Technology 1 83, 180-188.

Borghi, C.C., 2014. Continuous-flow magnetic separation with permanent magnets for water treatment, University of Bologna, Bologna, Italy.

Borghi, C.C. and Fabbri, M., 2014. Magnetic recovery of modified activated carbon powder used for removal of endocrine disruptors present in water. Environmental Technology 35(5-8), 1018-1026.

Boulos, L., Prévost, M., Barbeau, B., Coallier, J. and Desjardins, R., 1999. LIVE/DEAD® *Bac*Light™: application of a new rapid staining method for direct enumeration of viable and total bacteria in drinking water. Journal of Microbiological Methods 37(1), 77-86.

Bourikas, K., Vakros, J., Kordulis, C. and Lycourghiotis, A., 2003. Potentiometric mass titrations: Experimental and theoretical establishment of a new technique for determining the point of zero charge (PZC) of metal (hydr)oxides. Journal of Physical Chemistry B 107(35), 9441-9451.

Camper, A.K., LeChevallier, M.W., Broadaway, S.C. and McFeters, G.A., 1985. Evaluation of procedures to desorb bacteria from granular activated carbon. Journal of Microbiological Methods 3(3-4), 187-198.

Castro, C.S., Guerreiro, M.C., Goncalves, M., Oliveira, L.C. and Anastacio, A.S., 2009. Activated carbon/iron oxide composites for the removal of atrazine from aqueous medium. Journal of Hazard Materials 164(2-3), 609-614.

Çeçen, F. and Aktas, Ö., 2012. Activated carbon for water and wastewater treatment integration of adsorption and biological treatment, Wiley-VCH, Weinheim, Germany.

Centre d'expertise en analyse environnementale du Québec (CEAEQ), 2012. Détermination des métaux : méthode par spectrométrie de masse à source ionisante au plasma d'argon. M. 200 - Mét. 1..2, Rév. 3, p. 36, Ministère du Développement durable, de l'Environnement, de la Faune et des Parcs du Québec.

Chattopadhyaya, G., Macdonald, D.G., Bakhshi, N.N., Soltan Mohammadzadeh, J. and Dalai, A.K., 2006. Preparation and characterization of chars and activated carbons from Saskatchewan lignite. Fuel Processing Technology 87, 997–1006.

Cheng, W., Dastgheib, S.A. and Karanfil, T., 2005. Adsorption of dissolved natural organic matter by modified activated carbons. Water Research 39(11), 2281-2290.

Choo, K.H. and Kang, S.K., 2003. Removal of residual organic matter from secondary effluent by iron oxides adsorption. Desalination 154(2), 139-146.

Chun, J., Lee, H., Lee, S.H., Hong, S.W., Lee, J., Lee, C. and Lee, J., 2012. Magnetite/ mesocellular carbon foam as a magnetically recoverable fenton catalyst for removal of phenol and arsenic. Chemosphere 89(10), 1230-1237.

Cornell, R.M. and Schwertmann, U., 2003. The Iron oxides, Wiley-VCH, Weinheim, Germany.

Crittenden, J.C., H., B.J. and Montgomery, W.H., 2012. MWH's water treatment : Principles and design, John Wiley & Sons, Hoboken, N.J., USA.

Cui, X. and Choo, K.H., 2013. Granular iron oxide adsorbents to control natural organic matter and membrane fouling in ultrafiltration water treatment. Water Research 47(13), 4227-4237.

Cummings, D.L., Himmelblau, D.A., Oberteuffer, J.A. and Powers, G.J., 1976. Capture of small paramagnetic particles by magnetic forces from low speed fluid flows. AICHE Journal 22(3), 569-575.

Dastgheib, S.A., Karanfil, T. and Cheng, W., 2004. Tailoring activated carbons for enhanced removal of natural organic matter from natural waters. Carbon 42(3), 547-557.

Delgado, L.F., Charles, P., Clucina, K. and Morlay, C., 2012. The removal of endocrine disrupting compounds, pharmaceutically activated compounds and cyanobacterial toxins during drinking water preparation using activated carbon - a review. Science of the Total Environment 435-436, 509-525.

Dinali, R., Ebrahiminezhad, A., Manley-Harris, M., Ghasemi, Y. and Berenjian, A., 2017. Iron oxide nanoparticles in modern microbiology and biotechnology. Critical reviews in microbiology 43(4), 493-507.

Dinesh, R., Anandaraj, M., Srinivasan, V. and Hamza, S., 2012. Engineered nanoparticles in the soil and their potential implications to microbial activity. Geoderma 173-174, 19-27.

Do, M.H., Phan, N.H., Nguyen, T.D., Pham, T.T.S., Nguyen, V.K., Vu, T.T.T. and Nguyen, T.K.P., 2011. Activated carbon/Fe_3O_4 nanoparticle composite: fabrication, methyl orange removal and regeneration by hydrogen peroxide. Chemosphere 85, 1269-1276.

Edzwald, J.K. (ed) 2011. Water quality & treatment: A handbook on drinking water, sixth edition, McGraw-Hill, New York.

EPA, U.S.E.P.A., 2016. Contaminant Candidate List (CCL) and Regulatory Determination - Final CCL 4 Chemical Contaminants.

Essandoh, M., Wolgemuth, D., Pittmann Jr., C.U., Mohan, D. and Mlsna, T., 2017. Adsorption of metribuzin from aqueous solution using magnetic and nomagnetic sustainable low-cost biochar adsorbents. Environmental Science and Pollution Research 24, 4577-4590.

Evoqua, 2017. BIOMAG/COMAG–frequently asked questions, Evoqua Water Technologies, http://www.evoqua.com/en/brands/Envirex/productinformationlibrary/BC-BIOCOMAG-FAQ.pdf#search=Biomag/Comag%20-%20Frequently%20Asked%20Questions, 2017.

Faulconer, E.K., von Reitzenstein, N.V.H. and Mazyck, D.W., 2012. Optimization of magnetic powdered activated carbon for aqueous Hg(II) removal and magnetic recovery. Journal of Hazardous Materials 199–200(0), 9-14.

Feng, S., Chen, C., Wang, Q.F., Zhang, X.J., Yang, Z.Y. and Xie, S.G., 2013. Characterization of microbial communities in a granular activated carbon–sand dual media filter for drinking water treatment. International Journal of Environmental Science and Technology 10(5), 917-922.

Georgeaud, V., 1999. Adsorption des métaux lourds sur les oxydes magnétiques, vers des procédés magnétiques de décontamination et d'expertise des sites pollués, Université de Droit, d'Economie et des Sciences d'Aix-Marseille, Aix en Provence Cedex, France.

Gerber, R. and Birss, R.R., 1983. High gradient magnetic separation, Research Studies Press, Chichester; New York.

Gong, J.L., Wang, B., Zeng, G.M., Yang, C.P., Niu, C.G., Niu, Q.Y., Zhou, W.J. and Liang, Y., 2009. Removal of cationic dyes from aqueous solution using magnetic multi-wall carbon nanotube nanocomposite as adsorbent. Journal of Hazardous Materials 164(2-3), 1517-1522.

Gregory, R., Maloney, R.J. and Stockley, M., 1988. Water treatment using magnetite: A study of a sirofloc pilot plant. Water and Environment Journal 2(5), 532–544.

Gu, B., Schmitt, J., Chen, Z., Liang, L. and McCarthy, J.F., 1994. Adsorption and desorption of natural organic matter on iron oxide: mechanisms and models. Environmental Science & Technology 28(1), 38-46.

Halim, A.A., Aziz, H.A., Johari, M.A.M. and Ariffin, K.S., 2010. Comparison study of ammonia and COD adsorption on zeolite, activated carbon and composite materials in landfill leachate treatment. Desalination 262(1-3), 31-35.

Han, Z., Sani, B., Mrozik, W., Obst, M., Beckingham, B., Karapanagioti, H.K. and Werner, D., 2015. Magnetite impregnation effects on the sorbent properties of activated carbons and biochars. Water Research 70, 394-403.

He, S., Feng, Y., Ren, H., Zhang, Y., Gu, N. and Lin, X., 2011. The impact of iron oxide magnetic nanoparticles on the soil bacterial community. Journal of Soils and Sediments 11(8), 1408-1417.

Ho, Y.S. and McKay, G., 1998. Sorption of dye from aqueous solution by peat. Chemical Engineering Journal 70(2), 115-124.

Hu, X., Cook, S., Wang, P. and Hwang, H.M., 2009. In vitro evaluation of cytotoxicity of engineered metal oxide nanoparticles. Science of the Total Environment 407(8), 3070-3072.

Ilbay, Z., Sahin, S., Kerkez, Ö. and Bayazit, S.S., 2015. Isolation of naproxen from wastewater using carbon-based magnetic adsorbents. Internation Journal of Environmental Science and Technology 12, 3541-3550.

Jin, J.X., Liu, H.K., Zeng, R. and Dou, S.X., 2000. Developing a HTS magnet for high gradient magnetic separation techniques. Proceedings of the International Conference on Materials and Mechanisms of Superconductivity High Temperature Superconductors VI - Physica C 341, 2611-2612.

Jones, M., 1984. Nitrate reduction by shaking with cadmium: Alternative to cadmium columns. Water Research 18(5), 643-646.

Ju-Nam, Y. and Lead, J.R., 2008. Manufactured nanoparticles: An overview of their chemistry, interactions and potential environmental implications. The Science of the total environment 400(1-3), 396-414.

Kafayati, M.E., Raheb, J., Torabi Angazi, M., Alizadeh, S. and Bardania, H., 2013. The effect of magnetic Fe_3O_4 nanoparticles on the growth of genetically manipulated bacterium, *Pseudomonas aeruginosa* (PTSOX4). Iranian Journal of Biotechnology 11(1), 41-46.

Kahani, S.A., Hamadanian, M. and Vandadi, O., 2007. Deposition of magnetite nanoparticles in activated carbons and preparation of magnetic activated carbons. AIP Conference Proceedings 929, 183-188.

Kang, S.K. and Choo, K.H., 2010. Why does a mineral oxide adsorbent control fouling better than powdered activated carbon in hybrid ultrafiltration water treatment? Journal of Membrane Science 355(1-2), 69-77.

Kim, C., Lee, S.I., Hwang, S., Cho, M., Kim, H.S. and Noh, S.H., 2014. Removal of geosmin and 2-methylisoboneol (2-MIB) by membrane system combined with powdered activated carbon (PAC) for drinking water treatment. Journal of Water Process Engineering 4, 91-98.

Kim, S., Kim, J. and Seo, G., 2013. Iron oxide nanoparticle-impregnated powder-activated carbon (IPAC) for NOM removal in MF membrane water treatment system. Desalination and Water Treatment 51(31-33), 6392-6400.

Klaine, S.J., Alvarez, P.J., Batley, G.E., Fernandes, T.F., Handy, R.D., Lyon, D.Y., Mahendra, S., McLaughlin, M.J. and Lead, J.R., 2008. Nanomaterials in the environment: Behavior, fate, bioavailability, and effects. Environmental Toxicology and Chemistry 27(9), 1825-1851.

Koduru, J.R., Lingamdinne, L.P., Singh, J. and Choo, K.H., 2016. Effective removal of bisphenol A (BPA) from water using a goethite/activated carbon composite. Process Safety and Environmental Protection 103, 87-96.

Kondo, K., Jin, T. and Miura, O., 2010. Removal of less biodegradable dissolved organic matters in water by superconducting magnetic separation with magnetic mesoporous carbon. Physica C: Superconductivity 470(20), 1808-1811.

Kovalova, L., Knappe, D.R.U., Lehnberg, K., Kazner, C. and Hollender, J., 2013. Removal of highly polar micropollutants from wastewater by powdered activated carbon. Environmental Science and Pollutant Research 20, 3607–3615.

Lagergren, S., 1898. Zur Theorie der sogenannten Adsorption gelöster Stoffe. K. Sven. Vetenskapsakad. Handl. Band 24(4), 1-39.

Lead, J.R., Wilkinson, K.J., Balnois, E., Cutak, B.J., Larive, C.K., Assemi, S. and Becket, R., 2000. Diffusion coefficients and polydispersities of the Suwannee River fulvic acid: comparison of fluorescence corelation spectroscopy, pulsed-field gradient nuclear magnetic resonance, and flow field-flow fractionation. Environmental Science & Technology 34(16), 3508-3513.

Lebeau, T., Lelièvre, C., Buisson, H., Cléret, D., Van de Venter, L.W. and Côté, P., 1998. Immersed membrane filtration for the production of drinking water: Combination with PAC for NOM and SOCs removal. Desalination 117(1), 219-231.

Lebeau, T., Lelièvre, C., Wolbert, D., Laplanche, A., Prados, M. and Côté, P., 1999. Effect of natural organic matter loading on the atrazine adsorption capacity of an aging powdered activated carbon slurry. Water Research 33(7), 1695-1705.

Lee, J., Jin, S., Hwang, Y., Park, J.G., Park, H.M. and Hyeon, T., 2005. Simple synthesis of mesoporous carbon with magnetic nanoparticles embedded in carbon rods. Carbon 43(12), 2536-2543.

Leveillé, S., Carrière, A., Charest, S. and Barbeau, B., 2013. PAC membrane bioreactor as an alternative to biological activated carbon filters for drinking water treatment. Journal of Water Supply: Research and Technology-AQUA 62(1), 23-34.

Li, W., 2011. Elaboration par un procédé de précipitation de nanoparticules aux propriétés contrôlées. Application à la magnétite, Nancy-Université - Institut National Polytechnique de Lorraine (INPL), France.

Liu, N., Yin, L., Zhang, L., Wang, C., Lun, N., Qi, Y. and Wang, C., 2011. Ferromagnetic Ni decorated ordered mesoporous carbons as magnetically separable adsorbents for methyl orange. Materials Chemistry and Physics 131(1–2), 52-59.

Liu, Z., Zhang, F.S. and Sadai, R., 2010. Arsenate removal from water using Fe_3O_4-loaded activated carbon prepared from waste biomass. Chemical Engineering Journal 160(1), 57-62.

Lompe, K.M., Menard, D. and Barbeau, B., 2016. Performance of biological magnetic powdered activated carbon for drinking water purification. Water Research 96, 42-51.

Lompe, K.M., Menard, D. and Barbeau, B., 2017. The influence of iron oxide nanoparticles upon the adsorption of organic matter on magnetic powdered activated carbon. Water Research 123, 30-39.

Lu, A.H., Salabas, E.L. and Schuth, F., 2007. Magnetic nanoparticles: Synthesis, protection, functionalization, and application. Angewandte Chemie International Edition 46(8), 1222-1244.

Luo, X. and Zhang, L., 2009. High effective adsorption of organic dyes on magnetic cellulose beads entrapping activated carbon. Journal of Hazard Materials 171(1-3), 340-347.

Luyts, K., Napierska, D., Nemery, B. and Hoet, P.H.M., 2013. How physico-chemical characteristics of nanoparticles cause their toxicity: complex and unresolved interrelations. Environmental Science: Processes & Impacts 15(1), 23.

Ma, B., Wang, S., Li, Z., Gao, M., Li, S., Guo, L., She, Z., Zhao, Y., Zheng, D., Jin, C., Wang, X. and Gao, F., 2017a. Magnetic Fe_3O_4 nanoparticles induced effects on performance and microbial community of activated sludge from a sequencing batch reactor under long-term exposure. Bioresource Technology 225(377-385).

Ma, J., Yang, Q., Xu, D., Zeng, X., Wen, Y. and Liu, W., 2017b. Efficient removal of antibiotics in a fluidized bed reactor by facile fabricated magnetic powdered activated carbon. Environmental Science and Pollution Research 24, 3820-3828.

Magic-Knezev, A., Wullings, B. and Van der Kooij, D., 2009. *Polaromonas* and *Hydrogenophaga* species are the predominant bacteria cultured from granular activated carbon filters in water treatment. Journal of Applied Microbiology 107(5), 1457-1467.

Markarian, A., Carrière, A., Dallaire, P.O., Servais, P. and Barbeau, B., 2010. Hybrid membrane process: Performance evaluation of biological PAC. Journal of Water Supply: Research and Technology-AQUA 59(4), 209-220.

Marsh, H. and Rodriguez-Reinoso, F., 2006. Activated Carbon, Elsevier, Amsterdam, Netherlands.

Masuda, H., Higashitani, K. and Yoshida, H., 2006. Powder technology handbook, Taylor & Francis, Boca Raton, FL, USA.

Mayo, J.T., Yavuz, C., Yean, S., Cong, L., Shipley, H., Yu, W., Falkner, J., Kan, A., Tomson, M. and Colvin, V.L., 2007. The effect of nanocrystalline magnetite size on arsenic removal. Science and Technology of Advanced Materials 8(1-2), 71-75.

Mohan, D., Sarswat, A., Singh, V.K., Alexandre-Franco, M. and Pittman, C.U., 2011. Development of magnetic activated carbon from almond shells for trinitrophenol removal from water. Chemical Engineering Journal 172(2-3), 1111-1125.

Moore, M.N., 2006. Do nanoparticles present ecotoxicological risks for the health of the aquatic environment? Environment International 32(8), 967-976.

Moreau, M. (23-04-2013). Coûts unitaires, E-mail communication with Barbeau, B.

Morissette M.F., Vo Duy S., Arp H.P. and Sauvé S., 2015. Sorption and desorption of diverse contaminants of varying polarity in wastewater sludge with and without alum. Environmental Science: Processes & Impacts 17, 674-682.

MS-Engineering, 2006. Adsorption of Contaminants by MACs and Magnetic Separation, OSAKA, JAPAN, http://www.ms-engineering.co.jp/eng/index.htm, 2017.

Najm, I.N., 1996. Mathematical modeling of PAC adsorption processes. Journal of the American Water Works Association 88(10), 79-89.

Nakahira, A., Nishida, S. and Fukunishi, K., 2006. Synthesis of magnetic activated carbons for removal of environmental endocrine disrupter using magnetic vector. Journal of the Ceramic Society of Japan 114(1325), 135-137.

Nakahira, A., Nagata, H., Takimura, M. and Fukunishi, K., 2007. Synthesis and evaluation of magnetic active charcoals for removal of environmental endocrine disrupter and heavy metal ion. Journal of Applied Physics 101(9), 09J114-111-109J114-113.

Neal, A.L., 2008. What can be inferred from bacterium-nanoparticle interactions about the potential consequences of environmental exposure to nanoparticles? Ecotoxicology 17(5), 362-371.

Nethaji, S., Sivasamy, A. and Mandal, A.B., 2013. Preparation and characterization of corn cob activated carbon coated with nano-sized magnetite particles for the removal of Cr(VI). Bioresource Technology 134, 94-100.

Newcombe, G., Drikas, M. and Hayes, R., 1997. Influence of characterised natural organic material on activated carbon adsorption: II. Effect on pore volume distribution and adsorption of 2-methlylisobornoel. Water Research 31(5), 1065-1073.

Ni, S.Q., Ni, J., Yang, N. and Wang, J., 2013. Effect of magnetic nanoparticles on the performance of activated sludge treatment system. Bioresource Technology 143, 555-561.

Nicol, A.W. (ed) 1975. Physicochemical methods of mineral analysis, Plenum Press, New York, London.

Niemi, R.M., Heiskanen, I., Heine, R. and Rapala, J., 2009. Previously uncultured beta-Proteobacteria dominate in biologically active granular activated carbon (BAC) filters. Water Research 43(20), 5075-5086.

Oh, H.K., Takizawa, S., Ohgaki, S., Katayama, H., Oguma, K. and Yu, M.J., 2007. Removal of organics and viruses using hybrid ceramic MF system without draining PAC. Desalination 202(1-3), 191-198.

Ohara, T., Kumakura, H. and Wada, H., 2001. Magnetic separation using superconducting magnets. Physica C: Superconductivity 357-360(Part 2), 1272–1280.

Okamoto, T., Tachibana, S., Miura, O. and Takeuchi, M., 2011. Mercury removal from solution by superconducting magnetic separation with nanostructured magnetic adsorbents. Physica C: Superconductivity 471, 1516-1519.

Oligny, L., Bérubé, P. and Barbeau, B., 2016. Impact of PAC fines in fouling of polymeric and ceramic low-pressure membranes for drinking water treatment. Membranes 6(3), 1-14.

Oliveira, L.C.A., Rios, R.V.R.A., Fabris, J.D., Garg, V., Sapag, K. and Lago, R.M., 2002. Activated carbon/iron oxide magnetic composites for the adsorption of contaminants in water. Carbon 40(12), 2177-2183.

Pankhurst, Q.A., 2003. Applications of magnetic nanoparticles in biomedicine. Journal of Physics D: Applied Physics 36, R167–R181.

Park, H.S., Koduru, J.R., Choo, K.H. and Lee, B., 2015. Activated carbons impregnated with iron oxide nanoparticles for enhanced removal of bisphenol A and natural organic matter. Journal of Hazard Materials 286, 315-324.

Parlayici, S. and Pehlivan, E., 2017. Removal of metals by Fe_3O_4 loaded activated carbon prepared from plum stone (prunus nigra): kinetics and modelling study. Powder Technology 317, 23-30.

Partlan, E., Davis, K., Ren, Y., Apul, O.G., Mefford, O.T., Karanfil, T. and Ladner, D.A., 2016. Effect of bead milling on chemical and physical characteristics of activated carbons pulverized to superfine sizes. Water Research 89, 161-170.

Prescott, L.M., Harley, J.P. and Klein, D.A., 2005. Microbiology (Sixth Edition), The McGraw Hill Companies Inc., New York, NY, USA.

PubChem, 2017. Open chemistry database, p. CID 3386, National Center for Biotechnology Information, USA, https://pubchem.ncbi.nlm.nih.gov/, 2017.

Rahman, M.S., Whalen, M. and Gagnon, G.A., 2013. Adsorption of dissolved organic matter (DOM) onto the synthetic iron pipe corrosion scales (goethite and magnetite): Effect of pH. Chemical Engineering Journal 234, 149-157.

Rakshit, S., Sarkar, D., Elzinga, E.J., Punamiya, P. and Datta, R., 2013. Mechanisms of ciprofloxacin removal by nano-sized magnetite. Journal of Hazard Materials 246–247, 221– 226.

Reddy, L.H., Arias, J.L., Nicolas, J. and Couvreur, P., 2012. Magnetic nanoparticles: design and characterization, toxicity and biocompatibility, pharmaceutical and biomedical applications. Chemical Reviews 112, 5818−5878.

Rudge, S.R., Kurtz, T.L., Vessely, C.R., Catterall, L.G. and Williamson, D.L., 2000. Preparation, characterization, and performance of magnetic iron–carbon composite microparticles for chemotherapy. Biomaterials 21(14), 1411-1420.

Safarik, I., Nymburska, K. and Safarikova, M., 1997. Adsorption of water-soluble organic dyes on magnetic charcoal. Journal of Chemical Technology & Biotechnology 69(1), 1-4.

Safarik, I., Horska, K., Pospiskova, K., Maderova, Z. and Safarikova, M., 2013. Microwave assisted synthesis of magnetically responsive composite materials. Ieee Transactions on Magnetics 49(1), 213-218.

Saroyan, H.S., Giannakoudakis, D.A., Sarafidis, C.S., Lazaridis, N.K. and Deliyanni, E.A., 2017. Effective impregnation for the preparation of magnetic mesoporous carbon - application to dye adsorption. Journal of Chemical Technolgy and Biotechnology 92, 1899-1911.

Saucier, C., Karthickeyan, P., Ranjithkumar, V., Lima, E.C., Dos Reis, G.S. and De Brum, I.A.S., 2017. Efficient removal of amoxicillin and paracetamol from aqueous solutions using magnetic activated carbon. Environmental Science and Pollutant Research 24, 5918-5932.

Seo, G.T., Jang, S.W., Lee, S.H. and Yoon, C.H., 2005. The fouling characterization and control in the high concentration PAC membrane bioreactor HCPAC-MBR. Water Science and Technology 51(6-7), 77-84.

Servais, P., Anzil, A. and Ventresque, C., 1989. Simple method for determination of biodegradable dissolved organic carbon in water. Applied and Environmental Microbiology 55(10), 2732-2734.

Servais, P., Billen, G., Ventresque, C. and Bablon, G.P., 1991. Microbial activity in GAC filters at the Choisy-le-Roi treatment plant. Journal of the American Water Works Association 83(2), 62-68.

Shan, D., Deng, S., Zhao, T., Wang, B., Wang, Y., Huang, J., Yu, G., Winglee, J. and Wiesner, M.R., 2016. Preparation of ultrafine magnetic biochar and activated carbon for pharmaceutical adsorption and subsequent degradation by ball milling. Journal of Hazard Materials 305, 156-163.

Shi, S., Fan, Y. and Huang, Y., 2013. Facile low temperature hydrothermal synthesis of magnetic mesoporous carbon nanocomposite for adsorption removal of ciprofloxacin antibiotics. Industrial & Engineering Chemistry Research 52(7), 2604-2612.

Shindo, D. and Oikawa, T., 2002. Analytical electron microscopy for material science, Springer, Tokyo.

Simonet, B.M. and Valcarcel, M., 2009. Monitoring nanoparticles in the environment. Analytical and Bioanalytical Chemistry 393(1), 17-21.

Snoeyink, V.L. and Summers, R.S., 1999. Water quality and treatment: A handbook of community water supplies, pp. 13.11-13.83, American Water Work Association.

Spaldin, N.A., 2003. Magnetic materials : fundamentals and device applications, Cambridge University Press, Cambridge, Uk; New York.

Stoquart, C., Servais, P., Bérubé, P. and Barbeau, B., 2012. Hybrid membrane processes using activated carbon treatment for drinking water production: A review. Journal of Membrane Science 411–412, 1-12.

Stoquart, C., Barbeau, B., Servais, P. and Vázquez-Rodríguez, G.A., 2014a. Quantifying bacterial biomass fixed onto biological activated carbon (PAC and GAC) used in drinking water treatment. Journal of Water Supply: Research and Technology—AQUA 63(1), 11.

Stoquart, C., Servais, P. and Barbeau, B., 2014b. Ammonia removal in the carbon contactor of a hybrid membrane process. Water Research 67, 255-266.

Stoquart, C., Vázquez Rodríguez, G.A., Servais, P., Sauvé, S. and Barbeau, B., 2016. Micropollutant removal potential by aged powdered activated carbon. Journal of Environmental Engineering 142(11), 04016058.

Sudheer Khan, S., Bharath Kumar, E., Mukherjee, A. and Chandrasekaran, N., 2011. Bacterial tolerance to silver nanoparticles (SNPs): aeromonas punctata isolated from sewage environment. Journal of basic microbiology 51(2), 183-190.

Svarovsky, L., 2000. Solid-liquid separation, Butterworth-Heinemann, Oxford; Boston.

Tajabadi, M. and Khosroshahi, M.E., 2012. Effect of alkaline media concentration and modification of temperature on magnetite synthesis method using Fe_SO_4/NH_4OH. International Journal of Chemical Engineering and Applications 3(3), 206-2010.

Tarleton, S. and Wakeman, R., 2007. Solid/Liquid separation equipment selection and process design, Elsevier Science, Burlington, http://public.eblib.com/EBLPublic/PublicView.do?ptiID=282090.

Teja, A.S. and Koh, P.Y., 2009. Synthesis, properties, and applications of magnetic iron oxide nanoparticles. Progress in Crystal Growth and Characterization of Materials 55(1-2), 22-45.

Ternes, T.A. and Joss, A. (eds), 2006. Human pharmaceuticals, hormones and fragrances. The challenge of micropollutants in urban water management, IWA Publishing, London, UK.

Thommes, M., 2010. Physical adsorption characterization of nanoporous materials. Chemie Ingenieur Technik 82(7), 1059-1073.

Tuutijarvi, T., Lu, J., Sillanpaa, M. and Chen, G., 2009. As(V) adsorption on maghemite nanoparticles. Journal of Hazardous Materials 166(2-3), 1415-1420.

Valdiglesias, V., Fernández-Bertólez, N., Kiliç, G., Costa, C., Costa, S., Fraga, S., Bessa, M.J., Pásaro, E., Teixeira, J.P. and Laffon, B., 2016. Are iron oxide nanoparticles safe? Current knowledge and future perspectives. Journal of Trace Elements in Medicine and Biology 38, 53–63.

Vaughan Jr., R.L. and Reed, B.E., 2005. Modeling As(V) removal by iron oxide impregnated activated carbon using the surface complexation approach. Water Res 39, 1005-1014.

Velten, S., Hammes, F., Boller, M. and Egli, T., 2007. Rapid and direct estimation of active biomass on granular activated carbon through adenosine tri-phosphate (ATP) determination. Water Research 41(9), 1973-1983.

Velten, S., Boller, M., Köster, O., Helbing, J., Weilenmann, H.U. and Hammes, F., 2011. Development of biomass in a drinking water granular active carbon (GAC) filter. Water Research 45(19), 6347-6354.

Veolia Water, 2013. Opaline, la sécurité sanitaire en eau potable. Retrieved 15 october, 2013. Veolia Water, S.T. (ed), p. 2, http://www.veoliawaterst.com/opaline/fr/.

Vittori Antisari, L., Carbone, S., Gatti, A., Vianello, G. and Nannipieri, P., 2013. Toxicity of metal oxide (CeO_2, Fe_3O_4, SnO_2) engineered nanoparticles on soil microbial biomass and their distribution in soil. Soil Biology and Biochemistry 60, 87-94.

Wang, C., Liu, Q., Cheng, X.L. and Shen, Z., 1994. Adsorption and desorption of gold on magnetic activated carbon. Journal of Materials Science & Technology 10(2), 151-153.

Wang, D.W., Li, F., Lu, G.Q. and Cheng, H.M., 2008. Synthesis and dye separation performance of ferromagnetic hierarchical porous carbon. Carbon 46(12), 1593-1599.

Wang, T., Zhang, D., Dai, L., Chen, Y. and Dai, X., 2016. Effects of metal nanoparticles on methane production from waste-activated sludge and microorganism community shift in anaerobic granular sludge. Scientific reports 6(25857), 1-10.

Wang, Y., Yang, S. and Jingjing, L., 2012. Preparation and characterization of superparamagnetic porous carbon. Proceedings of 2012 2nd International Conference on Materials, Mechatronics and Automation (ICMMA 2012) - Lecture Notes in Information Technology 15, 459-462.

Wang, Y.X.J., 2011. Superparamagnetic iron oxide based MRI contrast agents: Current status of clinical application. Quantitative Imaging in Medicine and Surgery 1, 35-40.

Wang, Z., Lee, Y.H., Wu, B., Horst, A., Kang, Y., Tang, Y.J. and Chen, D.R., 2010. Anti-microbial activities of aerosolized transition metal oxide nanoparticles. Chemosphere 80(5), 525-529.

Weishaar, J.L., Aiken, G.R., Bergamaschi, B.A., Fram, M.S., Fujii, R. and Mopper, K., 2003. Evaluation of specific ultraviolet absorbance as an indicator of the chemical composition and reactivity of dissolved organic carbon. Environmental Science & Technology 37(20), 4702-4708.

Westwood, S.M., 1993. The physics of magnetic particle inspection, University of Durham.

Worch, E., 2012. Adsorption technology in water treatment. Fundamentals, processes, and modelling, De Gruyter, Berlin/Boston.

Yang, M., Xie, Q., Zhang, J., Liu, J., Wang, Y., Zhang, X. and Zhang, Q., 2010. Effects of coal rank, Fe_3O_4 amounts and activation temperature on the preparation and characteristics of magnetic activated carbon. Mining Science and Technology (China) 20(6), 872-876.

Yang, N., Zhu, S., Zhang, D.W. and Xu, S., 2008. Synthesis and properties of magnetic Fe_3O_4-activated carbon nanocomposite particles for dye removal. Materials Letters 62(4-5), 645-647.

Zahoor, M. and Mahramonlioglu, M., 2011. Adsorption of imidacloprid on powdered activated carbon and magnetic activated carbon. Chemical & Biochemical Engineering Quarterly 25(1), 55-63.

Zahoor, M., 2014. Removal of humic acid from water through adsorption–ultrafiltration hybrid processes. Desalination and Water Treatment 52(40-42), 7983-7992.

Zhang, D., Niu, H., Zhang, X., Meng, Z. and Cai, Y., 2011. Strong adsorption of chlorotetracycline on magnetite nanoparticles. Journal of Hazard Materials 192(3), 1088-1093.

Zhang, Q.L., Lin, Y.C., Chen, X. and Gao, N.Y., 2007. A method for preparing ferric activated carbon composite adsorbents to remove arsenic from drinking water. Journal of Hazardous Materials 148(3), 671-678.

Zhang, Z.Z., Cheng, Y.F., Bai, Y.H., Xu, L.Z.J., Xu, J.J., Shi, Z.J., Zhang, Q.Q. and Jin, R.C., 2018. Enhanced effects of maghemite nanoparticles on the flocculent sludge wasted from a high-rate anammox reactor: Performance, microbial community and sludge characteristics. Bioresource Technology 250, 265-272.

APPENDIX A SUPPLEMENTARY INFORMATION, ARTICLE 2

Journal: Water Research

Title: Removal of micropollutants by fresh and colonized magnetic powdered activated carbon

Authors: Kim M. Lompe, David Menard, Benoit Barbeau

Table A-1 : Studies of NOM adsorption on magnetic PAC.

Adsorbent and NOM	Characterization				Results	Reference
	K_F (mg/g) $(L/mg)^{1/n}$	$1/n$ (-)	Surface area (m^2/g)	Pore volume (mL/g)		
Rice hull PAC impregnated with magnetite NP, magnetization saturation of 6.27; 10.2 and 20.8 Am^2/kg, Fe_3O_4 mass fraction[a] of 7 %, 11 % and 23 %, Commercial HA (Wako)	-	-	-	-	30 % lower HA removal by MPAC with highest magnetite content compared to MPAC with lowest magnetite content. HA removal > 70 % by all MPAC from a 50 mg HA/L solution by addition of 5 g MPAC/L after 120 min.	(Anzai et al. 2016)
PAC (Norit) and MPAC* with maghemite and goethite NP, 20 % iron oxide mass fraction[c] HA (Sigma Aldrich)	15.4 6.9*	0.64 0.94*	1150 868 *	0.34 (micro) 0.21* (micro) 0.085 (meso) 0.065* (meso)	Reduced adsorption capacity for HA (121.2 mg/g vs. 95.7 mg/g) was attributed to lower surface area (BET isotherm).	(Zahoor 2014)
Heat treated wood (w) and coal (C) based PAC and MPAC* with magnetite NP, magnetization saturation of 6.75-8.04 Am^2/kg, Fe_3O_4 mass fraction[a] of ca. 8 %, NOM from IHSS	33.4(w) 19.4(w)* 3.0(C) 0.49(C) *	0.53(w) 0.87(w)* 1.49(C) 3.18(C) *	1239 (w) 835(w)* 959(C) 745(C) *	0.29(w) (micro) 0.19(w)*(micro) 0.22(C) (micro) 0.17(C)* (micro)	Among all heat-treated adsorbents, MPAC had lower adsorption capacities for NOM than PAC. Surface area and pore volumes measured via BET isotherms.	(Kim et al. 2013)
Lignite based PAC and MPAC impregnated with ferrihydrite*, hematite** and magnetite***, iron oxide mass fractions[b] of 2.6 %*; 2.2 %** and 1.8 %***, NOM concentrated from Water treatment plant, Daegu, Korea	0.08 6.82* 6.23** 5.42***	1.57 1.64* 0.90** 0.99***	631 323* 522** 622***	0.71 0.41* 0.68** 0.71***	Although surface area and pore volume decreased (BET isotherm), higher NOM adsorption rate and capacity achieved on MPAC (ferrihydrite > magnetite > hematite > PAC)	(Park et al. 2015)
Coconut based PAC* and MPAC impregnated with magnetite followed by heat treatment in CO_2 atmosphere, magnetization saturation 6.43 – 30.7 Am^2/kg, magnetite mass fractions[a] between 7 %** and 34 %, Commercial HA	-	-	928* 1190**	-	No difference of HA removal between MPAC and PAC when no CO_2- heat treatment was applied. HA removal by MPAC improved following CO_2-heat treatment which increased the BET surface area	(Kondo et al. 2010)

[a] Estimated from given saturation magnetizations (Am^2/kg) and the literature value for magnetite IONP of 90 Am^2/kg (Cornell and Schwertmann 2003)

[b] Estimated from given Fe-content and molecular weight of 168.7 g/mol*; 231.5 g/mol** and 159.7 g/mol***

[c] Estimated from the difference in bulk density

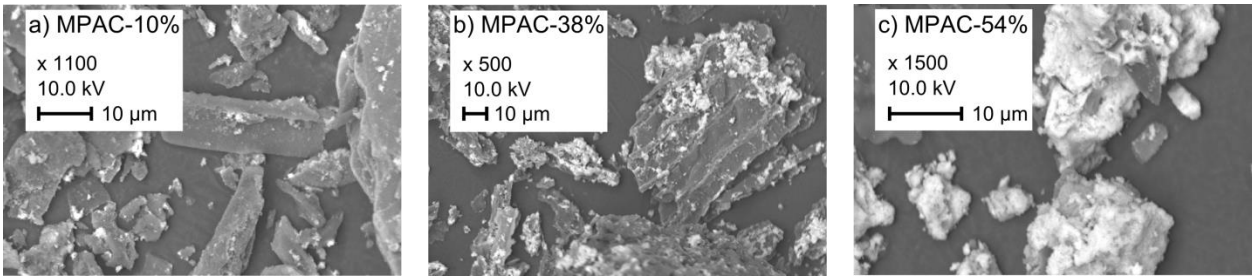

Figure A-1 : SEM images of MPAC with different IONP mass fractions a) 10 %, b) 38 % and c) 54 % show the distribution of IONP on the PAC particles. IONP are visible as white areas on the grey PAC particles. Particles of MPAC-10% and MPAC-38% samples appeared sparely covered with clumps of IONP whereas MPAC-54% samples show a more continuous IONP crust.

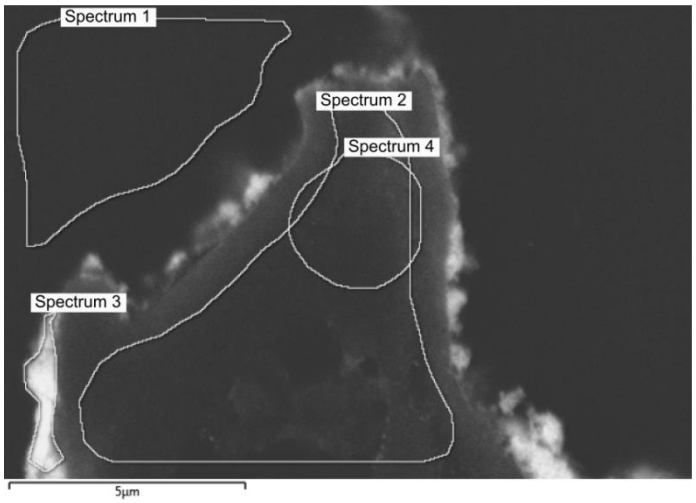

Figure A-2 : SEM image of a cross section of MPAC-54% particle embedded in a polished epoxy matrix showing the four regions used for EDS spectra recording. Region 1 is the epoxy matrix, region 2 is a large area inside the particle, region 3 is the IONP crust on the particle's surface and region 4 is a small area inside the particle.

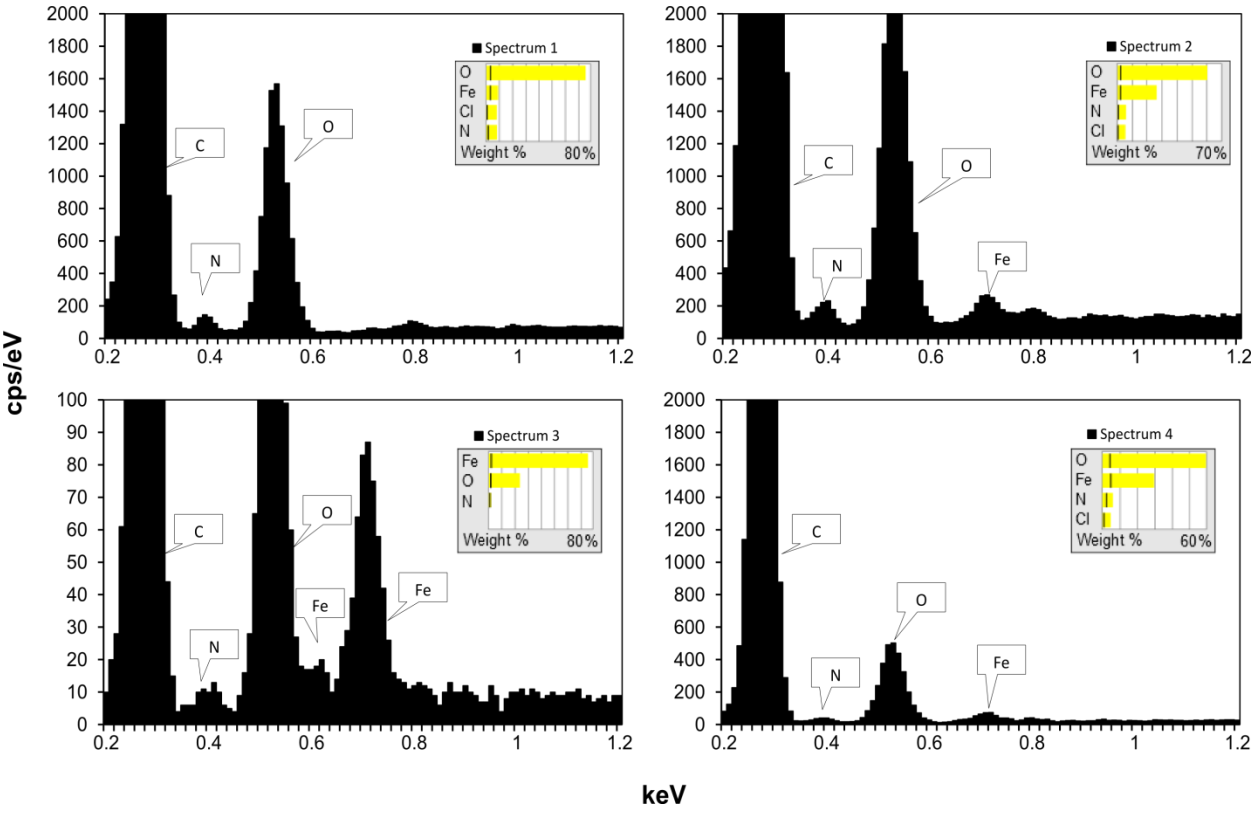

Figure A-3 : EDS spectra from regions 2 to 4 of the MPAC-54% particle show the presence of iron inside the particle and in the crust on the surface of the particle (region 3). Spectra 1 is the reference region 1 (epoxy matrix).

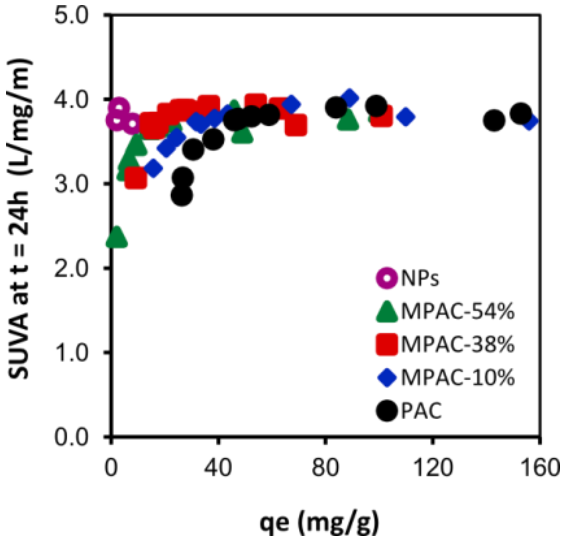

Figure A-4 : $SUVA_{254}$ indices of the SR-NOM solutions after adsorption isotherm experiments show no specific selectivity of IONP for the aromatic NOM fraction of SR-NOM.

Table A-2 : Distribution of pore volume (*V*) and surface area (*SA*) for PAC and MPAC.

Adsorbent	*SA* BET[b]	$V_{micro,DR}$[c]	V_{meso}[d]	V_{total}	NLDFT model[a]						
					$V_{prim.\ micro}$ < 0.8 nm	$V_{second.\ micro}$ 0.8 – 2 nm	V_{meso} 2 – 50 nm	V_{total}	*V* > 1 nm	*SA* total	*SA* >1nm
	(m²/g)	(mL/g)	(mL/g)	(mL/g)	(mL/g)	(mL/g)	(mL/g)	(mL/g)	(mL/g)	(m²/g)	(m²/g)
PAC	769	0.39	0.15	0.54	0.26	0.12	0.13	0.51	0.23	1256	238
MPAC-10%	521	0.24	0.17	0.41	0.15	0.08	0.17	0.39	0.24	783	215
MPAC-38%	575	0.25	0.38	0.63	0.13	0.06	0.38	0.57	0.55	751	275
MPAC-54%	417	0.18	0.55	0.72	0.08	0.05	0.46	0.59	0.64	443	173
Fe_2O_3 NP	-	-	-	-	-	-	-	-	-	64.3[c]	-

[a] non-local density functional theory, [b] Brunauer-Emmet-Teller model, [c] Dubinin-Radushkevich model in the relative pressure range $p/p_0 = 10^{-5} – 10^{-1}$, [d] as difference between $V_{total} – V_{micro,DR}$

Table A-3 : Pseudo-second order kinetic model parameters and HSDM parameters.

Adsorbent	Ref.	Pseudo-second order model			Homogeneous surface diffusion model		
		k_2 (g/mg/min)	R^2 (a)	*RMSE* (b)	D_s (m²/s)	R^2 (c)	*RMSE* (b)
PAC	This study	$1.21 \cdot 10^{-3}$ ($1.21 \cdot 10^{-3}$)*	0.999	0.044	$0.91 \cdot 10^{-14}$	0.916	0.170
MPAC-38%		$2.53 \cdot 10^{-3}$ ($1.57 \cdot 10^{-3}$)*	0.998	0.278	$1.21 \cdot 10^{-14}$	0.890	0.107
MPAC-54%		$1.89 \cdot 10^{-3}$ ($8.67 \cdot 10^{-4}$) *	0.996	0.009	$1.18 \cdot 10^{-14}$	0.875	0.055
PAC	(Zahoor 2014)	$7.50 \cdot 10^{-4}$	0.989		-	-	-
MAC	(Zahoor 2014)	$1.30 \cdot 10^{-2}$	0.998		-	-	-

(a) R^2 calculated for the linearized pseudo-second order model fit (Ho and McKay 1998): $\frac{1}{q_t} = \frac{1}{k_2 q_e^2} + \frac{1}{q_e} t$

(b) Root mean squared error *RMSE* calculated for the non-linearized pseudo-2nd order model (Ho and McKay 1998): $q_t = \frac{t k_2 q_e^2}{1 + k_2 q_e t}$

(c) R^2 calculated for the HSDM model (no linearized form of the model exists)

* Reaction constants k_2 (g PAC/mg/min) fitted to the data normalized to PAC mass fraction (mg DOC/g PAC)

APPENDIX B SUPPLEMENTARY MATERIAL, ARTICLE 3

Journal: Journal of Hazardous Materials (submitted 05-02-2018)

Title: Removal of micropollutants by fresh and colonized magnetic powdered activated carbon

Authors: Kim M. Lompe, Sung Vo Duy, Sigrid Peldszus , Sébastien Sauvé, Benoit Barbeau

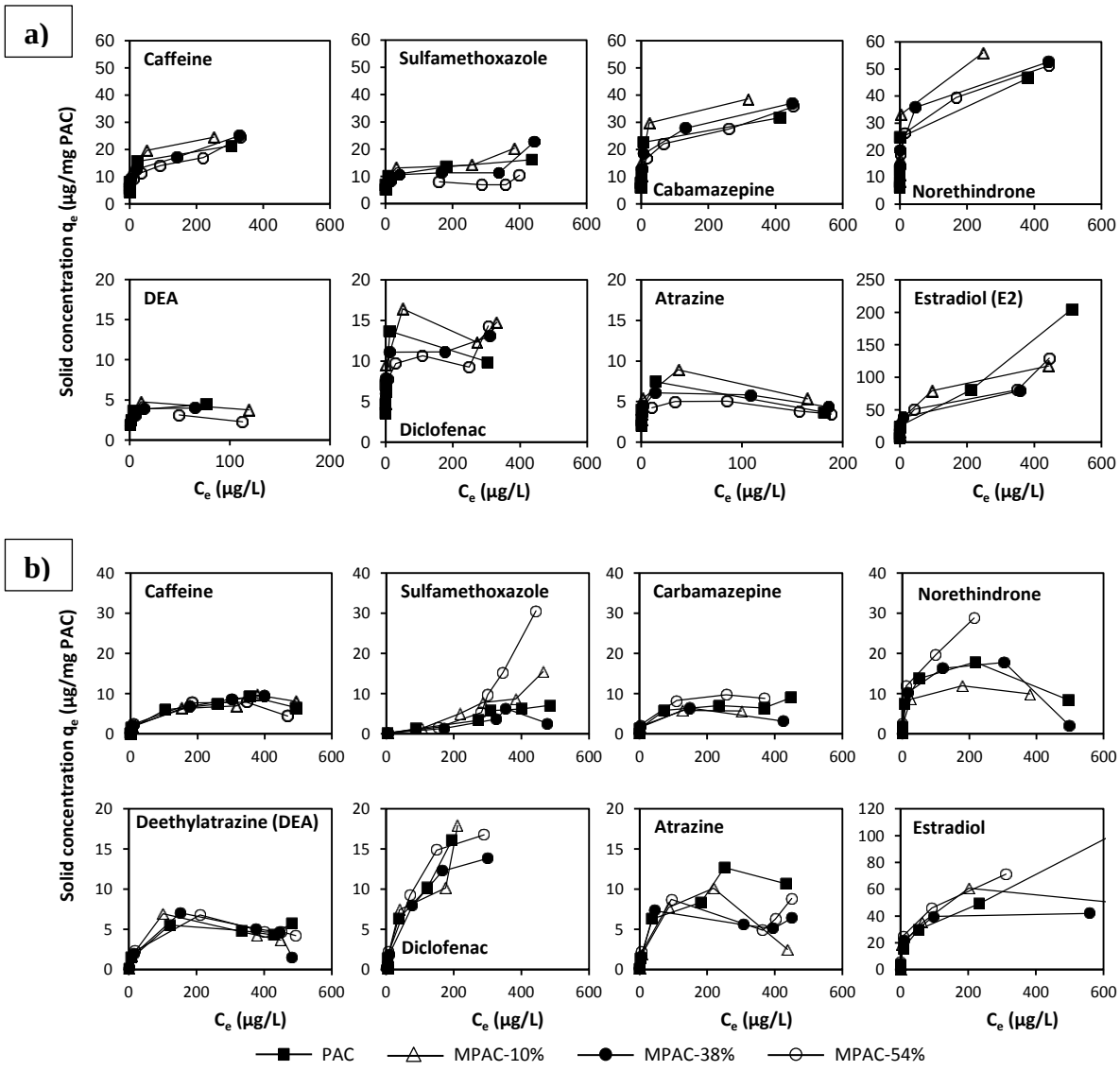

Figure B-1 : Micropollutant loadings q (µg/mg PAC) versus concentration c (µg/L) in equilibrium on a) non-colonized and b) colonized PAC and MPAC.

Table B-1 : Adsorption isotherm parameters for PAC & MPAC applying the Freundlich[a] model (datasets normalized to PAC content).

a) Non-colonized Pac and MPAC

MP	PAC				MPAC-10%				MPAC-38%				MPAC-54%			
	K_F (µg/mg) $(L/µg)^{1/n}$	*1/n*	R^2	*ARE* % [b]	K_F (µg/mg) $(L/µg)^{1/n}$	*1/n*	R^2	*ARE* %	K_F (µg/mg) $(L/µg)^{1/n}$	*1/n*	R^2	*ARE* %	K_F (µg/mg) $(L/µg)^{1/n}$	*1/n*	R^2	*ARE* %
CAF	6.81	0.22	0.97	10	7.80	0.22	0.98	7.4	6.46	0.22	0.98	6.0	4.54	0.26	0.93	7.7
SMX	6.12	0.16	0.94	7.6	6.51	0.17	0.91	11	3.83	0.26	0.81	22	-	-	-	-
DEA	2.38	0.16	0.85	10	2.69	0.19	0.95	26	2.29	0.17	0.84	30	-	-	-	
CBZ	13.1	0.17	0.93	16	14.6	0.19	0.97	10	12.5	0.17	0.99	4.3	9.44	0.21	0.98	3.7
ATZ	3.93	0.26	0.95	8.9	4.19	0.22	0.95	36	3.77	0.13	0.84	25	-	-	-	-
NOR	23.3	0.12	0.98	6.7	22.7	0.19	0.98	11	18.8	0.17	0.98	6.5	15.0	0.20	1.00	2.3
E2	31.4	0.18	0.99	8.0	36.8	0.18	1.00	4.8	25.4	0.19	1.00	3.4	22.2	0.25	0.97	7.4
DCF	6.85	0.12	0.75	21	8.00	0.14	0.89	19	7.40	0.10	0.88	8.5	6.49	0.10	0.56	9.7

b) Colonized Pac and MPAC

MP	PAC				MPAC-10%				MPAC-38%				MPAC-54%			
	K_F [b] (µg/mg) $(L/µg)^{1/n}$	*1/n*	R^2	*ARE* % [c]	K_F (µg/mg) $(L/µg)^{1/n}$	*1/n*	R^2	*ARE* %	K_F (µg/mg) $(L/µg)^{1/n}$	*1/n*	R^2	*ARE* %	K_F (µg/mg) $(L/µg)^{1/n}$	*1/n*	R^2	*ARE* %
CAF	0.35	0.55	0.91	37.5	0.35	0.55	0.91	33.1	0.36	0.57	0.96	20.7	0.45	0.48	0.86	46.5
DEA	0.26	0.53	0.90	37.7	0.29	0.50	0.77	60.9	0.32	0.44	0.64	66.8	0.33	0.47	0.87	35.8
ATZ	0.35	0.64	0.91	44.7	0.42	0.48	0.76	59.0	0.44	0.49	0.71	90.3	0.49	0.47	0.84	39.9
CBZ	0.45	0.51	0.86	46.9	0.44	0.50	0.79	41.4	0.49	0.42	0.74	71.0	0.59	0.53	0.91	36.2
SMX	0.05	0.80	0.98	17.0	0.04	0.92	0.95	27.0	0.07	0.65	0.89	34.2	0.03	1.01	0.86	60.1
DCF	0.11	0.95	0.70	108.3	0.15	0.90	0.84	65.9	0.16	0.84	0.94	33.6	0.25	0.81	0.95	31.8
NOR	1.14	0.49	0.72	102.5	0.94	0.48	0.77	77.7	1.19	0.38	0.51	158.8	1.38	0.62	0.90	54.4
E2	2.72	0.58	0.88	64.5	3.62	0.48	0.74	108.9	3.07	0.51	0.82	79.4	3.76	0.58	0.86	65.6

[a] Freundlich model $q_e = K_f \cdot C_e^{1/n}$, [b] As a measure for the quality of the non-linear fit the average relative error ARE (also known as mean absolute percentage error) was calculated as ARE (%) = 100/n * $\sum$ (|Δx|/x)

Table B-2 : Freundlich parameters for MP adsorption on magnetic activated carbons (MAC) in the literature (1).

Micropollutant	Water matrix	MAC Info	Main findings	Reference
Carbamazepine (Antiepileptic drug)	Wastewater (29 mg/L COD) from secondary sedimentation tank	MAC prepared with commercial PAC (Loba chemie, India) by co-precipitation of magnetite from $FeCl_2$ and $FeCl_3$ solution IONP:PAC ratio: 1:2; 1:4 and 1:8 M_S[a] 60 (IONP); 17 (1:2); 10 (1:4) and 5 (1:8) emu/g SA-BET[b] : 1378 (AC) ; 1241 (1:8) m^2/g	Freundlich constants for 25°C K_F (MAC 1:8) : 74.10 $(mg/g)(L/mg)^{1/n}$ 1/*n* (MAC 1:8) : 0.31 Kinetics model Elovich, intraparticle diffusion and pseudo-2nd order model fitted well k_2 (MAC 1:8, 15°C) : 0.015 mg/(µg min) k_2 (MAC 1:8, 30°C) : 0.022 mg/(µg min)	Baghdadi et al. (2016)
Bisphenol-A (Endocrine disrupter)	Adsorption capacity in the presence of 2.5 mg/L NOM (no details given)	MAC prepared with lignite PAC (Norit Darco A-51) by co-precipitation of ferrihydrite from a $Fe(NO_3)_3$ solution. Ferrihydrite was transformed to goethite in a vacuum oven at 70°C. IONP:PAC ratio: 42.8 (4.3 %); 45.7 (4.6 %) and 52.7 (5.3 %) mg Fe_2O_3/g SA-BET : 631 (AC) ; 717 (4.3 %); 622 (4.6 %); 522(5.3 %) and 115 (100 %) m^2/g PV-total[c]: 0.71 (AC) ; 0.93 (4.3 %); 0.71 (4.6 %); 0.68 (5.3 %) and 0.71 (100 %) mL/g	Freundlich model constants K_F (PAC) : 39.17 $(µg/g)(L/µg)^{1/n}$ K_F (MAC 4.3 %) : 97.27 $(µg/g)(L/µg)^{1/n}$ K_F (MAC 4.6 %) : 118.56 $(µg/g)(L/µg)^{1/n}$ K_F (MAC 5.3 %) : 187.21 $(µg/g)(L/µg)^{1/n}$ K_F (Goethite) : 12.94 $(µg/g)(L/µg)^{1/n}$ 1/*n* (PAC) : 0.613 1/*n* (MAC 4.3 %) : 1.281 1/*n* (MAC 4.6 %) : 1.706 1/*n* (MAC 42.3 %) : 2.089 1/*n* (Goethite) : 0.822 Pseudo-2nd order kinetics model fitted well k_2 (MAC) : 5 mg/(µg min)	Koduru et al. (2016)
Ciprofloxacin (Antibiotic)	In pure water	Mesoporous PAC (sucrose + sulphuric acid) template-free solvothermal reaction; IONP: Fe_3O_4 250 – 300 nm, spherically shaped ; M*s* 67.9 and 28.9 emu/g (IONP and MAC) –> IONP:PAC ratio 42.6 % IONP in MAC	Freundlich constants for 30 and 50°C K_F (MAC, 30°C) : 30.54 $(mg/g)(L/mg)^{1/n}$ K_F (MAC, 50°C) : 32.92 $(mg/g)(L/mg)^{1/n}$ 1/*n* (MAC, 30°C): 0.11 1/*n* (MAC, 50°C): 0.30 Pseudo-second-order kinetics model fitted well k_2 (MAC, 30°C) : 0.332 mg/(µg min)	Shi et al. (2013)

Table B-2 : Freundlich parameters for MP adsorption on MPAC in the literature (2).

Micropollutant	Water matrix	MPAC Info	Main findings	Reference
P-nitrophenol (intermediate for pharmaceuticals and pesticides)	In pure water	PAC produced from carrot dross immersed in IONP suspension produced by alkaline co-precipitation method $FeCl_2$ and $FeCl_3$ IONP are Fe_3O_4; 12 nm IONP (Fe_3O_4) : PAC ratio during preparation: 1/8 (12.5 %) and 1/5 (20 %) M_s : 70 (IONP), 2.22 (1/5) and 1.22 (1/8) emu/g Leads to assumption that IONP fraction is actually smaller (3 % and 1.7 %) SA-BET : 447 (AC) ; 435 (1/8) and 340 (1/5) m^2/g PV-micro[d] : 0.23 (AC); 0.22 (1/8); 0.17 (1/5) mL/g PV-total: 0.24 (AC; 1/8) and 0.18 (1/5) mL/g	Freundlich constants : K_F (AC) : 22.43 $(mg/g)(L/mg)^{1/n}$ K_F (MAC 1/8) : 20.32 $(mg/g)(L/mg)^{1/n}$ 1/*n* (AC) : 0.29 1/*n* (MAC 1/8) : 0.30 Pseudo-second order model fitted kinetics best k_2 (AC) : 0.125 mg/(µg min) k_2 (MAC 1/8) : 0.14 mg/(µg min)	Bastami and Entezari (2012)
Imidacloprid (Insecticide)	In pure water	MAC prepared with commercial PAC (Norit) in an alkaline co-precipitation method using $FeCl_3$, $FeSO_4$ and NaOH at 70°C. IONP:PAC ratio of 1:2 IONP: maghemite, magnetite and goethite SA : 1040 (PAC) ; 868 (1:2) ; 64 (IONP) PV-micro : 0.308 (PAC) ; 0.202 (1:2) ; 0.07 (IONP) PV-meso[e] : 0.07 (PAC) ; 0.065 (1:2)	Langmuir model parameter (best fit) Max adsorption capacities (q_m) q_m (AC): 110 mg/g q_m (MAC) (2:1) : 95 mg/g Freundlich constants: K_F (AC) : 71.08 $(mg/g)(L/mg)^{1/n}$ K_F (MAC 1/8) : 53.9 $(mg/g)(L/mg)^{1/n}$ 1/*n* (AC) : 0.26 1/*n* (MAC 1:2) : 0.37 Pseudo-second order model fitted kinetics best k_2 (AC) : 3.36 $*10^{-5}$ mg/(µg min) k_2 (MAC 1/8) : 5.01$*10^{-5}$ mg/(µg min)	Zahoor and Mahramonlioglu (2011)

[a] Saturation magnetization, [b] BET surface area, [c] total pore volume, [d] micropore volume, [e] mesopore volume

Table B-3 : Kinetic parameters[a] for micropollutant adsorption onto PAC and MPAC (based on PAC mass) for t = 0 to 60 min.

a) Non-colonized PAC and MPAC

MP	PAC			MPAC-10%			MPAC-38%			MPAC-54%		
	k_2 [a] mg/(µg min)	R^2	*ARE* % [b]	k_2 mg/(µg min)	R^2	*ARE* %	k_2 mg/(µg min)	R^2	*ARE* %	k_2 mg/(µg min)	R^2	*ARE* %
CAF	0.29	0.9997	5.0	0.05	0.9464	20.4	0.13	0.9708	13.4	0.15	0.9944	10.6
SMX	0.20	0.9641	23.1	0.03	0.7851	34.3	0.22	0.9693	18.5	2.19	0.9753	16.3
DEA	0.47	0.9958	13.7	0.03	0.8319	26.8	0.14	0.9589	17.1	0.35	0.9920	10.4
CBZ	1.45	0.9999	4.5	0.04	0.9443	18.7	0.09	0.9704	12.8	0.16	0.9911	14.8
ATZ	0.71	0.9989	9.3	0.03	0.8325	24.6	0.09	0.9503	16.2	0.20	0.9866	15.1
NOR	1.37	0.9999	3.8	0.03	0.9185	21.2	0.09	0.9622	13.6	0.17	0.9871	17.4
E2	2.69	1.0000	1.2	0.04	0.9462	19.6	0.08	0.9641	15.6	0.08	0.9795	17.5
DCF	0.44	0.9965	13.4	0.02	0.6932	35.1	0.10	0.9668	13.6	0.38	0.9801	23.6

b) Colonized PAC and MPAC

MP	PAC			MPAC-10%			MPAC-38%			MPAC-54%		
	k_2 [a] mg/(µg min)	R^2	*ARE* % [b]	k_2 mg/(µg min)	R^2	*ARE* %	k_2 mg/(µg min)	R^2	*ARE* %	k_2 mg/(µg min)	R^2	*ARE* %
CAF	4.83	1.0000	0.63	2.53	1.0000	1.51	0.85	0.9999	6.17	0.20	0.9989	16.53
DEA	6.72	1.0000	1.47	3.19	1.0000	3.41	1.16	0.9998	8.95	0.29	0.9971	20.31
ATZ	10.9	1.0000	1.11	4.88	1.0000	2.78	1.50	0.9998	8.71	0.36	0.9976	21.03
CBZ	12.9	1.0000	0.77	12.8	1.0000	1.11	2.50	0.9999	6.78	0.74	0.9992	15.61
FLUO	30.2	1.0000	0.33	16.0	0.9800	0.33	2.97	0.9999	3.76	1.28	0.9998	9.94
SMX	0.96	0.9997	7.51	0.42	0.9989	9.85	0.32	0.9990	8.28	0.07	0.9836	17.68
DCF	31.2	1.0000	0.59	16.9	1.0000	2.47	6.17	0.9997	10.78	1.64	0.9957	24.11
NOR	-			6.27	1.0000	1.02	2.96	0.9999	7.13	1.11	0.9994	14.70
E2	33.5	1.0000	0.62	33.0	1.0000	0.79	4.77	0.9999	5.86	1.54	0.9994	14.74

[a] Constant of the pseudo-second order kinetic model by Ho and McKay (1998) : $\frac{t}{q_t} = \frac{1}{k_2 q_e^2} + \frac{1}{q_e} t$, [b] As a measure for the quality of the non-linear fit the average relative error ARE (also known as mean absolute percentage error) was calculated as ARE (%) = 100/n * $\sum$ ($|\Delta x|/x$)

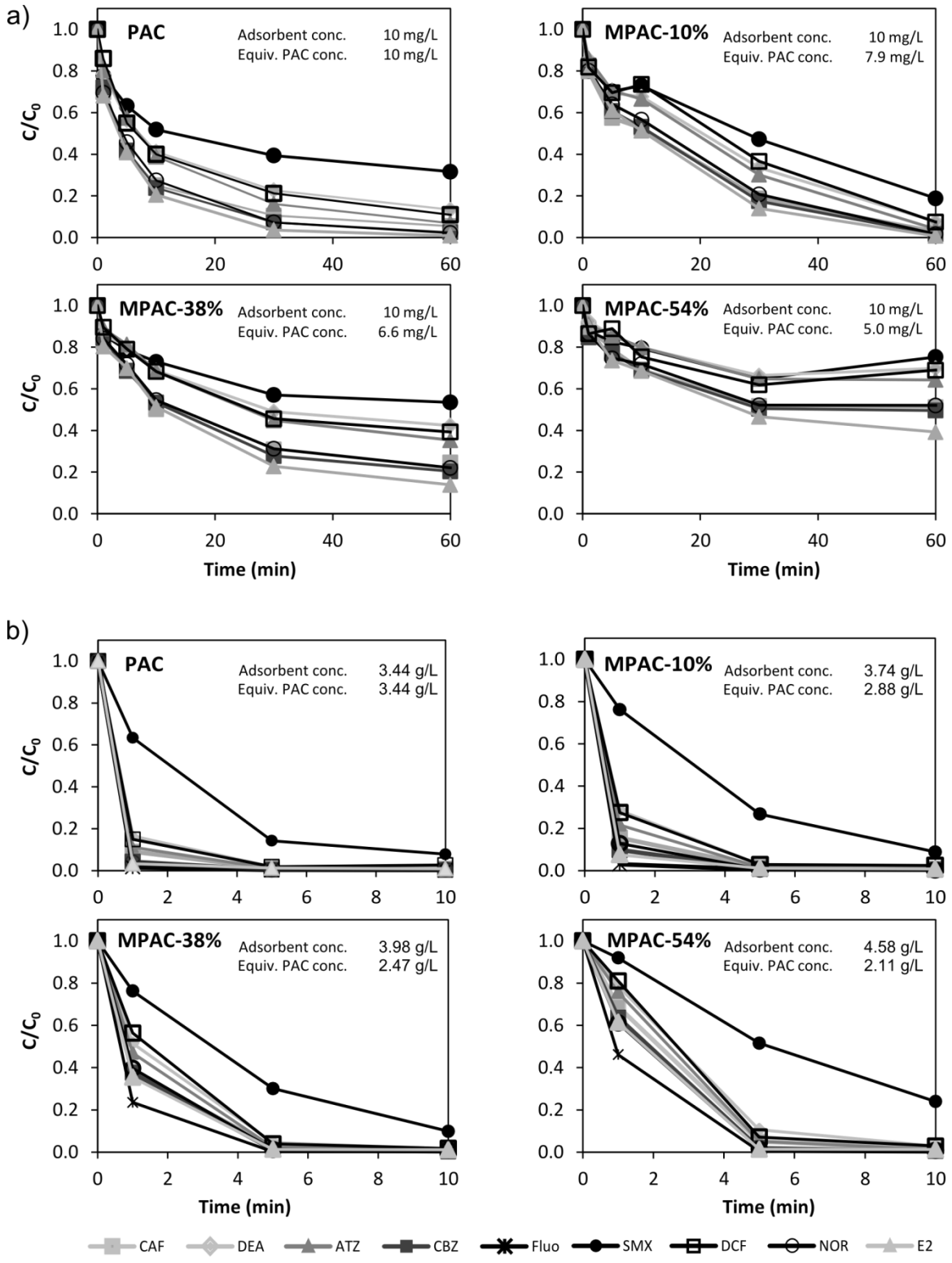

Figure B-2 : Adsorption kinetics of 9 micropollutants on a) non-colonized and b) colonized PAC and MPAC.

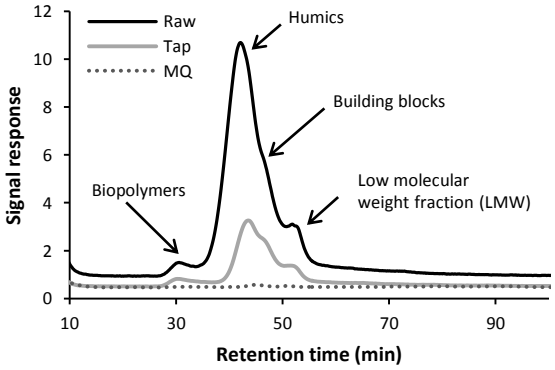

Figure B-3 : Size distribution of NOM of the three water types ultra-pure, tap and raw water.

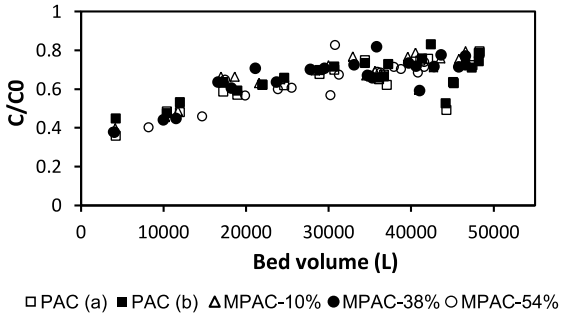

Figure B-4 : Breakthrough curve of DOC in 90 days of operation. While the adsorption capacity of the adsorbents decreases from the initial 60 % with increasing bed volume, the biodegradation of DOC increases leading to a constant DOC removal of 20 – 30 % when the adsorption capacity for DOC is already exhausted (after ca. 30000 bed volumes).

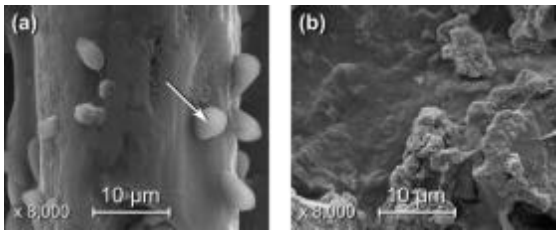

Figure B-5 : a) Precipitated minerals on the PAC surface (atomic percentage of 35 % C, 40 % O, 14 % Si, 9 % Ca), b) surface of aged MPAC-38% (after 90 days).

APPENDIX C MODELLING A MAGNETIC LAMELLA SEPARATOR – APPROACH AND RESULTS

In drinking water treatment, lamella separators are used for the removal of flocks formed during the coagulation/ flocculation step. Lamella separators accelerate the separation step by decreasing the distance the particles must fall. The parallel plates are generally inclined at a 60° angle to avoid the accumulation and blockage of the sedimentation channels. Instead, particles slide down the plates and accumulate at the bottom of the basin (Crittenden et al. 2012).

The objective of this study was to evaluate a lamella separator channel enhanced with permanent magnets alongside its lower plate as a magnetic separator for the removal of MPAC. First, particle sedimentation in a typical lamella separator was modelled for the removal of PAC and MPAC with increasing IONP content. Only gravitational and drag forces acting on the particles with different densities and a known particle distribution were considered. The lamella separator was designed according to criteria proposed by Crittenden et al. (2012). In a second step, a magnetic force acting perpendicular to the lower lamella plate was considered. The model allowed to identify separation times and particle size cut offs for 4 MPAC with mass fractions of 0%, 10%, 38% and 54% iron oxide content for typical flow velocities in the lamella.

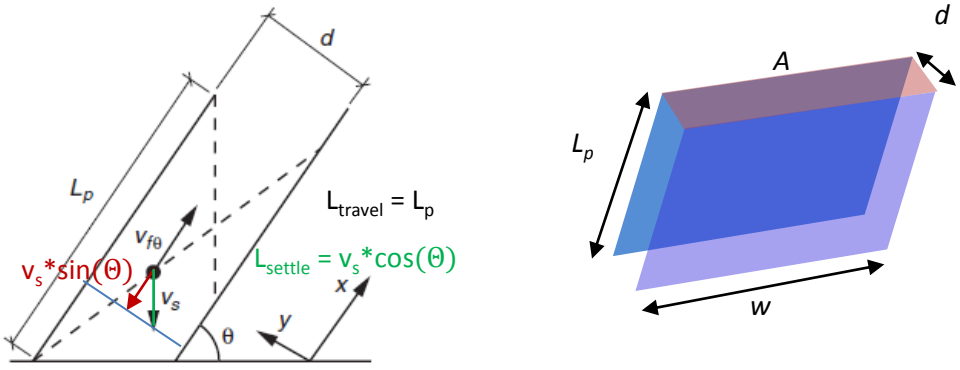

Figure C-1 : Lamella separator in 2D and 3D layout.

A) Modelling particle trajectories in a typical lamella separator

The chosen layout for the lamella separator (Figure C-1) consists of plates inclined at an angle θ of 60° operated with counter-current flow. To facilitate the calculations, the coordinate system was turned by 60°. The forces acting on a particle in the channel are the drag force and the gravitational force. A particle is separated in the lamella if the time for separation is smaller than the time the particle travels through the lamella.

The settling time can be calculated as:

$$t_s = \frac{L_{settle}}{v_s} = \frac{d}{v_s \cos(\theta)} \qquad \text{(Eq. C-1)}$$

Where L_{settle} is the length the particle falls to settle (Figure C-1) and v_s is the sedimentation velocity calculated with the Stoke's equation for laminar flow with η the dynamic viscosity of water, ρ_p the density of the wet MPAC particles, ρ_w the density of water and d_p the particle diameter given as a particle distribution.

$$v_s = \frac{g(\rho_p - \rho_w){d_p}^2}{18\eta} \qquad \text{(Eq. C-2)}$$

The travel time of the particle can be calculated with $L_{p,}$ the length the particle travels with the flow in x-direction, and the effective particle velocity in x-direction, calculated as the fluid velocity $v_{f\Theta}$ reduced by the settle velocity in the opposite x-direction.

$$t_p = \frac{L_p}{v_{f\theta} - v_s \sin(\theta)} \qquad \text{(Eq. C-3)}$$

The fluid velocity depends on the process flow rate Q, the number of lamellae N, the distance d between two lamellae and the width of the lamella or plate w.

$$v_{f\theta} = \frac{Q}{Ndw} \qquad \text{(Eq. C-4)}$$

So a critical particle settling velocity v_{crit} can be calculated below which the particle is still separated:

With $t_{settle} < t_{travel}$

$$v_{crit} = \frac{v_{f\theta} d}{L_p \cos(\theta) + d\, sind(\theta)} \qquad \text{(Eq. C-5)}$$

In our example a lamella separator was designed for a process flow rate Q of 10 000 m³/d and typical design parameters (Table C-1).

Table C-1 : Typical lamella settler characteristics.

Parameter	value	unit
Angle theta	60	Degrees
Spacing lamellae d	0.05	m
Fluid velocity in one lamella	0.15	m/min

A settler with the following parameters will be considered:

Table C-2 : Calculated lamella design.

Parameter	value	unit
Flow rate *Q*	10000	m³/d
	0.116	m³/s
Flow velocity v_f	0.151	m/min
Depth	2	m
width	4	m
Length of the plate *Lp*	2.31	m
Channel area *A*	0.2	m²
# channels	230	

The critical settling velocity is then (Eq. C-5):

$$v_{crit} = \frac{0.151 \frac{\text{m}}{\text{s}} * 0.05\ \text{m}}{2.31 * \cos(60) + 0.05\ \text{m} * \text{sind}(60)} = 1.13 * 10^{-4}\ \text{m/s}$$

With a critical settling time of 14.72 min.

With the given particle distribution of MPAC and PAC and their respective wet densities (Table C-3), the settling velocities of each MPAC distribution can be calculated and compared to the critical settling velocity (Figure C-2). With the information from the particle size distribution, the volume fractions that cannot be separated are calculated (Figure C-3). A volume fraction of 40 %

is not separated by the lamella separator of PAC particles without magnetite. These 40 % are represented by all particles < 17.89 µm. MPAC containing a mass fraction of 54 % magnetite are separated better and a volume fraction of 25 % leaves the separator with the fluid (all particles < 11.4 µm).

Table C-3 : Wet particle density of MPAC.

Density, particle, wet (kg/m³)			
MPAC-54%	MPAC-38%	MPAC-10%	MPAC-0%
2613	2228	1957	1650

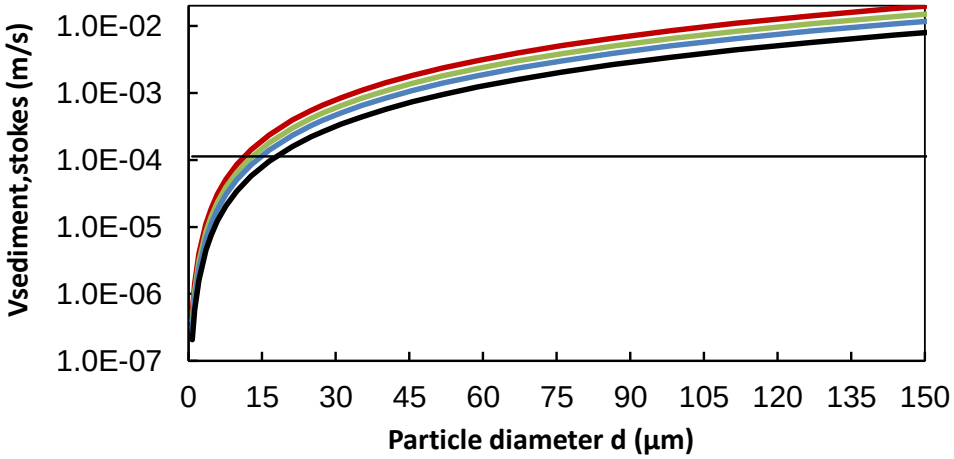

Figure C-2 : Sedimentation velocity (Stokes) for MPAC-54% (red). MPAC-38% (green), MPAC-10% (blue) and MPAC-0% (black. The horizontal line indicates $v_{crit.}$.

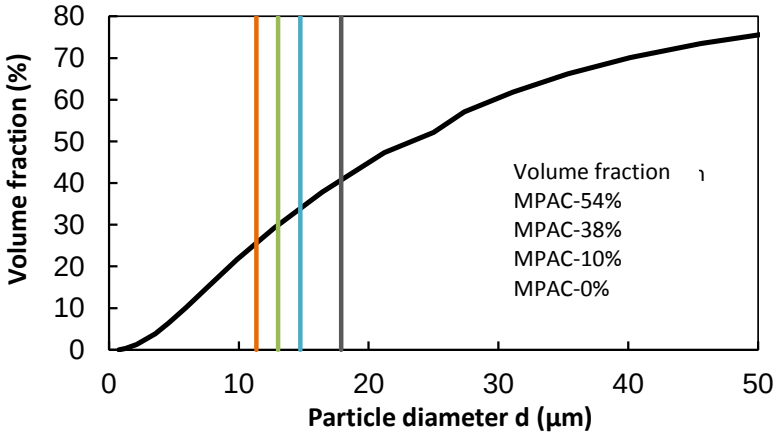

Figure C-3 : Volume fraction that is not separated in the lamella separator.

For the lamella separator we want to calculate the particle path and particle velocities based on a force-approach that allows us to add later the magnetic force. The forces considered here are the gravitational force $\vec{F}_G$ and the drag force $\vec{F}_D$. The drag force points in the opposite direction of the particle's flow direction. Considering a laminar flow the drag force can be written as following (Stokes' drag):

$$\vec{F}_D = -3\,\pi\,\eta\,d_p * \overrightarrow{v_r} \qquad \text{(Eq. C-6)}$$

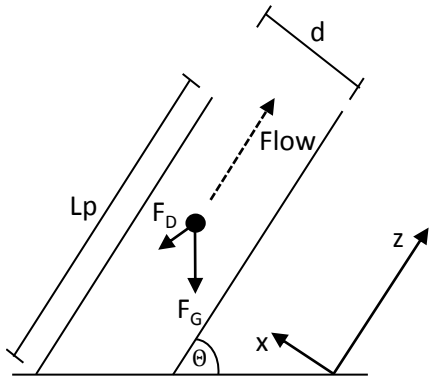

Figure C-4 : Forces acting on the particle in a typical lamella separator.

Where v_r is the resulting particle velocity when the particle sediments.

The gravitational force is

$$\vec{F}_G = -\vec{g} * m_p\,, \qquad \text{(Eq. C-7)}$$

where m_p is the mass of the MPAC particles. So the system of forces is:

$$\vec{F} = \vec{F}_D + \vec{F}_G. \qquad \text{(Eq. C-8)}$$

Considering that the fluid velocity in x-direction is zero, the equation of motion in x-direction is then:

$$\ddot{x} \cdot\ m_p = -3\,\pi\,\eta\,d_p \cdot \left(v_{px} - u_x\right) - g * m_p\,, \qquad \text{(Eq. C-9)}$$

$$\ddot{x}(t) = \frac{-3\,\pi\,\eta\,d_p}{m_p} \cdot \dot{x}(t) - g \cdot \cos(\theta)\,,$$

with $a = g \cdot \cos(\theta)$ and b $= \frac{3\,\pi\,\eta\,d_p}{m_p}$

we can write

$$\ddot{x}(t) = -b\dot{x}(t) - a \quad \text{(Eq. C-10)}$$

In z-direction:

$$\ddot{z}(t) = \frac{-3\,\pi\,\eta\,d_p}{m_p} \cdot \dot{z}(t) + \frac{3\,\pi\,\eta\,d_p}{m_p} \cdot u_z - g \cdot \sin(\theta) \quad \text{(Eq. C-11)}$$

With $c = -g \cdot \sin(\theta) + \frac{3\,\pi\,\eta\,d_p}{m_p} \cdot u_z$ and d $= \frac{3\,\pi\,\eta\,d_p}{m_p}$

$$\ddot{z}(t) = -d \cdot \dot{z}(t) + \text{c} \quad \text{(Eq. C-12)}$$

Both equations are linear differential equations that can be solved analytically.

With known initial conditions $\dot{x}(t_0) = 0$ and $x(t_0) = D$ we can solve (Eq. C-10) to find:

$$x(t) = \frac{1}{b^2} \cdot (-ae^{-bt} + Db^2 - abt + a) \quad \text{(Eq. C-13)}$$

With known initial conditions $\dot{z}(t_0) = 0$ and $z(t_0) = 0$ we can solve (Eq. C-12) find:

$$z(t) = \frac{1}{d^2} \cdot (ce^{-dt} - du_z e^{-dt} + du_z + cdt - c) \quad \text{(Eq. C-14)}$$

The velocity is then:

$$\dot{z}(t) = \left(u_z - \frac{c}{d}\right) e^{-dt} + \frac{c}{d} \quad \text{Eq. C-15}$$

The plots (Figure C-5) show the path and velocity in x- and z-direction of different MPAC particles with their characteristic min and max particle size and parameters (Table C-4).

Table C-4 : Properties of MPAC with increasing IONP content.

Parameter	Unit	MPAC-0%	MPAC-10%	MPAC-38%	MPAC-54%
Diameter min	µm	0.77	0.77	0.77	0.77
Diameter d50	µm	25.0	25.0	25.0	25.0
Diameter max	µm	163.5	163.5	163.5	163.5
Wet density	kg/m³	1650	1957	2228	2613

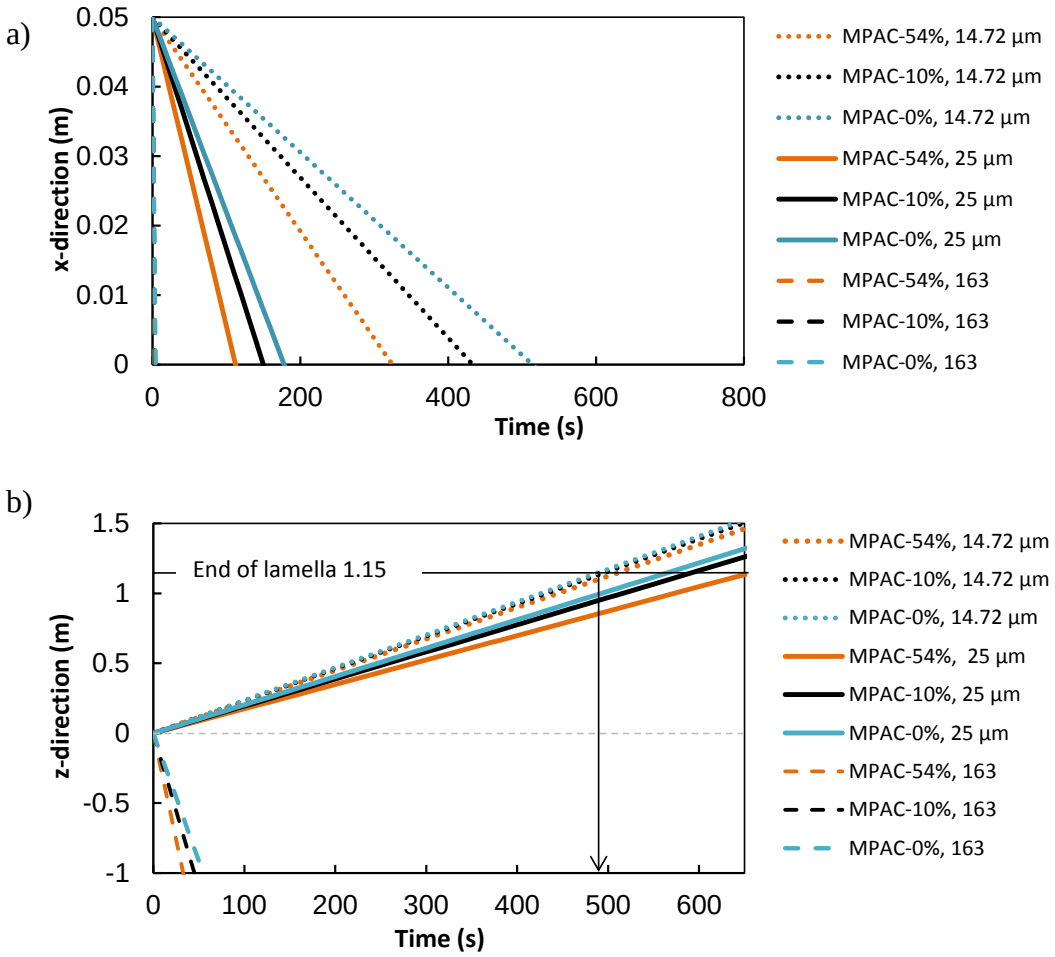

Figure C-5 : Particle motion a) x(t) and b) z(t) in the lamella separator.

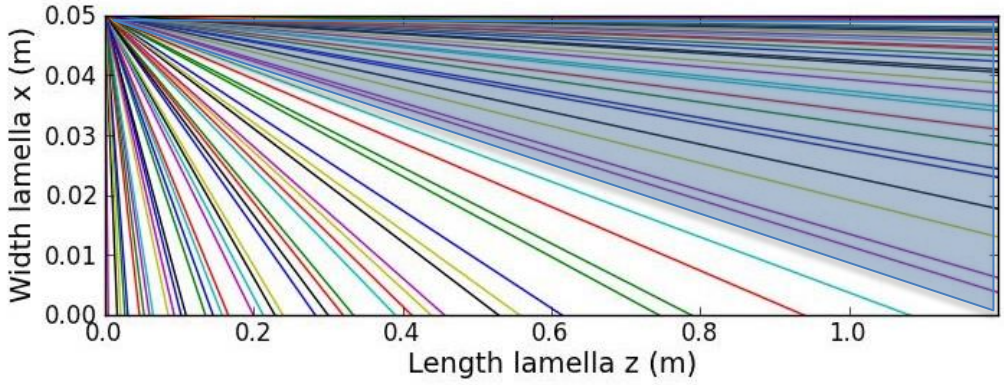

Figure C-6 : Trajectories in the lamella separator. All particles travelling in the blue area are not separated.

The model for a lamella separator allows to calculate the trajectories of MPAC particles in x and y direction. With known dimensions of the lamella, the critical particle size and particle type that cannot be separated under a given flow velocity can now be determined. The model allows as well calculating separation times. The particles that are the most difficult to remove are MPAC-0% particles with small diameters. A large fraction of those are exported from the separator. To avoid this from happening, the particle diameter is usually increased during coagulation/flocculation. PAC particles that are aggregated in larger flocks can then more easily be removed in the plate settlers. An alternative is to attract the particles to the particles to the lower plate of the lamella. For this reason the magnetic force will be considered in the model as a next step.

B) Magnetic lamella separator

In order to accelerate the separation or to catch also the small fraction of the magnetic particles, a permanent magnet could be attached to the lamella. We therefore consider a magnetic force that is directed vertically (in x-direction) to the lamella (Figure C-7).

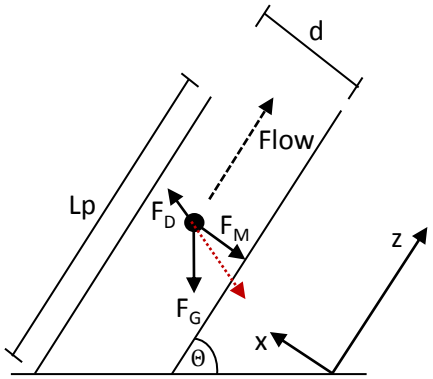

Figure C-7 : Particle trajectories in the lamella separator including the magnetic force.

The system of forces now looks like this:

$$\vec{F} = \vec{F}_D + \vec{F}_G + \vec{F}_m \qquad \text{Eq. C-16}$$

Considering that the magnetic force has only a component in x-direction, the equation of motion in z-direction remains the same:

In z-direction:

With $c = g \cdot \sin(\theta) - \frac{3\,\pi\,\eta\,d_p}{m_p} \cdot u_z$ and d $= \frac{3\,\pi\,\eta\,d_p}{m_p}$

$$z(t) = \frac{1}{b^2} \cdot (e^{-bt}) \cdot ae^{-bt} - a - bu_z e^{-bt} + bu_z + abt \qquad \text{Eq. C-17}$$

The velocity is then:

$$\dot{z}(t) = \left(u_z - \frac{a}{b}\right) e^{-bt} + \frac{a}{b} \qquad \text{Eq. C-18}$$

a)

b)

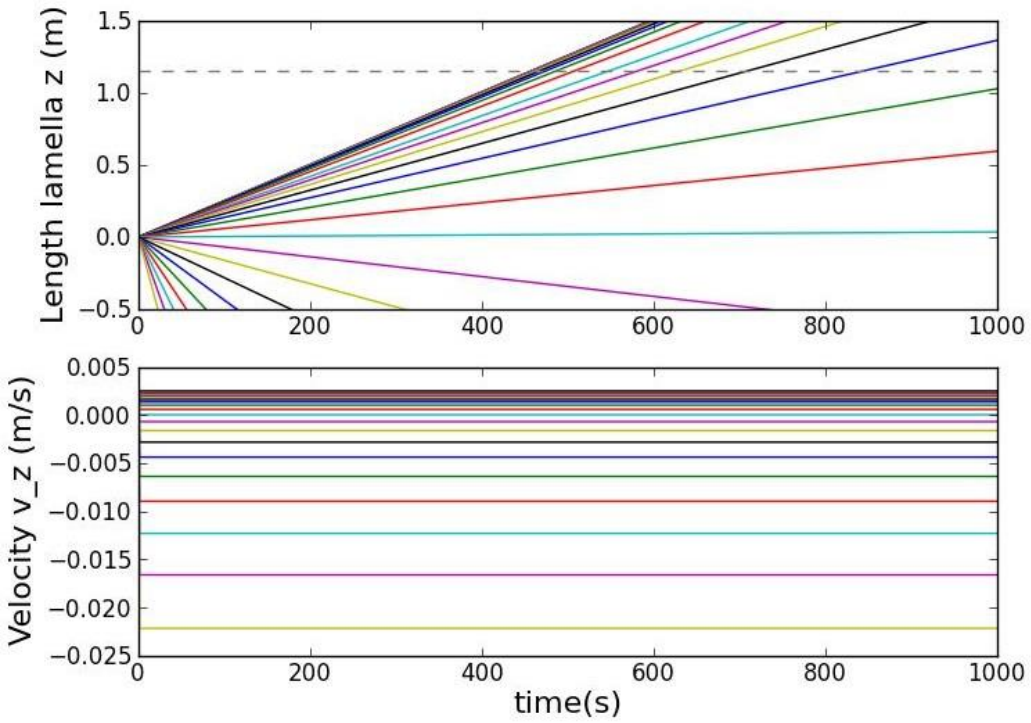

Figure C-8 : Result a) z(t) and b) v_z(t) for the magnetic lamella separator (heaviest particles are not transported upwards (negative velocity)).

In x-direction, however, the magnetic force has to be considered. The expression of the magnetic field for a permanent magnet has been simplified in a first approach with the magnetic field of a dipole and the force is the force between two dipoles (the permanent magnet and the magnetized MPAC particle). The magnetic force between two dipoles is defined as:

$$\vec{F}_m = \vec{m} \cdot grad\ \vec{B} \qquad \text{Eq. C-19}$$

$$\vec{F}_m(x) = \frac{3\mu_0}{2\pi} \cdot \vec{m}_1 \vec{m}_2 \cdot \frac{1}{x^4} \qquad \text{Eq. C-20}$$

For the x-direction we find with a fluid velocity in x-direction of zero:

$$\ddot{x}(t) = \frac{-3\,\pi\,\eta\,d_p}{m_p} \cdot \dot{x}(t) - g \cdot \cos(\theta) - \frac{m_1 m_2 \cdot 3\mu_0}{m_p \cdot 2\pi} \cdot \frac{1}{x^4} \qquad \text{Eq. C-21}$$

With $b = \frac{3\,\pi\,\eta\,d_p}{m_p}$, $a = -g \cdot \cos(\theta)$ and $c = \frac{m_1 m_2 \cdot 3\mu_0}{m_p \cdot 2\pi}$

We can write:

$$\ddot{x}(t) = -b\dot{x}(t) - \frac{c}{x^4} + a \qquad \text{Eq. C-22}$$

Eq. C-22 is a non-linear differential equation that has to be solved numerically e.g. with Python method ODEINT with the initial conditions $\dot{x}(t_0) = 0 \; and \; x(t) = d$ = 0.05 m. The magnetic moments m_1 and m_2 are dependent on the size and remanent magnetization of the permanent magnet and the saturation magnetization of the MPAC particles. For the permanent magnet and the surrounding fluid the following parameters were chosen:

Table C-5 : Parameter for the lamella separator.

Parameter	Value	Unit
Magnetic permeability in water μ0	$1.2566 \cdot 10^{-6}$	kg m/s²/A²
Length (z-direction) (m)	0.01	m
width (y-direction) (m)	0.01	m
Height (x-direction) (m)	0.01	M
Remanent induction Magnet Br	0.4	T

So the Magnetization of the magnet can be calculated to be

$$M_r = B_r/\mu_0 = 3.18 \cdot 10^5 \text{ A/m}$$

And the intensity of the magnetic dipole moment is

$$m_1 = M_r \cdot V = 0.318 \; Am^2$$

For three particles of the 3 magnetic MPAC the intensities of the magnetic moment m_2 were calculated

Finally, the trajectories and velocities can be plotted for MPAC with increasing IONP content (Figure C-9). As the MPAC particles approach the magnet its velocity increases exponentially due to the higher intensity of the magnetic force acting onto the particle. Indeed, the particle velocity increases inversely proportional to x^4 (Eq. C-20). Solving the equation for distances close to the magnet is a challenge as the behaviour of the velocity is asymptotic (changes in velocity per time step become very small), which can easily cause a numerical error.

Table C-6 : Characteristics of the MPAC particles for magnetic separation.

Parameter	Unit	IONP content in MPAC			
		0%	10 %	38 %	54 %
Diameter min	µm	0.77	0.77	0.77	0.77
Diameter d50	µm	25.0	25.0	25.0	25.0
Diameter max	µm	163.5	163.5	163.5	163.5
Dry bulk density	kg/m³	400	510	620	790
Saturation magnetization	Am²/kg	0	5.2	20.1	30.3
Magnetization	A/m	0	2652	12462	23937
Intensity of the magnetic moment m_2 (small)	Am²	0	$6.27 \cdot 10^{-16}$	$2.95 \cdot 10^{-15}$	$5.66 \cdot 10^{-15}$
Intensity of the magnetic moment m_2 (d50)	Am²	0	$2.17 \cdot 10^{-11}$	$1.02 \cdot 10^{-10}$	$1.96 \cdot 10^{-10}$
Intensity of the magnetic moment m_2 (biggest)	Am²	0	$6.07 \cdot 10^{-9}$	$2.85 \cdot 10^{-8}$	$5.48 \cdot 10^{-8}$

The graphics show how MPAC with higher IONP content are separated much faster than MPAC with low or no IONP. In the plotted examples, a MPAC-54% particle of 25 µm is attracted (and attached) to the magnet within 50 s after entering the lamella (Figure C-9 a) and this happens at the very bottom of the channel (after 9 cm) (Figure C-9 d). In contrast, a MPAC-10% particle of the same size needs 100 s to be separated (Figure C-9 b) and regular PAC of the same diameter needs 180 s (Figure C-9 c) as it is not influenced by the magnetic field. The size of the particles influences the magnetic separation as well (larger diameter and magnetic moment) and a MPAC-54% particle with a diameter of roughly 8.2 µm gets barely separated before the lamella ends (critical diameter for MPAC-54%) (Figure C-9 e). To increase the capture efficiency of a magnetic separator, the flow channels can be filled with a media that can be magnetized by the magnetic field of the permanent magnet. In that way, the distance between the particle and the magnet are decreased, the probability to come close to the magnetized elements increased and higher magnetic gradients (and thus higher forces) will make it possible to operate the separator at higher flow velocities. In Chapter 7 of this thesis, such a high gradient magnetic separator (HGMS) was tested at lab-scale. Modelling a HGMS, however, is more challenging as the magnetized filling media has to be represented. This can be done using e.g. a finite element approach, which would go beyond the scope of this thesis.

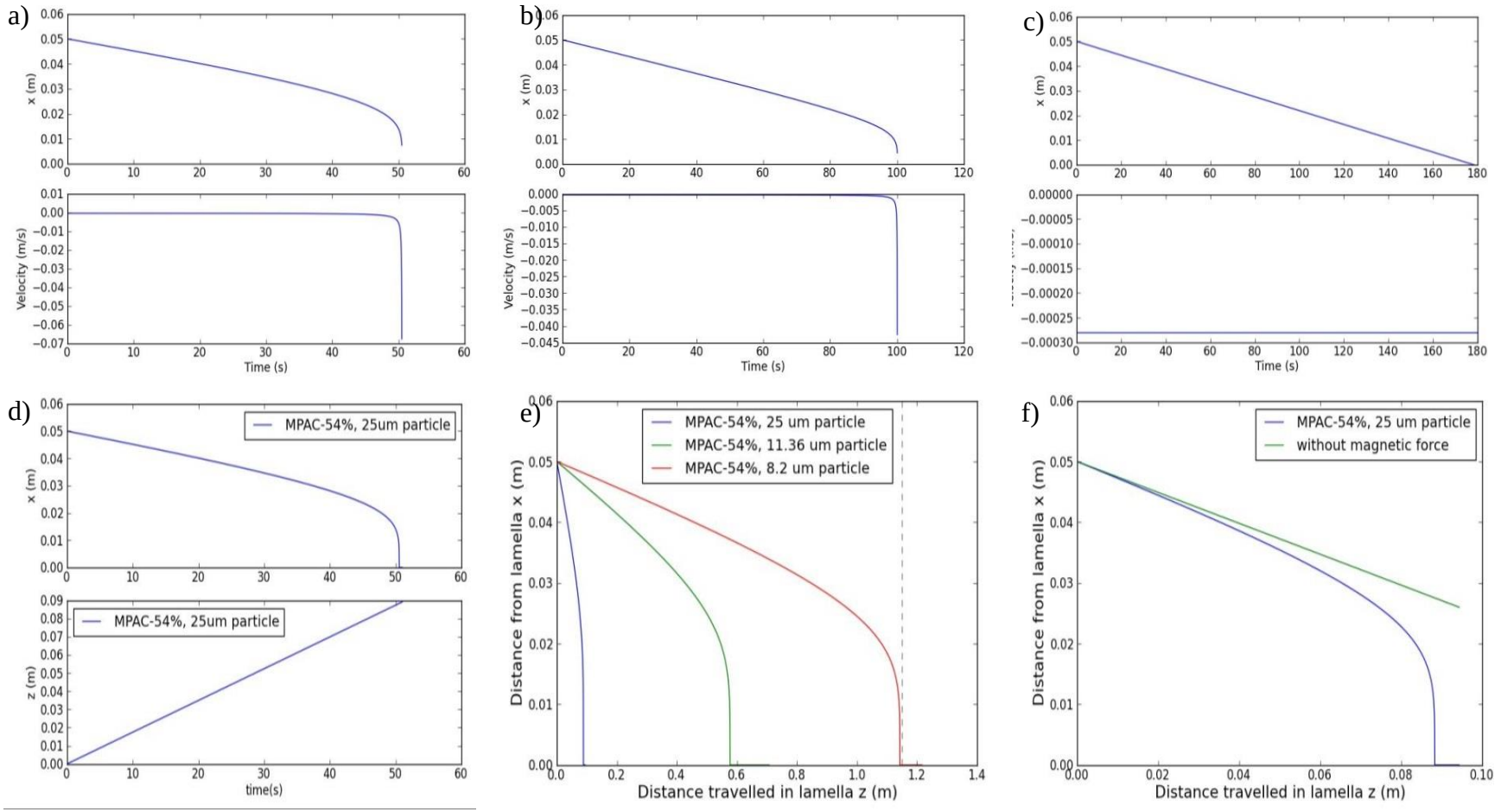

Figure C-9 : Trajectories x(t) and $\dot{x}(t)$ were solved numerically for a) MPAC-54% (25 µm), b) MPAC-10% (25 µm) and c) MPAC-0% (25 µm); the trajectories in x and z-direction were calculated in d) for MPAC-54% particles (25 µm); the trajectory in x-direction for 3 MPAC-54% particle sizes was calculated in e) and in f) a comparison between MPAC-54% particles of 25 µm with and without magnetic field is given.

APPENDIX D CALCULATION OF COSTS FOR MPAC

Unit costs for MPAC arise from the cost of PAC, iron salts, sodium hydroxide and energy costs for stirring and heating. In this project iron(III) chloride (hexahydrate) with the chemical formula $FeCl_3 \cdot 6H_2O$ and iron(II) sulphate (heptahydrate) with the formula $FeSO_4 \cdot 7H_2O$ were combined in the ratio 2:1 (Table D-1). Prices are current market prices for bulk orders and may vary according to the region (country/province), the delivery type (truck/train/tanks), product purity, raw materials, fluctuation of demand and order format. As can be seen in Table D-1, the price per tonne of active ingredient is highest for PAC followed by $FeSO_4$. The iron salt is expensive in East Canada, because these crystals are rare and have to be imported (Moreau 2013). With increasing IONP/PAC ratio, the cost per kg of MPAC increases (s. Figure 8.2). Additionally, to work at an equivalent PAC concentration, more MPAC has to be dosed to balance the lower PAC content. The costs of using MPAC instead of PAC are thus higher and increase proportionally to the IONP content.

Table D-1 : MPAC raw materials.

Product (aqu. solution)	Molar mass (g/mol)	Iron content (g/mol)	Content (g NaOH/kg and g Fe/kg)	Molar ratio (-)	Price ($/t)[a]	Price ($/t)[b]
NaOH (50 %)	40.0	0	500	8	330	660
$FeSO_4 \cdot 7H_2O$ (18 %)	278.05	55.85	180	1	180	1000
$FeCl_3 \cdot 6H_2O$ (13.8 %)	270.3	55.85	138	2	140	978
PAC	-	-	-	-	2500	2500

[a] metric liquid ton of the aqueous salt solution with given concentration, [b] price per tonne of the active ingredient

The costs for heating and stirring can be estimated by calculating the necessary quantity of heat energy to heat the volume of necessary PAC suspension to produce 1 kg of MPAC from 20°C to 70°C. As an approximation the heat capacity C_{water} for water was chosen (4181.3 J/(kg°C) at 25 °C) and a mass of water m_{water} of 15 kg to produce 1 kg of MPAC.

With an electricity price of 0.08 $/kWh in Quebec, the energy cost to heat water for producing 1 kg of MPAC can be calculated when knowing the necessary quantity of heat energy $Q_{Heat\ energy}$:

$$Q_{Heat\ energy} = m_{water} \cdot C_{water} \cdot (T_2 - T_1) \quad \text{(Eq. D-1)}$$

$$Q_{Heat\ energy} = 15\ kg \cdot 4181.3 \frac{J}{kg\ °C} \cdot (70°C - 20°C) = 0.836\ kWh$$

$$Energy\ cost = 0.836\ kWh * 0.08\ \$/kWh = 0.07\ \$/(kg\ MPAC)$$

The necessary power P for stirring the suspension at n = 700 rpm with a Rushton turbine impeller with the power number N_p = 3 and a diameter d of 5 cm can be calculated with:

$$P = N_P \cdot \rho \cdot n^3 \cdot d^5 \quad \text{(Eq. D-2)}$$

$$P = 3 \cdot 1000 \frac{kg}{m^3} \cdot (11.667\ 1/s)^3 \cdot (0.05\ m)^5 = 1.489\ Watt$$

For the small lab-scale reactor, the 5 cm impeller was stirring for 20 min a volume of only 300 mL for the production of max 15 g MPAC. To consider the production of 1 kg of MPAC, we approximate an industrial scale reactor with multiple 5 cm impellers.

$$Energy\ cost = 1.489\ Watt * 0.33\ h * \frac{1}{0.015} kg\ MPAC * 0.08 \frac{\$}{kWh} = 0.003 \frac{\$}{kg} MPAC$$

The total energy costs for the production of 1 kg MPAC from this rough estimate sum up to 0.07 $/kg MPAC. As can be seen in graphic Figure D-1, the price of the required energy represents around 2 % of the total costs of MPAC. In an industrial scale preparation of MPAC, these costs might be lower, as heat from the activation of PAC could be used to heat the co-precipitation reactor to 70°C, reactor designs such as its shape, agitation, chemical injection and insulation can dramatically influence the quality of the precipitated IONP and the required energy. A calculation of the real energy cost of MPAC production can only be carried out in the frame of a concrete large-scale project planning.

Table D-2 : Calculation of the unit price of MPAC.

Ratio IONP/PAC	PAC	Fe_2O_3	Iron	$FeCl_3$	$FeSO_4$	NaOH	Σ salts	PAC	Energy	MPAC
	(g/ g MPAC)						($/kg MPAC)			
1:1	0.50	0.50	0.362	1.201	0.584	0.711	2.227	1.250	0.070	3.547
1:2	0.67	0.33	0.241	0.801	0.389	0.474	1.485	1.667	0.070	3.221
1:3	0.75	0.25	0.181	0.600	0.292	0.355	1.114	1.875	0.070	3.058
1:4	0.80	0.20	0.145	0.480	0.233	0.284	0.891	2.000	0.070	2.961
1:5	0.83	0.17	0.121	0.400	0.195	0.237	0.742	2.083	0.070	2.895
1:9	0.90	0.10	0.072	0.240	0.117	0.142	0.445	2.250	0.070	2.765

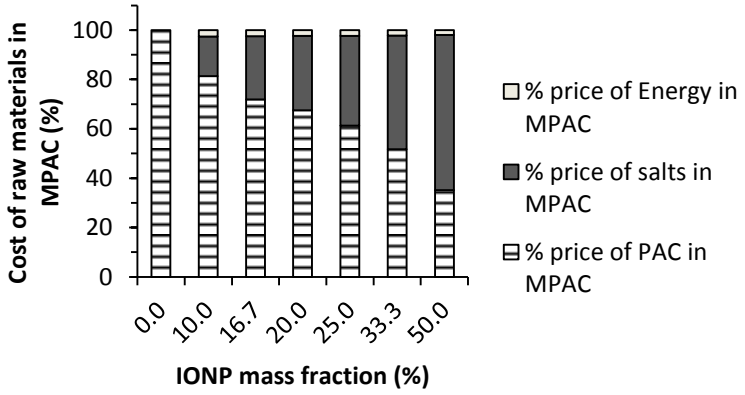

Figure D-1 : Composition of prices in MPAC.

APPENDIX E ADSORPTION OF MIB AND GEOSMIN ON PAC AND MPAC

Taste and odour removal is the main application of PAC in drinking water treatment plants and an important cost factor. Events of musty and earthy taste and odours occur mostly seasonal and are linked to the presence of two microbial metabolites: 2-methylisoborneol (MIB) and geosmin (GEO). With an odour threshold of only 5 – 10 ng/L, the dosage of PAC is often the most efficient treatment solution. The objective of this study was to compare PAC and MPAC with a mass fraction of 54 % IONP regarding the adsorption of these two molecules in three natural waters with increasing DOC concentrations.

Adsorption tests were carried out in pre-filtered raw waters of the Saint-Lawrence River, Rivière L'Assomption and Rivière des Mille-Îles at room temperature using the bottle-point technique. The waters were spiked with 100 ng/L of MIB and geosmin. PAC and MPAC-54% were added pre-wetted to obtain a concentration of 5 mg/L for a contact time of 15 min. The test conditions were chosen to represent water treatment plants in the metropolitan area of Montréal. The adsorption reaction was stopped via filtration through pre-washed glass fibre filters. Target compounds were extracted from the water samples using the Twister® system from Gerstel and analyzed with a gas chromatograph coupled to a mass spectrometer (GC-MS).

Results are normalized to the PAC content in the adsorbents and show (i) no relation between DOC concentration of the water matrix and adsorption performance and (ii) differences between PAC and MPAC are significant for MIB and geosmin removal when normalized to the mass of the active adsorbent (PAC), but not important. This reflects the previously observed behaviour when testing various organic micropollutants of anthropogenic origin.

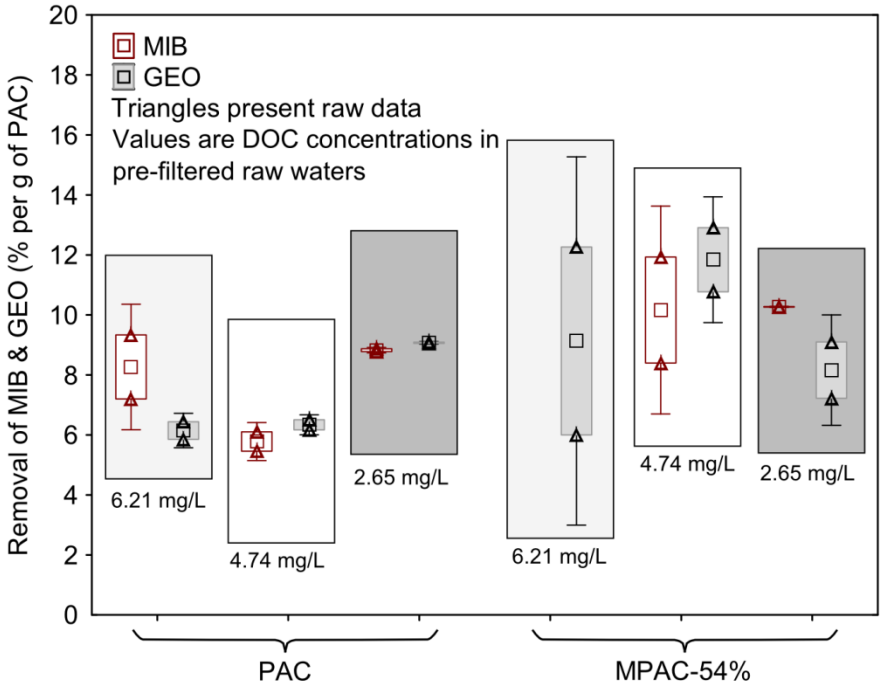

Figure E-1 : MIB and geosmin removal performance of PAC and MPAC-54% in three water matrices. Values are normalized to PAC content.